PATTERNING AND CROSS-LINKING OF FUNCTIONALIZED

POLYNORBORNENE POLYMERS

A Dissertation
Presented to
The Academic Faculty

by

Mehrsa Raeiszadeh

In Partial Fulfillment
of the Requirements for the Degree
Doctor of Philosophy in the
School of Chemical & Biomolecular Engineering

Georgia Institute of Technology
May 2012

PATTERNING AND CROSS-LINKING OF FUNCTIONALZIED

POLYNORBORNENE POLYMERS

Approved by:

Dr. Paul A. Kohl, Advisor
School of Chemical & Biomolecular
Engineering
Georgia Institute of Technology

Dr. Sue Ann Bidstrup Allen
School of Chemical & Biomolecular
Engineering
Georgia Institute of Technology

Dr. Michael A. Filler
School of Chemical & Biomolecular
Engineering
Georgia Institute of Technology

Dr. Dennis W. Hess
School of Chemical & Biomolecular
Engineering
Georgia Institute of Technology

Dr. Peter J. Ludovice
School of Chemical & Biomolecular
Engineering
Georgia Institute of Technology

Dr. Yonathan Thio
School of Material Science and
Technology
Georgia Institute of Technology

Date Approved: March 28, 2012

To my family

ACKNOWLEDGEMENTS

I would first like to thank my advisor, Prof. Paul kohl, for his guidance, support, and encouragement during my time at Georgia Tech. He is who encouraged me to join the Ph.D. program here at Georgia Tech and I wish to thank him for all the hope he has put on me even from the beginning. I would also like to thank my thesis committee members Prof. Yonathan Thio, Prof. Dennis Hess, Prof. Michael Filler, Prof. Pete Ludovice, and Prof. Sue Ann Bidstrup Allen for their helpful input during my Ph.D.

I would also like to give a very special thanks to the Kohl group members. Thank you in particular to Dr. Venmathy Rajarathinam, Dr. Nathan Fritz and C. Hunter Lightsey and also my undergraduate research assistants Noraica Davila, Christina Bins, Sang Lee, Chris Hilgert, Layla Marshall, Emily Korby, Jeremy Thompson, Robert McCormick, and Jackie Rand for their help with the work presented in this thesis. I would also like to thank Daphne Perry and my great friend, Dr. Ehsan Shah Hosseini, for their consistent help and support.

This work would not have been possible without the support of Promerus LLC, and I would like to acknowledge Dr. Ed Elce and Brian Knapp for their insight and support. Thank you to the MiRC Cleanroom staff specially Gary Spinner, Tran-Vinh Nguyen, and Walter Henderson for all their help throughout my time in the cleanroom.

Thank you to my parents and my oldest sister, without them I would have never even dreamed of making it to this point. Finally and most importantly I would like to thank my older sister, Mina, for being unbelievably supportive and helpful throughout the years. She has always inspired me to do great things and to be a better person.

TABLE OF CONTENTS

LIST OF TABLES

LIST OF FIGURES

LIST OF SYMBOLS

I/O	Input/Output
T_g	Glass Transition Temperature
3σ	Three Standard Deviation
γ	Contrast
D_0	The maximum exposure dose at which all of the negative-tone material is removed
D_{100}	The maximum exposure dose at which all of the negative-tone material is removed
S	Swelling
E_r	Reduced Modulus
H	Hardness
σ	Residual Stress
C	Capacitance
ε_r	Dielectric Constant

LIST OF ABBREVIATIONS

MEMS	Micro-Electro-Mechanical Systems
PNB	Polynorbornene
e-beam	Electron Beam
FTIR	Fourier Transform Infrared Spectroscopy
PAG	Photoacid Generator
LER	Line Edge Roughness
VFM	Variable-Frequency Microwave
CMOS	Complementary Metal–Oxide–Semiconductor
DOP	Degree of Planarization
BCB	Benzocyclobutene
CTE	Coefficient of Thermal Expansion
UV	Ultraviolet
DUV	Deep Ultraviolet
EUV	extreme Ultraviolet
SB	Soft Bake
PEB	Post-Exposure Bake
EBL	Electron-Beam Lithography
HSQ	hydrogen silsesquioxane
PMMA	polymethylmethacrylate
PAC	Photoactive Compounds
SEM	Scanning Electron Micrographs

RF	Radiofrequency
PGMEA	Propylene Glycol Monomethyl Ether Acetate
CPTX	1-Chloro-4-Propoxy-9*H*-Thioxanthen-9-One
TPEGE	Tetraphenylol Ethane Tetraglycidyl Ether
TGA	Thermal Gravimetric Analysis
DSC	Differential Scanning Calorimetry
BF	Base Formulation
BP	Base Polymer
DT	Developing Time
3-APS	3-Aminopropytriethoxy Silane
BOE	Buffered Oxide Etch
OD	Optical Density
PEG	Polyethylene Glycol
PDMS	Polydimethylsiloxane
PDF	Pressure Driven Flow
PECVD	Plasma Enhanced Chemical Vapor Deposition
LPCVD	Low-Pressure Chemical Vapor Deposition
ICP	Inductively Coupled Plasma
RIE	Reactive Ion Etching
HDMS	Hexamethyldisilazane
EOF	Electro-Osmotic Flow
IPA	Isopropanol
DAQ	Data Acquisition

SUMMARY

A challenging application space exists for high-aspect-ratio, high-fidelity dielectrics in micro-electro-mechanical system (MEMS), microelectronic, and photonic applications. Photosensitive polymers are widely used in these fields because they are relatively easy to process and pattern, and have good mechanical properties. Photosensitive polynorbornene (PNB)-based dielectrics have been shown to have high sensitivity, excellent photodefinition properties, and high mechanical strength making them suitable for MEMS, microelectronic packaging, and photonic applications. PNB-based dielectrics can be functionalized with epoxide, carboxylic acid, or fluorinated alcohol groups. Epoxy or carboxylic acid groups can be used to provide cross-linkable sites, resulting in improved chemical and thermal properties while fluorinated alcohol groups can provide solubility in aqueous base. The focus of this study has been on the epoxy-based cross-linking of ultraviolet and electron beam (e-beam) sensitive negative-tone PNB-based dielectrics.

The impact of multifunctional epoxy-based additives on the cross-linking, photolithographic properties, and adhesion properties of the photosensitive PNB dielectric was investigated. High aspect ratio features of 13:1 (height:width) were produced in 40 μm thick films (a single coat) with straight side-wall profiles and high fidelity. Contrast values as high as 33.4 were obtained at doses below 15 mJ/cm^2. To evaluate the polymer's suitability to MEMS and microelectronics applications, epoxy cross-linking reactions were studied as a function of processing condition through Fourier transform infrared spectroscopy (FTIR), nanoindentation, swelling and dielectric

measurements. The fully cross-linked films had an elastic modulus of 2.9 GPa and hardness of 0.18 GPa which can improve the mechanical compliance of the packaging device.

To explore the feasibility of the PNB dielectric as a highly sensitive e-beam resist for nano scale fabrication, the e-beam initiated reaction between PNB cross-linking sites and the multifunctional epoxy cross-linkers was investigated. In this study, the interaction of an e-beam with the PNB mixture and its compounds was investigated. The contrast, photodefinability, and e-beam activation of the components in the PNB formulations were studied. The PNB polymer had very high e-beam sensitivity and contrast. It was shown that the addition of a photoacid generator (PAG) to the polymer-epoxy mixture enhanced the contrast and sensitivity. Formulations with the additional cross-linker showed improved contrast, sensitivity, and substrate adhesion. 100 nm structures with 13.5 nm line edge roughness (LER) were fabricated. The influence of the developing time, the developer concentration, PEB, and film thickness on the contrast and sensitivity were studied. Structures with contrast values as high as approximately 8 were fabricated at doses as low as 0.38 $\mu C/cm^2$.

The acid-catalyzed epoxy ring opening reaction of the PNB dielectric was studied using FTIR spectroscopy. The photo and thermal acid generation initiated epoxy ring opening reactions and subsequent cross-linking of polymer. Additionally, polymer properties were characterized as a function of processing conditions for this polymer system. It was shown that thermal cure conditions have a substantial impact on the mechanical and electrical properties of the polymer. The rate and ultimate conversion of the epoxy ring opening reaction increased with increasing cure temperature, resulting in a

higher degree of cross-linking at cure temperatures above 140°C. Degradation reactions occurred at temperatures above 160°C, indicating loss of epoxide cross-linking groups and linkages. These hypotheses were supported by electrical and mechanical property studies. It was shown that curing the PNB polymer at 160°C for 1 h after develop resulted in full epoxy ring opening and highest cross-link density. This sample showed lower dielectric constant (3.9), residual stress (20 MPa), and solvent swelling (3.1%).

Variable frequency microwave (VFM) processing of the PNB dielectric was studied to investigate the rapid curing of the polymer at lower temperatures. The FTIR results showed that the microwave reaction rates were higher at each isothermal cure temperature compared to convective heating, indicating that the rapid VFM curing of PNB at low temperatures is feasible. The PNB film was fully cross-linked after 15 min VFM cure at the low temperature of 150°C. The shortest time to fully cure the polymer was found to be 5 min at 160°C. Also, the feasibility of rapid VFM curing of PNB in air was studied. All samples VFM-cured (140°C-180°C) in air showed no signs of oxidation. The electrical and mechanical properties of VFM-cured films were characterized and compared with thermally cured films to determine the effectiveness of the VFM processing. VFM-cured samples showed higher degree of cross-linking than thermally-cured samples, which was congruent with the FTIR results. Improved or equivalent properties were obtained for VFM-cured samples at shorter cure cycles and lower cure temperatures compared to thermally-cured films.

The PNB dielectric was also used as an overcoat material to make micro and nano fluidic channels. In this work, incorporation of advanced micro/nano fluidics with high-sensitivity photonic sensors was demonstrated. 500 nm to 50 μm channels were

fabricated by thermal decomposition of epoxy-based PNB polymers. Microdisks with quality factors of over 10^6 were presented in CMOS (complementary metal–xide–semiconductor) compatible SiN on oxide technology. These ultra-high quality factor SiN resonators were demonstrated in the visible range for the first time. The fluidic structures were interfaced with photonics for index and florescence sensing. This study was a collaboration with Dr. Ehsan Shahhosseini from the Photonics Group at Georgia Tech.

CHAPTER 1

INTRODUCTION

1.1 Dielectrics in Electronics

Advances in the semiconductor industry can benefit from increases in device speed, level of functionality, packing density, and shrinkage in component size as seen in high-performance, portable electronic devices. Bandwidth needs for future systems are expected to increase because of the large data requirements of such high-performance systems. As the frequency of I/O connections increases, the need for high-speed connections increases [1, 2].

Both optical and electrical connections are used for high-speed connections. However, optical links are preferred for long transmission lengths because they result in lower loss [1]. An optical fiber can transmit multiple data sets and therefore attain higher aggregate bandwidth than electrical connections. The limitation of applying optical links for short transmission lengths is due to the rigorous alignment tolerances and losses at sharp routing angles, resulting in challenging integration of optical connections [3].

On the other hand, electrical connections are simpler to integrate into electronic packages and can be improved by lowering the signal loss. The speed of an electrical signal through metal lines is a function of both the conductive metal and the surrounding dielectric material used in the connection [4, 5]. Enabling high-performance electronic systems require high density and high speed interconnects. To achieve these goals in electronic interconnects, losses in the metal line and dielectric material, and crosstalk noise need to be minimized.

The total delay in metal lines is a function of lumped resistance of interconnects and the capacitance coupling the line and its return path. One way to improve the chip

speed and decrease the loss is to improve the conductive properties of the metal. Replacing aluminum with a lower resistivity metal, such as copper, increases the signal speed. This increase in the signal speed is a direct consequence of decreasing the metal resistivity from 3.0 $\mu\Omega$.cm for aluminum to 1.7 $\mu\Omega$.cm for copper, which has been implemented in advanced processors [4, 6, 7].

The capacitive coupling between the lines (lateral or vertical) can be reduced by improving the dielectric properties of the surrounding dielectric material. The dielectric constant is a complex number which measures the ability of the material to store charge and its unrecoverable loss [4]. Decreasing the dielectric constant of the insulating layers can improve both the speed and density of electronic devices. The density can increase due to ability to place signal lines closer together without suffering undue current leakage (i.e. loss) and cross-talk. Incorporating low-dielectric constant materials into electronic devices is a major activity.

The transition from aluminum to copper for on-chip metal interconnects has reduced the delay. Improvements in process and properties of dielectric materials are key enablers in further reducing this delay and achieving high-speed, high-density electronic connections.

Many organic and inorganic dielectrics have been developed for various applications in electronic devices. Polymer dielectrics are of special interest because of their superior properties in certain applications. The dielectric constant for most polymers ranges from 2 to 4 fulfilling the electrical requirements. Also, polymers can more easily form planar structures compared to inorganic materials, which generally tend to coat features conformally [4]. Non-planarity is an important factor which causes difficulties in processing due to the propagation of any non-planar feature through subsequent layers as multiple layers of interconnect and insulators are deposited. Planarization effect is evaluated by degree of planarization (DOP) which is defined by Equation (1.1) [8, 9]:

$$\text{DOP} = \left(1 - \frac{T_2 - T_1}{T_0}\right) \times 100\% \qquad (1.1)$$

The requirements for the dielectric properties depend on its applications. The mechanical properties and thermal stability are also important properties for dielectric materials which can be achieved by polymer dielectrics.

Polymer dielectrics are divided into two main categories; thermosets and thermoplastics. Thermoset materials are polymers that are cured to produce a highly cross-linked polymer network. Thermoplastics soften at high temperatures and do not undergo a curing process [1]. Thermoset materials are common in electronic applications and undergo a chemical cross-linking reaction.

The most common polymer dielectrics are epoxies. The epoxy group is a three-member ring with two carbons and one oxygen as shown in Figure 1.1. Epoxies provide many advantages including their excellent adhesion to various materials, good mechanical properties, and good thermal stability. They also possess good solvent resistivity, which is created by cationic reactions. However, epoxies suffer from high dielectric constants (ε_r = 3.5 to 5) and high moisture uptake [1, 2]. Epoxies can be made photodefinable by incorporation of a photoacid generator that catalyzes epoxy ring opening and subsequent cross-linking leading to a negative-tone resist.
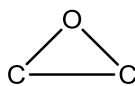
Figure 1.1 Chemical structure of epoxy.

Polyimides, which can be used as interlevel dielectrics, are typically derived from the reaction of dianhydride and diamine forming polyamic acid. Subsequently,

cyclodehydration is carried out either at a high temperature or by a dehydration agent [1]. The chemical structure of polyimide and the general structure of aromatic polyimide are shown in Figure 1.2 and 1.3 [1], respectively. The rigidity of polyimide is due to the large number of aromatic groups, which results in high glass transition temperature (T_g) and good mechanical properties. This polymer class possesses excellent solvent resistance, low loss, and good adhesion, making it a good dielectric candidate. However, the dielectric constant of polyimide changes with moisture uptake and ranges from 2.8 to 3.9. Additionally, photosensitive polyimides require high temperature cures to complete the imidization reactions and become insoluble [4].
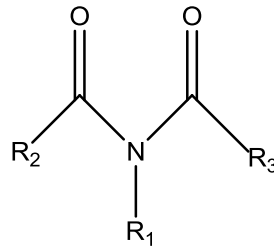
Figure 1.2 Chemical structure of polyimide.
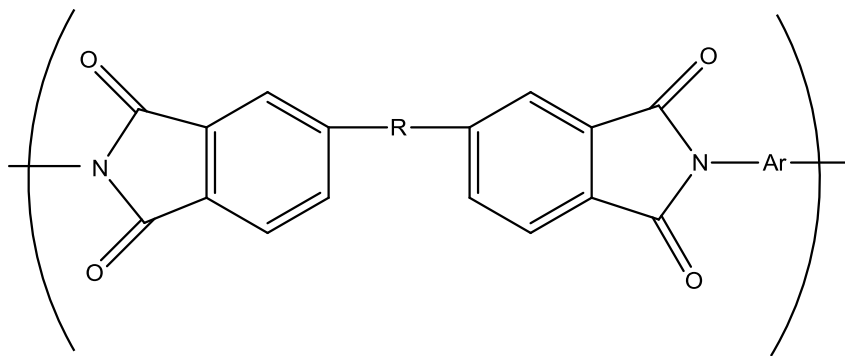
Figure 1.3 Chemical structure of aromatic polyimide.

Benzocyclobutene (BCB), which used in high-frequency applications, was developed by Dow Chemical under the trade name Cyclotene. The chemical structure of

BCB is shown in Figure 1.4. BCB provides many advantages including low dielectric constant (ε_r = 2.5 to 2.7), low loss factor, high T_g, and low moisture uptake. This polymer also has a high DOP with values greater than 90%. Additionally, BCB has a low cure temperature which results in a highly cross-linked network with high chemical resistance. However, a high degree of cross-linking in cured BCB results in high-stress in the films, which tends to crack the film if applied in layers thicker than 15 to 20 μm. The polymer is also costly and can have poor adhesion to substrates. An azide cross-linker is added to photodefinable formulations of BCB to provide cross-linking the irradiated regions of the polymer film [10, 11].
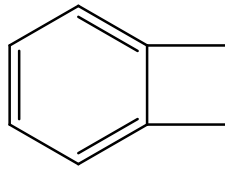
Figure 1.4 Chemical structure of BCB.

Polynorbornene (PNB) is a class of thermoset dielectric polymers, offering improved properties for MEMS and microelectronics applications.   Norbornene is a bridged cyclic hydrocarbon, as shown in Figure 1.5 and 1.6. The polymer can be prepared by variety of processes including vinyl-addition polymerization of norbornene and ring opening metathesis polymerization [1]. The resulting polymer is different in each case. The polymer obtained from the vinyl-addition process is marketed under the trade name Avatrel Dielectric Material. PNB has many advantages including low moisture uptake and good thermal stability, and excellent electrical properties: low dielectric constant (2.5) and low loss. However, this polymer itself suffers from poor adhesion to surfaces, high cost, and high coefficient of thermal expansion (CTE). The undesirable properties of PNB can be controlled by the addition of side groups. This class of polymer is discussed in more details later in this chapter.

5
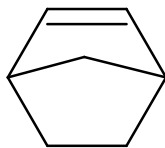
Figure 1.5 Chemical structure of norbornene molecule.
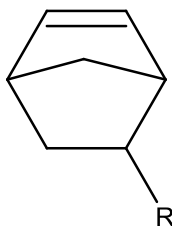
Figure 1.6 Chemical structure of functionalized norbornene molecule.

1.2 Photosensitive Dielectrics

1.2.1 Photodefinition and Photolithography

Photodefinition consists of two distinct steps: formation of a latent image in the polymer film by exposure to radiation and development of the image to give a three-dimensional structure for the next process step [12]. Both the material properties and process conditions affect the photodefinition. In most cases, material properties are hard to change for certain polymers. To get the optimum photodefinition, the process conditions of various steps need to vary. The key variables involved in processing steps of photolithography and their effects on the final image are discussed here.

Photolithography is a process used in micro-fabrication to transfer geometric shapes on a mask to photoresist material covering the surface of a semiconductor wafer [13, 14]. It uses light to transfer a pattern from a photo mask to a photoresist (light-sensitive chemical). The optical exposure tools use either visible, UV, deep ultraviolet (DUP), or extreme ultraviolet (EUV) light as the exposing radiation [15]. The light is

6

produced across a broad spectrum and it is filtered to select a single spectral line. A single iteration of photolithography combines the following steps in sequence: wafer cleaning; photoresist application (spin-coating); soft bake (SB); UV exposure; post-exposure bake (PEB); developing; and curing [16].

Wafer Cleaning: Substrate surfaces in semiconductor fabrication are normally metallic, semiconducting, or insulating. Organic, inorganic, and particulate contaminations are found on surfaces which may cause poor adhesion and defects. These defects raise issues such as non-uniform polymer coating, striation in coated films, and loss of line width control. Solvent treatment, plasma treatment, polishing, and thermal treatment are normally employed for surface cleaning. Main variables associated with the cleaning steps are the type of reagent and surface, time, temperature, and choice of cleaning equipment.

Spin Coating: In this step, the wafer is first mounted on the vacuum chuck of the spin coater. Then, a predetermined amount of polymer solution is dispensed on the wafer surface. The wafer is rapidly rotated to obtain a uniform, defect-free, adherent polymer film over the entire wafer. The acceleration stage is crucial to obtaining good uniformity since solvents begin evaporating from the polymer as soon as it is dispensed. The film uniformity across the substrate is essential to ensure good contact between the polymer film and the mask used in contact printing which is a pre-requirement for uniform and reproducible pattern and development time. The key variables that affect the spin coating process are the viscosity, molecular weight, boiling point, and composition of the polymer solution and the spin speed and acceleration of the spin-coater.

SB: After spinning , the wafers must undergo a SB on a hotplate or in an oven to dry off most of the solvent in the polymer, establish exposure characteristics, and release built-in stress due to the shear forces generated during the spin coating process [12, 15]. The dissolution rate in the developer is highly dependent on the solvent concentration in the final polymer film. Choosing the right bake time and temperature is important to

avoid excessive baking temperatures that could degrade or include undesired and premature chemical reactions in the polymer film. High-temperature soft bakes can actually begin to drive the photochemistry of the PAG, resulting in polymer dissolution of un-exposed regions during development. Typical soft-bake temperatures are 90-100°C. SB times range from 30 sec on a hotplate to 30 min in an oven [15]. It has been shown that varying the SB temperature, affecting the solvent concentration in the film, can improve the photodefinition for some polymers [12]. The solvent concentration remaining after SB is usually about 5% of the original concentration.

Exposure: After SB, the wafer is exposed. Here, the focus is on contact or proximity printing, which simply entailed flood-exposing a wafer with UV light through a mask as shown in Figure 1.7. The quality of the image is limited by many physical and chemical phenomena during the exposure step. The theoretical resolution capacity of contact printing for a mask consisting of equal lines and spaces is given by Equation (1.2):

$$2b_{min} = 3\sqrt{\lambda(s + (1/2)z} \qquad (1.2)$$

where $2b$ is the grating period, λ the wavelength of the exposing radiation, s the gap width between the mask and the surface of the polymer film, and z the polymer film thickness.
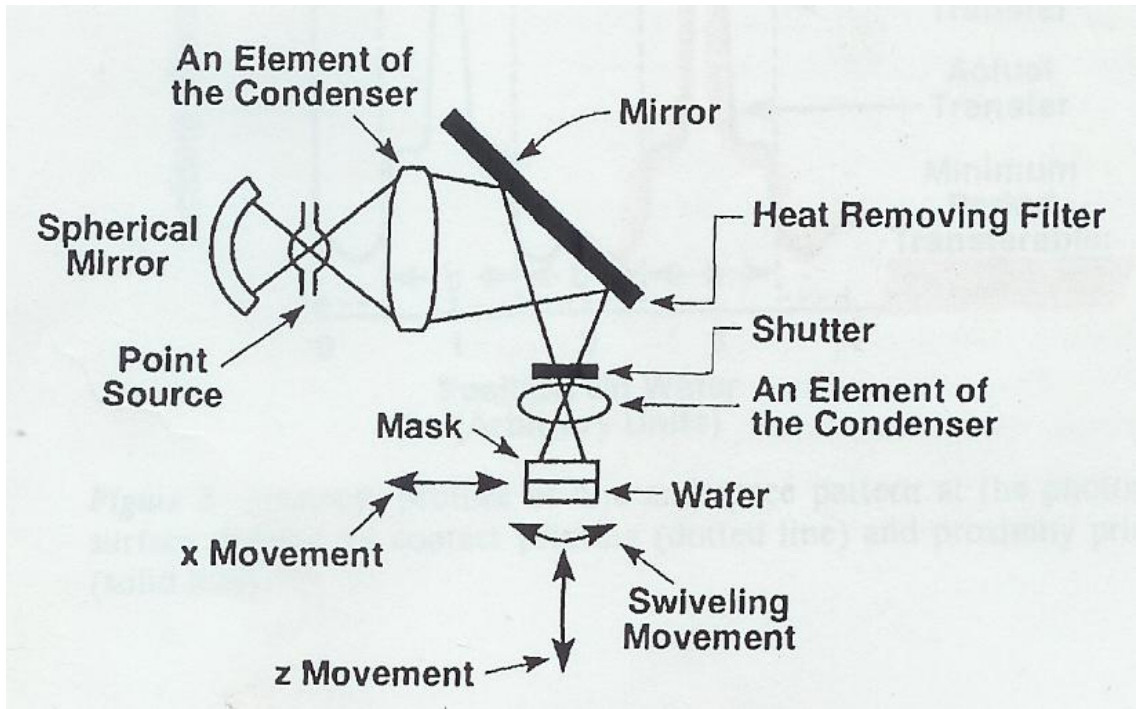
Figure 1.7 Schematic of contact printing [17].

The fundamental resolution limitation of contact printing is diffraction of light at the edge of an opaque feature on the mask as the light passes through an adjacent clear area. Even though the mask should transfer a sharp pattern to polymer film in contact printing according to geometrical optics, light may be diffracted or scattered at the edge of mask, introducing irradiation into unexposed areas. Light diffraction and scattering effects are shown in Figure 1.8.

Another important factor affecting the image profile of the polymer is the distribution of the light intensity in the polymer film, which is determined by both the absorption characteristics of the polymer and the material composition of the substrate. Light incident is absorbed by the polymer as it passes through the film. When incident light reaches the polymer-substrate interface, it partially reflects back to the polymer and is further absorbed. This process continues until it is fully absorbed. Standing waves are produced as these reflected beams interfere with each other. Light reflection in the

polymer film is shown in Figure 1.9. (Note that the light intensity of the beams in this figure is not scaled.) In summary, the distance between the mask and the polymer film, the light intensity, the exposure time, and the dose rate need to be controlled to improve the image quality.
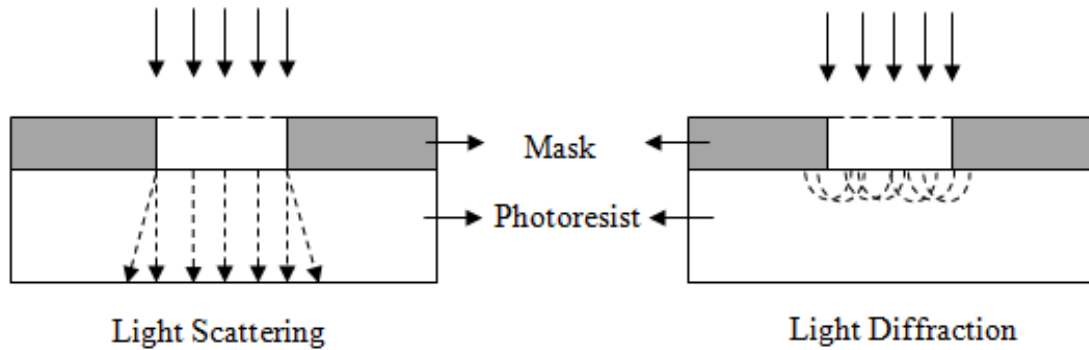
Figure 1.8 Illustration of light scattering and difraction during exposure.
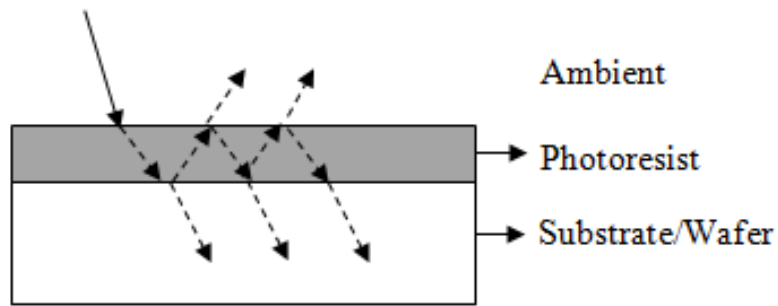
Figure 1.9 Multiple reflections occuring at the polymer-to-substrate inteface.

PEB: This is another important processing step which can affect the polymer cross-linking and pattern quality, specially in case of negative-tone systems. After exposure, the chemical raections are initiated in the exposed areas of the polymer film. As the cure temperature increased, the cure rate increases for the polymer having the

10

same concentration of cross-linking groups, resulting in a shorter cure time to reach the same degree of cross-linking [12, 18]. PEB is, therefore, essential to allow the desired reactions to continue after exposure. The PEB temperature must be controled to avoid thermal decomposition photoactive compounds (PAC) and undesired reactions. For acid-catalyzed reactive systems, cross-linking reaction rate is a function of PEB time and temperature, acid concentration, and acid diffusion rate in the polymer film. Therefore, optimization of these parameters is critical for improving the pattern quality, the line edge roughness and the pattern size.

Develop: After PEB, the wafer must be developed wich results in removal of unexposed areas of a negative-tone resist and dissolution of exposed regions of a positive-tone resist. This step has great influence on the polymer profile and is very temperature sensitive. Therefore, it is important to control the develop temperature to maintain an accurate control of the pattern linewidth.

Cure: High temperature cures are done after develop to fully cross-link the polymer and achieve the optimum mechanical stability and also to harden the polymer against furthur energetic processes such as ion implantation and plasma etching. Curing is only required for thermosest materials [1, 2]. The cure temperature and time can greatly affect the cross-link density in the polymer matrix, varrying the chemical, mechanical, electrical, and physical properties of the polymer. The cure temperature must be lower than the decomposition temperature of the polymer to avoid degredation reactions in the polymer. Traditional thermal cure and variable-frequency microwave (VFM) cure are two techniqes used for thermosets, which are discussed here.

Traditional thermal cure involves subjecting the polymer to a curing cycle in a conventional oven, which results in cross-linking of the polymer. However, some high-performance polymers require high thermal cure temperatures that are well above the degredation temperature of the substrates. Also, this method is usually lengthy. To

address theses issues of throughput and high temperature, low temperature processes such as microwave curing have been developed [1].

VFM processing of high-performance polymers has been studied as a low-temperature curign alternative to the traditional thermal cure process [19-22]. VFM processing provides the ability of quikly and repeatedly step through a range of frequencies. Irradiation of a polymer dielectric with microwave energy results in energy transfer due to the dielectric loss mechanisms. The principal mechanism of coupling microwave radiation to polymer dielectrics is through dipole orientation by the oscillating electric field [21, 23, 24]. The efficiency of coupling microwave energy into a material is dependent on a number of factors, including the dipole strength, mass, and mobility [21]. The amount of microwave energy per unit volume converted into heat is given by Equation (1.3) [21, 23].

$$P_{absorbed} = 2\pi f E_{rms}^2 \varepsilon_0 \varepsilon'' \qquad (1.3)$$

Where $P_{absorbed}$ is the dissipated or absorbed power per unit volume, f is the frequency, E_{rms} is the root mean square electric field strength, ε_0 is the permittivity of free space, and ε'' is the relative loss factor. VFM offers significant advantages over traditional fixed frequency system by providing uniform heat distribution and allowing processing of conducting materials. Previous studies have shown that VFM processing reduces the cure time and temperature without negative effect on the desirable properties of cured polymer [23].

In the cure process, therefore, the cure time, temperature, and tecnique can affect the polymer cross-linking and should be controlled to obtain the optimum chemical, mechanical, and electrical properties of the polymer.

Obviously, photolithography is a multidimensional process and its optimization is an important and challenging task.

1.2.2 Advantages of Photosensitive Polymers

Photosensitive polymers offer additional advantages over non-photosensitive polymers since they can be directly patterned by photolithography techniques, which simplifies the process steps and eases the integration [2, 23]. The patterning process for photosensitive and non-photosensitive, negative-tone polymers are compared in Figure 1.10. For photosensitive polymers, the coated polymer film is baked and exposed to UV radiation, which results in cross-linking in the exposed areas. The pattern is simply formed by developing after PEB, which dissolves the uncross-linked areas of the negative-tone polymer. On the other hand, non-photosensitive polymers require additional steps after SB: a layer of photoresist is applied on the polymer and baked. The photoresist is then patterned by exposure and developing. The pattern formed on the photoresist, which depends on whether a positive or negative resist is used, forms an etching mask. Then, wet or dry etching is used to pattern the polymer film. Finally, after removal of the photoresist, the patterned polymer is obtained. This patterning process in very complex and the pattern design is not reproducible due to the etching process which affects the polymer side-walls. Therefore, photosensitive polymers reduce process steps and improve the pattern quality

.
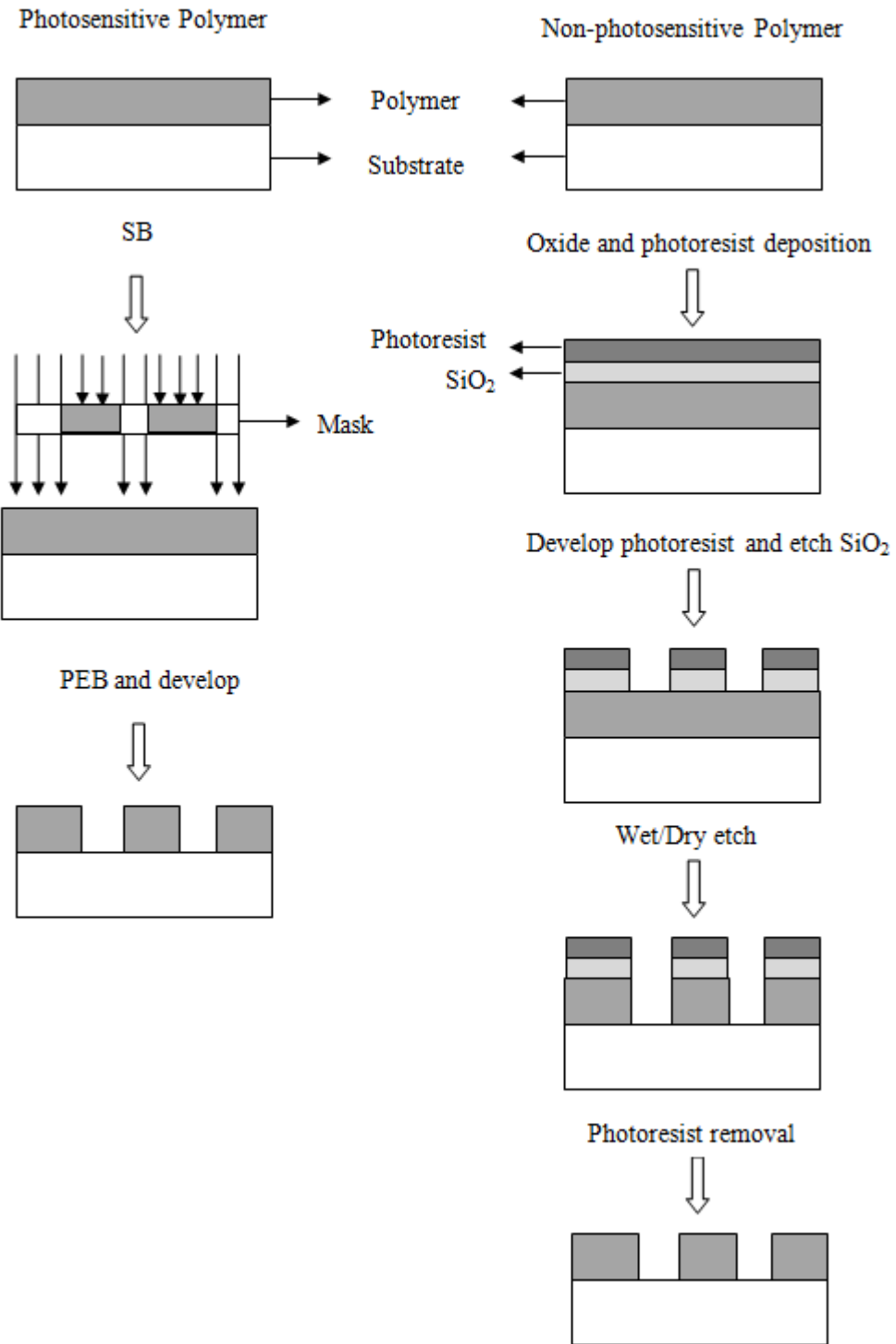
Figure 1.10 Schematic diagram comparing patterning of photosensitive and non-photosensitive, negative-tone polymers.

1.3 Electron-Beam Lithography and Resists

Electron-beam lithography (EBL) refers to a lithographic process that uses a focused beam of electrons to form the circuit patterns needed for material deposition on the resist, in contrast with optical lithography which uses light for the same purpose. The system is used to fabricate device components in semiconductor or insulator materials. EBL is an important patterning method for nanosystems and devices, such as molecular electronics [25, 26], high-precision mask making [27], and mold making for nanoimprint lithography [28] due to its high spatial resolution and versatile processing [29]. EBL is an established technique for the fabrication of small electronic device structures [30].

The purpose of EBL, as with photolithography, is to create very small structures in the resist, but EBL offers higher spatial resolution than optical photolithography because of the short wavelength of the e-beam possessed by the 10-50 keV electrons that it employs [14]. Therefore, the primary advantage of EBL is that it is one of the ways to beat the diffraction limit of light and make features in the nanometer regime. On the other hand, the key limitation of EBL is throughput due to the sequential nature of the exposure.

All e-beam systems require an electron source with high intensity (brightness) and uniformity, small spot size, good stability, and long-life [15]. The beam brightness is measured in units of amperes per unit volume per steradian. Electron removal from the cathode of the gun requires heating of the cathode (thermionic emission), applying electric field (field aided emission), a combination of the two (thermal field aided emission), or with light (photoemission). A typical electron gun for an EBL system is shown in Figure 1.11. The emitted electron current density is one of the primary figures of merit for the gun, which is given by Equation (1.4) [15]:

$$J_c = AT^2 e^{-E_w/kT} \qquad (1.4)$$

Where Jc is the electron current density, A is the Richardson's constant for the material, and E_w is the effective metal work function. The measure of the collected electron is the brightness. Although an increase in the emitted current density also generally increases the brightness, the percentage increase in the brightness is not as large as the percentage increase in the current density if the increase in brightness decreases the efficiency of electron collection [15].
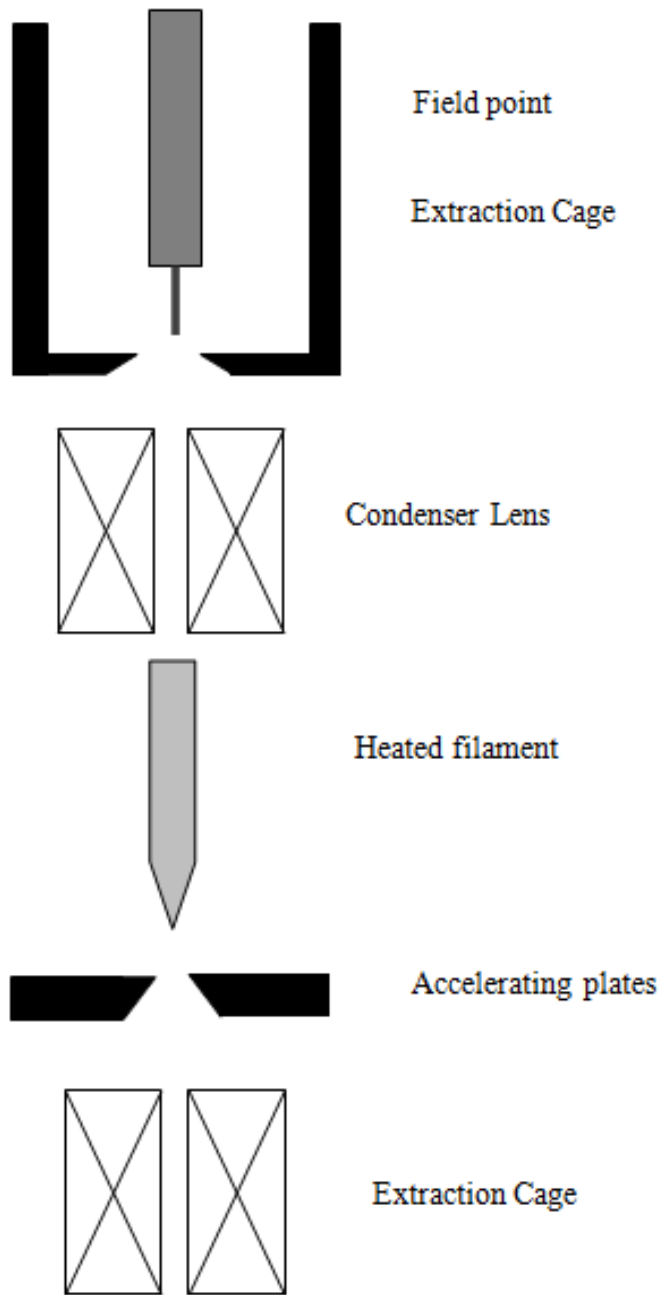
Figure 1.11 Simplified cross section schematics of field and thermoionic emission electron guns [15].

Image production in the e-beam resists is very different than in photoresists. In an optical process such as EBL, the energy of the absorbing photon is well defined. The energy of a photon depends only on its frequency (ν) or inversely, its wavelength (λ) as shown in Equation (1.5):

$$E = h\nu = \frac{h\,c}{\lambda} \qquad (1.5)$$

The photon energy for an i-line source is 3.4 eV. In contrast, exposure to e-beam produces high concentration of secondary electrons with a wide range of energies. E-beam resists must be designed so that the desired reaction occurs preferentially rather than designing it so that a single chemical reaction is driven by exposure. However, all the reactions that occur in this case should be considered. Additionally because the energetic beams penetrate the e-beam resist into the substrate, undesirable reactions must also be considered [15].

Some of the most common e-beam resists are ZEP (a copolymer of a-chloromethacrylate and a-methylstyrene) [31], hydrogen silsesquioxane (HSQ) [32, 33], and polymethylmethacrylate (PMMA) [29, 34], maN-2403 (a phenolic resin) [35]. These e-beam resists and their characteristics are explained below.

ZEP is a high-resolution positive-tone resist with better sensitivity compared to the other three resists and it also has excellent etch resistance. Due to its sensitivity and etch resistivity, ZEP can be used in both metal lift-off processes (slight overexposure results in an excellent undercut profile) and various dry-etch processes for pattern transfer to the underlying substrate. ZEP utilizes an inert solvent developer (100% n-amyl acetate).

HSQ shows high resolution [36-40], minimal LER [37] high etch resistivity [37-40], and high stability under scanning electron microscope (SEM) inspection [40, 41]. HSQ, which is sensitive to the time between coating and exposure, is best to expose immediately after coating samples. Two different schemes have been proposed for the description of the chemical structure of HSQ [32, 42-44]. In the first scheme a siloxane-based polymer is assumed where terminal silicon (Si) atoms is bond to two oxygen (O) atoms, one hydrogen (H) atom, and one OH bond and every other Si atom is bound to three oxygen (O) atoms and one hydrogen (H) atom. During cure, HSQ cross-links by condensation of Si–OH groups to Si–O–Si bonds. As a consequence, a three-dimensional network of the ladder structures is formed [43]. The second scheme describes the HSQ as caged oligomer structures with the general formula $(HSiO_{3/2})_{2n}$ [32]. The caged oligomers are opened during a cure and form a network structure [42-44]. If the network formation proceeds via conversion to silica [45] or via rearrangement reaction without a change in stoichiometry [46] depends on the process conditions.

PMMA is a very high-resolution positive-tone resist with relatively poor sensitivity (resolution scales directly and sensitivity scales inversely with molecular weight of the polymer). PMMA shows very poor plasma-etch resistance, hence it is used primarily to fabricate metal lines via liftoff processes; It offers ease of processing and utilizes an inert solvent developer. Improved pattern quality in micron and nano scale has been reported for PMMA [29, 47, 48].

ma-N 2403 is a negative-tone resist composed of a phenolic resin (novolak) as polymeric binder and a bisazide as PAC and is developed in aqueous-alkaline developers [49]. This resist works without chemical amplification consequently its processing does not comprise any critical steps. Ma-N 2403 with excellent dry-etch resistance, exhibits very good resolution (sub-100 nm) and moderate sensitivity.

These commonly used e-beam resists have high spatial resolution but relatively low sensitivity. The base dose of these e-beam resists with 100 kV accelerating voltage

is listed in Table 1.1. The low sensitivity of these resist requires them to have excessive

exposure time which can result in long write times for which beam drift or instability can

occur, and it tremendously increases the lithography process cost. Therefore, e-beam

imageable materials with high sensitivity are of special interest.

Table 1.1 Base dose of some commonly used electron-beam resists with 100 kV
accelerating voltage.

E-beam Resist	Base Dose ($\mu C/cm^2$)
ZEP	200
HSQ	450
PMMA	650
maN-2403	1200

1.4 Dielectric Property Requirements

The important properties of a dielectric material are electrical, mechanical,

thermal, chemical, and processability. Each of these properties, which are essential to

successful application of a dielectric, is discussed below. For photoresists and e-beam

resists, patteranability is also a critical property. Since the focus of the work presented in

this thesis is on photoresists and e-beam resists, this property is also discussed below.

The relative importance of each of these properties depends on the application of the

dielectric material.

Electrical properties: The primary role of a dielectric is electrical isolation.

Under alternating electric field, charge may be carried through the dielectric media.

Signal speed through the dielectric media is inversely proportional to the square root of

the dielectric constant as given by Equation (1.6) [1].

$$v_p = {}^c\!/\!{\sqrt{\varepsilon_r}} \qquad (1.6)$$

Where v_p is the signal propagation velocity, c is the speed of the light, and ε_r is the dielectric constant of the material. Thus, a lower dielectric constant material has higher signal speed and superior electrical performance. Additionally, a dielectric must have a maximum value of resistance to be useful and provide sufficient insulation. If a dielectric has poor electrical resistivity, electrical performance would be severely affected [1].

A dielectric must also have a low dielectric loss. Dielectric loss is a measure of electrical energy dissipated during one polarization cycle in a dielectric material. These energy losses are important in high-frequency signal transmission for radiofrequency (RF) and digital functions because they degrade the efficiency and change the impedance of the circuit. Another electrical property of interest for dielectric materials is the breakdown voltage. A dielectric, which is exposed to high magnitude of electrical field, must have a high breakdown voltage. That is, it must withstand high voltages without breaking down (bond breaking within the dielectric) [1].

Mechanical Properties: In addition to electrical isolation, mechanical stability of a dielectric can also be very important depending on the dielectric application. Elastic modulus, CTE, residual stress, elongation to break, and adhesion are the critical mechanical properties for dielectrics. Dielectrics with lower stress result in higher reliability. Thus, it is desirable to have a low-elastic modulus dielectric. Also, a lower CTE will result in lower stress on interconnects and the substrate. The elongation to break, which is the strain that can be applied to the film before it breaks, is also an important property and a lower elongation to break is desirable.

Adhesion is an important property for these materials. Regardless of the mechanical stability and strength, a dielectric must have good adhesion to the

surrounding materials. Multiple layers of wiring exist in electronics devices and good adhesion between the dielectric and the conductor, the substrate, and the overcoat material is necessary for the reliability of the device. Failure of adhesion between these layers creates stresses and results in delamination of the dielectric film after deposition of additional layers. Thus, dielectrics with good adhesion are desirable.

Thermal Properties: Dielectrics are required to have good thermal stability at all the processing temperatures the device may encounter, including all deposition, cure, and etch stages for each layer. If a dielectric is not thermally stable, it irreversibly mechanically or chemically changes over the temperature range of a process. One measure of thermal stability is T_g, the temperature at which the polymer gains segmental mobility and glassy regions of the polymer become amorphous [50]. Therefore, dielectrics must have a high T_g and a decomposition temperature to withstand high processing temperatures. Ideally, the device should not operate at temperatures substantially above the T_g of the polymers used in the processing for extended periods of time because the chemical and mechanical properties of the polymer can drastically change and also because cross-linked polymers are more susceptible to degradation than deformation at temperatures above their $T_{g\,[4]}$.

Processability: A dielectric with a high DOP creates flat surface, which is essential for formation of fine lines and spaces. High DOP of a dielectric is required both for lithography and metallization. Additionally, ease of deposition and thickness control are important in the process of a dielectric material. It is desirable to deposit the dielectric quickly and at moderate temperature either as a liquid or dry film. It should have good flow behavior to allow for planar layers [1]. Also, precise control of the dielectric thickness is needed. If vias are formed in a dielectric, etching, laser ablation, and drilling for photo-processing is needed. Patterning can be affected by the fillers in the dielectric. Dielectric fillers must be carefully evaluated for their effect on the drillability of the dielectric before incorporation.

Patternability and Resolution: The three most useful metrics of the performance of a resist (photoresist or e-beam resist) are sensitivity, resolution, and contrast. The sensitivity of a resist is the minimum exposure dose to obtain photodefinition at a fixed developing condition. The process for a resist with higher sensitivity is faster since a shorter exposure time will be necessary for a given exposure intensity. Resolution refers to the smallest feature size that can be produced in a resist. It depends on the ability of the resist to reconstruct a pattern from the areal image. Very small features may be patterned with a resist using a particular exposure tool, but they cannot be reliably used due to poor control of the dimensions of the feature. Therefore, resolution is a minimum feature size resolved that maintain a certain feature tolerance. A typical number is a three standard deviation (3σ) distribution of line-widths with no less than 10% variation [15]. Resolution strongly depends both on the exposure tool and the photoresist process. This characteristic of resists is not a fix number and carries with a considerable uncertainty even in a fixed exposure tool [15].

As resolution is highly dependent on the exposure tool, a function known as contrast is used to characterize the resist more directly. The contrast is obtained by measuring the resist thickness after developing, normalizing and plotting it versus the logarithm of the incident dose. Contrast curves for positive-tone and negative-tone resists are shown in Figure 1.12. Assuming the resist in a negative tone, the curve has three regions: low exposure dose where all the resist is removed, high exposure where almost all the resist remains, and the transition region between the two extremes. Contrast, γ, is the slope of the line connecting the maximum exposure dose in the low exposure dose region (D_0) and the minimum exposure dose in the high exposure dose region (D_{100}) and is described by Equation (1.7) [13]:

$$\gamma = \frac{1}{log_{10} \frac{D_{100}}{D_0}} \qquad (1.7)$$

Contrast is the measure of the resist to distinguish between the dark and light portions of the mask [15]. It depends on several factors including the exposing radiation, baking temperatures and times, the developing process, and surface reflectivity of the substrate. Resists with higher contrast are able to fabricate features with sharper lined edge and straight side walls. Contrast for typical photoresists is 2 to 4 [15].

Positive-tone resist

D_0

1.0 —

Normalized
thickness

D_{100}

10   100   1000

Logarithmic exposure dose (mJ/cm^2)

Negative-tone resist

D_{100}

1.0 —

Normalized
thickness

D_0

10   100   1000

Logarithmic exposure dose (mJ/cm^2)
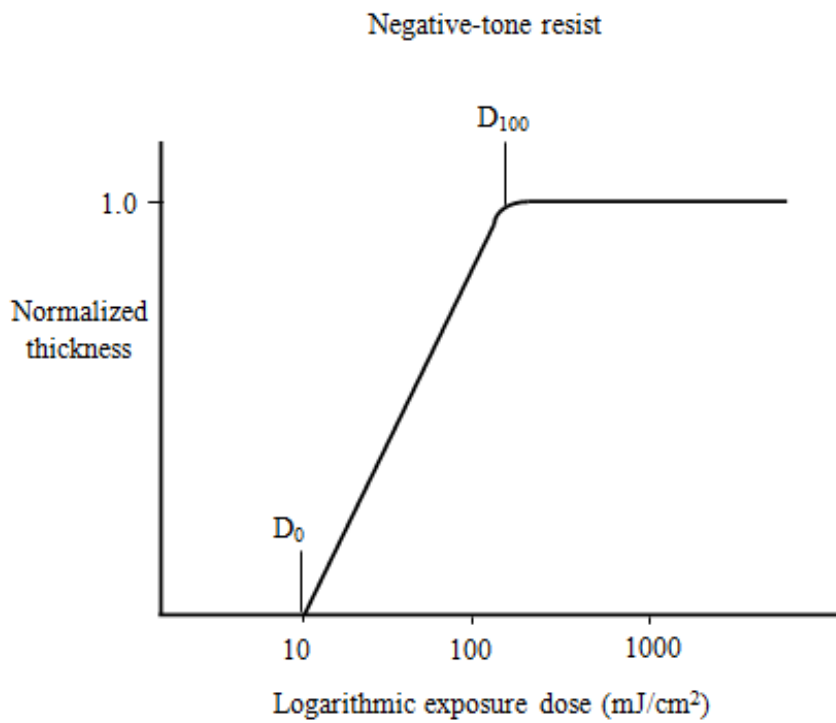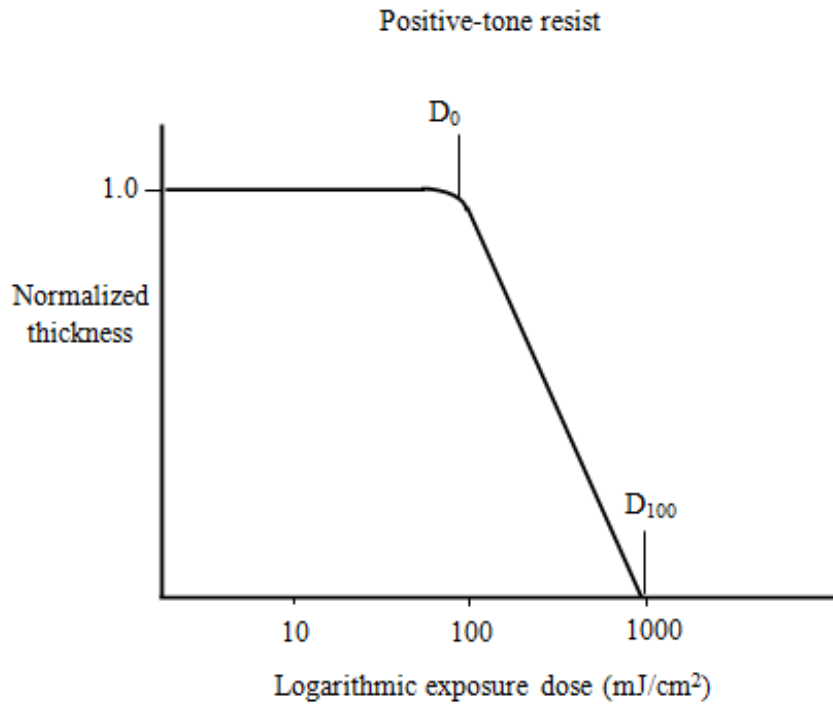
Figure 1.12 Contrast curves for positive-tone and negative-tone resists.

1.5 Polynorbornene-Based Dielectrics

Thin film polymer dielectrics are used in MEMS and microelectronics industry for a variety of applications [2, 51, 52] such as inter-level dielectrics, passivation layers, encapsulants, and underfills due to their superior mechanical, chemical, and electrical properties[21, 23, 53]. Photosensitive polymers offer additional advantages by reducing the processing steps. There has been extensive research and development focused on photosensitive polymers for MEMS and microelectronics applications [2, 54]. PNBs are attractive for these applications because they possess excellent electrical properties, good thermal stability, and low moisture uptake [55-57]. The bulky rigid nature of the PNB backbone has a T_g greater than 350°C and a decomposition temperature above 400°C [4]. Additionally, the hydrocarbon backbone of PNB has limited sites for moisture to hydrogen bond and therefore exhibits low moisture absorption [4].

Although PNB has suitable properties for MEMS and microelectronics applications, it suffers from poor mechanical properties and weak adhesion [1, 58]. PNB films, cast from solution, are brittle and possess low elongation to break due to the rigid polymer backbone. Also, these films, which are purely hydrocarbon chains, exhibit poor adhesion due to no direct chemical bond to substrates. However, the undesired properties of PNB can be improved by the addition of side groups that are substituted directly to the polymer backbone [59, 60]. The chemical structure of functionalized PNB is shown in Figure 1.3. The addition of any side group to PNB backbone increases chain flexibility and free volume, which can result in more mechanical stability [61]. Also, PNB film adhesion and reactivity can be improved by incorporation of appropriate adhesives as side groups and additives.

26
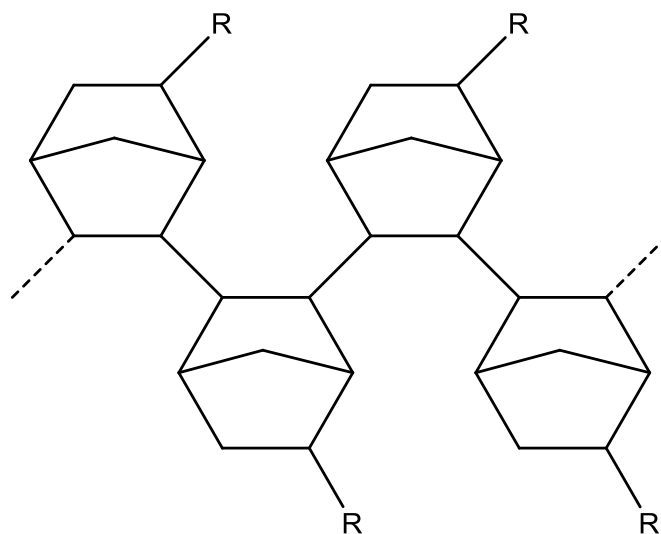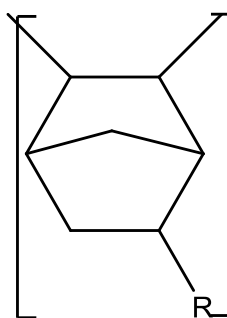
Figure 1.13 Chemical structure of polynorbornene.

To improve the mechanical properties, alkyl side chains can be substituted to the PNB backbone. The alkyl groups can increase the elongation to break of the PNB. The elongation to break has been shown to increase as the length of alkyl chain increase [4]. To improve the adhesion characteristics of PNB polymers epoxy polymers can be added the polymer. Epoxy polymers have excellent adhesion to various substrates and modest cure temperatures [53]. The acid catalyzed activation of epoxy groups is an efficient way to achieve cross-linking and enhance the polymer properties, especially adhesion and

[55]. Additionally, epoxide systems are known to form highly cross-linked systems, which can improve the mechanical stability of PNBs.

In the work presented in this dissertation, a photosensitive epoxy-added PNB polymer, Avatrel 8000P, was studied.   The polymer formulation is a mixture of the PNB polymer, multifunctional epoxy cross-linkers, a PAG, and an adhesion promoter. The PNB polymer is functionalized with alkyl groups with carboxylic and alcohol ending groups. Carboxylic acid functionalized side chains on the PNB backbone provide reactive sites for cross-linking with multifunctional epoxy additives. Fluorinated alcohol and carboxylic acid groups provide solubility in aqueous base for environmentally friendly developing process. The chemical structure of the aqueous base-developable PNB-based dielectric polymer, Avatrel 8000P, is shown in Figure 1.14.
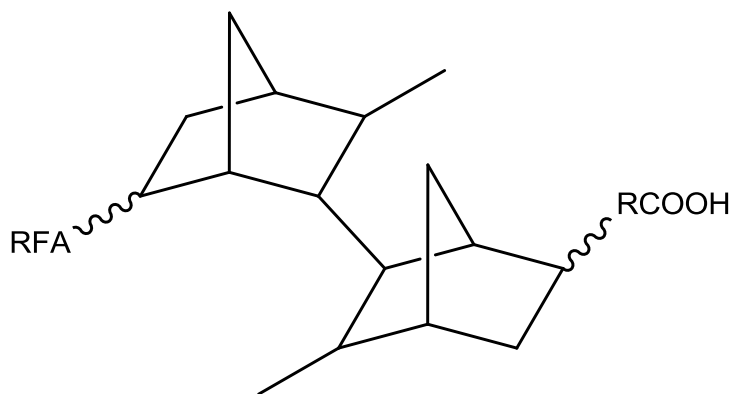
Figure 1.14 The chemical structure of Avatrel 8000P.

The epoxy-based cross-linking of the epoxy-functionalized PNB can be initiated by acid catalysis leading to a negative-tone, photodefinable dielectric material. This reaction has been studied for numerous epoxy systems [62-65]. The photoinitiated reaction is one which leads to the formation of a three dimensional cross-linked network [58, 66, 67]. During exposure to ultraviolet (UV) radiation or elevated temperature, the PAG decomposes to form a protic acid (HX) [68, 69]. The acidic proton (H+) reacts with

a lone pair of electrons on the epoxide oxygen, leading to epoxy ring opening and the formation of a hydroxyl group and a carbocation (C+). Cross-linking occurs when the carbocation reacts with either a pendant carboxylic acid group of a neighboring polymer chain to form a carboxylic ester linkage or with a second epoxy ring to form a polyether linkage. The cross-linking reaction between a PNB-based polymer and epoxy-based cross-linkers are shown in Figure 1.15.
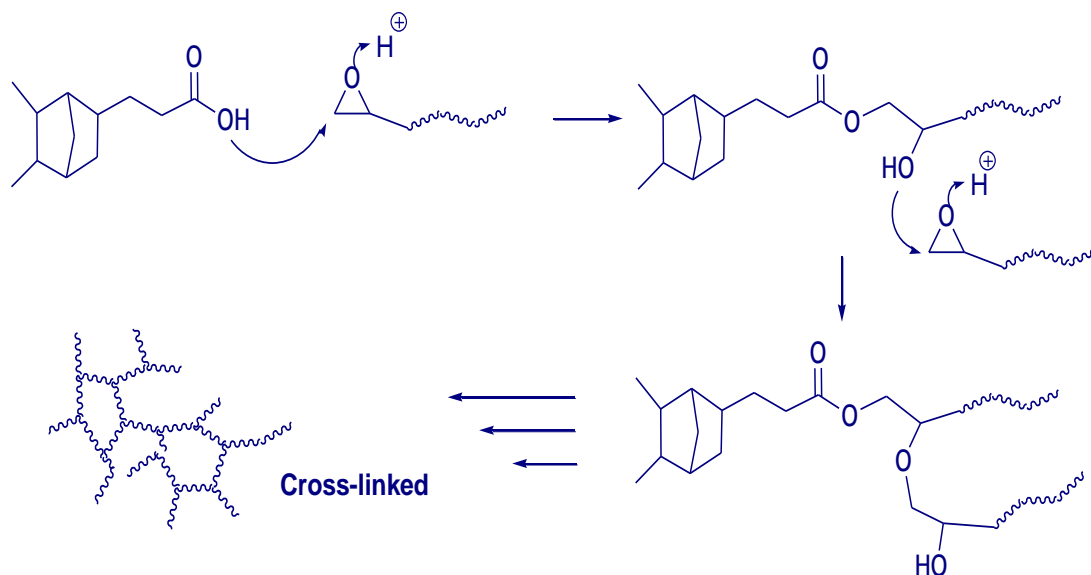
Figure 1.15 The cross-linking reaction between a PNB-based polymer and epoxy-based cross-linkers.

Previously, Rajarathinam et al. have shown that an epoxy cross-linked polynorbornene polymer formulation has straightforward processing parameters [53]. The polymer was characterized in terms of contrast and optical properties.[1] Their work showed that Avatrel 8000P can be exposed to UV radiation and can form high-aspect-ratio structures.   High contrast formulations (contrast = 12.2) were developed in aqueous-base. High-fidelity features with aspect ratios of 7:1, and vertical side-walls were fabricated in thick films. The PNB formulation with a high epoxy content exhibited

appealing mechanical strength and residual stress. The elastic modulus and hardness were reported as 2.9 GPa and 0.18 GPa, respectively, for the fully cross-linked films [53].

In this work, the ultraviolet and e-beam induced cross-linking of the epoxy-based PNB formulations were studied. The effect of epoxy-based cross-linking additives with different functionalities on the PNB cross-linking, photolithographic properties, and adhesion characteristics was also investigated.   Thermal and variable-frequency microwave cross-linking of the PNB were studied and their effect on the mechanical, electrical, and chemical properties of the polymer was evaluated. The properties of the PNB polymer formulations were characterized for various processing conditions, and the application of the PNB polymers for MEMS, microelectronics and photonics was investigated.

CHAPTER 2

EXPERIMENTAL TECHNIQUES

2.1 Materials

The materials used in this study are epoxy-functionalized PNB polymers. The PNB polymer (Avatrel 8000P), shown in Figure 1.14, was obtained from Promerus LLC (Brecksville, OH). The photosensitive PNB, Avatrel 8000P, is a mixture of the PNB polymer with a PAG, a UV absorbing sensitizer, multifunctional epoxy cross-linkers, and an adhesion promoter in propylene glycol monomethyl ether acetate (PGMEA). 4(methylphenyl)-4'-(1-methylethylphenyl) iodonium tetrakis (pentafluorophenyl) borate (Rhodorsil PI 2074), shown in Figure 2.1, was used as a PAG in this study, as described previously.[55, 58, 70] 1-chloro-4-propoxy-9*H*-thioxanthen-9-one (CPTX) was used as the UV absorbing sensitizer in the PNB formulations [55, 58]. The chemical structure of CPTX is shown in Figure 2.2.
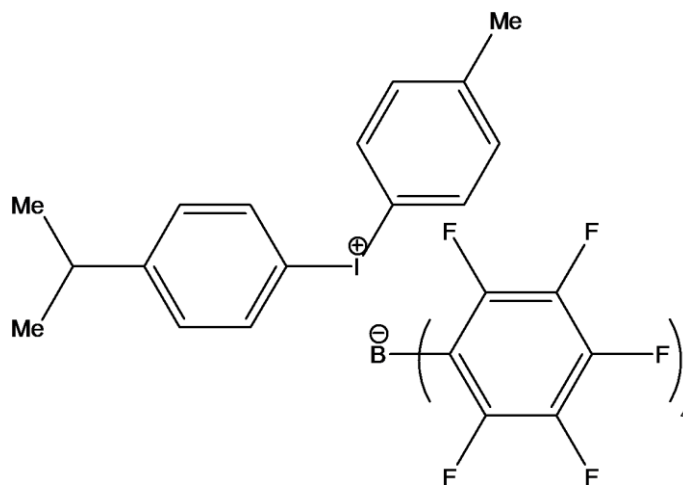
Figure 2.1 The chemical structure of Rhodorsil PI 2074.
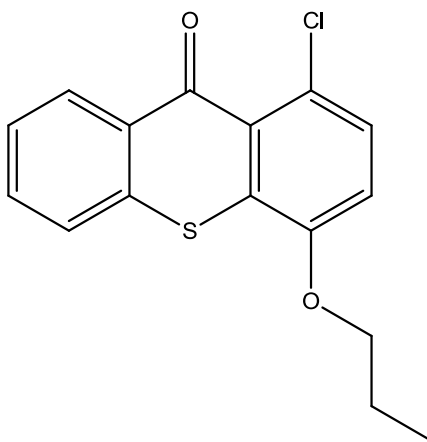
Figure 2.2 The chemical structure of 1-chloro-4-propoxy-9*H*-thioxanthen-9-one.

Avatrel 8000P is mixed with different ratios of two multifunctional epoxy cross-linkers: polypropylene glycol diglycidyl ether (Figure 2.3) and trimethylolpropane triglycidyl ether (Figure 2.4), which are readily soluble in PGMEA. Tetraphenylol ethane tetraglycidyl ether (TPEGE) was used as a tetra-functional epoxy cross-linker in this study and its chemical structure is shown in Figure 2.5. Triphenylol methane triglycidyl ether (3-EP) and bisphenol-F diglycidyl ether (2-EP) were used as additional tri-functioanl and di-functioanl epoxy cross-linkers and their chemical structures are shown in Figure 2.6 and 2.7, respectively. PGMEA, CPTX and all epoxy-based cross-linkers were purchased from Aldrich Chemical Co.Shipley MF-319 0.26N tetramethyl ammonium hydroxide (TMAH), purchased from MicroChem Co. was used as the developer for PNB formulations.
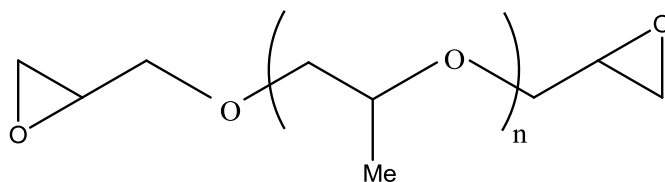
Figure 2.3 The chemical structure of polypropylene glycol diglycidyl ether.
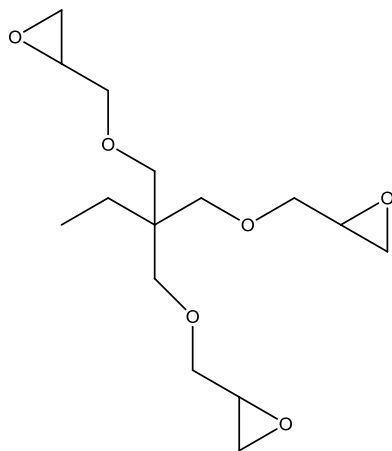
Figure 2.4 The chemical structure of trimethylolpropane triglycidyl ether.
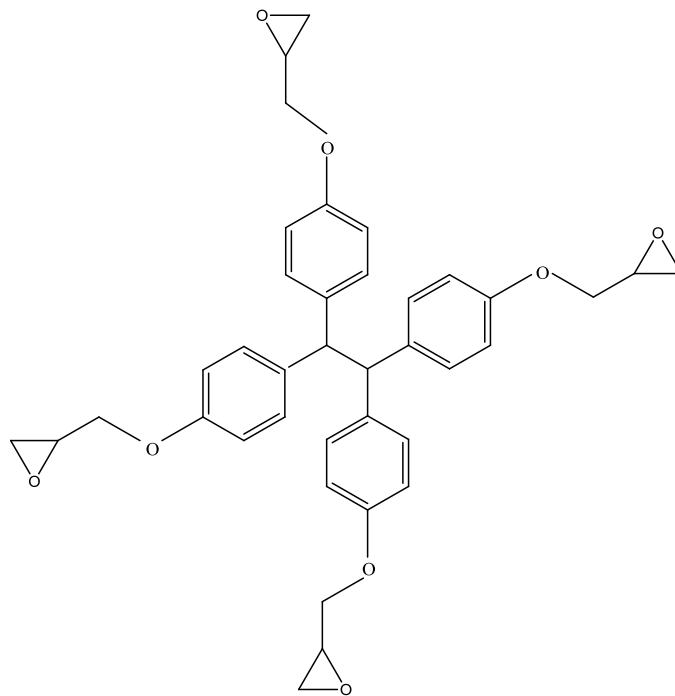
Figure 2.5 The chemical structure of TPEGE.
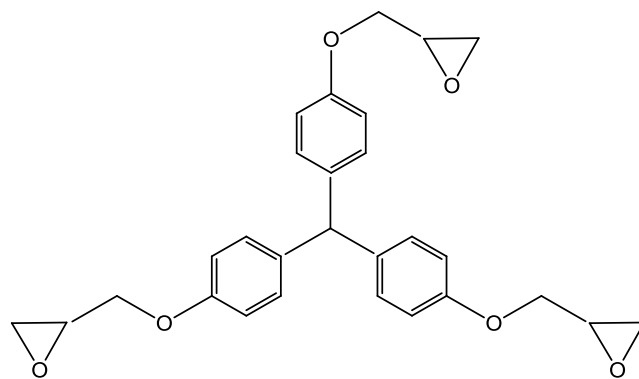
Figure 2.6 The chemical structure of 3-EP.
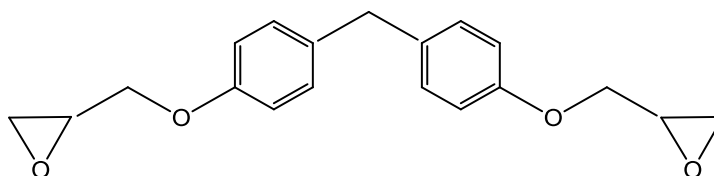
Figure 2.7 The chemical structure of 2-EP.

2.2 Polymer Film Preparation

For thick-film samples of Avatral 8000P, the polymers were spin-coated on

<100> silicon wafers using a CEE 100CB Spinner at 1000 rpm for 30 s producing ca. 40

μm thick films. The spin speed curve for Avatrel 8000P is shown in Figure 2.8.   The

films were soft-baked at 100°C for 10 min in an oven (air ambient) to remove residual

solvent. The effect of exposure dose was studied using a variable-density optical mask

(Opto-line International Inc.). Contact printing was used to evaluate the aspect-ratio of

the photodefined structures. UV exposures were performed using a Karl Suss MA-6

Mask Aligner with a 365-nm filter. The operating parameters for a Karl Suss MA-6

Mask Aligner are listed in Table 2.1. EBL was performed using a JEOl JBX-9300FS tool

at 100 kV acceleration voltage and 50 pA beam current. The operating parameters for a

34

JEOl JBX-9300FS is listed in Table 2.2. The samples were post-exposure baked in an oven at 100°C for 8 min. The thin-film samples (25 μm) were spin-coated on 100 mm diameter <100> silicon wafers using a CEE 100CB Spinner at 1500 rpm for 30 s. Polymers were soft-baked and hard-baked at the same conditions, which was 100°C for 5 min in an air ambient atmosphere oven. ALL polymer films were developed for 3 min at room temperature using the TMAH developer. After developing, the films were cured in either in a furnace or with a microwave system. Thermal cures were performed in a nitrogen-ambient furnace at the desired temperature. The temperature was ramped at 5°C/min and held at temperature for 1 hr. The furnace was allowed to cool slowly to ambient temperature by natural convection. The film thickness was measured after the PEB with a Veeco Detak profilometer.
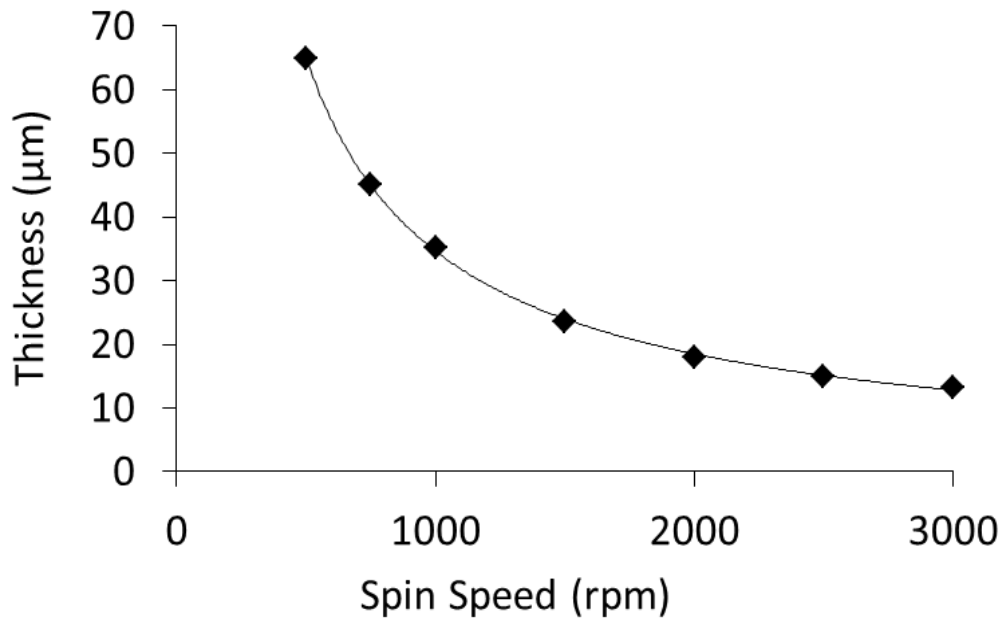
Figure 2.8 The spin speed curve for Avatrel 8000P.

Table 2.1 Karl Suss Ma6 mask aligner operating parameters. [71]

Maximum Substrate Size	6"
Maximum Mask Size	7"
Exposure Modes	Soft, Hard, Low Vacuum, Vacuum, Flood Exposure
Wavelength Range	UV400, UV300, UV200
Proximity	Exposure gap 1-300 μm
Resolution	Down to 0.4 μm
Intensity Uniformity	±5%

Table 2.2 JBX-9300SF E-beam lithography operating parameters. [72]

Maximum Wafer Size	12"
Maximum writing area	9"
E-beam Diameter	4 nm
Accelerating Voltage	50 kV/100kV
Current Range	50 pA-100 pA
Scan Speed	50 MHz

2.3 Chemical Properties

2.3.1 Fourier Transform Infrared Spectroscopy (FTIR)

FTIR spectroscopy was used to follow the epoxy ring-opening reactions using a Magna 560 spectrometer (Nicolet Instruments). Scans were collected in transmission mode on potassium bromide (KBr) substrates with 512 scans being averaged for each measurement at a resolution of 2.00 cm^{-1}. Samples were prepared by coating each KBr

plate at 1500 rpm for 30 sec producing ca. 25 μm thick films. Samples were soft-baked and post-exposure baked at 100˚C for 5 min. After exposure to UV light, the edge and back of KBr disk were covered by Parafilm to prevent film delamination and dissolution of the KBr disc in the TMAH developer. Samples were developed in TMAH developer for 3 min. To monitor conversion, the epoxy ring opening reaction was monitored by following the disappearance of the 844 cm^{-1} peak, associated with the oxirane ring C-O-C stretch.

In the study presented in Chapter 7, VFM curing of the PNB dielectric, films prepared for FTIR analysis were spun on 50 mm diameter, double side polished silicon wafers using a CEE 100CB Spinner at 1500 rpm for 30 sec resulting in ca. 30 μm thick films. Samples were soft-baked and post-exposure baked at 100°C for 5 minutes on a hotplate in air. UV exposures were performed at a dose of 450 mJ/cm^2 using a Karl Suss MA-6 Mask Aligner with a 365 nm filter. Polymer films were developed for 3 min using the TMAH developer.

2.3.2 Cross-Link Density

Swelling experiments were performed by soaking in PGMEA on the samples used for nanoindentation. The swelling of cured polymer films was evaluated by measuring the increased sample weight versus the exposure time in the PGMEA solvent. The measurements were taken using an Ohaus Voyager Pro balance with readability of 0.0001 g and linearity of $\pm$ 0.0002. The mass of each sample was measured at least 6 different times during the 24 h swelling period. The percent increase in weight was calculated using Equation (2.1). Each data point is the average of four measurements. The average of standard deviation was less than 0.0003.

$$S = \frac{W_t - W_0}{W_0} \qquad (2.1)$$

Where S is the swelling, and W_t is the weight of sample swollen with solvent at time t, and W_o is the sample weight in dry state [73, 74].

2.4 Mechanical Properties

2.4.1 Reduced Modulus and Hardness

To characterize mechanical properties of samples such as reduced modulus and hardness, nanoindentation was used as a depth sensing technique. Researchers have used this technique to characterize materials such as metallic alloys [75] and ceramics [76]. However, the nanoindentation of polymeric materials is challenging due to their viscoelastic and viscoplastic response [77], low hardness [78], and resulting strain-rate dependence of deformation [79]. In this work, quasi-static nanoindentation was performed on PNB samples using a Tribo indenter nano-indenter (Hysitron Inc. Minneapolis, MN) with a Berkovich tip. The hardness (H) was defined as the applied load per unit area of indentation, as given by Equation (2.2) [80].

$$H = \frac{P_{max}}{A(h_c)} \qquad (2.2)$$

Where P_{max} is the maximum load and the projected contact area, $A(h_c)$, for an indenter where the tip imperfection is defined by Equation (2.3).

$$A(h_c) = 24.5h_c{}^2 + \sum_{i=0}^{7} a_i h_c{}^{1/2^i} \qquad (2.3)$$

Where h_c was estimated for a geometrical constant (ε) by using the Oliver and Pharr model, Equation (2.4).

$$h_c = h_{max} - \varepsilon \frac{P_{max}}{S} \qquad (2.4)$$

Where S is the stiffness of the contact. The indenter was located on an anti-vibration table and enclosed in an acoustic housing. The peak load was varied between 250 μN and 6250 μN. The tip was loaded to maximum load within 10 sec, held for 10 sec, and unloaded in 2 sec. In order to minimize the impact of the substrate on the indentation results, the maximum force was chosen such that less than 5% of the total polymer film thickness, 25 μm, was indented [54]. Additionally, a 5×5 array of points was indented in the center of the samples to exclude edge effects. The maximum drift rate of the experiments was set at 0.1 nm/s over a period of 40 sec. The curvature of the Berkovich tip was between 250 nm and 970 nm. The Oliver-Pharr model was used to analyze the load-depth curves [53]. The reduced modulus was extracted from the 20% to 95% portion of the unloading curve [4]. To eliminate the impact of thermal drift, the first data points were discarded so that the average hardness and modulus only included indents above 500 nm.

Each nanoindentation data point shown in the results sections is the average of all measurements performed on all samples at each processing condition [54]. In each set of

experiments, multiple calibrations were performed to minimize drift in the calibration and ensure the precision of the data collected [81]. It is necessary to calibrate the tip with a standard having a modulus similar to the sample to obtain a valid area function over the indentation depths of the film [53]. Fused silica (quartz) is a commonly used standard because its elastic modulus does not change significantly with indentation depth and it does not have a surface oxide as metals.[81] However, it has been shown that it is necessary to calibrate the tip with a standard having a modulus similar to the sample to obtain an area function valid over the indentation depths of the sample [53]. In this work, a Hysitron polycarbonate calibration standard with a modulus of 3.1 GPa was used to calculate the area function.

2.4.2 Residual Stress

The residual film stress was measured at room temperature using a He—Ne laser-based Flexus Tencor stress analyzer (Model F2320) [82]. Residual stress levels for 25 μm thick films were determined by measuring changes in the curvature of <100> silicon wafers as a result of the deposition and subsequent curing of the polymer film. The residual stress, σ, was calculated using Stoney's equation, which relates the residual stress of a film to the change in the radius of curvature of the supporting substrate, Equation (2.5).

$$\sigma = \left(\frac{E}{1-v} \right) \frac{h^2}{6Rt} \qquad (2.5)$$

Where is E/(1-v) is the biaxial elastic modulus of the substrate (1.805 × 1011 Pa for <100>-oriented silicon), h is the substrate thickness, and t is the thickness of the film in meters. R is the reduced change in radius, given by Equation (2.6).

$$\frac{1}{R} = \frac{1}{R_2} - \frac{1}{R_1} \qquad (2.6)$$

Where R_1 is the radius of curvature of the uncoated substrate and R_2 is the radius of curvature of the substrate after film coating and processing. Stoney's equation represents the average biaxial stress acting within a film deposited on a substrate for film thickness less than 10% of the substrate thickness [83]. The polymer film thickness was measured after cure with a Veeco Detak profilometer.

2.5 Electrical Properties

Dielectric measurements were conducted by the fabrication of parallel-plate capacitors on <100> silicon wafers. The bottom plate of the capacitor was a full surface film of sputtered aluminum (400 nm thick) deposited on the silicon surface by DC sputtering. The polymer was spin-coated on the aluminum layer at 1000 rpm for 30 sec producing a ca. 10 μm thick film. The sample was soft-baked and post-exposure baked at 100°C for 5 min, and exposed at 450 mJ/cm². The edge of the sample was covered with Parafilm to prevent delamination during developing. The sample was developed in TMAH developer for 3 min, and then cured at the desired temperature. The top electrode consisted of 400 nm aluminum and was deposited on top of the polymer film with a DC sputterer. The aluminum was patterned with photoresist and wet etched to form the top plate of the parallel plate capacitor, Equation (2.7).

41

$$C = \varepsilon_r \varepsilon_o \left(\frac{A}{t}\right) \qquad (2.7)$$

Where C is the capacitance, ε_r is the relative dielectric constant, ε_0 is the permittivity of free space, A is the area, and t is the thickness of the dielectric. Conductance and capacitance were measured at 10 kHz using a Hewlett Packard 4236 LCR meter on a Karl Suss probe station. The ASTM correction, D 150, for fringing fields was performed, Equation (2.8) [84].

$$C_e = \left(0.0041\, \kappa_{\chi'} - 0.00334 \ln t + 0.0122\right)P \qquad (2.8)$$

Where $\kappa_{\chi'}$ is the approximate value of the dielectric constant and P is the perimeter of the top measuring electrode.

2.6 Thermal Properties

2.6.1 Thermogravimetric Analysis (TGA)

To track the weight loss of the polymer films during a thermal excursion a TA Instruments Q50 thermogravimetric analyzer was used. The samples were prepared for analysis by placing about 4 g of dry polymer in an aluminum TGA test pan. A nitrogen purged convective heating unit completely surrounds the test pan. The system was calibrated with an empty test pan and the experiments were performed in a dynamic mode. The temperature inside the sample chamber was increased at a rate of 5°C/min from 27°C to 500°C under nitrogen atmosphere. This technique is very sensitive to

subtle changes in the sample weight. The polymer weight loss is monitored as a function of time and temperature.

2.6.2 Differential Scanning Calorimetry (DSC)

The glass temperature of the polymer films was measured using a TA Instruments Q20 differential scanning calorimeter. This technique monitors the heat flux in a sample relative to an inert reference as the sample is heated. The difference in the heat flux between the sample and the reference is recorded as a function of time and temperature. The samples were prepared for analysis by placing about 4 g of dry polymer in an aluminum DSC test pan.   The DSC chamber was purged with nitrogen to reduce the oxygen content to less than 50 ppm after the sample was placed in the DSC chamber on the sample heater. This technique was only used for fully cured samples to avoid pressure built up in the chamber and melting the aluminum test pan at high temperatures due to the cross-linking reactions and solvent evaporation.

2.7 Patternability

Scanning electron micrographs (SEM) were obtained using a Zeiss Ultra 60 to observe the morphology of patterns in polymer films. For SEM imaging, polymer films were coated with titanium metal to prevent charging and increase the conductivity of the polymer sample using EFFA Sputter Coater at 25 watts. The thickness of the titanium was around 60 nm, which will not affect the surface morphology. The wafers were cut into small pieces using a diamond scribe. For side-profile observation, the wafer was cut at the center of the pattern to avoid geometry effects. The sample pieces were then mounted on a sample holder using silver adhesive.

CHAPTER 3

PHOTO-CROSS-LINKING OF POLYNORBORNENE DIELECTRIC

Numerous photosensitive and non-photosensitive polymers have been developed for MEMS and microelectronics applications [55, 58, 77, 85-89]. Furthermore, several studies of photodefinable, high-aspect-ratio materials have recently been reported [53, 55, 90-92]. Among the most desirable attributes for photosensitive polymers is the ability to achieve high-aspect-ratio (depth-to-width) structures with excellent adhesion and high sensitivity. In this work, the effect of different epoxy-based cross-linkers on the physical and photochemical properties of the PNB-based dielectric, Avatrel 8000P, was investigated, in an effort to enhance the resolution, aspect ratio, adhesion, and photo-speed. The base polymer formulation used in this study was the same as that of Rajarathinam et al., and the results were compared with the results reported previously [53].

3.1 Experimental

The epoxy-based cross-linkers used in this study are TPEGE, polypropylene glycol diglycidyl ether, and trimethylolpropane triglycidyl ether, which will be identified as I, II and III, respectively, hereafter. The base polymer used in Avatrel 8000P, shown in Figure 1.14 was used as the base polymer formulation used in this study. The PNB polymer was mixed with different ratios of II and III to form a base polymer formulation (BF) which replicates the formulation of Rajarathinam et al [53]. A summary of the formulations made with compounds I, II, and III are listed in Table 3.1. X is defined as the mole fraction of epoxy moieties in each formulation, where X=1 in the case of BF, as was used previously [53]. In the base formulation, the value of X for compounds II, III,

44

and adhesion promoter are 0.86, 0.09, and 0.05, respectively. The epoxy cross-linkers
were dissolved in PGMEA and ball-milled with the PNB resin for 72 h.

Table 3.1 PNB polymer formulations.

Polymer Formulation	X	Title
Base polymer	1	BF
BF with 1 wt% supplementary I	1.07	A
BF with supplementary II, III, and CPTX	1.07	B
BF with supplementary II	1.07	C
BF with supplementary III	1.07	D
BF with supplementary II and CPTX	1.07	E
BF with supplementary III and CPTX	1.07	F

A 1 wt% solution of 3-aminopropytriethoxy silane (3-APS) in ethanol (90%
ethanol) was applied on the substrate surface in all experiments to enhance the film-to-
substrate adhesion. The solution was spin-coated at 300 RPM for 10 sec followed by a
higher-speed spin at 1500 RPM for 20 s. To remove excess ethanol, the samples were
baked at 130°C for 15 min on a hotplate. A 15 s ethanol rinse was performed to remove
excess materials. All films were cured in a nitrogen-purged furnace at 225°C for 1 h after
developing.

High-aspect ratio structures were fabricated on metalized silicon wafers
composed of sputtered Ti/Cu/Ti (300Å, 3000Å, 300Å). The metal was deposited on
silicon wafers with a Unifilm sputterer. SiO_2 (1.5 μm thick) was deposited on the final
titanium layer using a Unaxis PECVD to improve the film-to-substrate interface. The

epoxy polymers formulations were also spin-coated using the same procedure as described earlier. After the samples were developed, the samples underwent a descum step using a Plasma-Therm-RIE. The final polymer thickness was 38 to 40 μm. The SiO_2 and top surface of titanium were etched using buffered oxide etch (BOE) for 7 min. The exposed copper surface was then suitable for electroplating copper metal in the regions where the polymer was developed away. An acid copper sulfate plating bath was used. The copper electroplating bath contained 120 g of copper sulfate ($CuSO_4.5H_2O$) and 139 ml of sulfuric acid in 1500 ml of deionized water. The bath also contained 0.189 g of hydrochloric acid to reduce anode polarization and eliminate striated deposits and 1.134 g of polyethylene glycol (PEG) as a carrier, lever, and brightener. The current density was 10 to 15 mA/cm^2 yielding a plating rate of 20 μm/h.

3.2   Results and Discussion

The behavior of the three epoxy cross-linkers, I, II, and III, were studied and their effect on the physical and photochemical properties of the base polymer formulation was investigated. The photosensitivity and contrast of the BF was first evaluated. Generally, high contrast is needed to make vertical-walled, high-aspect-ratio features. High contrast is achieved when an incremental increase in cross-linking leads to insolubility of the polymer film [13]. High contrast can lead to high aspect-ratio, vertical-walled structures, if adhesion of the resist to the substrate can be maintained during development of the latent image. To evaluate the impact of compound I on the sensitivity, contrast, and aspect ratio of BF, the contrast of formulation A (Table 3.1) was compared to the contrast of BF. The mole fraction of epoxy moieties in formulation A was increased to X=1.07, compared to the normalized value of X=1.00 for the base formulation, by addition of 1 wt% of epoxy compound I. That is, 1 wt% of compound I (weight percent solids in the formulated solution) corresponds to 7 mole% of total epoxy in BF, making X=1.07 for the final solution. Front-side, normal incident exposure was conducted and the contrast

46

curves are shown in Figure 3.1. The resulting 25-µm tall structures using formulation A and BF are shown in Figure 3.2. Structures patterned with formulation A had higher contrast, vertical side-walls, and same line and spacing.
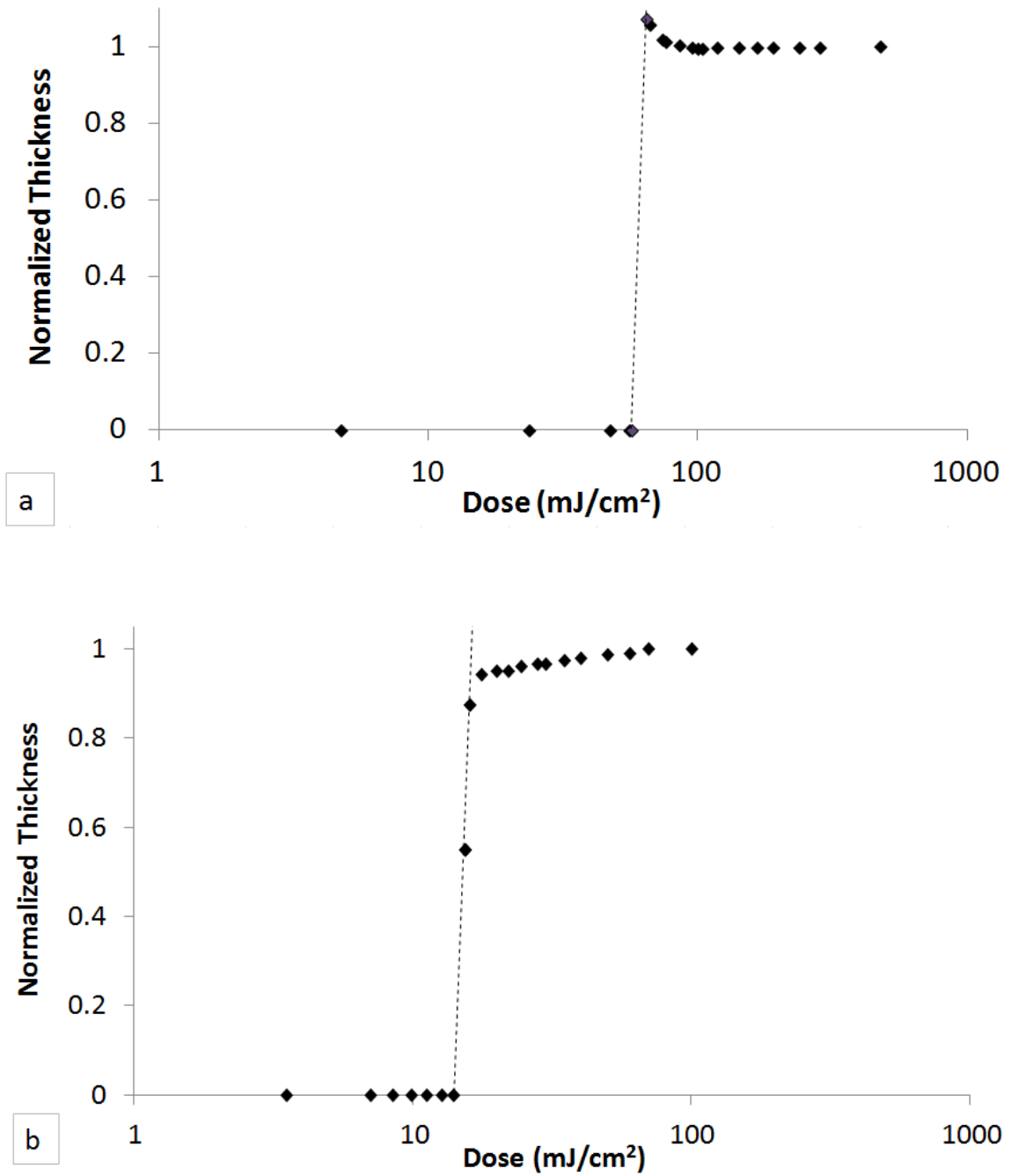
Figure 3.1 (a) Contrast curve for Avatrel 8000P (b) Contrast curve for Avatrel 8000P with supplementary I. The dashed line shows the slope used to obtain the contrast.

47
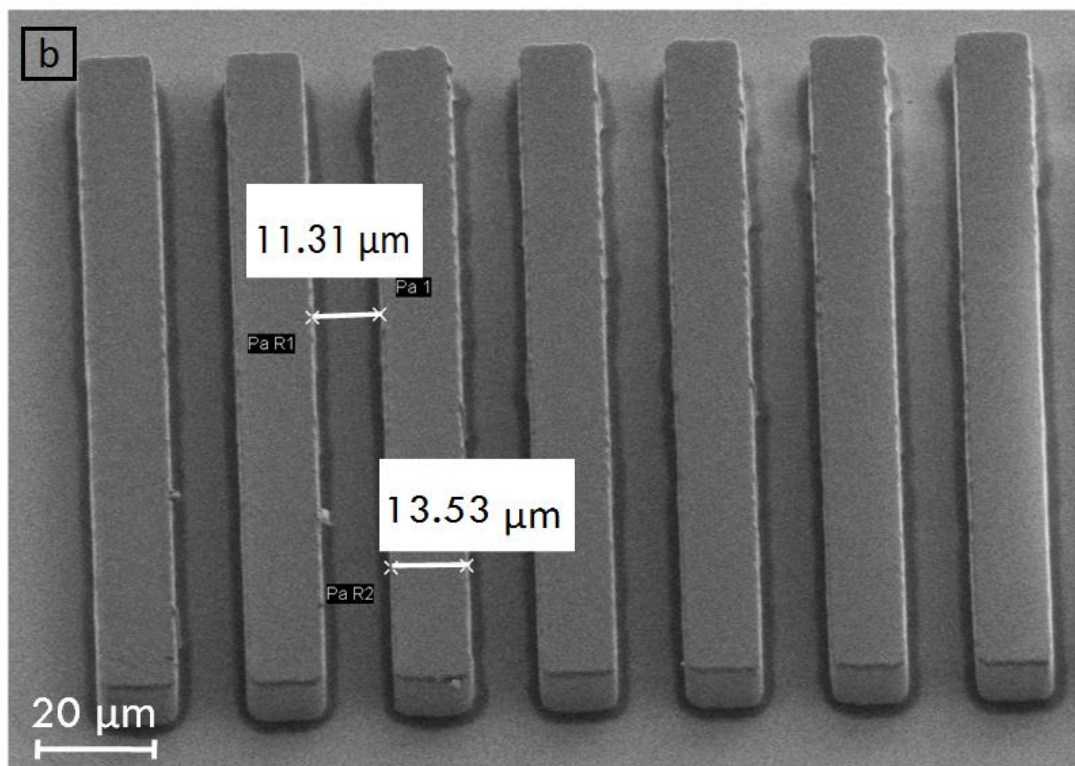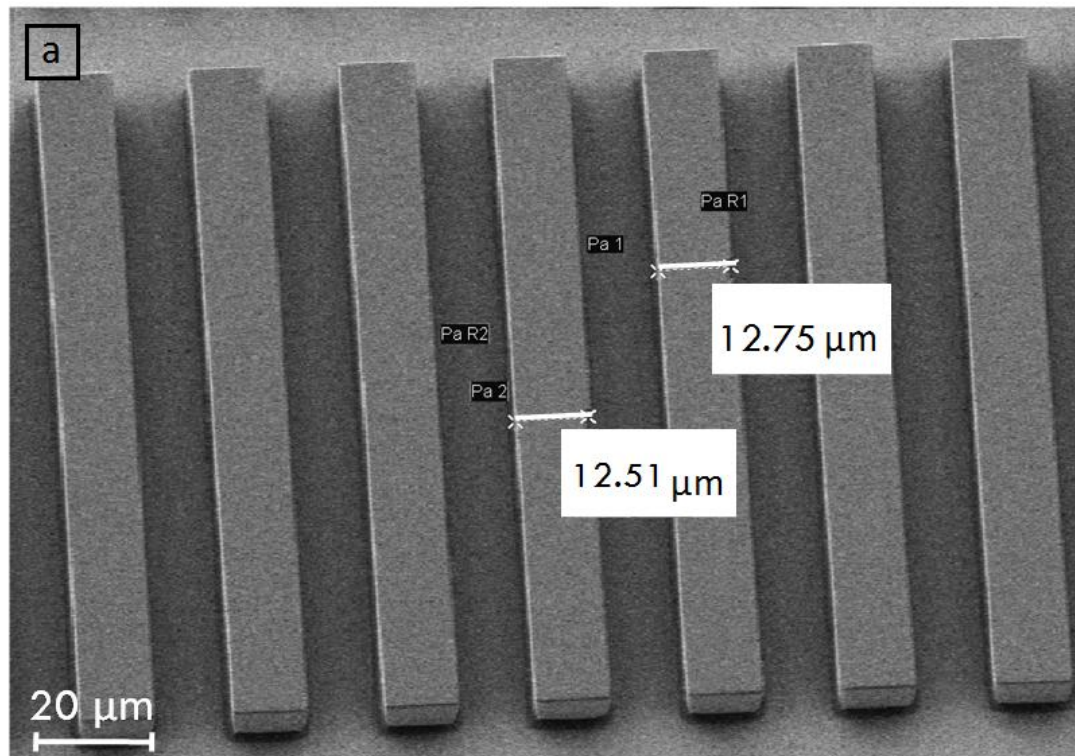
Figure 3.2 SEM image of (a) formulation A; (b) Avatrel 8000P photopatterned with an exposure dose of 400 mJ/cm^2.

The contrast values were calculated from the slope of the line in the contrast curve where there is a transition from essentially full development (film removal) to no development (full or partial film remaining). Using the slope of the line in the contrast curve, and interpolation of the values of D_0 and D_{100}, avoids possible errors in having to pick a single value for D_0 and D_{100}. Formulation A yielded a contrast of 24.2, which is exceptionally high, even compared to that for BF ($\gamma=7.4$). This 3.3 fold improvement in contrast compared to that for BF, was solely due to the 1 wt% addition of the tetra-functional epoxy. As can be discerned from Fig. 3.1B, the contrast value obtained for formulation A is an accurate value as a result of multiple data points defining the slope of the contract curve between D_0 and D_{100}. It should be noted that the contrast value for BF, Fig. 3.1A, is a minimum contrast value due to the fact that only D_0 and D_{100} were observed. Thus, the true slope is at least as great as the value obtained by connecting D_0 and D_{100}.

In the case of BF, the value of D_{100} is at a thickness value greater than one and the resulting contrast is somewhat misleading because the films exposed at doses near D_{100} suffered from poor adhesion to the substrate. The value of thickness was greater than one in Fig. 3.1A because the film delaminated from the surface at the edge of the exposed region. Rajarathinam showed that epoxy activation at the polymer-to-substrate interface is critical for adhesion [53]. In front-side, normal incident exposures, the UV intensity at the surface of the film is high. However, the optical intensity at the polymer-substrate interface is attenuated by UV absorption within the film resulting in a lower exposure dose at depths within the film. Rajarathinam showed this by comparing front-side and back-side exposures [53]. If the top surface is exposed to doses at or near D_{100}, then the exposure dose at the polymer-substrate interface will be below D_{100}, especially for thick-film samples.

The absorption of UV radiation results in activation of the PAG and creation of an acid which initiates epoxy ring opening and polymer cross-linking. The lower exposure

dose at the polymer-substrate interface results in fewer epoxy units being activated at the wafer surface and can lead to poor adhesion and delamination. The addition of compound I to the BF, as in formulation A, increases the optical density (OD) of the film at 365 nm. The OD of the incident UV radiation for formulation A at the polymer-substrate interface was less than that of BF, due to the increased absorption of compound I within the film. Thus, the superior adhesion of formulation A must be due to the presence of the tetra-functional epoxy, compound I, (within the film and at the polymer-substrate interface) and its higher efficacy for producing adhesion, compared to the other epoxy compounds used in BF.

The addition of the tetra-functional epoxy, compound I, affected the solubility of the unexposed film in the aqueous-base developer. The developing time for formulation A was 4.50 minutes compared to 3.00 minutes for BF. The increased adhesion and longer developing time with formulation A could have been due to fractional epoxy ring opening after spin-coating and baking (SB and PEB). This was investigated in unexposed samples using FTIR spectroscopy. The FTIR peak corresponding to the epoxy rings (844 cm^{-1}) showed a 12% decrease after PEB (with no exposure) compared to the same film after spin coating (no exposure or baking steps) showing that some the epoxide rings had reacted resulting in some degree of cross-linking in the unexposed regions after the 100°C bake. Epoxy ring opening can occur during thermal treatments or can be acid activated, if some of the PAG was thermally activated. It was also noted that the less swelling occurred in the exposed regions of formulation A, compared to BF, which will be discussed in more detail later in the paper when swelling is discussed. Enhanced epoxy ring opening and polymer cross-linking was also seen, as shown later in the FTIR data.

The sensitivity or photospeed of the polymer is a critical attribute of each formulation. The absorption of ultraviolet radiation within the polymer film results in activation of the PAG producing an acid within the polymer film. The photogenerated

acid catalyzes epoxy ring opening reaction, which leads to polynorbornene cross-linking. The absorption of UV radiation can be increased by adding a sensitizer to the polymer formulation, as was done with BF. Energy transfer occurs between the sensitizer and the PAG, creating the acid catalyst. However, the sensitizer does not participate in polymer cross-linking and remains in the polymer film as a low molecular weight additive. The D_{100} value, obtained from the contrast curves, was improved from 66 mJ/cm^2 for BF to 18 mJ/cm^2 for formulation A. Thus, UV radiation is significantly more effective at activating the PAG and initiating cross-linking after PEB, when the tetra-functional epoxy, I, is present.

To evaluate the impact of compound I on the polymer sensitivity at 365 nm, a series of UV absorption experiments were conducted. The absorbance of PGMEA, BF, and dilute solutions of I, II, and III in PGMEA were measured in the ultraviolet and visible regions. PGMEA, II, and III had very low absorbance at wavelengths from 300 nm to 400 nm. Compound I was found to have high molar absorptivity in the UV. The absorptivity of compound I in PGMEA was compared to the absorptivity of a dilute solution of the sensitizer used in BF, CPTX, in PGMEA, as shown in Figure 3.3. The molar absorbance of I and CPTX are 172,287 L.mol^{-1}.m^{-1} and 395,779 L.mol^{-1}.m^{-1}, respectively.
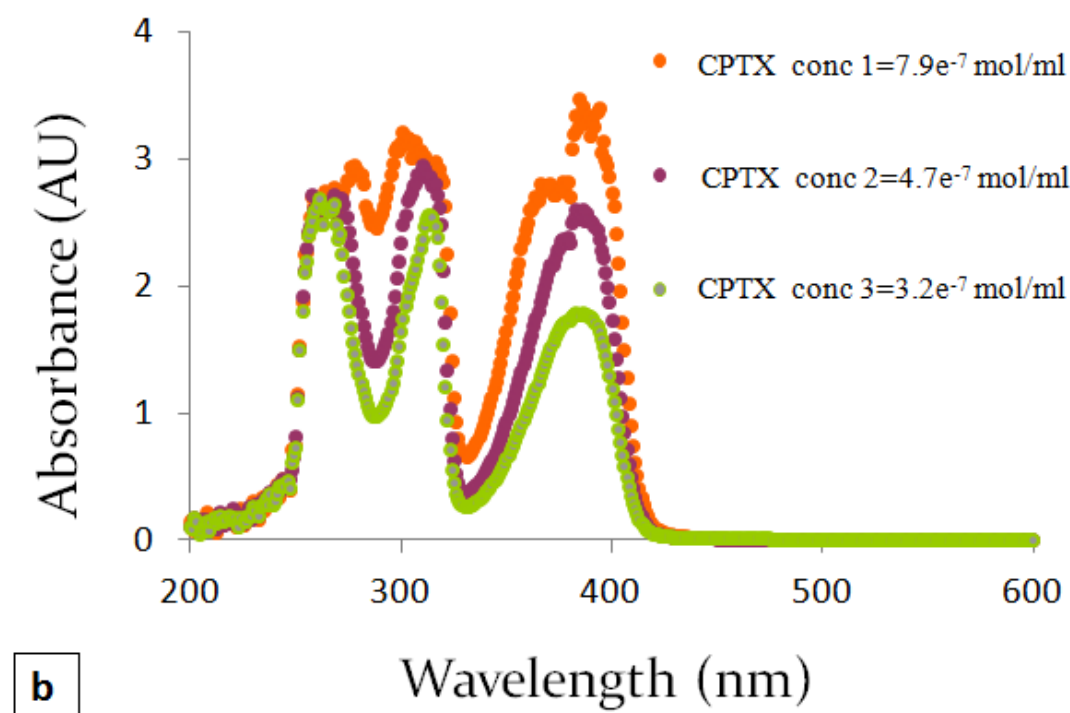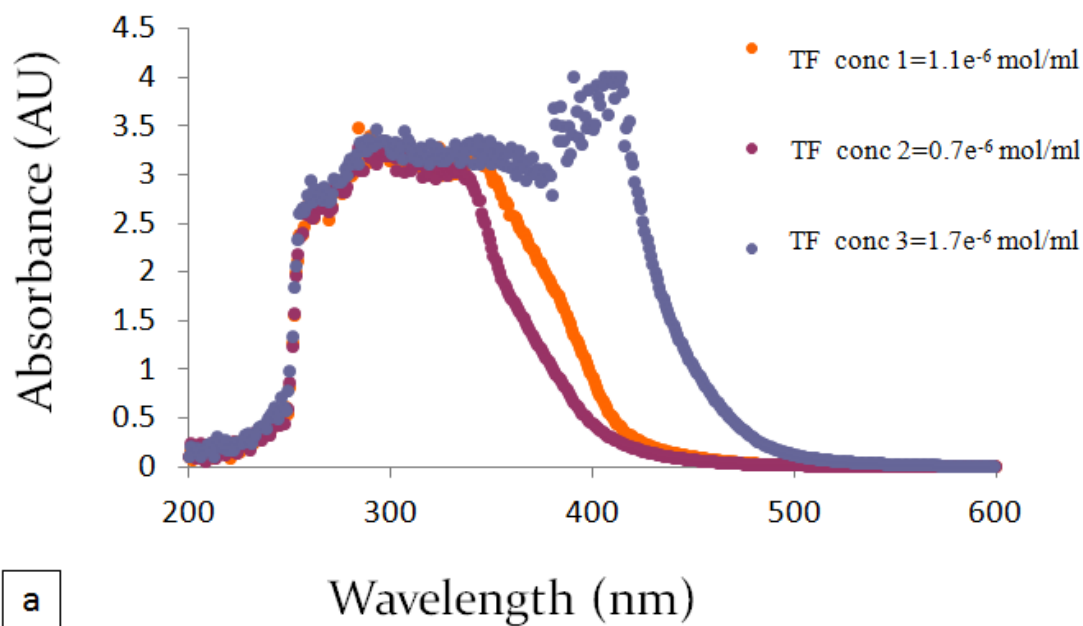
Figure 3.3 Changes in UV-vis spectrum of dilute solution of I in PGMEA from 200 nm to 600 nm (b) Changes in UV-vis spectrum of dilute solution of CPTX in PGMEA from 200 nm to 600 nm.

The higher absorbance of formulation A, compared to BF, by itself does not account for the improved adhesion and sensitivity of the tetra-functional epoxy. In the case of a partially cross-linked polymer, a higher degree of functionality within the cross-linker will lead to a higher degree of cross-linking in the polymer film. That is, the overall cross-link density using compound I, will be higher than that of compound II or III, for a given mole fraction of epoxy moieties, when the films are partially cured (same degree of curing) because compound I has a higher degree of functionality. Thus, the higher cross-link density of the tetra-functional epoxy is an asset when the film is partially cross-linked, as in the case of soft baked or post exposure baked films. This point will be revisited in greater detail later in the paper.

These results show that the increase in the sensitivity of formulation A, compared to BF, is at least partly due to the higher absorbance of compound I at 365 nm, and subsequent activation of the PAG and creation of the acid catalyst, compared to the other epoxy compounds. To compare the effect of simply adding more epoxy to BF, polymer formulations containing an identical quantity of epoxy moieties, using II and III, were studied. Formulation B was prepared so as to contain the exact number of equivalents of epoxy as formulation A. Since compound I has a higher molar absorptivity than compounds II or III, CPTX was added to formulation B so the new mixture had the same absorbance at 365 nm as A. Thus, B had the same mole ratio of epoxy as A and identical absorbance at 365 nm due to the additional CPTX. As shown in Figure 3.4, the sensitivity of B was evaluated by measuring D_{100}, which was 18 mJ/cm^2, essentially the same as formulation A. Thus, the improved sensitivity of formulation A, compared to BF, was due to the higher OD of the tetra-functional epoxy, and subsequent energy transfer with the PAG creating the acid catalyst. The relative efficiency for energy transfer between compound I and PAG vs CPTX and PAG could have been different but was beyond the scope of this study.
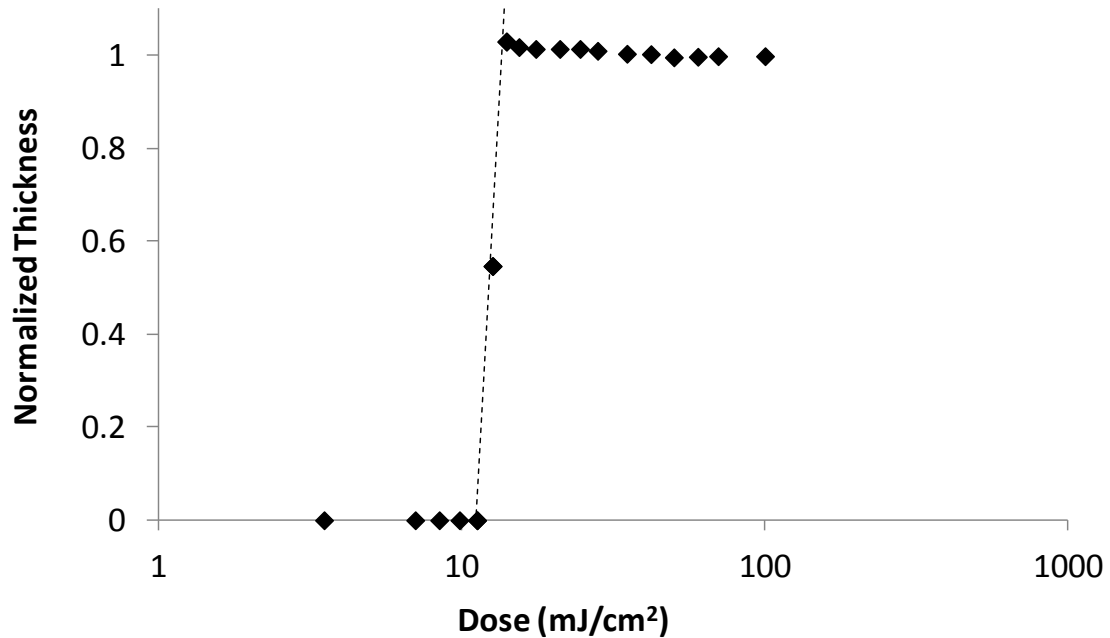
Figure 3.4. (a) Contrast curve for Avatrel 8000P (b) Contrast curve for Avatrel 8000P
with supplemented CPTX, II and III.

The contrast for formulation B was measured to be γ=9.96, which is higher than

BF, due to the added epoxy and CPTX, however, it is lower than that of formulation A,

γ=24.2. This result is congruent with the previous observation that the higher contrast

obtained with formulation A is not simply due to a higher epoxy content or higher

absorbance of the tetra-functional epoxy. The addition of compound I did provide greater

surface adhesion and swelling resistance in the cross-linked regions of the film. The

improved adhesion is critical to extending the developing time and allowing full

development of the features, especially at exposure doses at or just greater than D_{100}. For

example, the developing time needed for formulation A was 4.50 min, compared to 3.33

min for formulation B, and 3.00 min for BF. The longer develop time for formulation B,

compared to BF, is attributed to a modest degree of cross-linking from the addition of II

and III. Also, it improves the adhesion at the film-to-substrate interface in the exposed

regions. The poor adhesion at doses just above D_{100} was visually observed in the films

and is reflected in Figures 3.1 A and 3.4. In Fig. 3.4, the thickness values greater than

100% thickness at doses just above D_{100} correspond to delaminated films. The poor adhesion at D_{100} observed with the BF formulation was slightly improved in formulation B by addition of epoxy compounds II and III.

The ability to make high aspect ratio features is a function of the contrast, adhesion characteristics, and sensitivity of a photodefinable material. Since the addition of 1 wt% of compound I had a significant effect on these parameters in formulation A, the ability to form high-aspect-ratio features was investigated. Hollow-core structures, Figure 3.5, were chosen for this work since they are the difficult to fabricate because the transport of developer into the core of the structure is restricted, compared to the transport of developer to the outside of the structure. Films were spin-coated at 1000 rpm and photopatterned at an exposure dose of 200 mJ/cm^2 at 365 nm resulting in 38.7 μm tall, hollow-core, triangular shaped structures. Dissolving the unexposed polymer from the region at the center of the structure before delamination occurred at the outside edge of the polymer structure is a critical test of adhesion. To confirm complete development of the center core region, copper was electroplated in the hollow core portions of the film after a 2 min plasma (RIE) descum. If the polymer was not fully developed from the center core, electroplating would not occur. Hollow-core features, 38.7 μm thick with 3 μm diameter (length of a side) opening, were fabricated using formulation A, as shown in Figure 3.6. The resulting aspect ratio was 13:1.
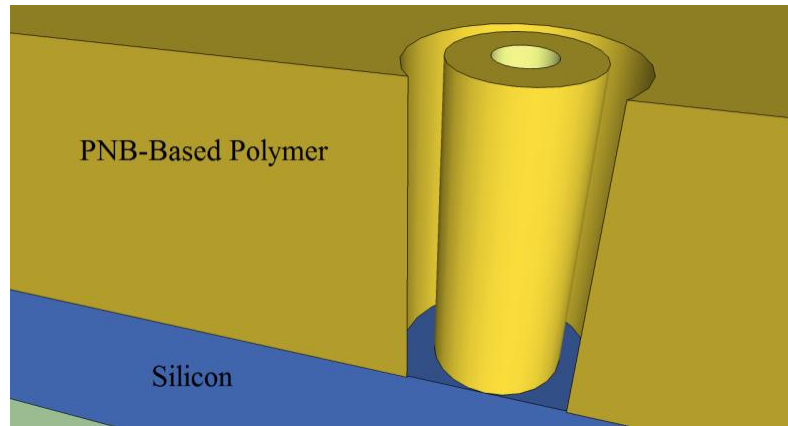
Figure 3.5 High -aspect- ratio annular structure with hollow center.
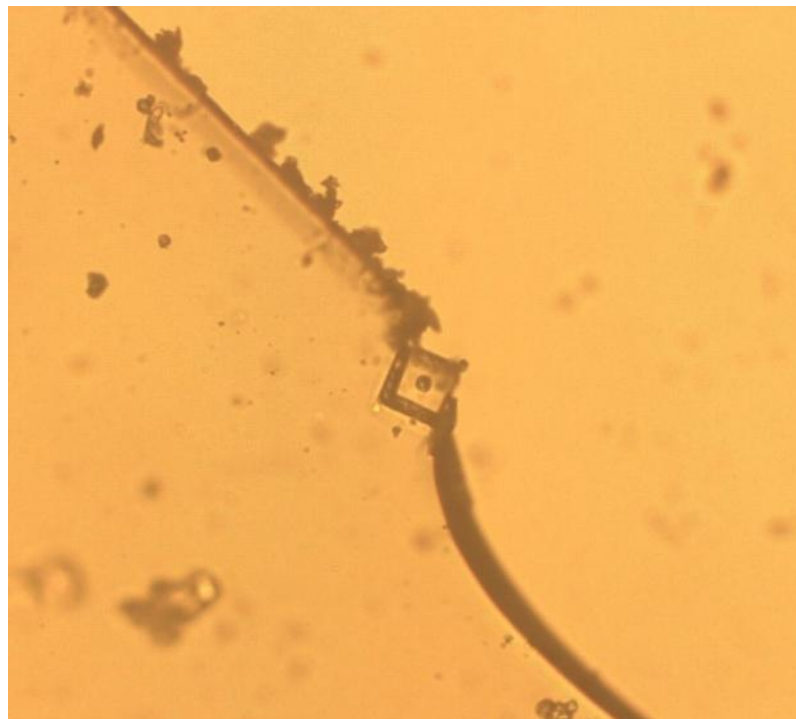
Figure 3.6 Microscopic image of a 13:1 (height:width) hollow-core
structure photopatterned with Avatrel 8000P with supplementray I.

The center core of the structures was fully developed since copper electroplating
was observed in the center region after development. The electroplated copper filled the
center region of the cavity. The polymer shell around the copper was removed and the
sidewall of the copper features was examined. The sidewalls were relatively straight-

walled in comparison with the results reported previously by Rajarathinam et al [53]. For comparison, 13:1 aspect-ratio structures were formed with BF at a higher exposure dose of 400 mJ/cm^2 and 11:1 aspect-ratio hollow structures were made with formulation B at an exposure dose of 200 mJ/cm^2. The same process as above was performed, however incomplete developing occurred in the cavities of both BF and formulation B, as shown by a lack of copper plating. In both cases, longer developing time was needed to fully develop the center core, which led to film delamination and lifting due to the lack of film-to-substrate adhesion. Thus, only formulation A had sufficient adhesion and contrast to produce features with aspect ratio greater than 13:1. It can be concluded that 1 wt% of compound I improved the contrast, sensitivity, and film-to-substrate adhesion of formulation A and led to higher aspect-ratio features with straight side-walls and high fidelity. The properties investigated for BF, formulation A, and formulation B are summarized in Table 3.2.

Table 3.2 Properties of PNB formulations.

Polymer Formulation	Sensitivity (D_{100}, mJ/cm^2)	Contrast (γ)	DT (min)	Aspect Ratio
BF	66	7.37	3	5:1
A	18	24.2	4.5	13:1
B	66	9.96	3.3	5:1

The reduced modulus and hardness of BF and formulations A and B were compared using nanoindentation. All samples were tested after a 225°C cure for 1h. Formulations A, BF, and B had a reduced modulus of 2.80 GPa, 2.82 GPa, and 2.83 GPa,

respectively. The hardness values for A, BF, and B were 0.17 GPa, 0.16 GPa, 0.18 GPa, respectively. This shows that no significant change in mechanical properties occurred due to the additional epoxy-based cross-linkers in formulations A and B.

The extent of cross-linking can play an important role in the properties of the polymer [93, 94]. To evaluate the effect of compounds I, II, and III on the cross-link density of the cured polymer, the average molecular weight between cross-links (M_c) and effect of cross-link functionality (f_c) were calculated and compared assuming fully reacted and cross-linked films. In addition, two formulations were made to experimentally compare the effect of cross-linking (Table 3.1). In one case, formulation C, compound II was added to BF to provide an equivalent number of epoxide groups as in formulation A. In the second case, formulation D, compound III was added so that the total molar epoxy content was the same as formulation A. The values of M_c and f_c were calculated using Equations (3.1) and (3.2), which assumes that all the epoxy moieties have reacted, and each has resulted in backbone cross-linking.

$$M_c = \frac{2(M_e + \sum_{f=2}^{\infty} \frac{M_f}{f} \Phi_f)}{\sum_{f=3}^{\infty} \Phi_f} \qquad (3.1)$$

$$f_c = \frac{\sum_{f=3}^{\infty} \Phi_f}{\sum_{f=3}^{\infty} (\frac{\Phi_f}{f})} \qquad (3.2)$$

Where M_e is the epoxide equivalent weight of the resin, f is the functionality of the cross-linker, M_f is the molecular weight of the f-th functional cross-linker, and Φ_f is the mole fraction of epoxy moles provided by the f-th functional cross-linker [95, 96]. With full conversion of the cross-linkers, M_c and f_c were calculated. The calculated network parameters are summarized in Table 3.3. In the work of Crawford et al. [95], full

conversion was achieved. That is, the calculation assumes that all polymer sites were reacted with epoxy groups, and no cross-linking occurred between epoxy groups.

Table 3.3 Network properties.

Polymer Formulation	$\bar{M}_c$ (gr/mol)	f_c
BF	446	3
A	449	3
C	491	3
D	441	3

The results show that there is little difference between the M_c and f_c values for the various formulations. This implies that compounds I, II, III could each result in nearly the same cross-link density. This result is consistent with the mechanical property measurements shown above where the properties for the formulations with compounds I, II, III are essentially identical. As shown in Table 3.2, the model predicts a similar average molecular weight between cross-links for BF, and the other formulations with slightly higher epoxy content. In the films this occurs because there are enough sites on the polymer backbone for complete cross-linking for all the epoxy units in each formulation. Thus, the addition of a small amount of epoxy does not change M_c by very much. This will be confirmed in the next section where it is shown that the solvent swelling within the polymer is a function of the mole fraction of epoxy only, and not the functionality of the epoxy different epoxy additives. The M_c value obtained for formulation C is slightly higher than the other formulations due to the higher molecular weight per epoxy moiety for compound II compared to compounds I and III. The same

M_c value would be obtained for all formulations with the same mole fraction of epoxy, if the molecular weight per epoxy functionality for the different cross-linkers was identical.

Swelling experiments were performed to investigate the actual degree of cross-linking. A larger value of M_c (lower degree of cross-linking) will result in greater solvent swelling [94]. Swelling tests were performed in PGMEA. Formulations were made so that the molar content of epoxide and OD were constant for the different experiments. The optical absorbance of epoxies II and III was less than that of compound I. Thus, CPTX was added to formulations with II and III so that the formulations had the same OD. Formulations E and F, Table 3.1, have the same molar quantities of epoxy and OD as formulation A. The swellings of BF, A, E, and F were measured after the PEB and the final cure. Figure 3.7 shows an increase in weight with swelling time for the cured samples.
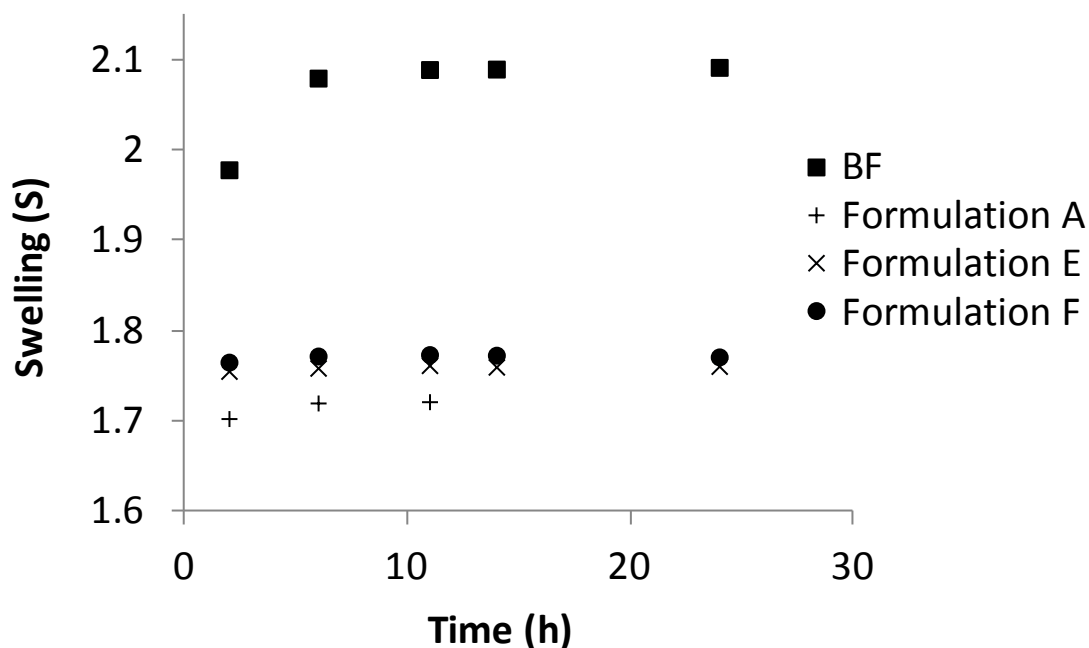
Figure 3.7 Influence of di-functional, tri-functional and tetra-functional cross-linker on swelling of fully cross-linked cured polymer.

No significant difference was found between the various formulations when the epoxy content was identical. This agrees with the calculation of M_c for the different formulations. That is, each epoxy compound resulted in a similar degree of cross-linking. The degree of swelling was greater for BF because it has a slightly lower molar epoxy content than the other formulations. In the model calculations above, it was assumed that all the polymer reaction sites were fully reacted through an epoxy reaction with the cross-linkers. However, there is an excess of reactive sites on the polymer so that after reaction with the epoxy, unreacted sites will remain on the polymer. The addition of a cross-linker to the polymer increases the degree of cross-linking between the epoxy and the polymer reaction sites, regardless of the functionality of the cross-linker.

The swelling tests were replicated after PEB, as shown in Figure 3.8. As in Fig. 3.7, there was no swelling dependence on cross-linker functionality. However, a high degree of film lifting and delamination occurred across the film for formulation F. A lower degree of delamination around the corners of the film was observed for formulation E. Due to the adhesion improvement with compound I, no delamination of formulation A was observed anywhere on the silicon surface. The diversity in the degree of delamination observed for compounds I, II, and III shows the complex nature of adhesion caused by the epoxy reaction for PNB and epoxy cross-linkers.
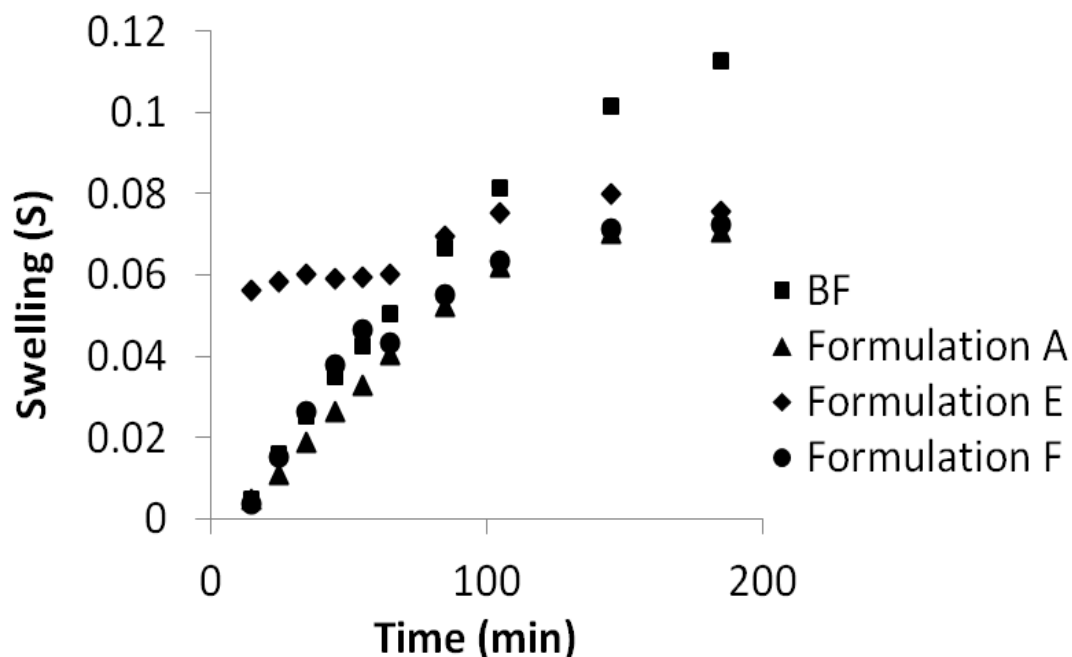
Figure 3.8 Influence of di-functional, tri-functional and tetra-functional cross-linker on swelling of cross-linked baked polymer.

To study the reactivity of the cross-linkers, the degree of epoxy ring opening for formulations BF, A, and E after PEB was investigated using FTIR spectroscopy. All formulations show epoxy ring-opening after PEB suggesting that some cross-linking has occurred. The IR spectra for the thin-film BF from 700 cm^{-1} to 950 cm^{-1} are shown in Figure 3.9. The FTIR peak corresponding to epoxy was not observed after curing at 225°C in all cases showing that the epoxide rings had reacted resulting in adequate adhesion after curing for all formulations. The exact nature of the improved adhesion for compound I, beyond its higher epoxy functionality and absorbance, was not investigated and may be the subject of future publication. Even though the cross-linkers show the same degree of swelling resulting in the same cross-link density, they result in a significantly different degree of adhesion. These observations confirm the results obtained from previous experiments; excellent film-substrate adhesion can be obtained by the addition of small amount of tetra-functional epoxy at the 1 wt% level.
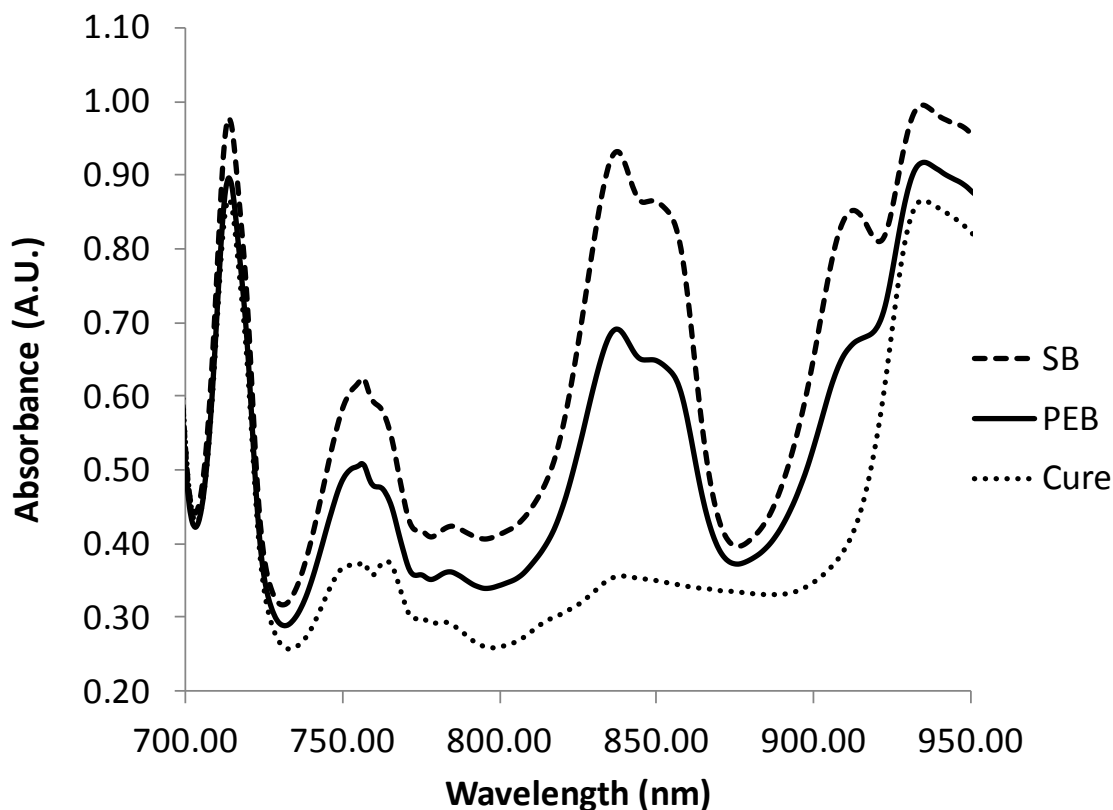
Figure 3.9 Change in FTIR spectrum of the thin-film Avatrel 8000P from 700 cm^{-1} to 950 cm^{-1} as a function of processing steps (SB: 100°C for 5 min; exposure: 250 mJ/cm^{2}; PEB: 100°C for 5 min; Cure: 1 h at 225°C).

3.3 Conclusions

The tetra-functional epoxy-based cross-linker, TPEGE, showed a significantly different behavior compared to the di-functional and tri-functional cross-linkers studied. TPEGE showed a high UV absorption between 250 nm and 400 nm and the sensitivity of the polymer with 1 wt% supplementary TPEGE was enhanced by a factor of 3.7. A minor increase in the contrast of the base polymer was observed by addition of di-functional and tri-functional cross-linkers while the contrast value of the base polymer, 7.36, was increased to 24.2 by 1 wt% addition of TPEGE. The base polymer with

supplementary TPEGE shows excellent adhesion at the film-substrate interface enabling the fabrication high-aspect ratio structures (13:1 aspect ratio) with high-fidelity and straight side-walled photo-defined structures.   The addition of TPEGE to the base polymer resulted in high contrast, high sensitivity, excellent adhesion, and the ability to make high-aspect- ratio features, making the polymer films suitable for MEMS and microelectronics applications.

CHAPTER 4

ADVANCED PHOTO-PATTERNING OF POLYNORBORNENE

DIELECTRIC

It was shown in Chapter 3 that the addition of as little as 1wt% of TPEGE significantly improved the photodefinition properties of Avatrel 8000P. The contrast improved from 7.37 for Avatrel 8000P (identified as the base formulation (BF)) to 24.2 for the formulation with the addition of 1 wt% TPEGE (formulation A). Additionally, TPEGE showed high UV absorbtivity at 365 nm. The sensitivity of the polymer was enhanced by a factor of 3.7 by the addition of 1wt% TPEGE. In BF, CPTX, a non-cross-linking UV absorber, was used as the photosensitizer. Additives such as CPTX, which do not become a part of the final polymer matrix, reside within the final polymer structure and can result in property degradation compared to purer formulations. In this work, the feasibility of using TPEGE, which is a tetra-functional cross-linker with a high UV absorbtivity, was investigated as the only UV absorber in the polymer mixture. New formulations with 1 wt% TPEGE (formulation B) and 3 wt% TPEGE (formulation C) (no CPTX) were investigated. The sensitivity and photodefinability of the polymers were compared to those of BF and formulation A. The mechanical properties and the degree of moister uptake of the formulations were studied to determine the effectiveness of using TPEGE as the photosensitizer and cross-linker on the properties of the cured films

4.1 Experimental

All epoxy-based cross-linkers were purchased from Aldrich Chemical Co. A summary of the formulations made with the multifunctional epoxy cross-linkers TPEGE, 3-EP, and 2-EP are listed in Table 4.1. The epoxy cross-linkers were dissolved in

PGMEA and ball-milled with the PNB resin for 72 h. After developing, the films were cured in a nitrogen-purged furnace at 160°C for 1 h [54].

Table 4.1 Polynorbornene formulations.

Polymer Formulation	Title
Base polymer (Avatrel 8000P)	BF
BF with no CPTX	BC
BF with supplementary 1 wt% TPEGE	A
BC with supplementary 1 wt% TPEGE	B
BC with supplementary 3 wt% TPEGE	C
BF with supplementary 1 wt% 2EP	D
BF with supplementary 1 wt% 3EP	E

4.2 Results and Discussion

Contrast experiments were performed to compare the contrast and sensitivity of the formulations. The contrast curves for formulation B and C are shown in Figure 4.1. The addition of TPEGE increased the developing time for the polymer. The developing time for BF was 3.00 min, while the developing time for formulation B and C were higher at 4.30 and 4.50 min, respectively. These results show that, TPEGE improved the polymer-to-substrate adhesion and also affected the solubility of the unexposed film in the aqueous-base developer. The increased adhesion and longer developing time with formulation B and C is due to higher degree of epoxy ring opening and resulting reaction with the surface. That is, in the presence of TPEGE, epoxy rings are fully reacted, improving the polymer-to-substrate adhesion. Additionally, TPEGE resulted in fractional

epoxy ring opening after spincoating and baking (SB and PEB). This effect was investigated previously in unexposed samples using FTIR spectroscopy where it was shown that some of the epoxide rings had reacted, resulting in some degree of cross-linking in the unexposed regions after the 100˚C PEB [97]. These effects were only observed in the presence of TPEGE, showing that TPEGE significantly improved the polymer adhesion characteristics and affected the polymer dissolution behavior.

67
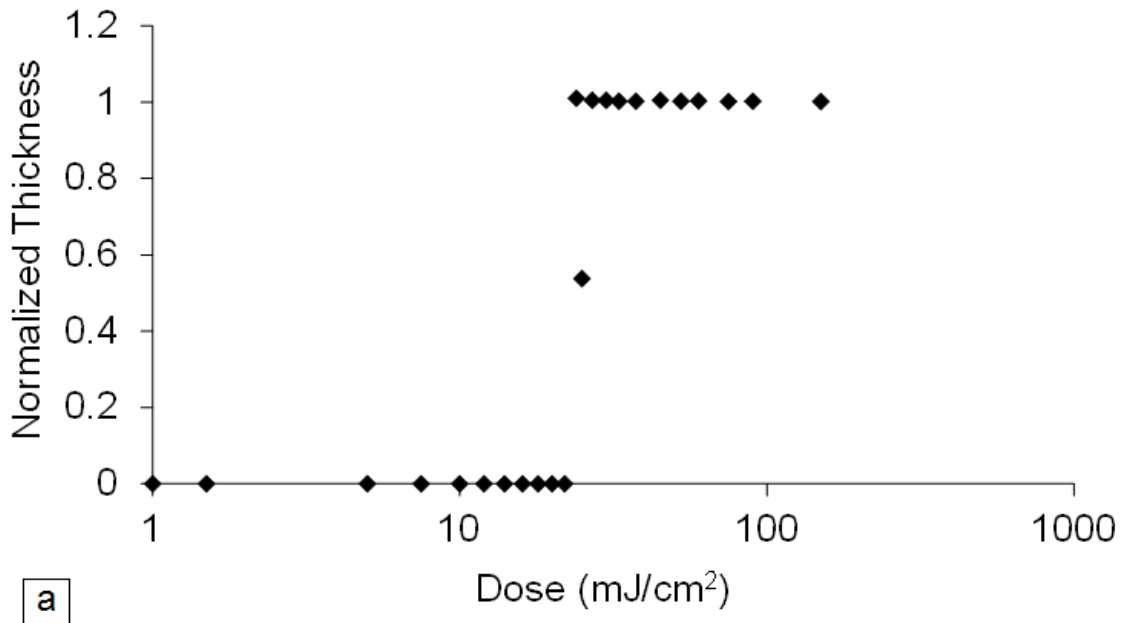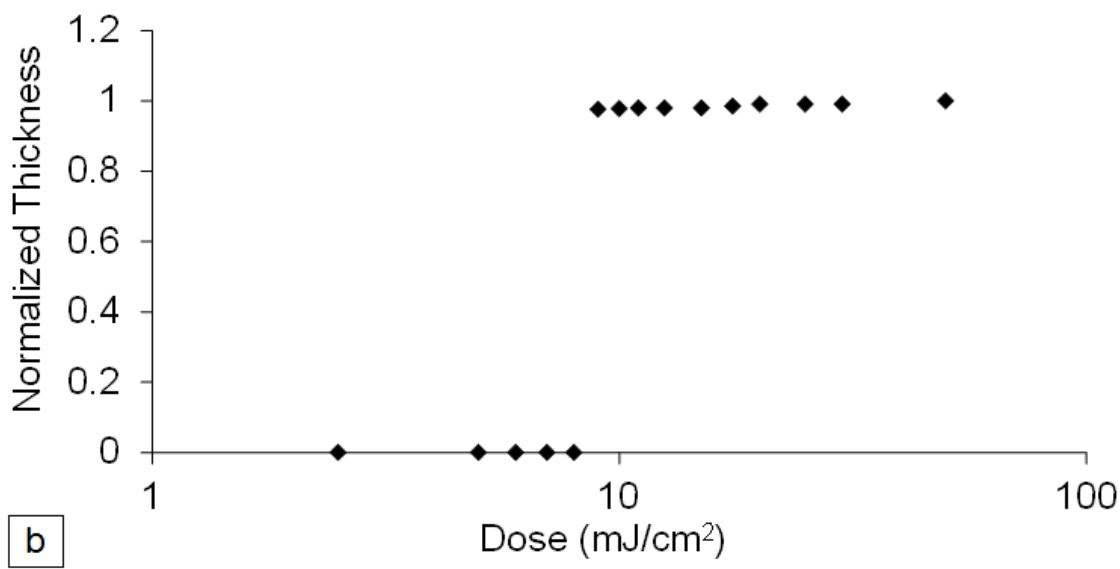
Figure 4.1 Contrast curve for (a) formulation B, (b) formulation C.

Photosensitivity is one of the critical characteristics of a photoresist or permanent dielectric. Upon the absorption of UV radiation within the polymer film, PAG activates and produces an acid within the polymer film, catalyzing the epoxy ring opening reaction, which leads to polymer cross-linking. In BF, the UV absorption was increased by adding CPTX as the sensitizer to the polymer formulation. In this case, energy transfer occurred between the sensitizer and the PAG, creating the acid catalyst. As shown in Fig. 4.1a, structures were patterned with formulation B at doses as low as 16 mJ/cm^2, which is an extremely low value compared to the D_{100} value for BF, 66 mJ/cm^2. This improvement in the sensitivity for the mixture containing TPEGE, compared to BF, is attributed to greater interaction between the UV sensitizer and the acid catalyst. That is, although TPEGE has less UV absorbtivity compared to CPTX (used in BF), it is more effective than CPTX because once it absorbs UV radiation and activates the PAG (via energy transfer), the epoxy functionalities are guaranteed to be within close proximity of the photogenerated acid.

68

Formulation B showed slightly higher sensitivity compared to formulation A (16 mJ/cm^2 for formulation C compared to 18 mJ/cm^2 for formulation A). One reason could be the more effective energy transfer between TPEGE and PAG (compared to that of CPTX and PAG) since CPTX does not participate in polymer cross-linking and remains in the polymer film as a low molecular weight additive. The same effect was observed in formulation C (Fig. 4.1b). The sensitivity of formulation C improved compared to that of BF and the D_{100} value deceased from 66 mJ/cm^2 for BF to 14 mJ/cm^2 for formulation C. It can be concluded that the addition of TPEGE to the polymer in the absence of CPTX results in more efficient energy transfer and creation of the acid catalyst (compared to the use of CPTX as a sensitizer), which results in greater cross-linking.

To further investigate the effect of TPEGE on the photodefinability of the polymer, contrast values were calculated from the slope of the line connecting D_0 to D_{100}. As it can be seen from Fig. 4.1a, the addition of 1 wt% TPEGE to BF in the absence of CPTX significantly improved the contrast. The contrast value increased from 7.37 for BF to 26.5 for formulation B. Commonly used photoresists have been reported to have a contrast of 2 to 3 [21, 98, 99]. This improvement in contrast of the polymer is due to the addition of 1 wt% TPEGE and omission of CPTX. The addition of TPEGE resulted in more effective cross-linking within the polymer due to its higher functionality (four epoxy units per molecule) compared to the di-functional and tri-functional cross-linkers in BF. TPEGE has a greater chance of cross-linking two or more PNB polymer strands. This should result in greater cross-linking and lower solubility at low exposure doses (closed to D_0 where the not all the epoxy has reacted), and improved contrast. We also note that photosensitive materials with higher sensitivity, e.g. TPEGE formulations, also generally have higher contrast.

Contrast experiments were also performed for formulation C which had a higher TPEGE concentration. As shown in Figure 4.1b, the addition of 3wt% of TPEGE further improved the polymer contrast resulting in an extremely high value of 33.4. This contrast

value is one of the highest contrast values reported for photosensitive materials in the literature. This improvement in contrast is due to the same reasons mentioned above: achieving a critical degree of cross-linking at lower doses, higher epoxy functionality for the cross-linker, and higher sensitivity of the polymer due to the addition of TPEGE. These results show that the addition of TPEGE to BF as the UV sensitizer significantly improved the polymer cross-linking, contrast, and photosensitivity.

The ability to fabricate high aspect ratio features is a function of the contrast, sensitivity, and adhesion characteristics of the photosensitive material. Since formulations B and C showed significant improvement in these parameters compared to BF, the ability to fabricate high-aspect-ratio features was investigated and compared to that of BF. For this work, hollow-core structures were chosen since they are difficult to fabricate due to the restricted transport of the developer into the spatially restricted core of the structure compared to the transport of the developer to the outside of the structure. Thick films were photopatterned at an exposure dose of 100 mJ/cm^2, at 365 nm, with formulation B resulting in 39-µm tall, hollow-core, triangular-shaped structures. Double coating was performed for formulation C which resulted in 97 µm thick films. Due to the improved polymer-to-substrate adhesion with TPEGE, the unexposed polymer film at the center of the structure were fully dissolved before delamination occurred at the outside edge of the polymer structure. Hollow-core features with 3 µm diameter openings were fabricated in 39 µm thick films using formulations B. Hollow-core features with 7 µm diameter openings were fabricated in double-coated, 97 µm thick films using formulations C. The resulting aspect ratio for formulation B was 13:1, while that of formulation C was 14:1. As shown previously, the highest aspect ratio achieved for BF in 39-µm films was 5:1. Fabrication of higher aspect ratio structures with BF required longer developing time to fully develop the center core, which led to film delamination and lifting. Thus, only formulations with the additional TPEGE cross-linker had sufficient adhesion, contrast, and sensitivity to produce features with an aspect ratio of

greater than 13:1. It can be concluded that the use 3wt% TPEGE with no CPTX resulted in higher contrast, sensitivity, film-to-substrate adhesion, and aspect ratio (formulation C).

To study the effect of TPEGE on the cross-link density and mechanical properties of formulations B and C, the reduced modulus and hardness of these formulations were compared with those of BF using nanoindentation. All samples were tested after a 160°C cure for 1h. BF, formulations B, and formulation C had a reduced modulus of 2.80, 2.84, and 2.86 GPa, respectively. The hardness values for BF, formulation B and formulation C were 0.13, 0.14, and 0.14 GPa, respectively. These results show that TPEGE resulted in a slight improvement in the mechanical properties.

In order to investigate the actual degree of cross-linking, swelling experiments were performed. A lower degree of cross-linking will result in greater solvent absorption and swelling [94]. Swelling tests were performed in PGMEA after a final cure at 160°C for 1 h. The mass of each sample was measured at eight different times during a 24 h swelling period. The percent increase in weight are shown in Figure 4.2. Each data point is the average of four measurements, and the standard deviation was less than 0.0003.

As shown in Fig. 4.2, the sample weight increased with the swelling time. The sample weight of BF significantly increased compared to that of the formulations with additional TPEGE. These observations agree with the previous results discussed above. The degree of swelling decreased from 2.1 for BF to 1.2 and 1.0 for formulations B and C, respectively. The degree of swelling was greater for BF because it had a lower molar epoxy content than the other formulations, resulting in a lower cross-link density and higher water uptake. The addition of the TPEGE cross-linker to the polymer increased the degree of cross-linking between the epoxy and the polymer reaction sites, especially in the case of formulation C.
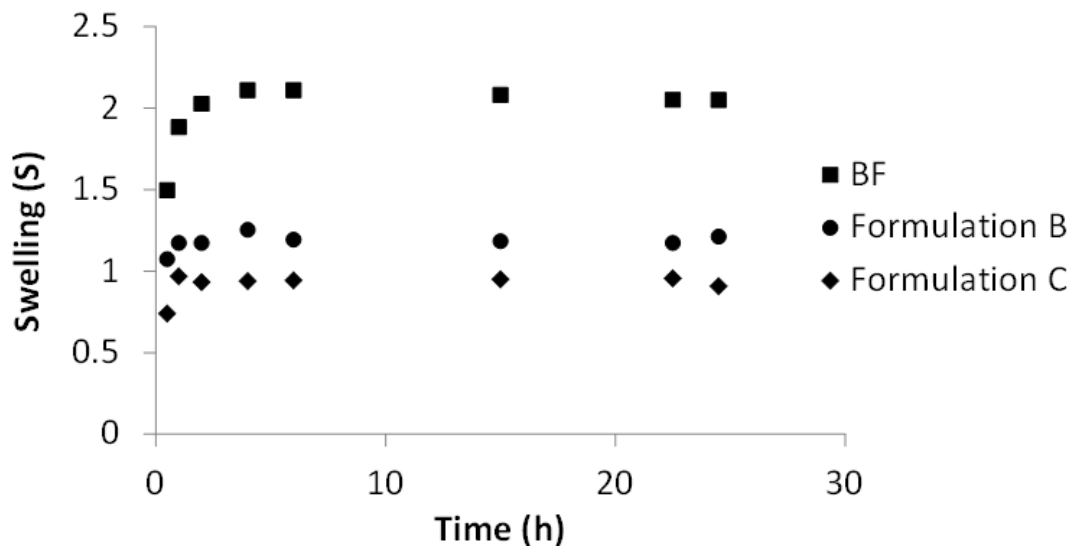
Figure 4.2 Influence of TPEGE on swelling of a fully cross-linked cured polymer.

It was shown that the addition of TPEGE to BF improved the polymer photosensitivity and photodefinability. To study the effect of having the UV absorbing moiety within the epoxy cross-linker (compared to non-UV absorbing epoxy with added sensitizer), new formulations were made with 2-EP and 3-EP which have negligible UV absorption compared to TPEGE. 2-EP and 3-EP compounds have similar structures to TPEGE, except for the number of pendant epoxy rings. The organization of the TPEGE pendant groups leads to high UV absorbance, not found in 2-EP and 3-EP. Formulation D and E were prepared (with 2-EP and 3-EP compounds, respectively) so as to contain the exact number of equivalents of epoxy as formulation A, Table 4.1. To evaluate the impact of 2-EP and 3-EP on the polymer photosensitivity at 365 nm, a series of UV absorption experiments were conducted. The absorbance of dilute solutions of 2-EP, and 3-EP were measured in PGMEA, which were transparent in the wavelength range of interest [97]. 2-EP had very low absorbance at wavelengths from 300 to 400 nm while 3-EP had higher molar absorptivity in the UV, Figure 4.3. However, the absorptivity of 3-EP in PGMEA was low compared to the absorptivity of a dilute solution of TPEGE and

CPTX in PGMEA. The molar absorbance of 3-EP, TPEGE and CPTX are 113, 172,287 , and 395,779 (L/mol.m), respectively. The high UV absorptivity of TPEGE from 300 to 400 nm is due to the conjugation of the double bonds because of the chemical structure of the TPEGE molecule.
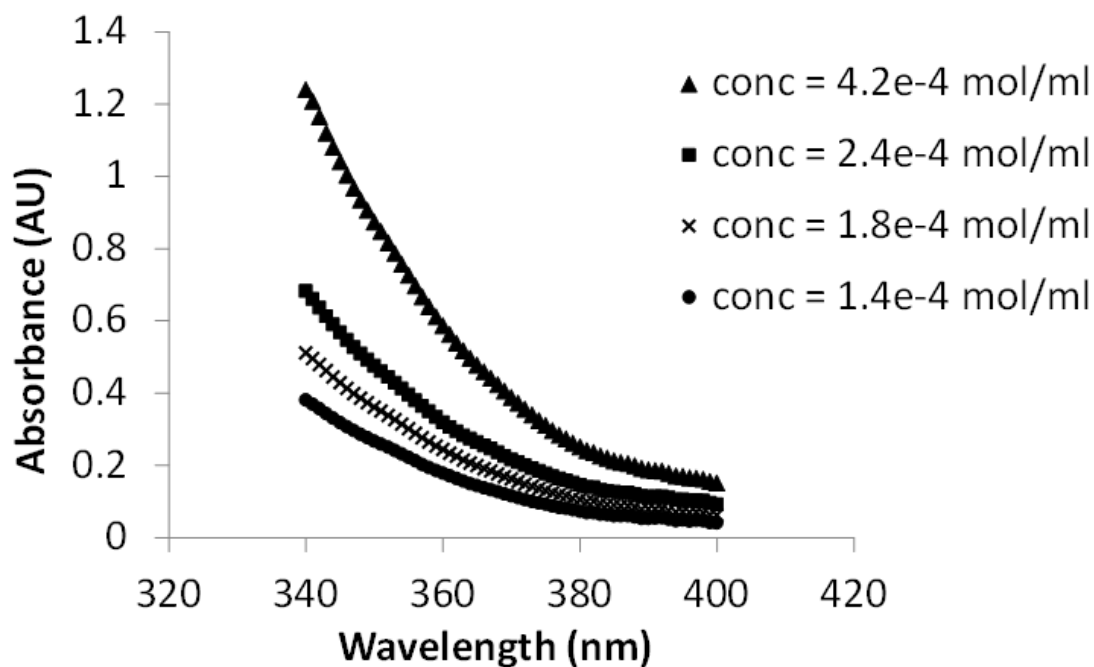
Figure 4.3 Changes in UV-vis spectrum of dilute solution of 3-EP in PGMEA from 200 to 600 nm.

Contrast experiments were performed to compare the sensitivity and the contrast of the formulations. As shown in Figure 4.4, contrast values of 11.4 and 11.5 were obtained for formulation D and E, respectively. The contrast values for formulations D and E were higher than that for BF (γ=7.4), because of the added epoxy; however, it is lower than that of formulation A (γ=24.2). The developing time also increased from 3.00 min to 3.40 min for formulations B and C, respectively, due to the higher epoxy content of these formulations. This shows that additional epoxy cross-linker affected the solubility of the unexposed polymer and somewhat improved the polymer-to-substrate adhesion. The D_{100} value of these formulations was similar to that of BF, Table 4.2,

showing that 2-EP and 3-EP did not affect the polymer sensitivity. This result is
congruent with the previous observation that 2-EP and 3-EP have very low UV
absorbtivity at the wavelength of interest.
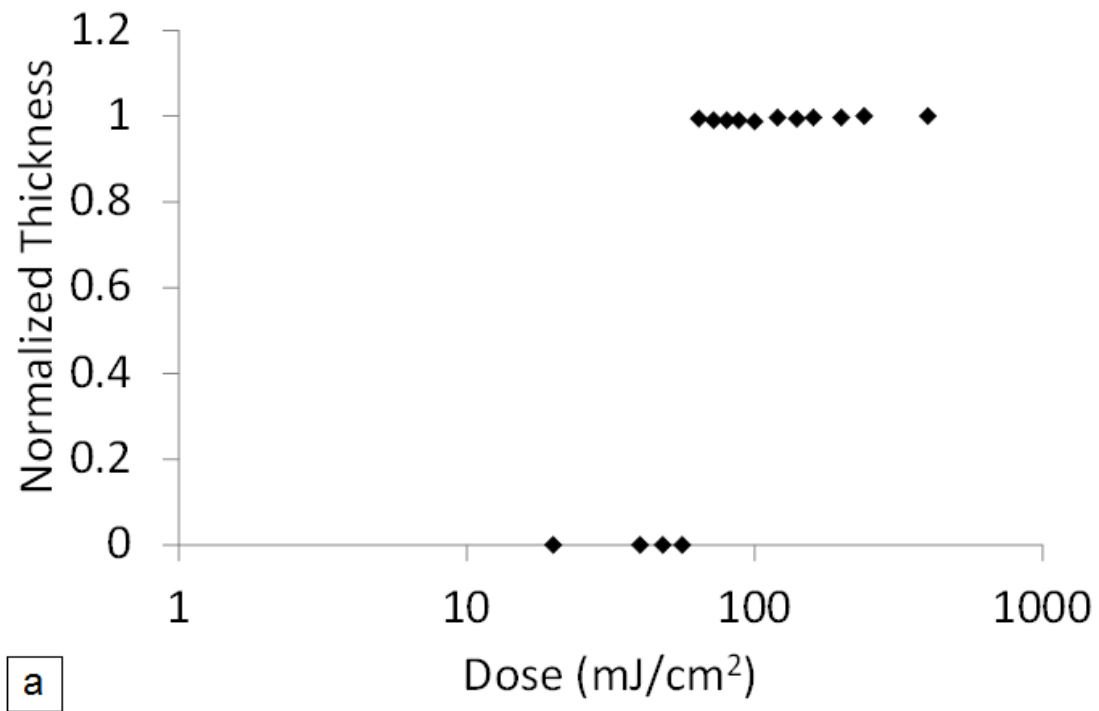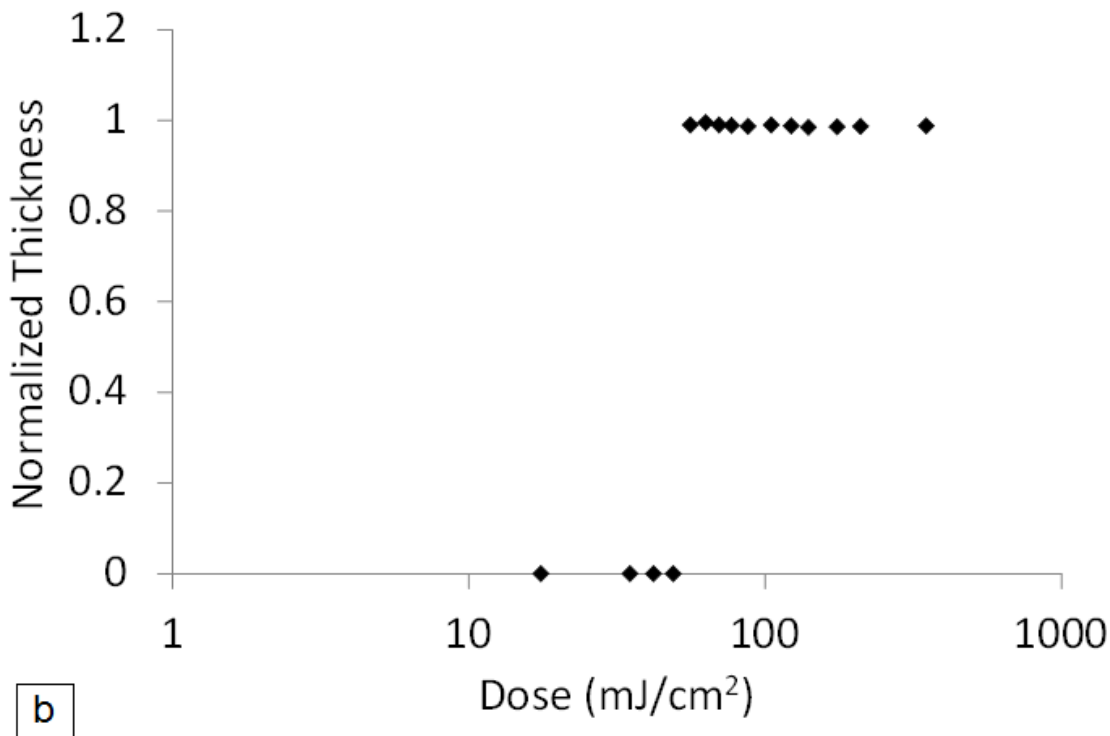
Figure 4.4 Contrast curve for (a) formulation D, (b) formulation E.

The ability to fabricate high-aspect-ratio structures is one of the most desirable attributes of a photosensitive polymer. The effect of 2-EP and 3-EP cross-linkers on the patternability of high-aspect-ratio features was evaluated. Hollow-core features with 3 μm diameter opening were fabricated in 39-μm thick films using formulation D and E. Both formulations resulted in 5:1 aspect-ratio structures, and the development of higher-aspect-ratio structures resulted in film delamination. Previously, an aspect-ratio of 5:1 and 13:1 were obtained for BF and formulation A, respectively [97]. This shows that only TPEGE improved the polymer ability to pattern high-aspect-ratio structures because of the improved sensitivity, contrast and adhesion.

Table 4.2 Properties of PNB formulations.

Formulation	Contrast (γ)	D_{100} (mJ/cm^2)	DT (min)	Aspect Ratio	Modulus (GPa)	Hardness (GPa)
BF	7.37	66	3	5:1	2.80	2.13
A	24.2	18	4:30	13:1	2.84	2.14
B	26.5	16	4:15	13:1	2.84	2.14
C	33.4	14	4:50	14:1	2.86	2.14
D	11.4	65	3:40	5:1	2.85	2.14
E	11.5	65	3:40	5:1	2.84	2.14

Nanoindentation was used to evaluate the reduced modulus and hardness of formulation A, D, and E, compared to BF. The reduced modulus of formulations A, D, and E (160°C cure for 1 h) was 2.84, 2.85, and 2.84 GPa, respectively. All formulations resulted in a hardness value of 0.14 GPa. The results show that there was no significant difference between the mechanical properties of the various formulations with additional epoxy cross-linker, which implies a similar cross-link density. The lower modulus value for BF is simply due to the lower epoxy content, resulting in a lower number of cross-links.

Swelling experiments were performed to investigate the relative degree of cross-linking. The mass of each sample was measured at six different times during a 26-hour swelling period. Each data point is the average of four measurements and the average of standard deviation for each point was less than 0.0003. Figure 4.5 shows an increase in weight with swelling time. No significant difference was found between formulation A, D, and E when the epoxy content was identical. This shows that the addition of a cross-

linker to the polymer increases the degree of cross-linking between the epoxy and the polymer reaction sites, regardless of the functionality of the cross-linker. This agrees with the nanoindentation results, showing that each epoxy compound resulted in a similar degree of cross-linking. The degree of swelling was greater for BF because it has a lower molar epoxy content than the other formulations.
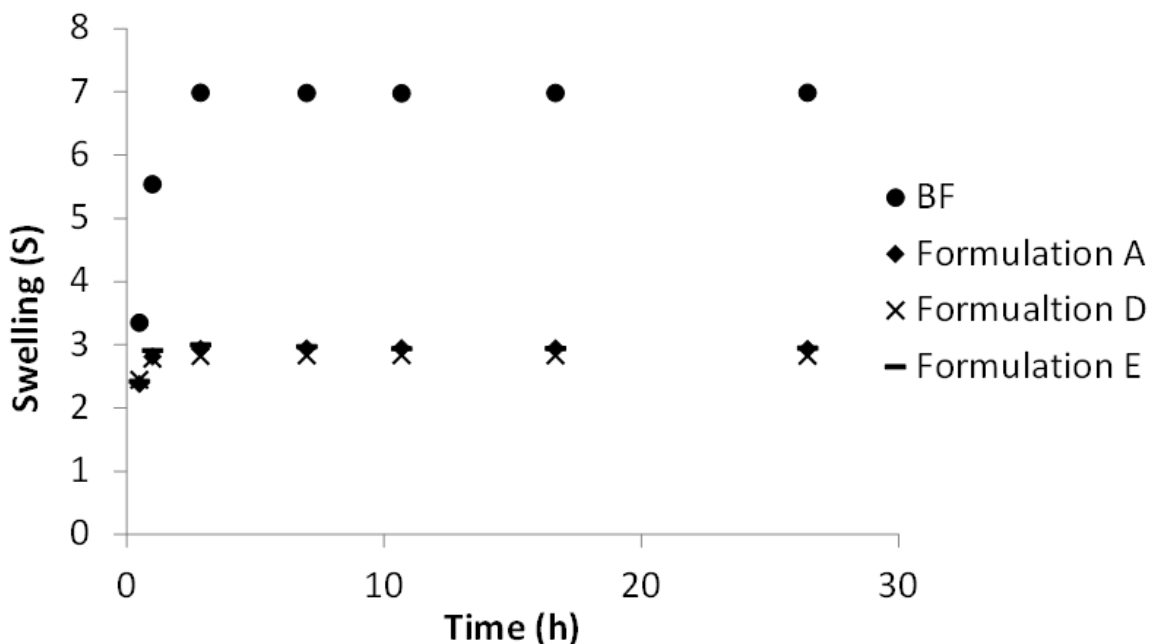
Figure 4.5 Influence of 2-EP, 3-EP, and TPEGE crosslinker on swelling of crosslinked cured polymer.

4.3 Conclusions

The tetra-functional epoxy-based crosslinker with high UV absorbtivity at 365 nm, TPEGE, was used as the photosensitizer in the polymer. TPEGE was used to replace the non-crosslinking UV sensitizer in the polymer resulting in improved photolithographic characteristics and sensitivity. TPEGE resulted in a more effective acid-catalyzed route to epoxy cross-linking within the polymer compared to the non-crosslinking photosensitizer. The addition of a small quantity of TPEGE (3 wt% of solution) resulted in improved UV sensitivity of the polymer at 365 nm. The di-

functional and tri-functional crosslinkers (with similar chemical structures) showed no significant effect on the polymer sensitivity. The contrast value of the polymer, 7.4, increased to 33.4 by the addition of 3wt% of TPEGE. A minor increase in the contrast of the base polymer was observed through the addition of the di-functional and tri-functional crosslinkers. The polymer with additional TPEGE crosslinker showed excellent polymer-to-substrate adhesion enabling the fabrication of 14:1 high-aspect ratio structures with high-fidelity and straight side-walls. It can be concluded that TPEGE can replace the photosensitizer in the polymer formulation and improve the polymer patternability and photosensitivity. The addition of TPEGE to the polymer resulted in high contrast, high sensitivity, excellent adhesion, and the ability to make high-aspect-ratio structures, making this polymer suitable for MEMS and microelectronics packaging applications.

CHAPTER 5

CROSS-LINKING OF POLYNORBORNENE DIELECTRIC BY ELECTRON-BEAM LITHOGRAPHY

Electron beam lithography (EBL) is an important patterning method for nanosystems and devices due to its high spatial resolution and versatile processing [29]. However, EBL has low throughput due to the sequential nature of the exposure, which can be mitigated to some extent by increasing the sensitively of the material to be imaged. Epoxy-based polymers have been e-beam cross-linked [100-103]. They possess high sensitivity but the resolution can be limited by swelling during developing [104]. Recently, chemically amplified, epoxy-based resists have been reported to have high sensitivity for nano-scale EBL [104-106]. The high sensitivity of these materials comes from the chemical amplification mechanism where the e-beam generated acid catalyzes the epoxy cross-linking [104]. Molecular e-beam resists have been shown to somewhat mitigate excess LER problems caused by diffusion of the acid catalyst into unexposed regions [105, 107-109].

In this study, the lithographic characteristics of e-beam induced cross-linking of Avatrel 8000P were studied in a effort to explore the feasibility of using this material as a high contrast, high sensitivity electron-beam imageable dielectric material. The e-beam initiated reaction between PNB cross-linking sites and the epoxy cross-linkers was investigated and the spatial resolution of the PNB dielectric material was evaluated. The relationship between sensitivity and processing conditions were investigated as a function of mixture formulation. The process parameters were optimized for forming lithographic patterns in the 100 nm regime.

5.1 Experimental

The polymer mixture was formulated using PGMEA as the solvent with PNB, Rhodorsil PI 2074, multifunctional epoxy cross-linkers (polypropylene glycol diglycidyl ether and trimethylolpropane triglycidyl ether), CPTX, and an adhesion promoter. This formulation, with all components present, will be identified as the base formulation (BF) hereafter. The formulation containing only PNB and adhesion promoter in PGMEA solvent is identified as the base polymer, BP. PNB mixtures were diluted with PGMEA to different degrees to produce different thickness films by spin coating. The solutions were each rolled on a ball-mill for 72 h. The polymer films were spin-coated on 100 mm diameter <100> silicon wafers using a CEE 100CB Spinner at 2000 rpm for 30 s to produce 200 nm and 1100 nm thick films.   The polymers were soft-baked and post-exposure baked at 100°C for 2 min on a hotplate. The polymers were e-beam irradiated using a JEOl JBX-9300FS tool at 100 kV acceleration voltage and 50 pA beam current.

5.2 Results and Discussion

Thin films of PNB and its mixtures are highly soluble in aqueous base (0.26N TMAH). A 202 nm BF film dissolved in the TMAH developer in less than 10 s after soft-bake to remove the PGMEA casting solvent. This corresponds to the development step of the unexposed Avatrel 8000P film. The addition of 1 wt% of supplementary TPEGE to the BF did not change the dissolution time, as shown in Figure 5.1. This establishes that a 10 s immersion in 0.26N TMAH is an adequate developing time for the formulations used here. Hereafter, all samples in this study were developed for 10 s, unless otherwise stated.
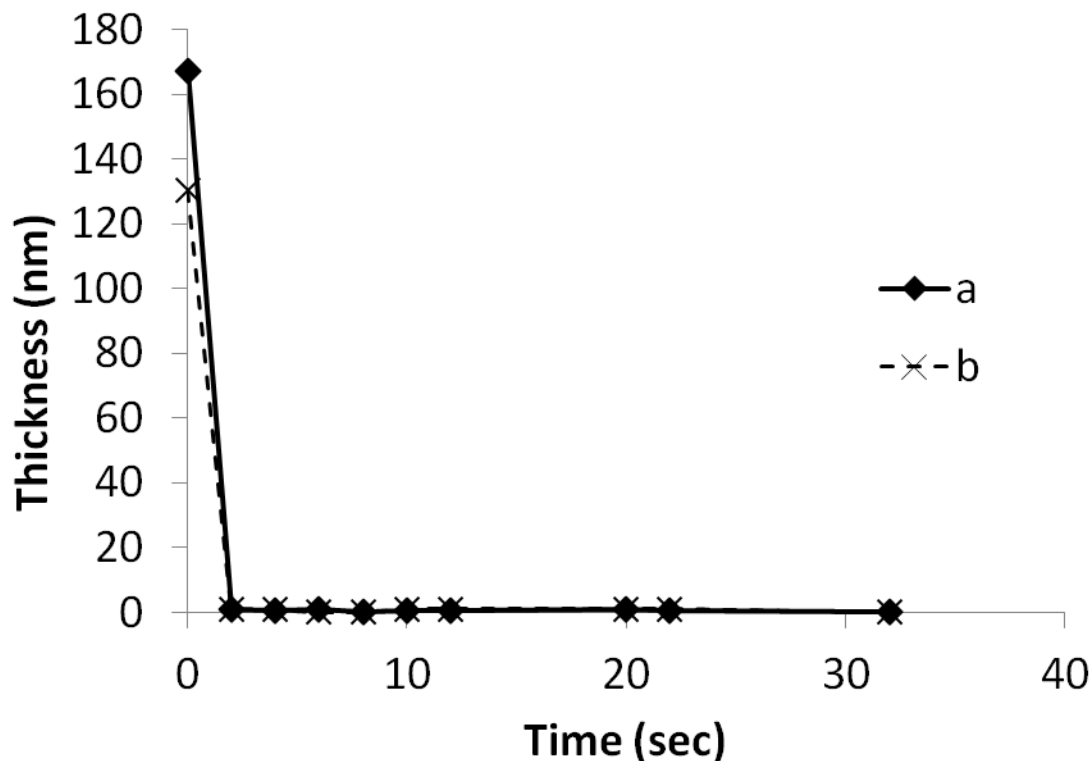
Figure 5.1 The developing profile for (a) BF; (b) BF with additional 1 wt% TPEGE.

Previously, TPEGE was shown to significantly improve the photo-patterning and sensitivity of Avatrel 8000P [110]. To evaluate the impact of TPEGE on the e-beam sensitivity and contrast of Avatrel 8000P, different concentrations of TPEGE were added to the PNB BF. The contrast curves for thin-films of the BF with varying concentration of TPEGE are compared to PNB (identified as BP) in Figure 5.2. This shows that PNB by itself (i.e. BP) is e-beam patternable. E-beam exposure causes random bond breaking and formation resulting in PNB cross-linking and insolubility in TMAH (10 s develop time) at doses greater than 1000 μC/cm^2. E-50, the dose at which 50% of the resist film is retained after development, for this formulation is 290 μC/cm^2. This dose is comparable to the E-50 values reported for known e-beam resists [111-115]. Hereafter, the contrast sensitivity of the formulations is defined by E-50.
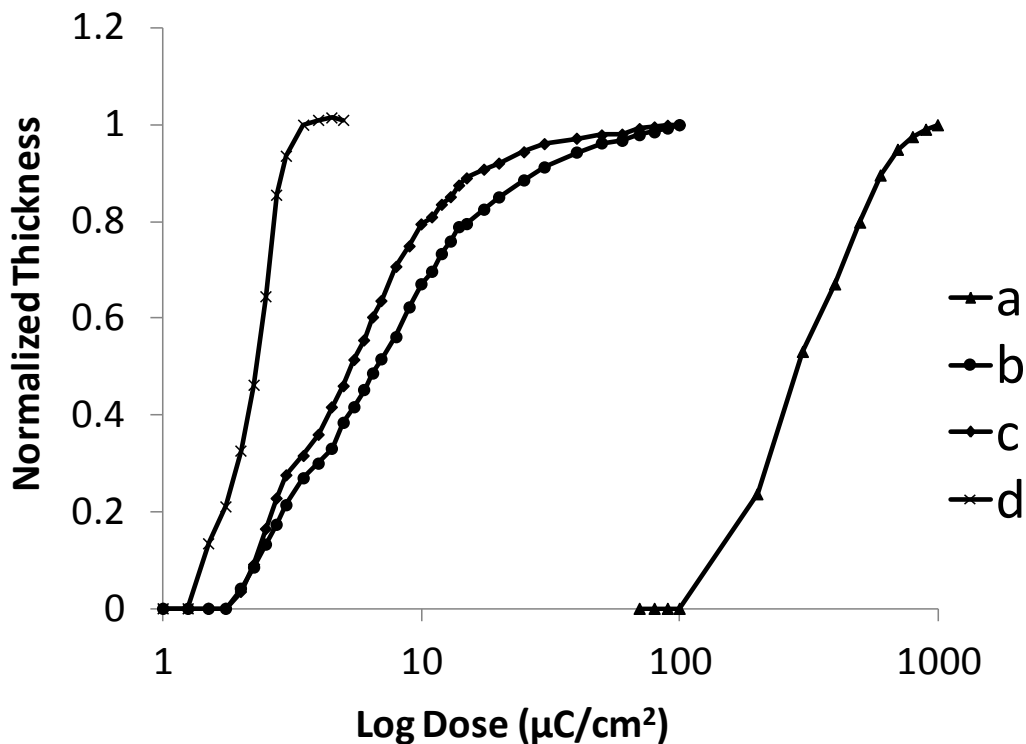
Figure 5.2 E-beam contrast curves for PNB formulations (a) BP with no additives; (b) BF; (c) BF with additional 1 wt% TPEGE; (d) BF with additional 3 wt% TPEGE.

To investigate the effect of the tetra-functional epoxy cross-linker and other components in the BF mixture, the contrast for BF and BF with TPEGE is also shown in Fig. 5.2. The contrast curve for BF in Fig. 5.2 shows that it has a very high sensitivity to e-beam radiation. The E-50 dose for this formulation decreased to 7 $\mu C/cm^2$. That is, the addition of the PAG, epoxy-based cross-linkers, and the sensitizer to the PNB polymer (BF) significantly improved the e-beam activation and cross-linking of the PNB polymer. The contribution of each of the components in the BF to the e-beam activation process will be examined later in this chapter.

The contrast value for each of the films in Fig. 5.2 was calculated from the slope of the line in the contrast curve where there is a transition from full development (film removal) to 50% normalized film thickness [105]. A similar slope was observed for BF and BP, resulting in similar contrast values for the two formulations. As shown in Fig.

5.2, E-50 decreased to 5.4 $\mu C/cm^2$ by the addition of 1 wt% TPEGE to BF, and the contrast increased from 0.8 to 1.1. The addition of 3 wt% TPEGE to BF increased the sensitivity and further improved the contrast of BF. The contrast increased to 2.1 for BF with 3 wt% TPEGE, andE-50 decreased to 2.3 $\mu C/cm^2$. These results show that the addition of TPEGE to BF decreased its solubility in aqueous base after e-beam exposure as a result of polymer cross-linking and interconnectivity. TPEGE has also been used in other negative-tone systems to improve the cross-link density of the polymer [103, 105].

The formulated PNB mixture, BF, was significantly more sensitive than the PNB base polymer, BP (without epoxy, PAG, or sensitizer), as shown in Fig. 5.2. The effect of CPTX on the sensitivity of the PNB material was examined first. As CPTX is used in optical photoresists to increase the absorption coefficient in the UV regions of the spectrum, it was not expected that its inclusion in the formulated PNB mixture had any effect on the mixture's sensitivity. Two new formulations of BP were made with different concentrations of the sensitizer. An amount equal to half the concentration of that contained in BF and an amount equal to the concentration of that contained in BF were added to BP. Contrast experiments were performed and are shown in Figure 5.3. As expected, the addition of sensitizer to the base polymer had no effect on the e-beam activation of the cross-linking reaction.
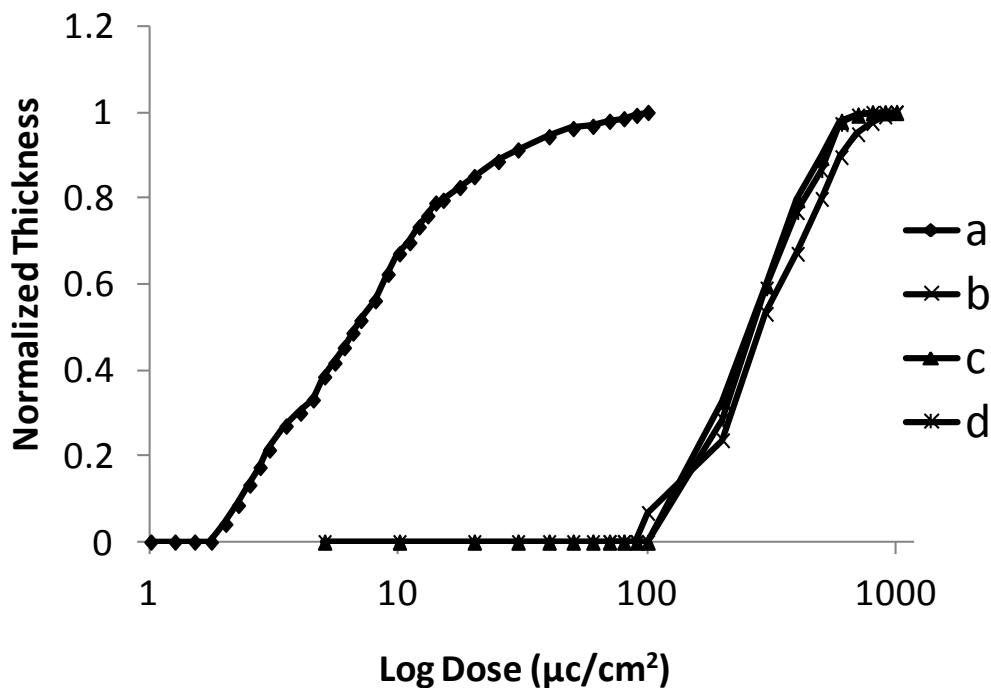
Figure 5.3 Effect of CPTX on e-beam contrast and sensitivity of PNB formulations (a) BP; (b) BP with 0.5X CPTX; (c) BP with 1X CPTX; BF.

The enhanced sensitivity of the formulations containing epoxy cross-linkers, shown in Fig. 5.2, is due to a higher degree of epoxy ring opening and cross-linking. Ring opening of the epoxide structures can occur through thermal treatment, acid activation, or direct e-beam irradiation. Thermal activation is unlikely here since the samples did not experience high temperature. Thus, it is important to understand the contribution of direct electron bombardment and ring opening vs. PAG activation by e-beam exposure and subsequent acid generation, followed by epoxide ring opening. The activated epoxy quickly leads to cross-linking between PNB molecules or between epoxy molecules themselves. In either case, the higher molecular weight products inhibit the rate of dissolution in aqueous base.

To study the affect of PAG, new formulations were made with different amounts of PAG and/or epoxy. Figure 5.4 shows the contrast curves for 200 nm thick films. The contrast and sensitivity of the base polymer, BP, was compared to the BP with 0.2X,

0.5X and 1X PAG, where X is the concentration of PAG in BF (i.e. X=1 in the case of BF). As shown in Fig. 5.4, base polymer formulations with different PAG concentrations (0.2X, 0.5X, and 1X PAG) resulted in the same contrast and sensitivity as BP. That is, PAG had no effect on the sensitivity and contrast of the base polymer. This result shows that cross-linking of PNB by itself, as occurred in Fig. 5.2, is not acid activated. The creation of an acid by e-beam activation of PAG did not result in cross-linking.

When epoxy was added to the base polymer with different amounts of PAG, the sensitivity of the mixture to e-beam irradiation increased. Mixtures of base polymer, BP, with epoxy cross-linkers and no PAG showed higher sensitivity and similar contrast compared to BP with no epoxy. The E-50 value of 67 $\mu C/cm^2$ was obtained for BP in the presence of the epoxy cross-linkers compared to 290 $\mu C/cm^2$ for BP with no epoxy. This result shows that the epoxy cross-linkers are activated by e-beam exposure and results in polymer network formation even in the absence of the PAG. Adding a small amount of PAG to the base polymer with epoxy (0.2X total PAG) slightly increased the sensitivity. E-50 decreased from 67 $\mu C/cm^2$ for BP with epoxy and no PAG to 55 $\mu C/cm^2$ for BP with epoxy and 0.2X of PAG. Further additions of PAG (i.e. 0.75X, 0.9X, and 1X) substantially increased the sensitivity, and E-50 decreased to the low dose of 7 $\mu C/cm^2$. The increase in the PAG concentration from 0.75X to 0.9X or 1X did not affect the contrast.

These results show that a certain amount of PAG is effective in initiating epoxy cross-linking within the polymer. That is, the irradiated PAG affects the e-beam activation and the rate of epoxy ring opening within the polymer mixture but does not affect the random PNB cross-linking (epoxy free cross-linking). A higher concentration of PAG results in a higher degree of cross-linking. However, there is an optimum range of PAG concentrations which can initiate the cross-linking reactions and provide the required degree of epoxy activation to obtain adequate cross-linking.
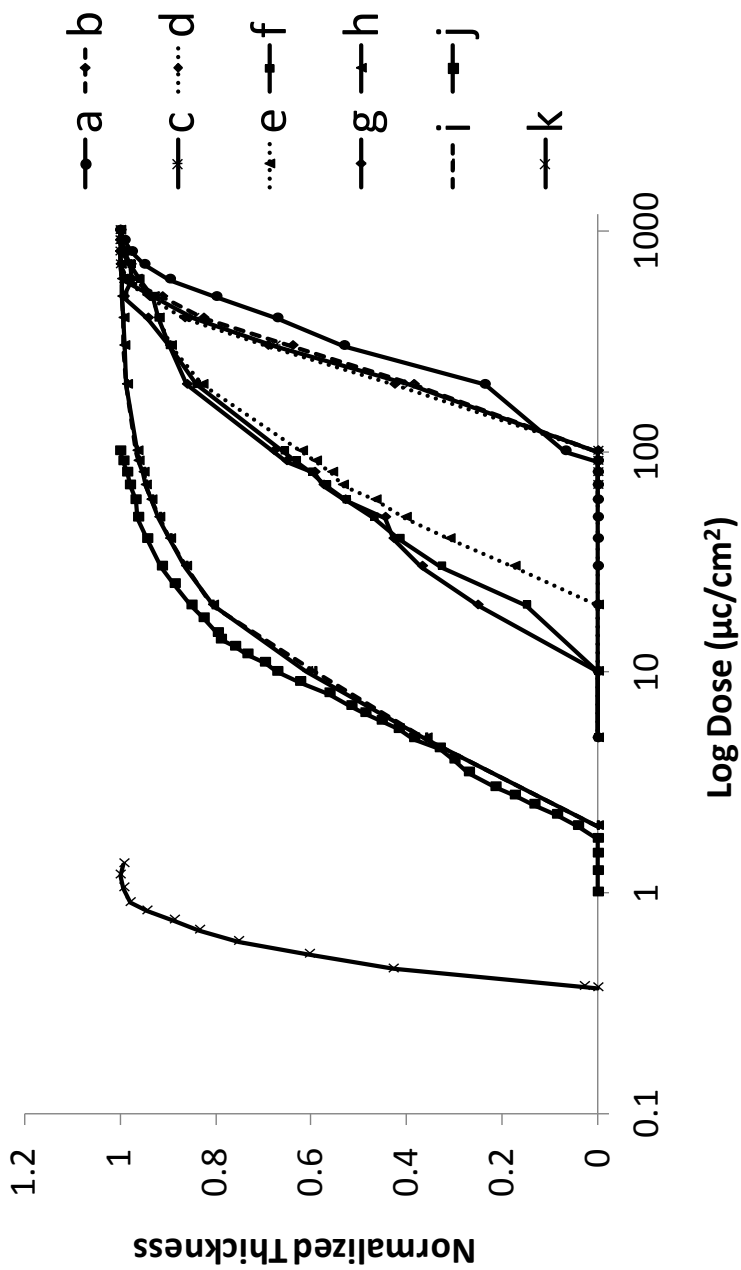
Figure 5.4 Effect of PAG on contrast and sensitivity of the PNB formulations (a) BP; (b) BP with 0.2X PAG; (c) BP with 0.5X PAG; (d) BP with 1X PAG; (e) BP with epoxy and no PAG; (f) BP with epoxy and 0.2X PAG; (g) BP with epoxy and 0.5X PAG; (h) BP with epoxy and 0.75X PAG; (i) BP with epoxy and 0.9X PAG; (j) BF; (k) BF with no CPTX and 3.4X PAG.

To investigate the effect of even higher concentrations of PAG on the cross-linking and sensitivity of the polymer, an additional mixture was made with higher concentration of PAG: 3.4X (PAG concentration was 3.4 times that in BF). The sensitizer was not added to the polymer mixture since it was shown to have no e-beam activation. BF with PAG showed significantly higher contrast and sensitivity, Fig. 5.4. The contrast was 4.4, which is high compared to known e-beam resists. This high sensitivity formulation was used to pattern 50 μm square patterns at the low E-50 dose of 0.48 μC/cm^2. Higher concentrations of PAG result in greater quantities of acid generation and epoxy ring opening, increasing the polymer cross-linking.

The experiments presented thus far were performed on thin-films, 200 nm to 300 nm thick. To evaluate the effect of film thickness on imaging characteristics of the polymer, the electron-beam contrast experiments were replicated on thicker samples, 1025 nm thick. The contrast curves for 200 nm and 1025 nm thick films of the base formulation, BF, are shown in Figure 5.5. Thin-film and thick-film samples were developed in the TMAH developer for 10 s and 12 s, respectively, to create a 50 μm square pattern. No residue was observed in the developed images. As shown in Fig. 5.5, the thicker film resulted in a higher contrast (γ=1.9) compared to the thin-film sample, whose contrast was 0.8. However, the minimum dose required to induce patterning (a 50 μm square) of the thicker film increased from 2 μC/cm^2 for the 200 nm thick sample to 4 μC/cm^2 for the 1025 nm thick sample.
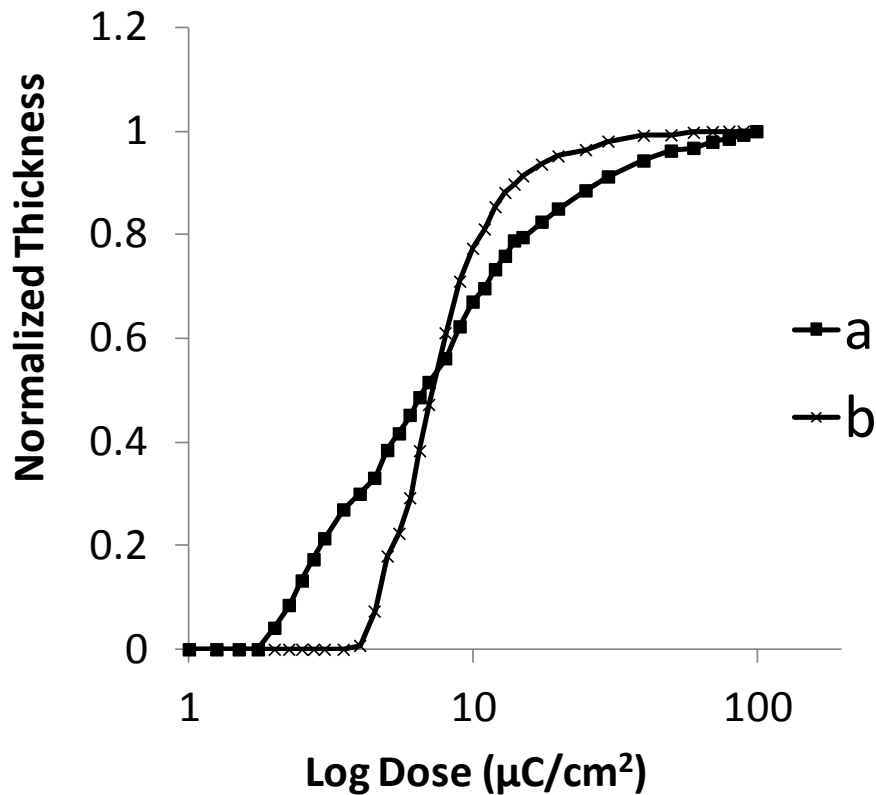
Figure 5.5 E-beam contrast curves for Avatrel 8000P with two different film thicknesses (a) 200 nm; (b) 1025 nm.

The effect of developing time on the sensitivity and contrast of 1025 nm thick BF was investigated. BF samples, 1025 nm thick, were developed in 0.26N TMAH yielding features with sharp corners and edges with no residue. Figure 5.6 shows the contrast curves for three developing processes. First, a sample was developed in 0.26N TMAH for 12 s. A 50 µm square was observed at doses as low as 4 µC/cm^2, and E-50 of 7 µC/cm^2 was obtained. The second sample was developed in TMAH developer for 7 s, rinsed with deionized (DI) water for 30 s, and immersed in the developer for an additional 5 s. The DI rinse allowed time for dissolution of the soluble products which had been neutralized by base. 50 µm squares were observed at a dose of 1 µC/cm^2 and a E-50 of 1.1 µC/cm^2 was obtained. The contrast increased from 1.9, for the first sample, to 3.7 for the second sample. TMAH which penetrates into the film results in

neutralization of the acidic protons and the development process becomes dissolution limited creating an opportunity for enhanced development in DI water without degradation in base during the water soak. The dissolution limited aspect (after penetration of base) was further demonstrated by developing a film in diluted TMAH developer, diluted 2:1 by weight with DI water, for 19 s. As shown in Fig. 5.6, the sample had the same contrast and sensitivity as the second sample (with DI soak), confirming the developing process is limited by the dissolution of the neutralized PNB and not the penetration of the TMAH.
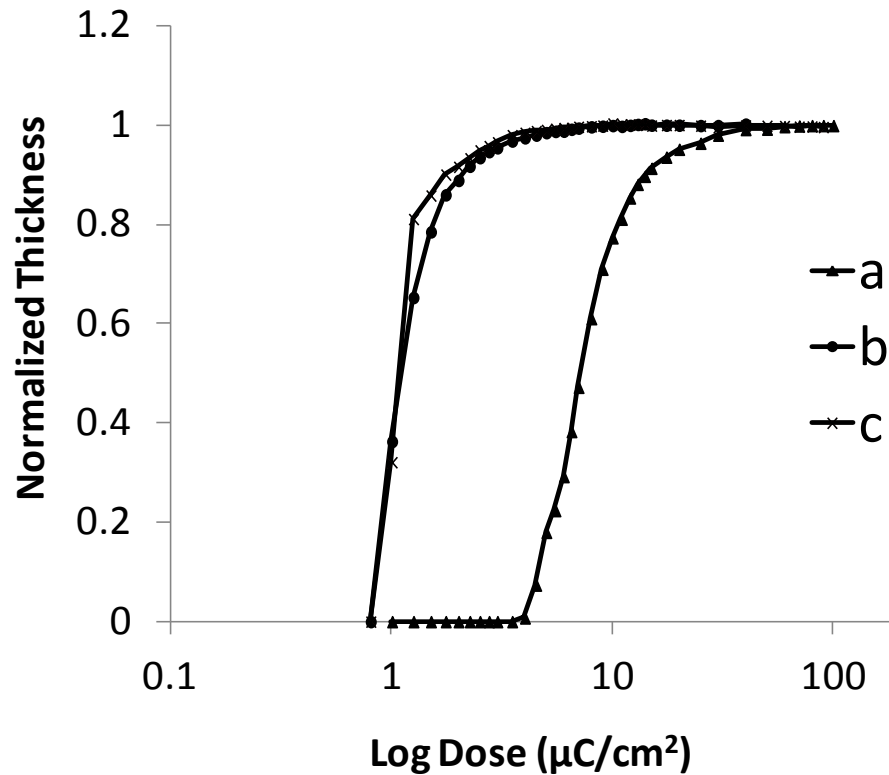
Figure 5.6 Effect of developing on e-beam contrast and sensitivity of Avatrel 8000P (a) developed in TMAH for 12 s; (b) developed in TMAH for 7 s, rinsed with DI water for 30 s, and immersed in TMAH for an additional 5 s; (c) developed in diluted TMAH (2:1 by weight with DI water) for 19 s.

The effect of the developer concentration was also evaluated on thin-film BF samples with and without additional TPEGE (1wt% and 3wt% TPEGE). 300 nm thick films were developed in diluted TMAH developer (2:1 by weight with DI water) for 15 s and compared to those developed in 0.26N TMAH for 10 s. The samples developed in the diluted developer resulted in poorer LER at low doses. The longer developing time, which was required to fully remove polymer residue in the unexposed regions, degraded the sharpness of the exposed edges. Thus, in next experiments the contrast and sensitivity of thick-film samples were compared to the thin-film samples developed in 0.26N TMAH developer for 10 s.

The film thickness and the developing time affected the sensitivity and the pattern quality of the developed polymer. The affect of thickness and developing time on BF with additional TPEGE was also evaluated (1wt% and 3 wt% additional TPEGE). The contrast and sensitivity of thick-film samples, 1100 nm thick, were compared to values obtained for 300 nm-thick samples. As shown in Figure 5.7, the thin-film BF sample with 1 wt% TPEGE developed in 0.26N TMAH for 10 s had a contrast of 1 and E-50 of 5.4 $\mu C/cm^2$ (results are not shown here). The thick-film sample developed in the TMAH developer for 16 s showed improved contrast and sensitivity compared to the thin-film sample. The contrast was 2.5 and the E-50 was 1.27 $\mu C/cm^2$. The effect of developing a 1100 nm thick BF film containing an additional 1 wt% TPEGE in diluted TMAH (2:1 by weight with DI water) for 25 s resulted in similar contrast and sensitivity to the film developed in TMAH developer for 16 s. The addition of the tetra-functional epoxy allowed the develop time to be extended to longer values because the film had enhanced film-to-substrate adhesion. The longer develop time resulted in higher contrast and sensitivity. It has been shown previously that enhanced adhesion of TPEGE is due to epoxy ring opening and polymer cross-linking [110].
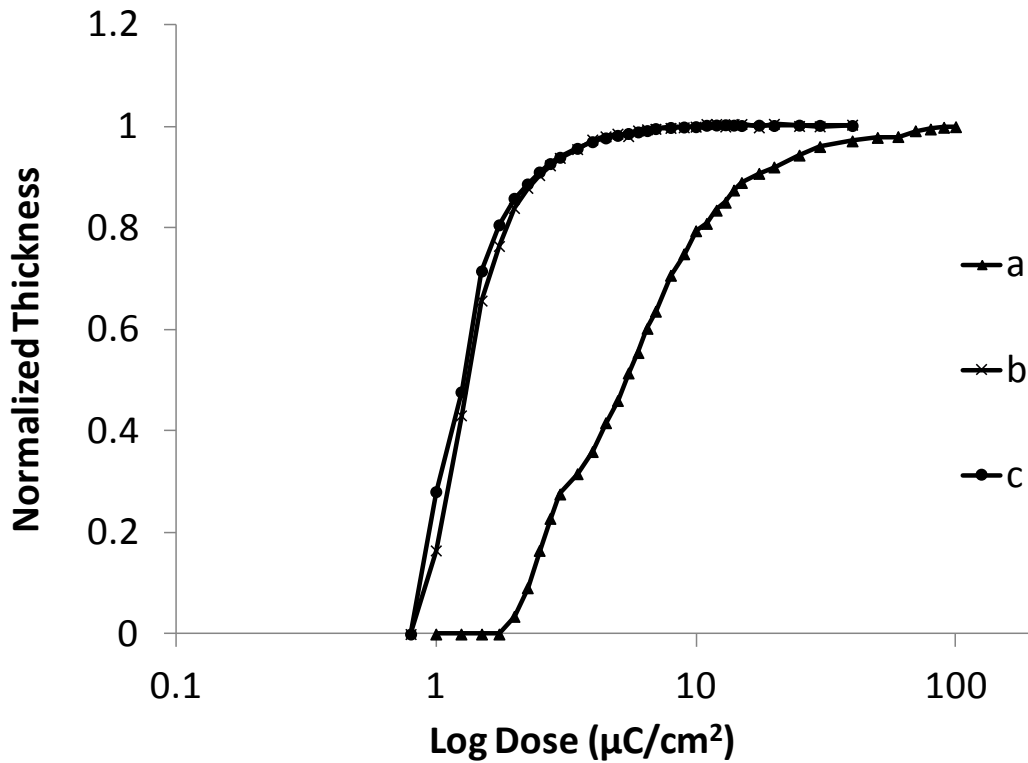
Figure 5.7 Effect of film thickness and developing on e-beam contrast and sensitivity of Avatrel 8000P with 1wt% TPEGE (a) 300 nm film developed in TMAH for 5 s; (b) 1100 nm film developed in TMAH for 16 s; (c) 1100 nm film developed in diluted TMAH for 25 s.

The contrast and sensitivity of BF with 3wt% TPEGE was investigated as a function of thicknesses and developing conditions, Figure 5.8. Nearly the same contrast (γ=2.1) and sensitively (E-50 of 2.3 μC/cm^2) can be obtained by changing the developer concentration and time over a limited range of values. The thick-film sample was developed in 0.26N TMAH developer for 16 s. Developing the thick-film sample in diluted TMAH developer (2:1 with DI water) for 30 s showed no significant change in the sensitivity and contrast. The longer developing time could be used in these experiments because the films had greater adhesion from the inclusion of 3wt% TPEGE.
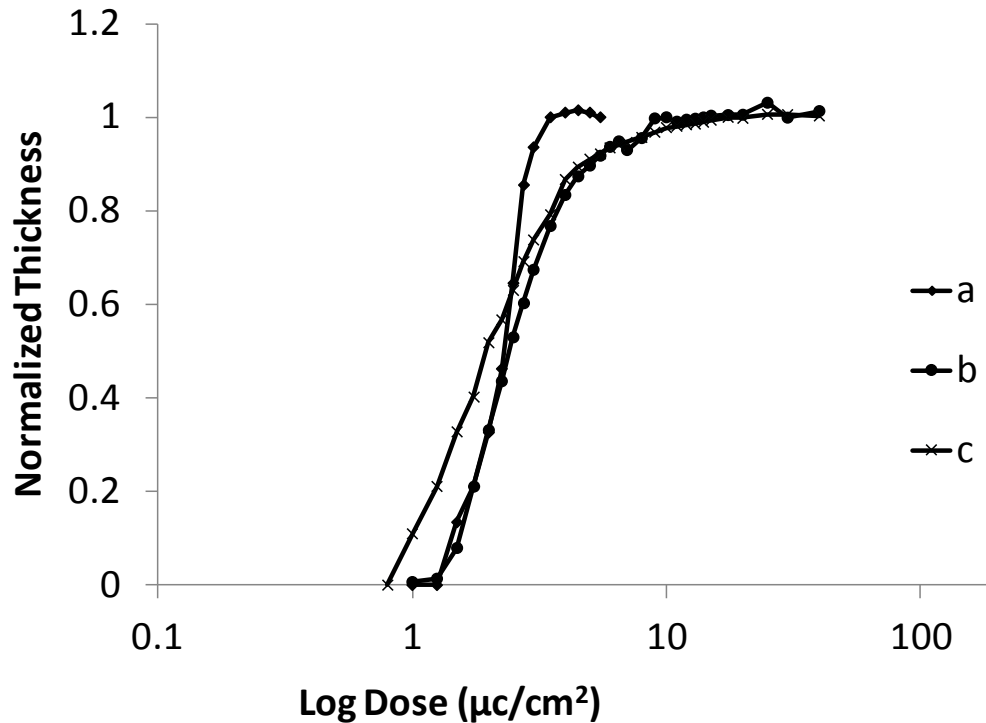
Figure 5.8 Effect of film thickness and developing on e-beam contrast and sensitivity of Avatrel 8000P with 3wt% TPEGE (a) 300 nm film developed in TMAH for 10 s; (b) 1100 nm film developed in TMAH for 16 s; (c) 1100 nm film developed in diluted TMAH for 30 s.

In the results discussed above, It was shown that the develop time affected the sensitivity of thick-film BF samples. PEB is another important processing step which can affect the polymer cross-linking and pattern quality. Three different PEB times (100°C) were used to investigate the impact of PEB on the sensitivity and contrast of thick-film samples. Figure 5.9 shows the e-beam contrast curves for BF samples post-exposure baked for 2, 4, and 6 min. All samples were developed in 0.26N TMAH developer for 12 s and the developed features had sharp edges and no residue. The sample with shorter PEB time had lower sensitivity but similar contrast to the samples with shorter PEB. The longer PEB time resulted in a higher degree of epoxy reaction (higher cross-linking), improved substrate adhesion, and lower residual solvent in the film.
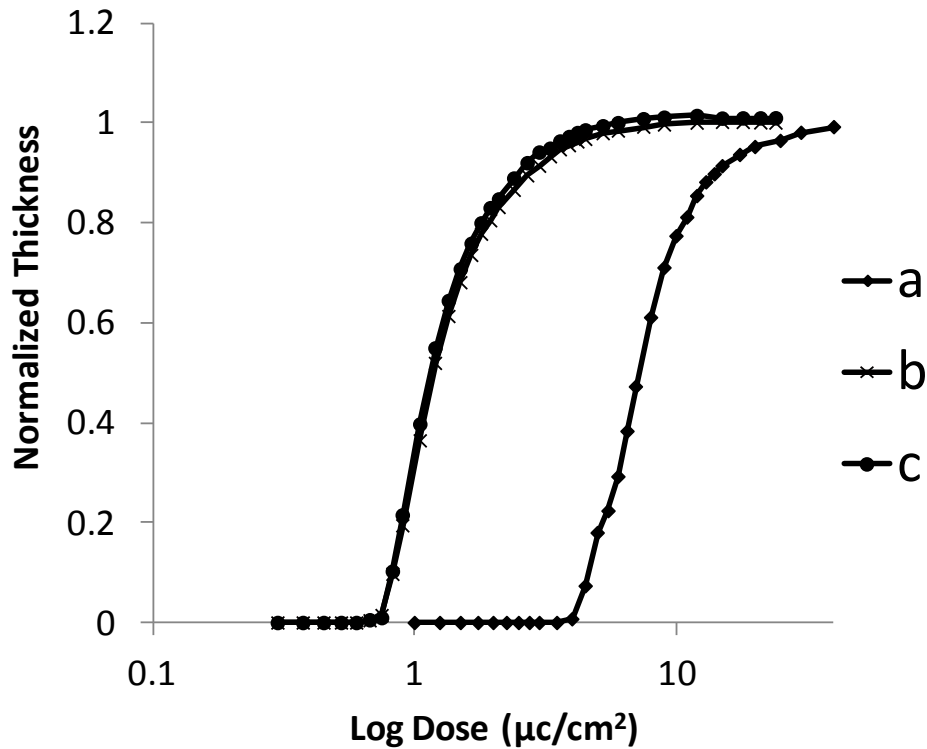
Figure 5.9 Electron-beam contrast curves for Avatrel 8000P at three different 100˚C PEB times (a) 2 min; (b) 4 min; (c) 6 min.

The impact of PEB time on the minimum exposure dose of the most sensitive formulation, BF with 3.4X PAG and no CPTX, was investigated. Two PEB times (100°C PEB) were investigated on 950 μm thick films. As shown in Figure 5.10, the longer PEB time did not affect the sensitivity of the polymer, and the contrast was slightly improved. The sample post-exposure baked for 6 min yielded a contrast of 7.9.
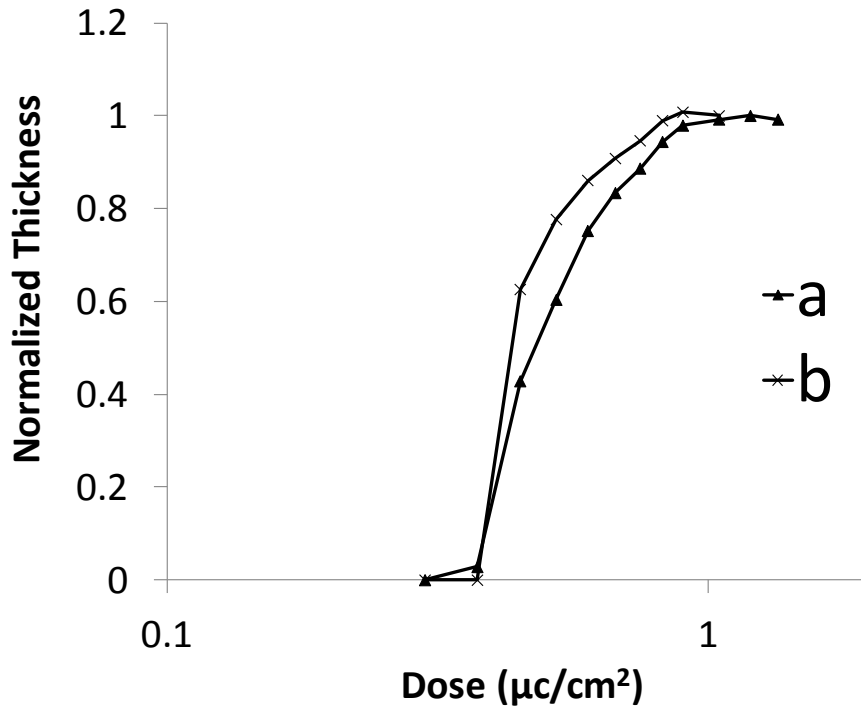
Figure 5.10 Electron-beam contrast curves for base formulation with 3.4 X PAG and no CPTX at two different 100˚C PEB times (a) 2 min; (b) 4 min.

Based on the results presented above, the exposure process was optimized for the BF samples. Lines 100 nm to 500 nm in width were fabricated using e-beam dose from 5 $\mu C/cm^2$ to 50 $\mu C/cm^2$. The resolution and LER of the 200 nm thick lines were compared. The optimum dose needed to resolve the 200 nm, 300 nm, 400 nm, and 500 nm wide lines was 40 $\mu C/cm^2$, 20 $\mu C/cm^2$, 15 $\mu C/cm^2$, and 10 $\mu C/cm^2$, respectively. Patterns produced at lower exposure dose suffered an unacceptable degree of swelling resulting in excessive LER. Figure 5.11 shows four of the exposure doses for the 200 nm wide lines: 5 $\mu C/cm^2$, 10 $\mu C/cm^2$, 25 $\mu C/cm^2$, and 40 $\mu C/cm^2$. The lines exposed at low doses were distorted (not straight) due to a high degree of swelling along with inadequate surface adhesion caused by low cross-link density in the films. The highest resolution was obtained at doses greater than 40 $\mu C/cm^2$. The 100 nm lines were not printed without excessive distortion.
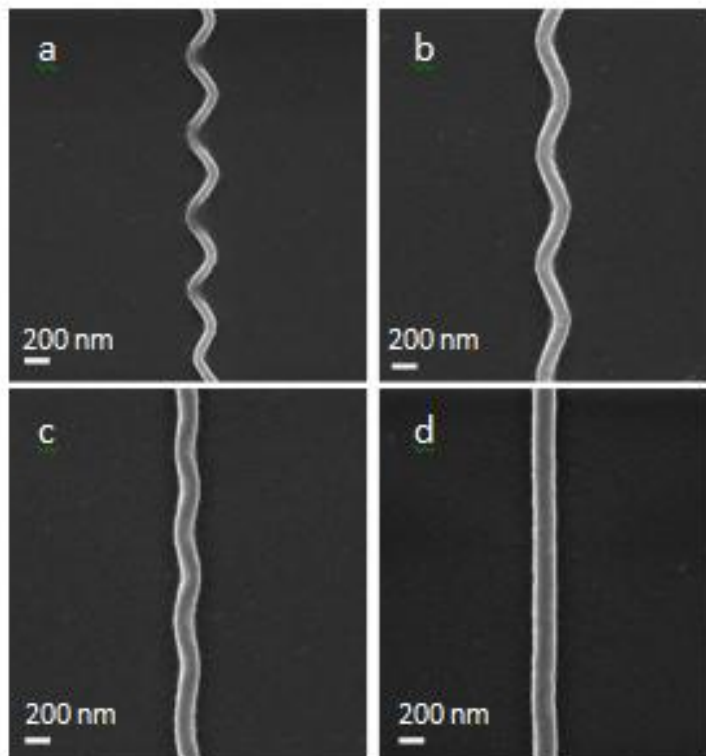
Figure 5.11 SEM images of Avatrel 8000P demonstrating 200 nm resolution at different exposure doses (a) 5 $\mu C/cm^2$; (b) 10 $\mu C/cm^2$; (c) 25 $\mu C/cm^2$; (d) 40 $\mu C/cm^2$.

The addition of TPEGE to the BF improved the cross-link density of the polymer and substrate adhesion. The exposure process was optimized for BF samples with 1wt% TPEGE to investigate the effect of the additional cross-linker on the resolution and pattern quality of the patterns. 200 nm thick films were exposed to doses from 5 $\mu C/cm^2$ to 50 $\mu C/cm^2$. A similar trend to the BF samples was observed, and the minimum exposure dose increased with the line width. However, a lower dose was required to pattern the 200 nm (35 $\mu C/cm^2$) and 300 nm (15 $\mu C/cm^2$) wide lines compared to the BF samples. In addition, it was possible to pattern 100 nm wide lines when TPEGE was added to BF, whereas these lines could not be resolved without TPEGE. The optimum dose for the 100 nm wide lines was 45 $\mu C/cm^2$. As shown in Figure 5.12, the 100 nm

wide lines at doses below 45 µC/cm^2 suffered from poor adhesion and curling. They

showed a high degree of swelling, especially at doses below 20 µC/cm^2. It can be

concluded that the addition of the tetra-functional epoxy cross-linker improved the

polymer cross-linking density and substrate adhesion as measured during the develop

cycle.
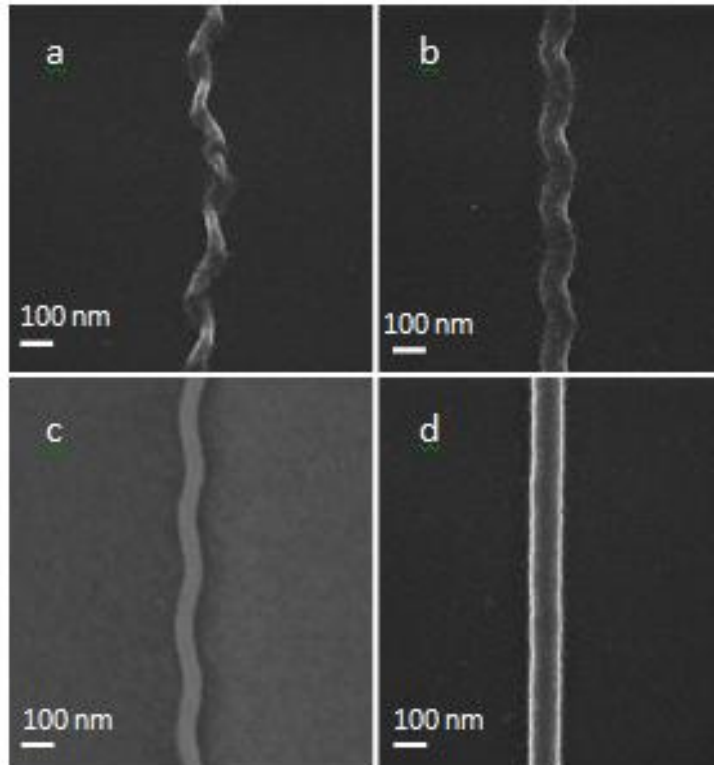
Figure 5.12 SEM images of Avatrel 8000P with 1 wt% TPEGE demonstrating 100 nm
resolution at different exposure doses (a) 10 µC/cm^2; (b) 20 µC/cm^2; (c) 35 µC/cm^2; (d)
45 µC/cm^2.

In addition to improved resolution, the LER also improved by adding the tetra-

functional cross-linker to the polymer mixture. The LER values were calculated by the

method described by Leunissen et al using an inspection length of 500 nm and

magnification of 300k [116]. The LER (3σ) was 17.9 nm for 200 nm BF lines and 13.5

nm for 100 nm BF lines with 1 wt% additional TPEGE. Formulations with higher

concentrations of TPEGE (3 wt% and 5 wt% TPEGE) resulted in larger LER for the 100 nm lines, which could be the result of higher cross-linking within the polymer. At high TPEGE concentrations, the mole ratio of TPEGE to PNB increased resulting in greater interconnectivity and cross-linking, increasing the LER.

Overall, the PNB formulations with the epoxy and PAG showed extremely high sensitivity compared to known e-beam resists.[111-115] The contrast, sensitivity and processing conditions of the PNB formulations are summarized in Table 5.1. Previously described chemically amplified e-beam resists have also been shown to have high e-beam sensitivity.[117, 118] PNB formulations with PAG and epoxy have higher sensitivity than and comparable contrast to other e-beam sensitive materials.[32, 119] The minimum resolution for isolated lines found for PNB formulations was 100 nm with a LER of 13.5 nm. Molecular e-beam resists have been shown to have high resolution and lower LER values due to the lower average molecular weight of the cross-linked materials.[29, 102, 105, 120] The PNB used in this study was significantly higher in molecular weight than the molecular resists used in the past. Improvements in minimum feature size and LER may be expected with lower molecular weight PNB formulations. The optimum cross-linking to produce the highest resolution and lowest LER was not investigated here and may be subject of future reports.

Table 5.1 The list of processing conditions, contrast, and sensitivity of PNB formulations.

Formulations	Thickness (nm)	PEB (min)	DT (s)	Developer	Contrast (γ)	E-50 (μC/cm^2)
BF	200	2	10	TMAH	0.8	7
BF	1025	2	12	TMAH	1.9	7
BF	1025	4	12	TMAH	1.9	1.2
BF	1025	6	12	TMAH	1.9	1.2
BF	1025	2	7/DI rinse/5	TMAH	3.7	1.1
BF	1025	2	19	diluted TMAH	3.7	1.1
BF with 1 wt% TPEGE	300	2	10	TMAH	1.1	5.4
BF with 1 wt% TPEGE	1100	2	16	TMAH	2.5	1.27
BF with 1 wt% TPEGE	1100	2	25	diluted TMAH	2.5	1.27
BF with 3 wt% TPEGE	300	2	10	TMAH	2.1	2.3
BF with 3 wt% TPEGE	1025	2	16	TMAH	2.1	2.3
BF with 3 wt% TPEGE	1025	2	30	diluted TMAH	2.1	2
BP (no additives)	200	2	10	TMAH	0.8	290

Table 5.1 Continued.

Formulations	Thickness (nm)	PEB (min)	DT (s)	Developer	Contrast (γ)	E-50 ($\mu C/cm^2$)
BP with 0.2X PAG	200	2	10	TMAH	0.8	230
BP with 0.5X PAG	200	2	10	TMAH	0.8	230
BP with 1X PAG	200	2	10	TMAH	0.8	230
BP with epoxy and no PAG	200	2	10	TMAH	0.8	67
BP with epoxy and 0.2X PAG	200	2	10	TMAH	0.7	55
BP with epoxy and 0.5X PAG	200	2	10	TMAH	0.7	55
BP with epoxy and 0.75X PAG	200	2	10	TMAH	0.8	7
BP with epoxy and 0.9X PAG	200	2	10	TMAH	0.8	7
BF	200	2	10	TMAH	0.8	7
BF with 3.4X PAG (no CPTX)	200	2	10	TMAH	4.4	0.48
BF with 3.4X PAG (no CPTX)	950	2	12	TMAH	4.4	0.48
BF with 3.4X PAG (no CPTX)	950	6	12	TMAH	7.9	0.43

5.3 Conclusions

Avatrel 8000P, a negative tone epoxy-based polynorbornene dielectric, has been shown to have very high e-beam sensitivity and acceptable resolution for 100 nm size features. The e-beam interaction with the components in the polymer formulation was studied. It was shown that the addition of a PAG to the polymer-epoxy mixture enhanced the contrast and sensitivity. Formulations with the additional tetra-functional cross-linker, TPEGE, showed improved contrast, sensitivity, and substrate adhesion. 100 nm structures with 13.5 nm LER were fabricated. The influence of the developing time, the developer concentration, PEB, and film thickness on the contrast and sensitivity were studied. Structures with contrast values as high as approximately 8 were fabricated at doses as low as 0.38 μC/cm^2.

CHAPTER 6

THERMAL CROSS-LINKING OF POLYNORBORNENE DIELECTRIC

In epoxy resins, degradation of the polyether type linkages is known to occur at temperatures in excess of 250°C [19]. Previously, Chiniwalla, et al. proposed a similar degradation scheme for polyether cross-linking degradation in cationically cured epoxy cross-linked PNB polymers at temperatures approaching 160°C based on the observation of changes in the mechanical properties of the cross-linked network with increasing cure temperature [66, 67]. In the study, the PNB is linked to a three dimensional cross-linked epoxy network through carboxylic ester bonds which prevent severing the PNB polymer backbone from the cross-linked epoxy network during degradation. Such degradation must, therefore, occur in the multifunctional epoxy additives included in the formulation. The proposed degradation mechanism results in cleavage of the polyether linkages reducing the density of cross-links in the developing a three dimensional cross-linked network. Similar decomposition mechanisms have been proposed for diglycidyl ethers of bisphenol A (DGEBA) type epoxies at temperatures in excess of 250°C [66, 67, 121].

In this report, the reactions that occur during epoxide ring opening, cross-linking, and degradation of Avatrel 8000P were tracked by FTIR. Film properties were a function of the degree of cross-linking in the polymer [93, 94]. The impact of cure conditions and degree of cross-linking on the electrical and mechanical properties of Avatrel 8000P were evaluated. The dielectric constant, reduced modulus, film residual stress, and solvent absorption in polymer films cured at different temperatures were studied. The relationship between the cure conditions and material properties were optimized to obtain high-quality Avatrel 8000P films.

6.1 Results

The multifunctional epoxide cross-linking and post-cure degradation reactions determine the overall degree of cross-linking in Avatrel 8000P and affect the electrical and mechanical properties of the polymer film [53]. In this work, the cure temperature of Avatrel 8000P was varied so as to optimize the dielectric and mechanical properties in the cured polymer film. The extent of epoxide ring opening was studied using FTIR to help determine the degree of cure. A 25 µm thick film of Avatrel 8000P was spin-coated onto a KBr disk and taken through a process sequence consisting of SB, exposure, PEB, and three successive cure cycles, each for 1 h at 160°C. The infrared spectra from 700 cm^{-1} to 950 cm^{-1} was obtained after each process step in roughly the same location on the KBr disk, Figure 6.1. Three peaks corresponding to asymmetric and symmetric epoxide ring stretches were observed at 913 cm^{-1}, 844 cm^{-1}, and 760 cm^{-1}. A significant degree of epoxy ring opening occurs as a result of the UV exposure and PEB processes, resulting in some degree of cross-linking before the final cure step.
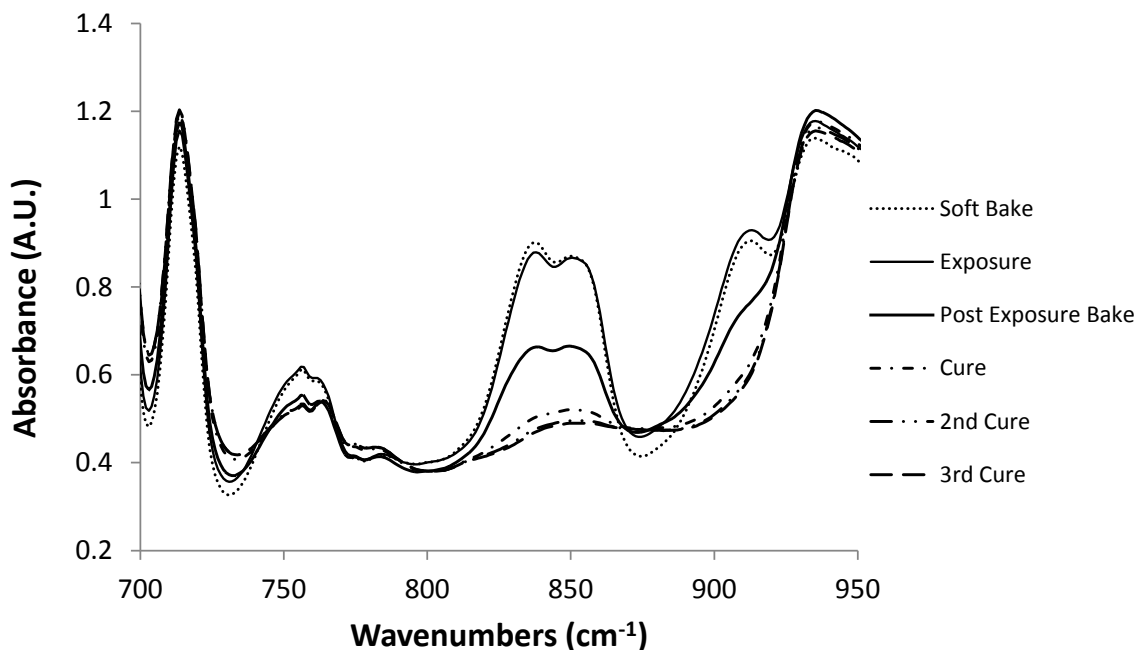
Figure 6.1 Changes in infrared spectrum of thin film Avatrel 8000P on KBr disc from 700 cm^{-1} to 950 cm^{-1} as a function of processing steps (SB: 100°C for 5 min; exposure dose: 170 mJ/cm^2; PEB: KBr plate inverted onto the hotplate, 100°C for 5 min; cure at 160°C for 1 h).

In this experiment, the PEB steps were performed using a KBr disk inverted onto a silicon wafer when placed on the hotplate. The inverted structure was needed because the 4 mm thick KBr disk has a lower thermal conductivity than the 0.525 mm thick silicon wafer, which was used as the substrate in all other experiments. When the KBr disk was PEB in the right-side up configuration, the film on the top surface of the KBr disk did not reach the desired temperature during the soft-bake and PEB. Inversion of the KBr disk onto a silicon wafer during hotplate bake brings the polymer film into thermal contact with the hotplate in a way that more closely replicates that of an Avatrel 8000P film directly on a silicon wafer baked in the right side up configuration.

After curing at 160°C for 1 h, the magnitude of the FTIR epoxy peaks decreased. When the cured sample was heated again to 160°C for 1 h, there was a small decrease in the peaks, suggesting that the epoxy ring opening reaction had not been taken to

completion after the first one hour cure. The third cure cycle at 160°C, Fig. 6.1, showed

no significant change in the FTIR spectra, indicating that complete epoxide ring opening

of the Avatrel 8000P had occurred after two hours at 160°C.

A significant reduction in the magnitude of the epoxide ring peak height was

observed in Fig. 6.1 after the UV exposure and PEB. The absorbance after PEB was

further investigated by repeating the experiment with the KBr disk placed on the hotplate

in the face-up condition, rather than in the face-down configuration, as in Fig. 6.1. Figure

6.2 shows the epoxide absorbance after PEB in the face-up condition, where the lower

conductivity of the KBr disk affected the polymer heating. As shown in Fig. 6.2, there is

no significant change in the IR spectra between the SB and PEB steps. This confirms

that the thermal insulation of the KBr disk indeed mitigates the effect of the PEB heat

treatment.
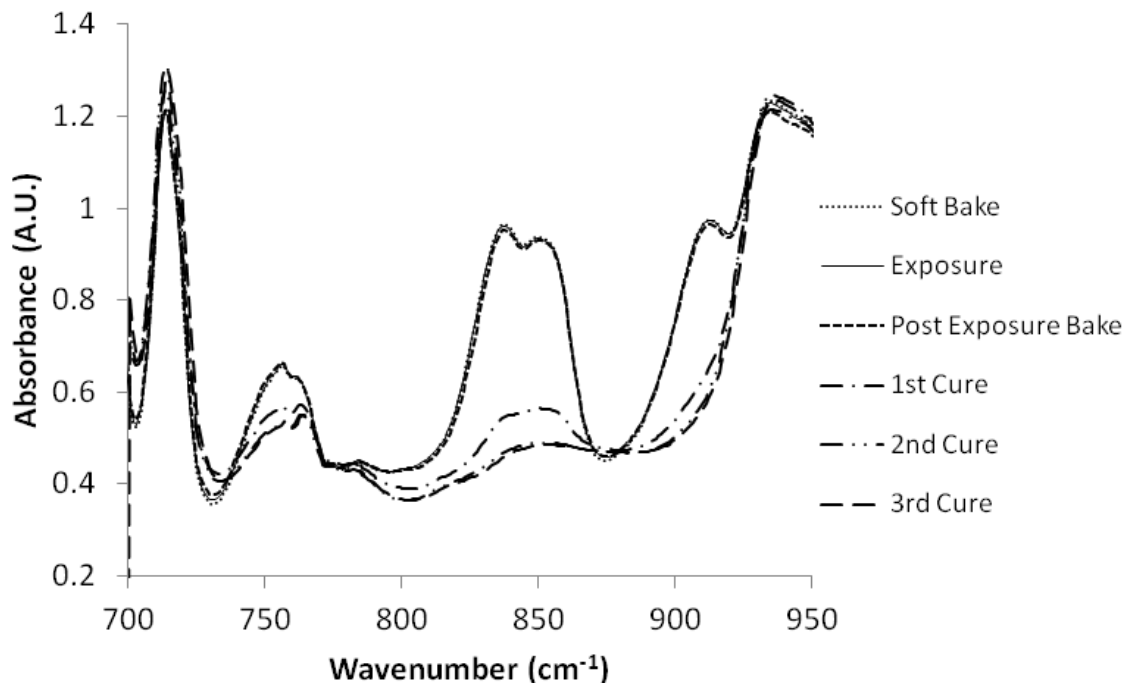
Figure 6.2 Effect of PEB method on Avatrel 8000P cross-linking (SB: 100°C for 5 min; exposure dose: 170 mJ/cm^2; PEB: KBr disc in up-right configuration on the hotplate, 100°C for 5 min; cure at 160°C for 1 h).

The peak height and area corresponding to the epoxide ring after the first cure at 160°C for 1 h were similar (relative to the background) to the corresponding ones in Fig. 6.1. To quantify the chemical changes in the cured film, the relative absorbance of the two samples were compared after the first cure step by using the height of the SB peak ($h_{soft\ bake}$) at 844 cm^{-1} as a spectral reference. The infrared absorbance corresponding to the epoxy group was compared using Equation (6.1).

$$\text{normalized absorbance} = \frac{h_{cure\ @\ 844\ cm^{-1}}}{h_{soft\ bake\ @\ 844\ cm^{-1}}} \qquad (6.1)$$

Where h is peak height using a background drawn by connecting the points at 800 cm^{-1} and 870 cm^{-1} of the spectrum. The peak height of the cured spectrum (h_{cure}) is used to

quantify changes in absorbance. The normalized absorbance after cure for the Avatrel 8000P film inverted on the hotplate (Fig. 6.1) and the sample baked in the face-up position (Fig. 6.2) were 0.18 and 0.27, respectively. The results show that the sample baked in the inverted PEB condition had a higher degree of epoxy ring opening after cure at 160°C for 1 h than the one which was post-exposure baked in the film-up configuration. Thus, not only does the PEB assist in creating a latent image for later development (the usual benefit of PEB), it also has an effect on how rapidly the film is cured at the final cure temperature. Hereafter, all FTIR samples on KBr in this study were post-exposure baked in the inverted configuration. The silicon substrates were all post-exposure baked in the up-right configuration.

To examine the effect of exposure of the Avatrel 8000P polymer film to developer (e.g. TMAH) on the extent of the epoxy ring opening reaction, new samples were prepared and were exposed to TMAH developer for 3 min after exposure to 170 mJ/cm^2 of 365nm UV radiation. As described above, all samples were post-exposure baked. This exposure dose was chosen because it represents full exposure of the Avatrel 8000P, which will be shown later. Figure 6.3 shows that there is very little change in the magnitude of the FTIR epoxy peak after the PEB and develop steps. However, a notable difference was observed between the sample cured after it was developed, Fig. 6.3, and the sample cured without being developed, Fig. 6.1. The normalized absorbance after cure was 0.18 for the undeveloped sample (Fig. 6.1), and was 0.12 for the developed sample (Fig. 6.3). This shows that a higher degree of epoxy ring opening occurred when the sample was exposed to the aqueous base developer prior to the first cure for 1 h. Further, there was no significant change in the FTIR after multiple cure cycles (each for 1h) when the sample had been developed, Fig. 6.3, showing that complete epoxy ring opening occurred after the first cure at 160°C for 1 h. Previous studies ignored the develop step during their cure studies assuming that it has no effect on curing [53]. However, the corresponding sample cured without having been developed, Fig. 6.1, did

eventually come to the fully cured state after multiple cure cycles at 160°C for 1 h in each cure cycle. This result shows that developing in TMAH assists in the epoxy ring opening and final cure.
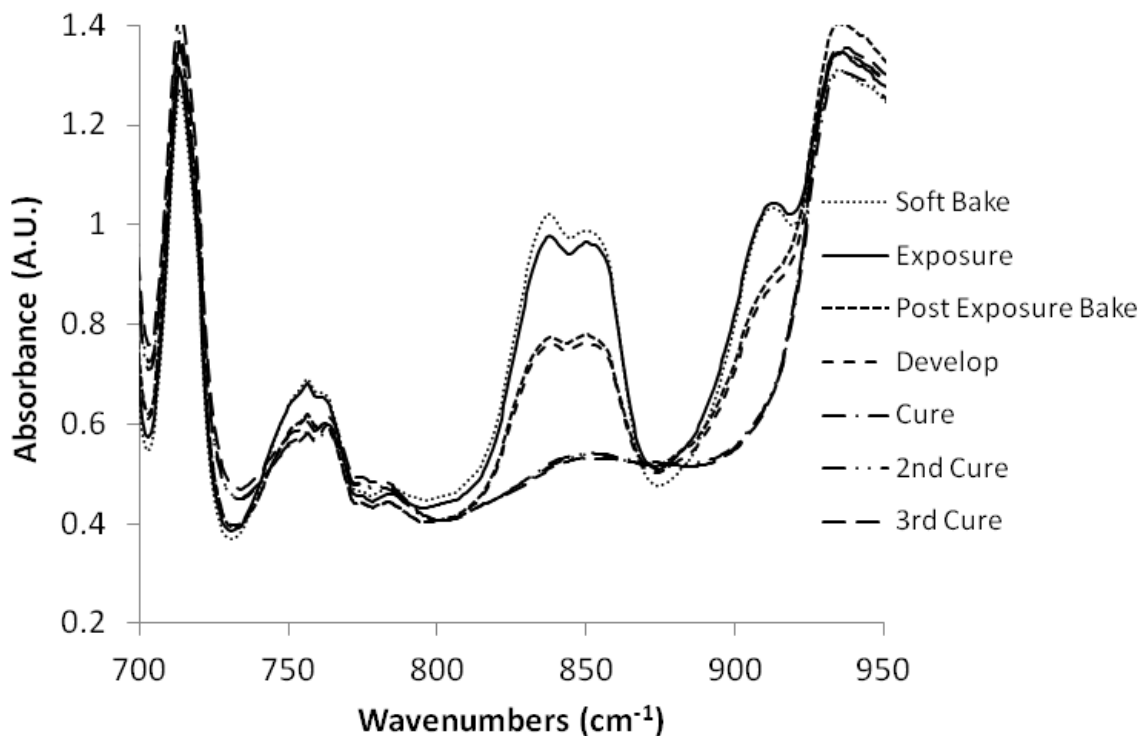
Figure 6.3 Effect of developing on epoxide ring opening of Avatrel 8000P (soft bake: 100°C for 5 min; exposure dose: 170 mJ/cm^2; post-exposure bake: KBr disc inverted onto the hotplate, 100°C for 5 min; develop for 3 min; cure at 160°C for 1 h).

There are several possible reasons for an exposure to TMAH assisting in the final cure. Exposure of the Avatrel 8000P film to aqueous base could cause some degree of neutralization and dissolution of the photogenerated acid created during exposure. The PAG itself and byproducts (e.g. conjugate base) may also dissolve during developing. While leaching out the acid from the polymer film decreases the amount of acid catalyst, it may provide more free volume and thus higher mobility for the activated epoxy moieties within the film to move. Alternatively, incorporation of the TMAH base in the

PNB can plasticize the film. This observation is congruent with the fact that the residual stress in the film decreases after developing in the TMAH, as shown later in this paper. Additionally, the TMAH developer can act as a catalyst for the reaction of the carboxylic acid pendant on the polymer with the epoxy groups contained in the multifunctional cross-linkers. This would improve the cross-linking within the polymer. In any event, the beneficial effects of the developing step are clear. The exact nature of the improved cross-linking with development may be subject of a future publication.

The cross-linking of Avatrel 8000P films can be activated either photolytically or thermally. In the photocross-linking of the polymer, the PAG is activated by UV radiation creating a proton which can catalytically activate epoxy ring opening on the multifunctional additive cross-linkers. The activated epoxy can react with the carboxylic acid groups pendent from the PNB backbone. In the thermal cross-linking of Avatrel 8000P, the PAG can be thermally activated followed by acid catalyzed epoxy activation. Figure 6.4 shows the contribution of the thermal activation of the PAG on the epoxy ring opening reaction. The sample was not exposed to UV radiation and was cured at the same condition as in Fig. 6.1 (160°C for 1 h). The 100°C, 5 min bake, which was identified as PEB in Fig. 6.1, resulted in no ring opening in Fig. 6.4, where no exposure occurred. That is, the PEB results in ring opening only when the sample is photolytically activated (exposed to UV radiation). However, the 1 h, 160°C cure does result in epoxy ring opening regardless of UV exposure, although the UV exposure increases the percent of epoxy ring opening. The normalized absorbance of the epoxy groups after cure was 0.29 in Fig. 6.4, compared to 0.18 for the exposed sample in Fig. 6.1. This results show that to achieve complete cross-linking of Avatrel 8000P at low cure temperature of 160°C, both photo and thermal activation of epoxide rings are required.
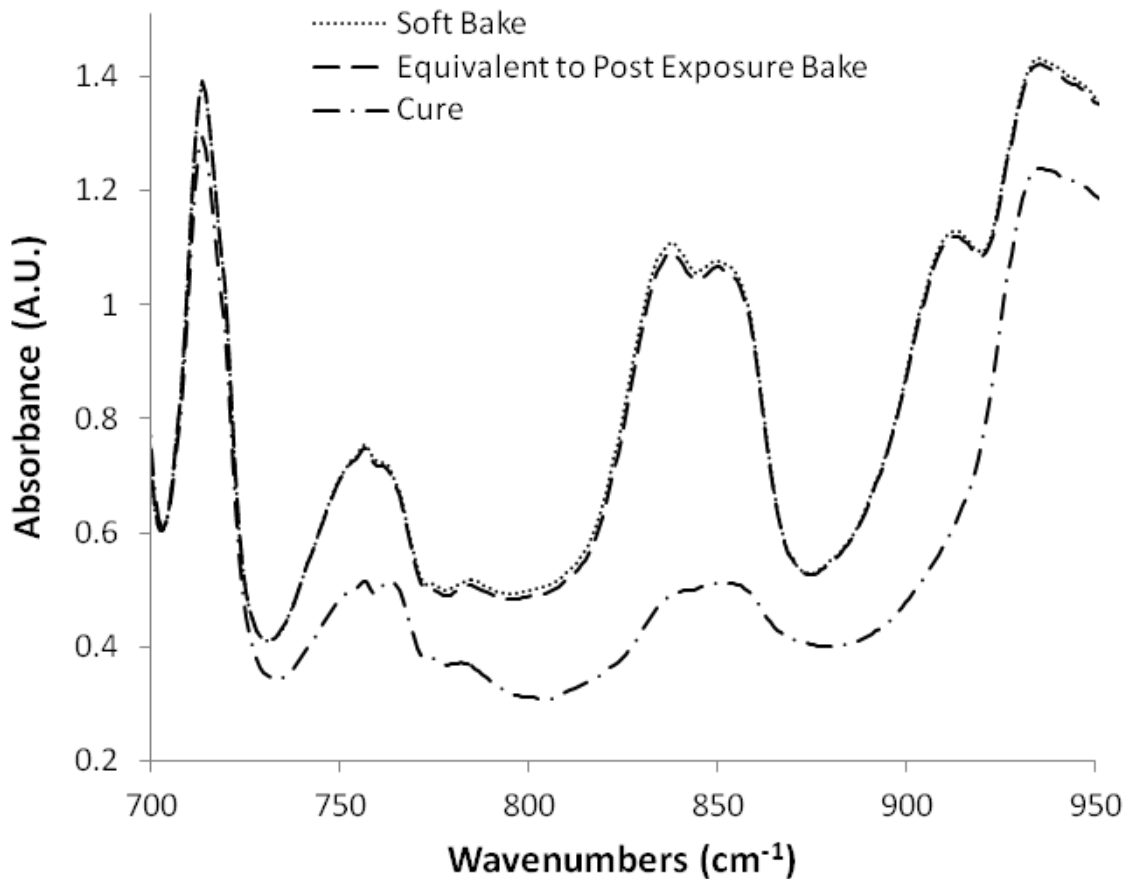
Figure 6.4 Effect of thermal cure on cross-linking of unexposed Avatrel 8000P (SB: 100°C for 5 min; PEB: KBr disc inverted onto the hotplate, 100°C for 5 min; cure at 160°C for 1 h).

Since UV exposure is critical to developing and curing of the polymer, the effect of UV exposure dose on the degree of conversion of the epoxy ring opening reaction in the polymer film was studied. A UV exposure dose sufficient to fully activate the PAG is desired after which higher doses have little or no effect on cure. An Avatrel 8000P film was exposed to a 450 mJ/cm^2 UV dose (compared to the 170 mJ/cm^2 used in Fig. 6.1) and the FTIR spectrum was obtained, Figure 6.5. After the PEB step, it can be seen that the 450 mJ/cm^2 exposure dose caused more epoxy conversion compared to the 170 mJ/cm^2 dose. After PEB, the peak at 844 cm^{-1} decreased by 55% for the 450 mJ/cm^2 exposure dose, compared to a 38% decrease for the 170 mJ/cm^2 exposure dose, Fig. 6.1.

Additionally, there is essentially no change in the epoxy absorbance between the first cure at 160°C for 1 h and the second and third cure at 160°C (1 h each) because the film was fully cured after the first cure cycle, whereas there was a slight decrease in the epoxy peak after first cure in Fig. 6.1. This shows that there is a slight difference in the cure time when a higher UV dose was used. This change in epoxy absorbance between the first and second cure, Fig. 6.1, was not viewed as a significant change since 170 mJ/cm^2 was a sufficient dose for full development of the latent image.
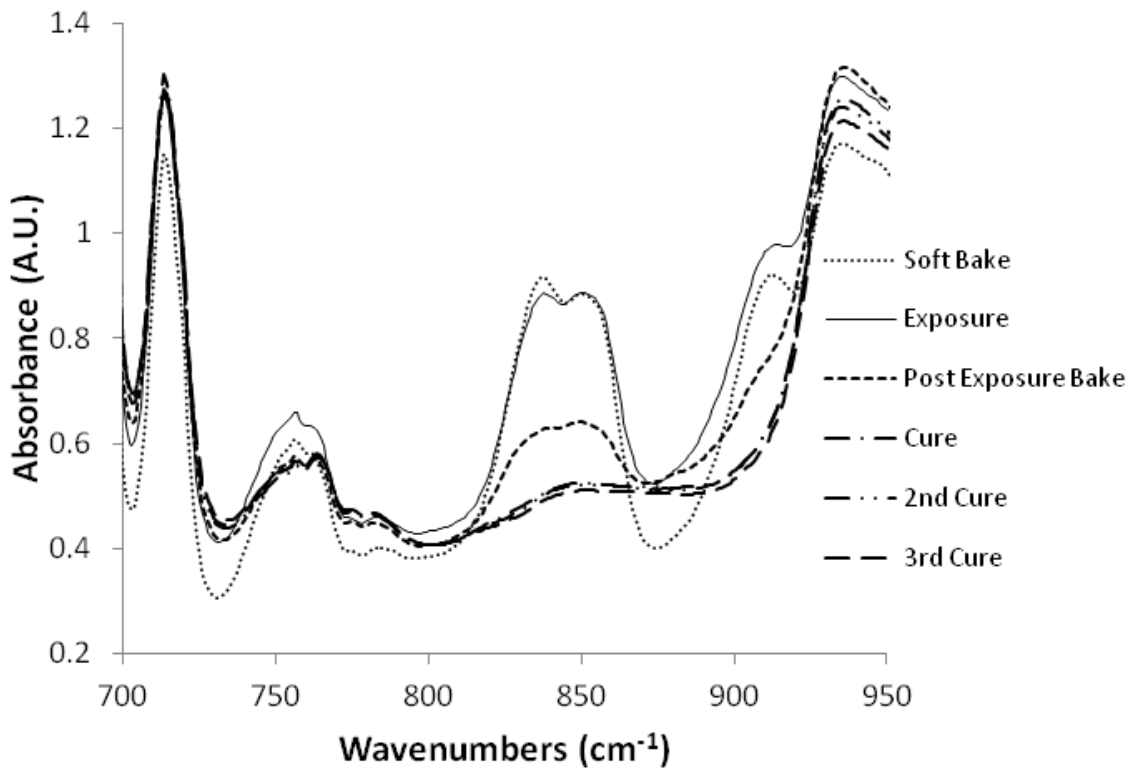
Figure 6.5 Effect of exposure dose on cross-linking degree of Avatrel 8000P (SB: 100°C for 5 min; exposure dose: 450 mJ/cm^2; PEB: KBr disc inverted onto the hotplate, 100°C for 5 min; cure at 160°C for 1 h).

The effect of exposure dose on the mechanical properties of cured Avatrel 8000P was investigated for UV doses ranging from 100 mJ/cm^2 to 1728 mJ/cm^2. The mechanical properties were measured by nanoindentation as a function of exposure dose

110

for a set of samples cured at 160°C for 1 h, and for a set of samples cured at 200°C for 1 h. Nanoindentation was performed on the samples, and the reduced modulus was calculated. Higher values of reduced modulus indicate a higher cross-link density for the cured films. The reduced modulus values increased nearly 45% for the samples exposed at doses from 100 mJ/cm^2 to 200 mJ/cm^2, as shown in Figure 6.6a. The increase in modulus is attributed to a higher cross-link density due to UV exposure, all other variables held constant. At exposure doses above 400 mJ/cm^2, the reduced modulus was essentially constant at 2.8 GPa (the standard deviation was 0.02). This suggests that at doses above 400 mJ/cm^2, the maximum PAG activation was achieved and doses higher than 400 mJ/cm^2 resulted in no further increase in acid catalyst concentration. These results were consistent with the results obtained from the samples cured at 200°C for 1 h, as shown in Fig. 6.6b. The average modulus for films cured at 200°C was 2.6 GPa with a range of 3.8% for all values from 200 mJ/cm^2 to 1575 mJ/cm^2. The decrease in modulus for films cured at 200°C, compared to the values at 160°C, is attributed to the slight degradation of the polyether crosslinking linkages between multifunctional epoxy additives at 200°C. It should be noted that at 200°C, the minimum dose required for PAG activation to obtain full cross-linking is lower than that for samples cured at 160°C. This is due to thermal activation of the PAG.
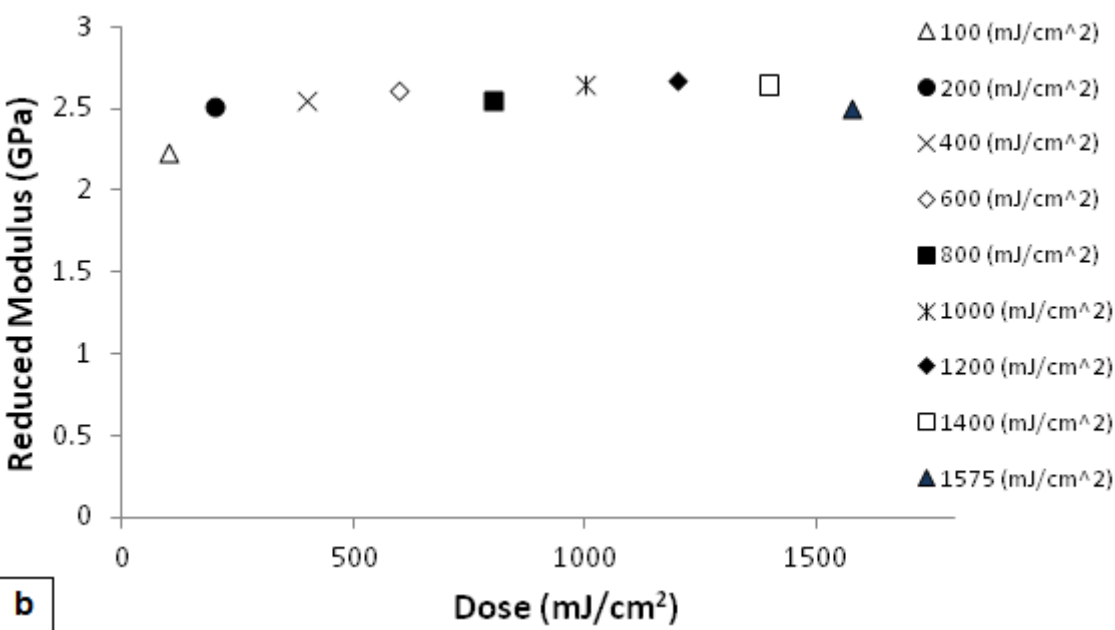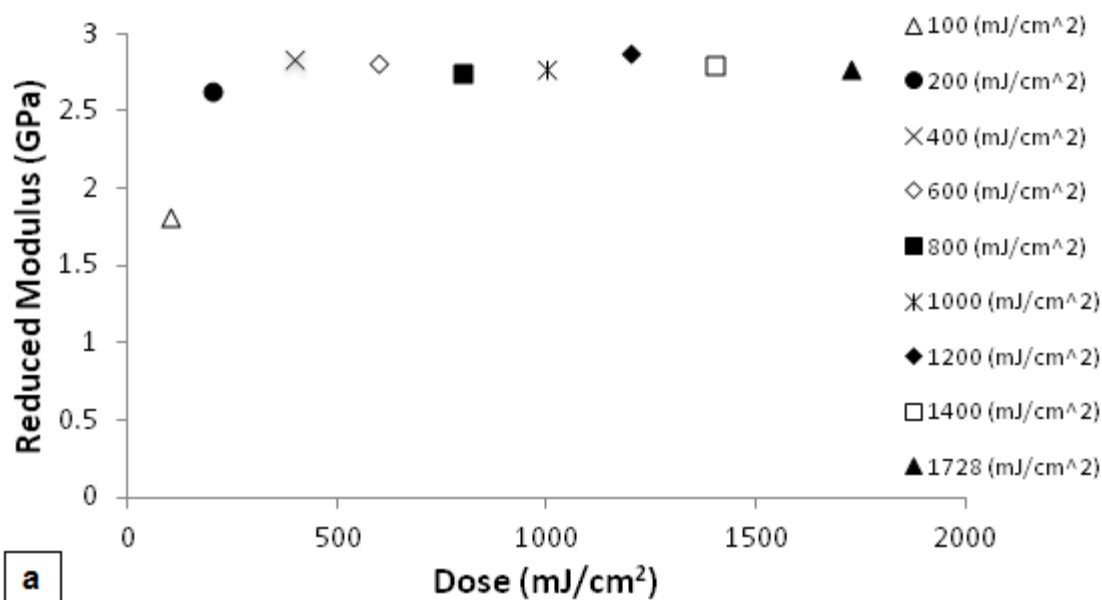
Figure 6.6 Reduced modulus dependence of cured Avatrel 8000P on exposure dose (a) cure at 160°C for 1 h; (b) cure at 200°C for 1.

Thus far, it has been shown that the method of the PEB, exposure to the TMAH developer, and concentration of the acid catalyst result in a higher degree of epoxide ring opening and cross-linking. FTIR spectra were taken after each step for an Avatrel 8000P

sample exposed to a 450 mJ/cm^2 (365 nm) UV dose, post-exposure baked on an inverted

KBr disk on a hotplate, and cured at 160°C for 1 h after development for 3 min. As

shown in Figure 6.7, full epoxide ring opening was achieved after cure. The samples

cured for extended periods of time at 160°C showed no detectable change in the height of

the epoxy peaks in the IR spectra. This confirms that the epoxy ring opening reaction

was complete after curing at 160°C for 1 hour. Compared to Fig. 6.1, which showed a

small change in epoxide ring opening (normalized absorbance of 0.18) after the first cure

at 160°C for 1 h, Fig. 6.7 shows a fully cured polymer (normalized absorbance of 0.11)

after the first 1 h cure.
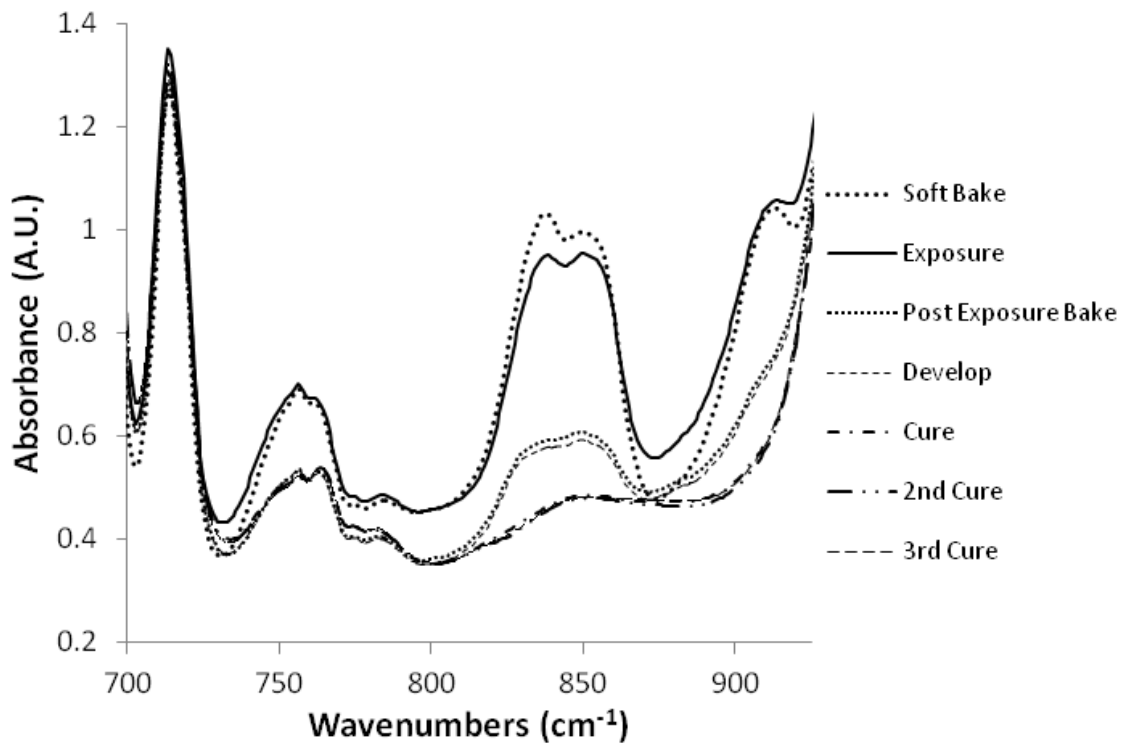
Figure 6.7 Changes in spectrum of Avatrel 8000P from 700 cm^{-1} to 950^{-1} as a function of processing conditions (SB: 100°C for 5 min; exposure dose: 450 mJ/cm^2; PEB: KBr disc inverted onto the hotplate, 100°C for 5 min; develop for 3 min; cure at 160°C for 1 h).

Lowering the cure temperature is important in some packaging applications due to

the presence of temperature sensitive materials and as a way to lower the overall thermal

profile of the process. To investigate the lowest cure temperature to achieve full cross-linking of Avatrel 8000P after 1 h cure, samples cured at 140°C and 150°C for 1 h were prepared. All other processing variables were held constant. The FTIR analysis of the samples cured at 140°C for 1 h showed incomplete epoxy ring opening, suggesting a reduced degree of cross-linking. Thus, a higher cure temperature or longer cure time at 140°C is required for full curing of Avatrel 8000P. A sample cured at 150°C, Figure 6.8, showed that very little epoxy remained after being cured for 1 h suggesting that a 150°C cure for 1 h may too be adequate. There was only a slight change in the epoxy peak after the second cure at 150°C.

The extent of cross-linking plays an important role in establishing the properties of the cured polymer [93, 94]. To evaluate the effect the cure temperature on the mechanical stability of the cured Avatrel 8000P, films cured at temperatures between 140°C to 240°C were evaluated using nanoindentation. Nanoindentation was performed on 2 to 4 samples prepared at each cure temperature. The nanoindentation results were repeated on each sample 2 or 3 times. Table 6.1 shows the number of samples for each cure temperature and the number of indentation measurements performed on each sample. It was found that it is especially important to calibrate the nanoindentation tool before, during and after a set of experiments to make sure no drift occurred in the calibration. In each set of experiments, multiple calibrations were performed to ensure accuracy. In addition, each set of measurements were performed during a single 96 h period.
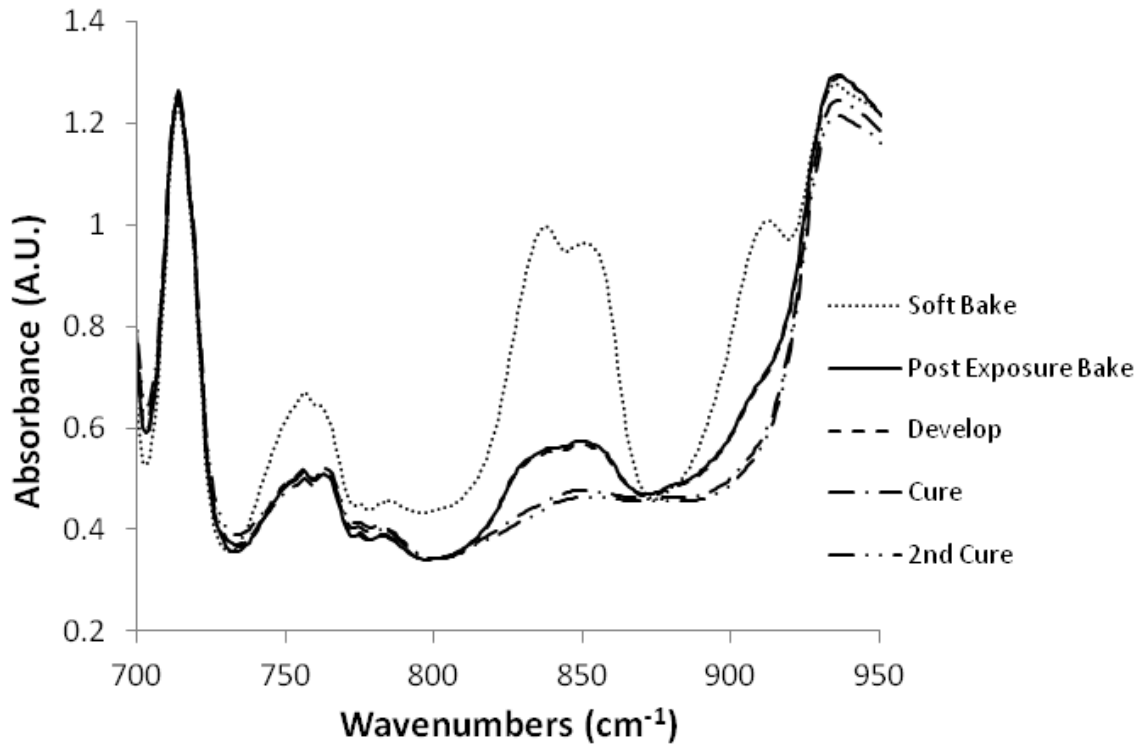
Figure 6.8 Changes in spectrum of Avatrel 8000P from 700 cm^{-1} to 950^{-1} as a function of processing conditions (SB: 100°C for 5 min; exposure dose: 450 mJ/cm^2; PEB: KBr disc inverted onto the hotplate, 100°C for 5 min; develop for 3 min; cure at 150°C for 1 h).

Table 6.1 Summary of nano-indentation samples.

Cure Temperature. (°C)	# Sample	# meas./sample
140	2	3
160	4	3
180	3	2
200	4	2
220	4	3
240	2	2

Figure 6.9 shows the reduced modulus of developed Avatrel 8000P as a function of cure temperature using a 1 h cure. Each data point is the average of all measurements performed on all samples cured at each temperature. The reduced modulus value increased nearly 10% for the samples cured between 140°C and 160°C. The modulus reached the maximum value of 2.8 GPa. The increase in modulus is likely due to a higher cross-link density as the cure temperature increased. When the cure temperature was increased from 160°C to 240°C, the reduced modulus decreased from 2.8 GPa to 2.4 GPa due to a higher degree of degradation of the polyether cross-links between the multifunctional epoxy additives at the higher cure temperature. The maximum reduced modulus value, 2.8 GPa, was obtained after curing at 160°C for 1 h.
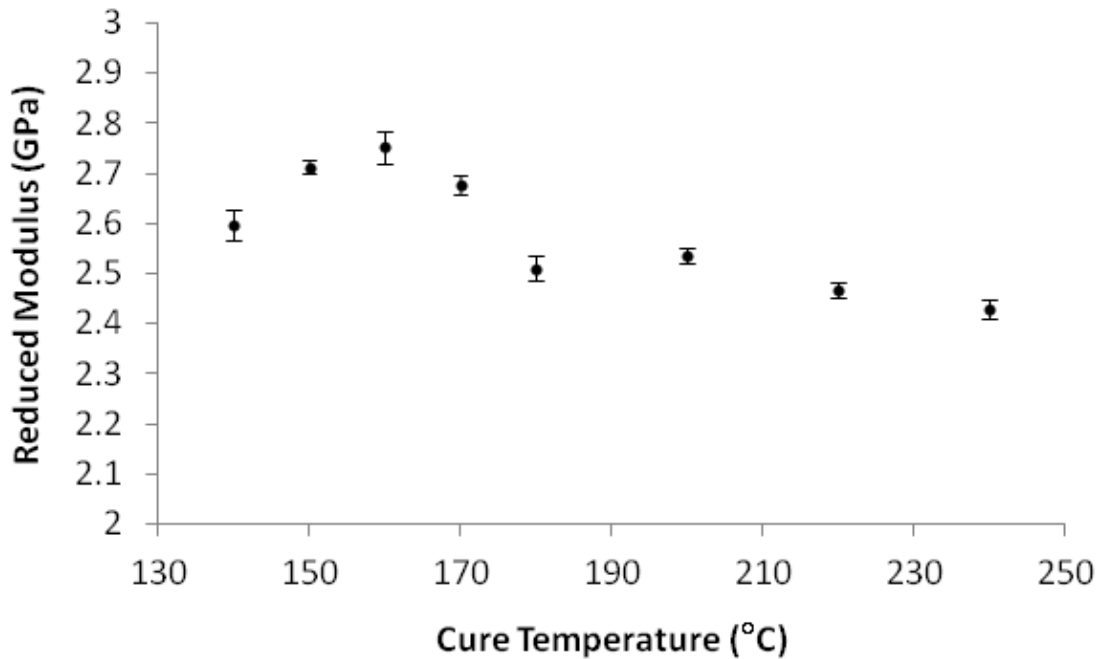
Figure 6.9 The reduced modulus of developed Avatrel 8000P films as a function of cure temperature from 140°C to 240°C.

The same trend was observed for the samples that were not exposed to the TMAH developer, Figure 6.10. The maximum reduced modulus value, 2.8 GPa, was obtained

for the sample cured at 160°C for 1 h. However, the reduced modulus dropped 15%

when the temperature was increased from 160 °C to 240 °C compared to 12% drop for the

developed samples. The difference between the developed and non-developed samples

could be linked to the contribution of the TMAH developer to curing, as noted above.

The hardness values showed the same trend and the highest hardness value, 0.13 GPa,

was achieved after cure at 160°C for both developed and non-developed samples (results

are not shown here).
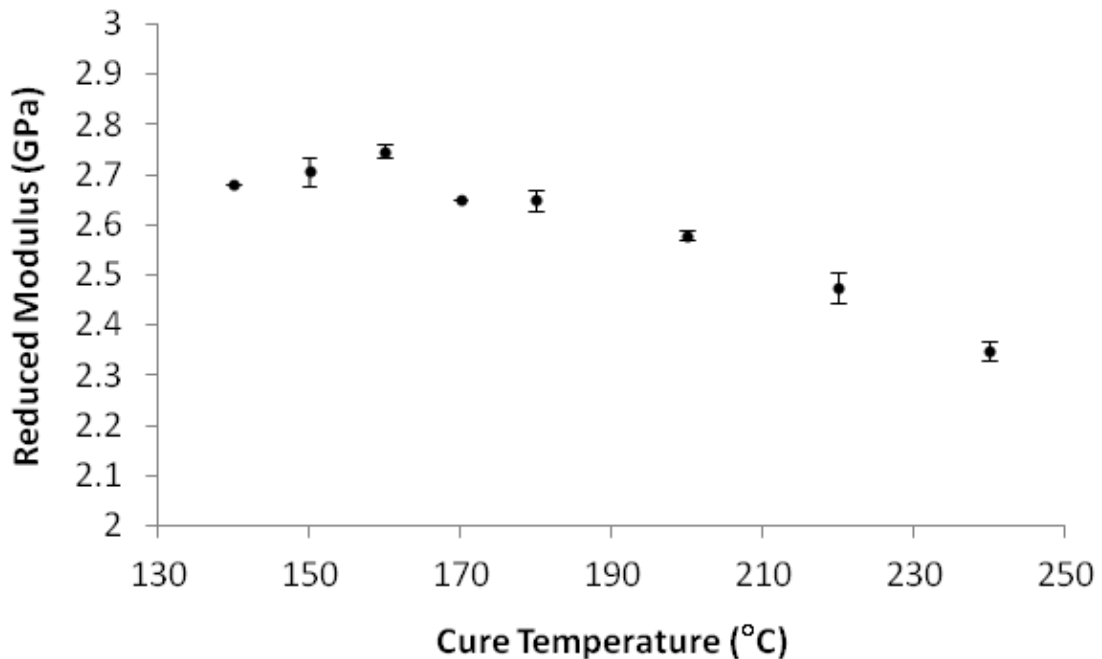
Figure 6.10 The reduced modulus of Avatrel 8000P films without developing as a
function of cure temperature from 140°C to 240°C.

Swelling experiments were performed to investigate the degree of Avatrel 8000P

cross-linking. The solvent swelling in a polymer film is inversely related to the degree of

cross-linking between polymer chains, other factors remaining constant [50, 94, 122,

123]. 25 μm thick polymer films made by spin-coating on silicon wafers were UV

exposed at 450 mJ/cm^2 and cured for 1 h. The mass of each sample was measured at 7

different times during the 25 h swelling period and each data point is the average of four measurements. Figure 6.11 shows an increase in weight with swelling time. The swelling ratio was less for samples cured at 160°C compared to those cured at 140°C. This shows that curing at 160°C for 1 h leads to higher cross-link density than samples cured at 140°C. Raising the cure temperature from 160°C to 240°C increased the swelling from 3.1% to 4.1%. The decrease in the cross-link density, as noted above, for films cured at higher temperature is likely due to degradation of polyether cross-links between the multifunctional epoxy additives at higher cure temperatures. This data is consistent with the hardness and reduced modulus results.
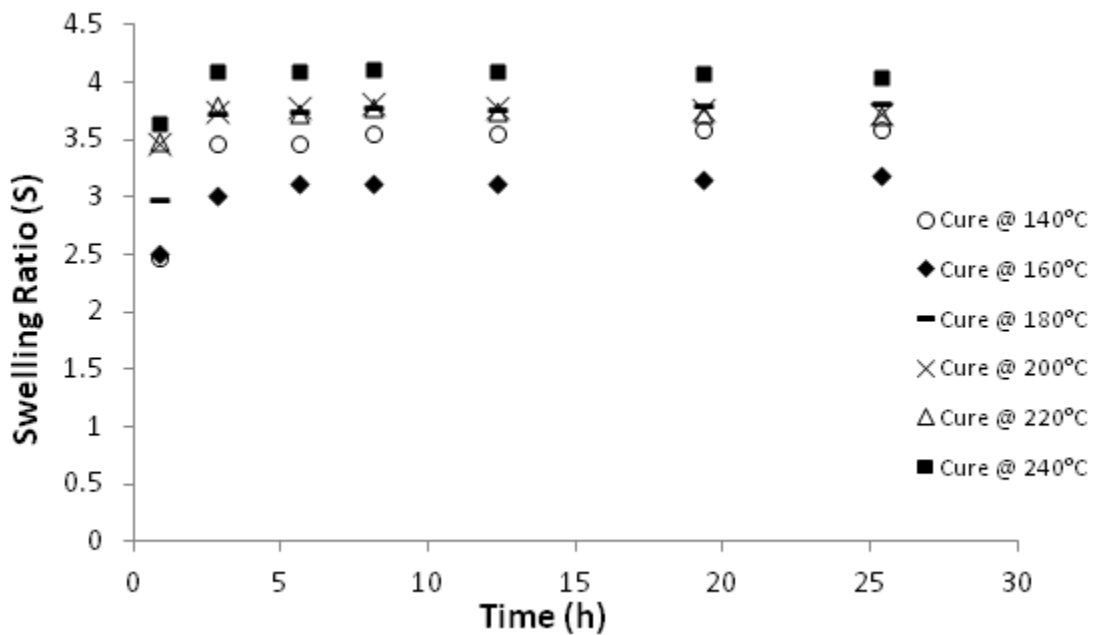
Figure 6.11 Effect of cure temperature on swelling ratio of Avatrel 8000P.

The cure temperature and quality of the three-dimensional cross-link network can have a dramatic effect on the residual stress of the polymer film. Residual stress in a polymer-coated substrate is generated as a result of solvent evaporation, shrinkage during the cross-linking of the polymer film, and mismatch of the thermal expansion coefficient between the polymer film and the substrate. The magnitude of the film stress is related to the CTE, Poisson's ratio, biaxial modulus of the polymer film, and stress neutral temperature of the polymer film, all of which can change with cure temperature, especially the stress neutral temperature [124].

To evaluate the effect of cure temperature, the residual stress of Avatrel 8000P films was characterized for samples after each process step and cure temperature. The measurements were repeated on four different samples (10 measurements each) for each processing step and the standard deviation for all measurements was 0.78. As shown in Figure 6.12, the residual stress of a 45 μm thick Avatrel 8000P films ranged from 13 MPa after soft-bake to 20 MPa after cure at 160°C for 1 h. The creation of residual stress in the soft-baked film was primarily because of solvent removal and subsequent shrinkage of the polymer film. The CTE mismatch during the thermal process also contributes to the stress build-up in the soft-baked film. After PEB, the modulus of the polymer film increased due to the acid-catalyzed cross-linking within the film, resulting in an increase in stress of the post-exposure baked film. The decrease in the Avatrel 8000P film stress after developing can be the result of film softening and swelling. The high residual stress of 20 MPa after cure was due to the high cross-link density of the polymer and the CTE mismatch.
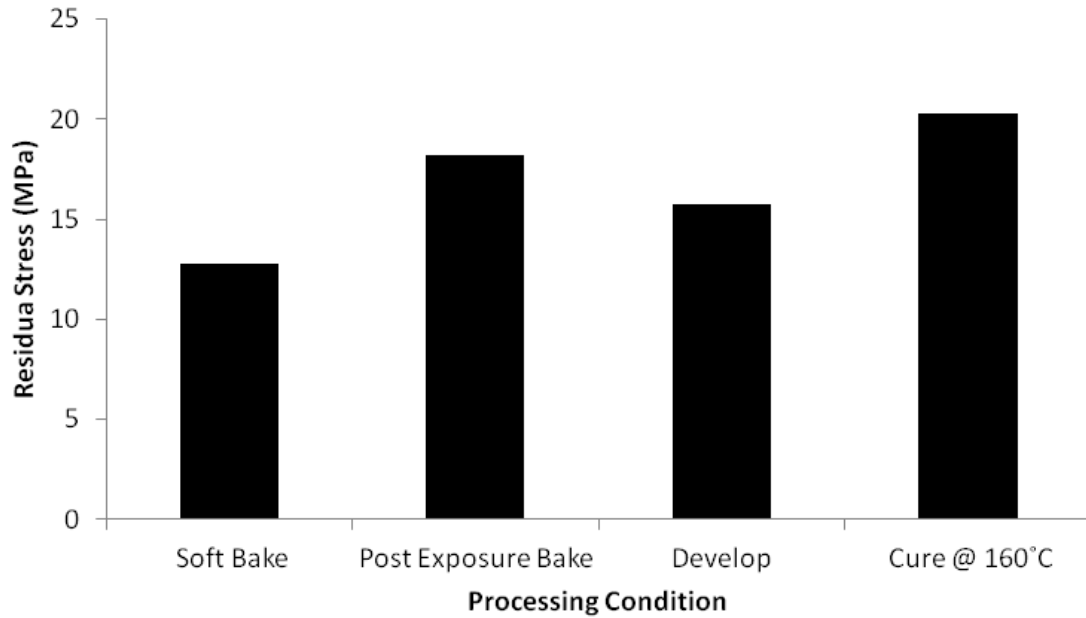
Figure 6.12 Changes in internal film stress of Avatrel 8000P as a function of processing conditions (SB: 100°C for 5 min; PEB: 100°C for 5 min; develop for 3 min; cure at 160°C for 1 h).

The residual stress of Avatrel 8000P was investigated for cure temperatures ranging from 140°C to 220°C. The measurements were performed on two different samples at each cure temperature and 10 values were taken on each sample. The results are presented in Figure 6.13, where each data point is the average of all measurements performed on all samples at each cure temperature. The residual stress of the polymer ranged from 18 MPa to 25 MPa with increasing cure temperature (each for 1 h), as shown in Fig. 6.13. The increase of residual stress values for samples cured from 140°C to 160°C is likely due to higher cross-link density and increased rigidity of the polymer. The drop in the film stress for the film cured at 180°C, compared to those cured at slightly lower temperatures, can be attributed to degradation of polymer at high cure temperature. The increase in stress at even higher temperatures may be due to a higher stress neutral temperature, although the trend is not as obvious as the other physical properties discussed above. Overall, the film stress increased about 30% from the lowest

to highest value for cures from 180°C to 220°C. The individual contributions of the different factors (i.e. stress neutral point, CTE mismatch, modulus of the film, and rate of the degradation reaction) was not resolved.
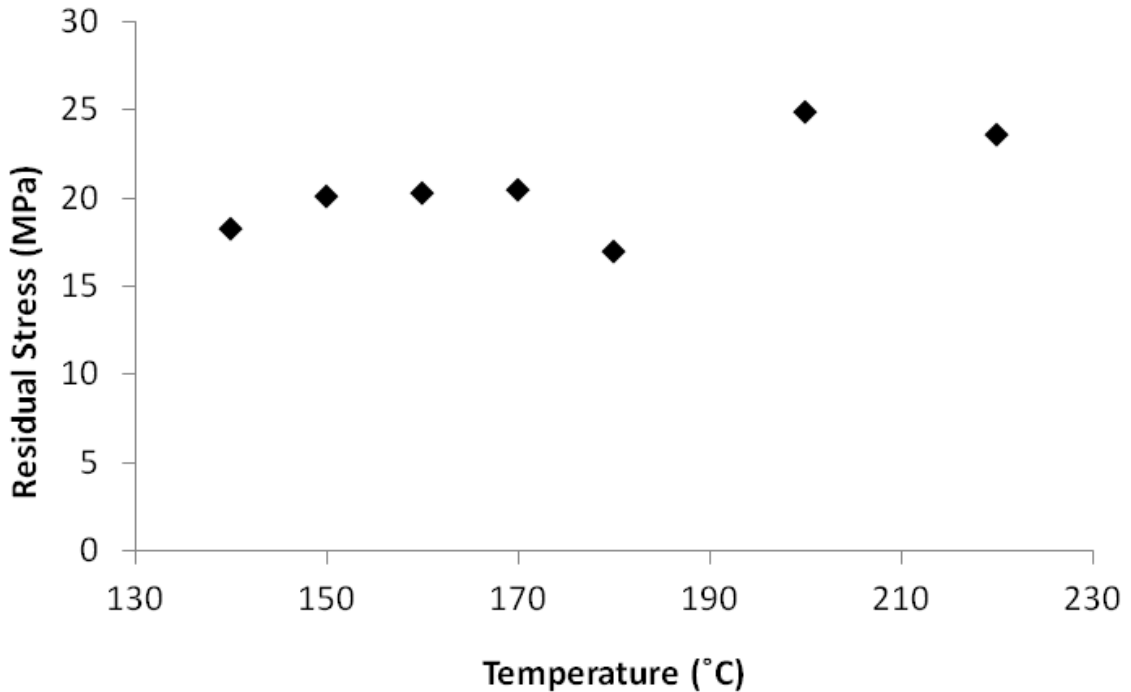
Figure 6.13 Residual stress of Avatrel 8000P as a function of cure temperature from 140°C to 240°C.

In addition to mechanical integrity, a polymer film must also have a high level of thermal stability for successful implementation of polymer microstructures in MEMS, microelectronics, and photonics applications. To evaluate the thermal stability of Avatrel 8000P, decomposition versus temperature of Avatrel 8000P was characterized through TGA. Figure 6.14 shows the TGA scans of Avatrel 8000P cured at 160°C for 1 h which resulted in the decomposition temperature of 328°C. To obtain the T_g for the cured film, DSC was performed which resulted in the T_g of 268°C.
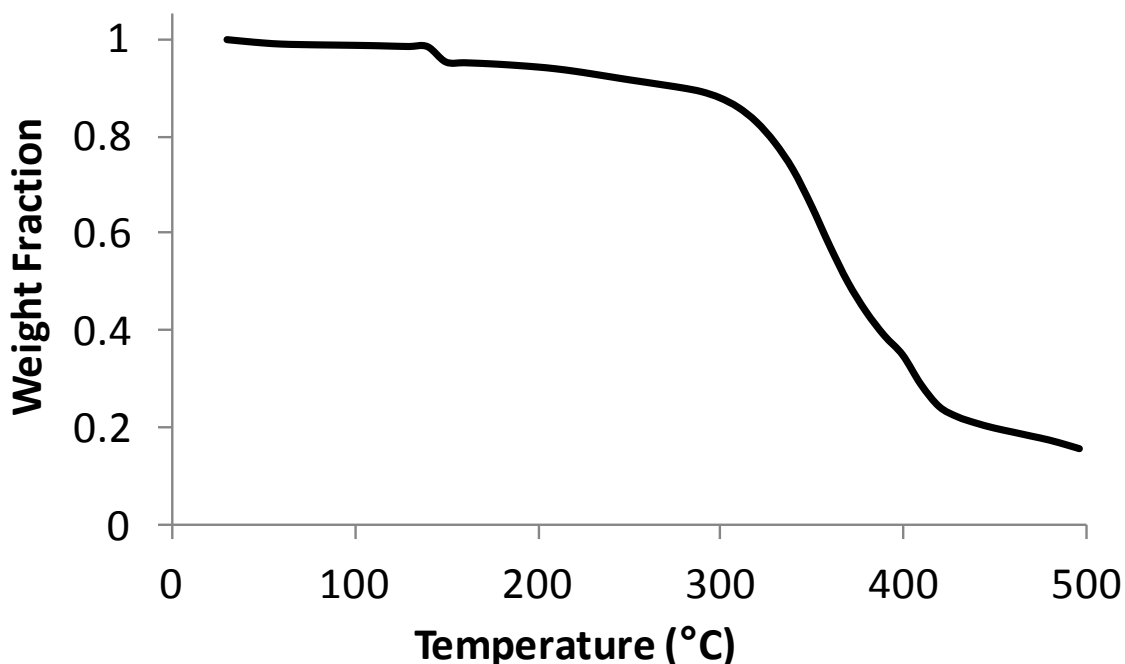
Figure 6.14 TGA scans for cure Avatrel 8000P (SB: 100°C for 5 min; exposure dose: 450 mJ/cm^2; PEB: 100°C for 5 min; develop for 3 min; cure at 150°C for 1 h).

The extent of cross-linking can change the dielectric properties of Avatrel 8000P due to the polarizability of the structures and products. The impact of cure temperature on dielectric constant of polymer films cured at temperatures from 160°C to 220°C was evaluated. Parallel plate capacitors were fabricated, as described in Chapter 2. Measurements were repeated four times for each cure temperature. The standard deviation for all cure temperatures was 0.072. The dielectric constant values for the samples cured from 160°C to 220°C are shown in Figure 6.15. The dielectric constant of the cured Avatrel 8000P increased from 3.9 to 4.4 with increasing cure temperature. The increase in the dielectric constant with cure temperature is due to the higher polarizability of the structures in the cured film at each temperature. For example, the degradation reaction at high cure temperature could result in C=O bond production with a dipole moment of 2.3, which is higher than the dipole moment of the C-O (0.7) bonds [125]. As a result, degradation of the fully cross-linked polymer results in higher electron and

induced dipole polarization. In summary, curing Avatrel 8000P at 160°C for 1 h resulted

in the lowest relative dielectric constant, $\varepsilon_r = 3.9$. This cure temperature agrees well with

the cross-linking and modulus results shown above.
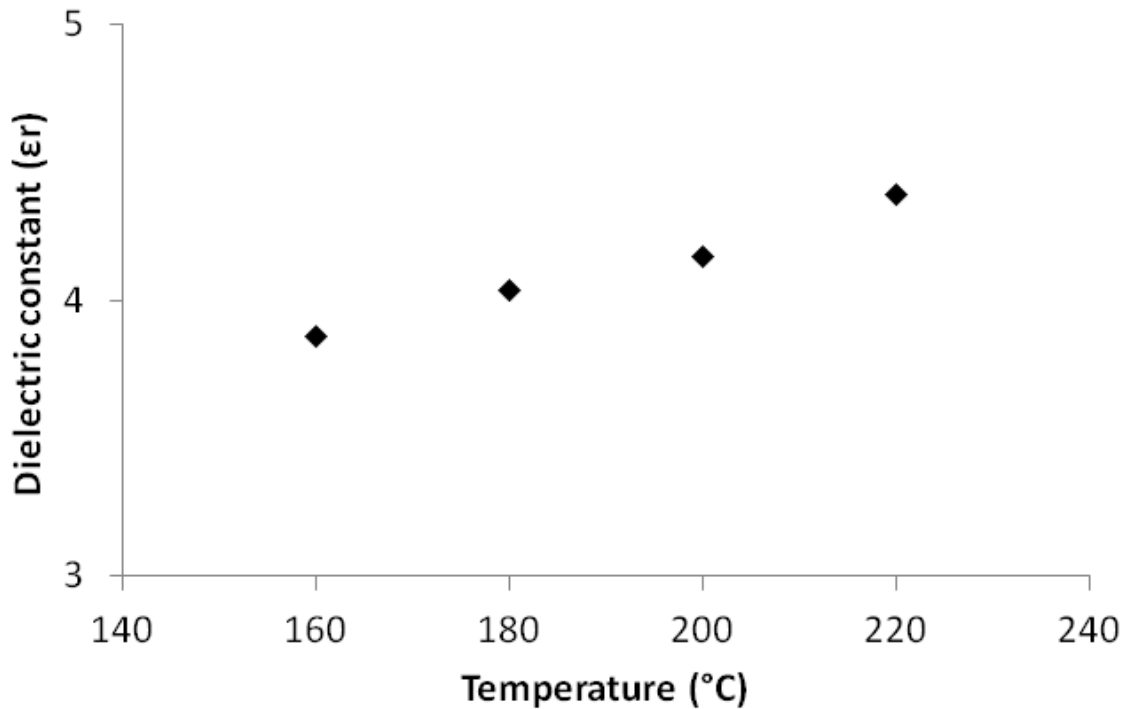
Figure 6.15 Dielectric constant of Avatrel 8000P at cure temperatures of 160°C, 180°C, 200°C, and 220°C.

6.2 Discussion

The cure temperature for optimal mechanical and electrical properties of Avatrel

8000P was experimentally identified. The optimal cure temperature is a compromise

between formation of cross-links within the polymer and degradation of structures. The

highest cross-link density and optimum properties were achieved for samples exposed to

365 nm radiation, exposed to TMAH developer, and cured at the relatively low

temperature of 160°C for 1 h. Several important results were found. The optimal cure

temperature for this polymer was found to be lower than other PNB-based systems

studied previously [53, 66, 67, 110]. The addition of multifunctional cross-linkers to this polymer mixture results in higher mobility and easier access of the cross-linkable sites to each other, compared to epoxy-functionalized PNB polymers (i.e. PNB with pendant epoxy moieties). The high cross-link density of Avatrel 8000P at low cure temperatures is also attributed to the efficient activation of the multi-functional epoxy additive. As discussed earlier, cross-linking can be achieved by both photo and thermally activation of the PAG. However, as shown in Fig. 6.4, if one were to rely only upon the thermal activation of the PAG to initiate crosslinking of the epoxy compounds, a higher temperature and/or longer curing cycle would be required to achieve full epoxy ring opening and cross-linking within the polymer.

It was also found that thermal activation of the acid catalyst during PEB, which assists in development of the latent image, also assists in achieving full epoxy ring opening during thermal curing at low temperature, as shown in Fig. 6.2. The extent of photo-crosslinking can be improved by excess UV exposure, resulting in a higher degree of PAG activation and greater epoxy conversion, Fig. 6.5.

The increase in the rate of the epoxy ring opening reaction as a result of TMAH exposure prior to curing is an unexpected benefit of developing in aqueous base. This could be due to an increase in mobility of the multifunctional cross-linkers, or catalysis of the crosslinking reaction due to absorbed TMAH, resulting in improved network interconnectivity. This corroborates with the reduced modulus measurements presented in Fig. 6.9 and Fig. 6.10. The reduced modulus of the developed samples decreased less (12%) when the cure temperature increased from 180°C to 240°C compared to the reduce modulus of the undeveloped sample which decreased 15%. The action of the developer also results in a lower residual stress value for the developed sample, shown in Fig. 6.12, possibly due to plactization of film by the TMAH. These factors contribute to full cross-linking of the polymer at a relatively low cure temperature of 160°C, resulting in the

highest measured hardness and modulus, and lowest dielectric constant and residual stress.

6.3 Conclusions

The acid-catalyzed epoxy ring opening reaction of a photodefinable polynorbornene-based dielectric formulation was studied using FTIR spectroscopy. The photo and thermal acid generation initiates epoxy ring opening reactions and subsequent cross-linking of polymer. This reaction is limited by the diffusive mobility of reactive groups (epoxy ring opening and acid catalyst). The rate and ultimate conversion of the epoxy ring opening reaction increases with increasing cure temperature, resulting in a higher degree of cross-linking at cure temperatures above 140°C. Degradation reactions likely occur at temperatures above 160°C, indicating loss of epoxide cross-linking groups and linkages. These hypotheses were supported by electrical and mechanical property studies. It was shown that curing Avatrel 8000P at 160°C for 1 h after develop resulted in full epoxy ring opening and highest cross-link density. This sample showed lower dielectric constant (3.9), residual stress (20 MPa), and solvent swelling (3.1%).

CHAPTER 7

CROSS-LINKING OF POLYNORBORNENE DIELECTRICS BY
VARIABLE FREQUENCY MICROWAVE

Fully curing polymer dielectrics can require lengthy cure cycles. VFM processing has been shown to be an effective rapid-curing technique for dielectric polymers [24, 126, 127]. Microwave irradiation of a polymer dielectric results in energy transfer due to the dielectric loss mechanism. The principal mechanism of coupling microwave radiation to polymer dielectrics is through dipole orientation by the oscillating electric field [21, 23, 24]. Microwave-induced reactions and curing can occur at temperatures lower than convective heating systems due to localized energy absorption, resulting in faster thermal curing of polymer dielectrics.

The extent of cross-linking plays an important role in establishing the mechanical properties of the cured polymer [54, 93, 94], and is a function of the reaction time and temperature. In Chapter 6, processing conditions for Avatrel 8000P were optimized and it was shown that the dielectric can be fully cured at 160˚C for 1 h in a conventional, conventional oven [54]. Curing of epoxy-based materials via VFM processing has also been previously investigated [128-131]. In addition, the cure ovens were purged with nitrogen to minimize the extent of oxidation of the PNB or other polymer during the extended cure time at high temperature, which degrades the polymer properties [4, 53, 54, 66, 67, 97].

In this study, VFM curing of the PNB dielectric was investigated and three specific questions were addressed: (i) can equivalent or better properties of the PNB dielectric be obtained at a lower temperature cure using VFM processing compared to thermal curing, (ii) can equivalent or better polymer properties be obtained in shorter time through the use of VFM curing compared to thermal curing, and (iii) can the

126

shortened cure cycle of VFM processing allow curing in air rather than an inert atmosphere. The effect from VFM curing on the chemical, electrical, and mechanical properties of the epoxy-functionalized PNB was studied under different processing conditions and compared to conventional thermal curing.

7.1 Experimental

All VFM samples were processed in a Microcure 2100 system from Lambda Technologies Inc. The five most important parameters that were controlled in the VFM system include the central frequency, frequency bandwidth, sweep rate, power, and temperature ramp rate [19]. The VFM oven maintains the desired temperature by adjusting the power level, thus permitting the control of the film temperature and ramp rate. In this work, an infrared pyrometer was used to monitor the temperature in the VFM furnace cavity. The central frequency of the VFM sweep was 6.425 GHz. The sweeping bandwidth was 1.15 GHz and the sweep rate was 0.1 s. This variable frequency process eliminates the non-uniformity in temperature that occurs in traditional single frequency microwave systems [131-134].

To evaluate the effect of VFM cure on the PNB polymer, the material was also cured according to standard thermal cure process studied previously [54]. The preparation of the thermally-cured films, including spin coating, bakes, UV exposure, and developing, was identical to that for VFM-cured films. Thermal curing was performed in a furnace with the same ramp rate as calculated for the VFM process for each cure temperature. Samples were allowed to cool for the same amount of time as used for the VFM cured films for each cure temperature. All VFM-cured and thermally-cured samples were exposed at dose of 450 mJ/cm^2.

The UV absorbance of polymer films was measured using an ultraviolet-visible spectrometer (Hewlett Packard 8543 UV) with 100 mm diameter <100> glass wafers to

investigate the oxidation effects of curing the polymer in air. PNB films were spin-coated at 1500 rpm for 30 sec on a glass wafer and baked at 100°C for 10 min on a hotplate in air. Nanoindentation was performed on 2 to 4 samples prepared at each cure temperature and time. The nanoindentation results were repeated three times on each sample. Each set of measurements were performed during a single 48 h period. Each nanoindentation data point shown in the results section is the average of all measurements performed on all samples cured at each temperature [54].

7.2 Results

Prior to investigating the effects of VFM curing on PNB, the VFM system was characterized by studying the effect of substrate temperature as a function of VFM power and time. Then, the effect of cure temperature and environment were investigated to evaluate the effectiveness of VFM curing. The cure temperature was varied from 140 to 180°C in both an air-filled VFM cavity and a nitrogen-purged VFM cavity. Cure times ranging from 1 to 30 min were used. The chemical, mechanical, and electrical properties of these samples were measured and compared to those of thermally-cured films.

The heating rate during exposure to VFM radiation is an important parameter for polymer films because the polymer reaction begins before the final cure temperature is reached. The wafer temperature was studied as a function of time during exposure to 100 W VFM power. The temperature profile for a bare silicon wafer, a bare silicon wafer with 1 μm thermally-grown silicon dioxide, and an oxide coated silicon wafer with 10 μm PNB coated on one side were compared. All three samples reached the set temperature within 100 s. However, the PNB-coated silicon wafer showed a more rapid rise in temperature due to the high absorptivity of the PNB at the microwave frequencies used. In the first 100 s of microwave exposure at 100 W, the bare wafer, the oxide coated wafer, and the oxide coated wafer with PNB reached 90, 95, and 110°C, respectively.

At higher VFM power, the temperature rise was more rapid and a higher steady-

state temperature could be reached. To quantify this effect, the PNB-coated wafer was irradiated at constant power ranging from 100 to 500 W. The samples irradiated at 100, 300, and 500 W reached the maximum temperature of 110, 150, and 250°C, respectively. This shows that rapid heating of the PNB was possible. In each of the cure experiments, a constant heating rate (degrees per minute) was achieved by controlling the VFM power.

The degree of epoxide ring opening and resulting cross-linking for Avatrel 8000P affect the electrical and mechanical properties of the polymer film [54]. In addition, excessive time at higher temperature can result is a slight degradation of the film properties due to deterioration of the polyether linkages between multifunctional epoxy moieties. In this study, Avatrel 8000P curing was studies as a function of time and temperature in an attempt to shorten the cure time VFM, and to optimize the dielectric and mechanical properties for VFM cured films. The epoxy ring opening reaction and chemical changes occurring in the PNB films were monitored using FTIR spectroscopy. A 30-μm thick PNB film was spin-coated on an oxide coated silicon wafer. The sample was taken through the normal lithographic sequence consisting of SB, exposure, PEB, and cure. The infrared region from 700 cm^{-1} to 950 cm^{-1} was examined after each process step to determine the extent of ring opening, as shown in Figure 5.1.
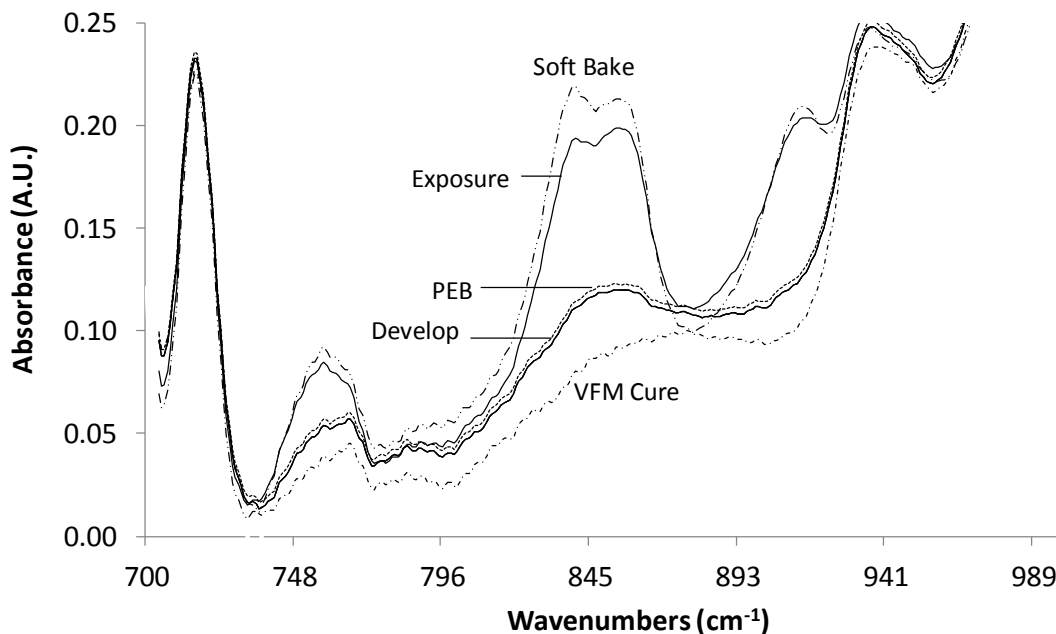
Figure 7.1 Changes in infrared spectrum of thin film Avatrel 8000P from 700 cm^{-1} to 950 cm^{-1} as a function of processing steps (SB: 100°C for 5 min; exposure dose: 170 mJ/cm^2; PEB: 100°C for 5 min; cure at 150°C for 15 min).

Three peaks corresponding to the asymmetric and symmetric epoxide ring stretches were observed at 913 cm^{-1}, 844 cm^{-1}, and 760 cm^{-1}. As seen in Fig. 7.1, a significant degree of epoxy ring opening occurred as a result of the UV exposure and PEB. This results in cross-linking allowing the latent image to be developed before the final cure step. The magnitude of the FTIR epoxy peaks decreased further after curing at 150°C for 15 min. To quantify the chemical changes in the processed films, the absorbance of the samples after each step were compared by measuring the decrease in peak height compared to a fully cured sample where no epoxy rings exist. The extent of epoxy ring opening after each process step was evaluated by measuring the epoxy absorbance at 844 cm^{-1}. The epoxy content after, $h_{soft\ bake}$, was assumed to have no ring-opening and peak height after extensive curing, $h_{final-cure}$, was taken as no epoxy remaining, Equation (7.1). After SB is the first instance where the film exists.

$$\text{Extent of Reaction (\%)} = \frac{h_{\text{soft bake @ 844 cm}^{-1}} - h_{i \text{ @ 844 cm}^{-1}}}{h_{\text{soft bake @ 844 cm}^{-1}} - h_{\text{final-cure @ 844 cm}^{-1}}} \times 100 \qquad (7.1)$$

The background for the 844 cm^{-1} peak from 800 cm^{-1} and 870 cm^{-1} was used as the basis for calculating the absorbance in Equation (7.1). The epoxy peak height after different processing steps (h_i) was used to quantify the extent of reaction. The extent of reaction for the fully cured sample by definition is 100%.

A series of experiments were performed at constant temperature from 140˚C to 180˚C in a traditional, thermal oven and in the VFM system at different cure conditions. Figure 7.2 summarizes the extent of cure data from the FTIR results for the processed films as a function of cure temperature, time, and atmosphere. The average extent of epoxy ring opening for the exposed and post-exposure baked samples were 14% and 82%, respectively, with a standard deviation of 4%. The first issue addressed is to determine if PNB can be cured at lower temperature by VFM. Samples were VFM-cured for 30 min in air at 140˚C to 180˚C. The extent of reaction for VFM cured films for 30 min in air are shown in Fig. 7.2. The extent of reaction increased with the cure temperature, as expected. The sample cured at 140˚C for 30 min showed 92.5% epoxy ring opening, while samples cured at higher temperatures showed 100% conversion (fully reacted). This FTIR result shows that full epoxy ring-opening was achieved after 30 min at 150°C by VFM curing.
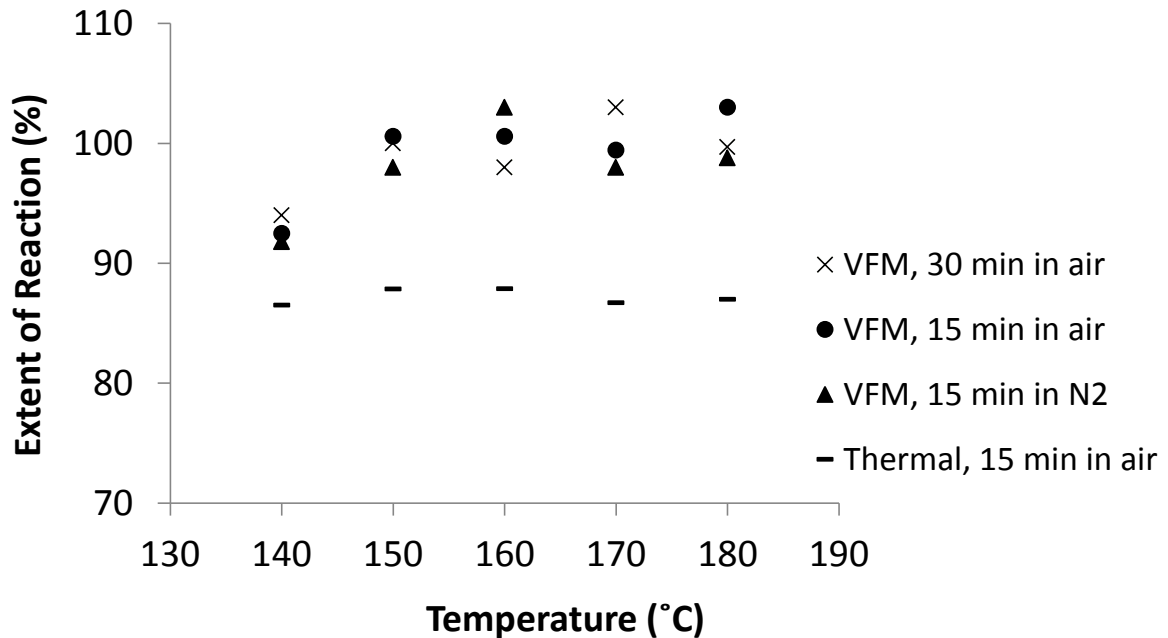
Figure 7.2 Extent of cure of Avatrel 8000P, cured in VFM and convectively heated oven at different processing conditions, as a function of cure temperature from 140˚C to 180˚C.

To investigate the feasibility of shorter cure times, samples were VFM cured for 15 min in air. As shown in Fig. 7.2, the lowest temperature that resulted in full epoxy ring-opening was 150˚C for the 15 min cure cycle in air. These results show that full epoxy ring-opening can be achieved at the relatively low cure temperature of 150˚C for periods as short as 15 min by VFM processing. Previously, it was shown that full conversion (100% extent of reaction) of the PNB can be achieved after a 1 h thermal cure at 160˚C. For comparison, a 60 min thermal cure at 150°C gave only 95% reaction [54]. This means that a 15-min VFM cure at 150°C gave the same extent of cure as the thermal oven treated sample 160°C for 1 h [54].

To further investigate the effectiveness of VFM processing, the PNB films were cured under identical conditions in a traditional, thermal oven for 15 min as the control. The cure temperature was varied from140˚C to 180˚C, and the extent of reaction was measured by FTIR. The spectra for the VFM and thermally cured films were essentially identical. As shown in Fig. 7.2, the extent of reaction for the thermally cured samples for

132

15 min was about 87% showing that for each cure condition, a higher degree of epoxy ring-opening and cross-linking was achieved by VFM processing. This demonstrates the efficacy of VFM processing in driving reactions to completion. That is, a higher extent of cure could be achieved at lower temperature for the same cure time for the VFM samples.

To investigate the feasibility of VFM-curing the polymer in air, the experiments were repeated with the cavity purged with nitrogen. The temperature was varied from 140°C to 180°C. A PNB film cured in nitrogen for 15 min was used as a control. The extent of reaction at each cure temperature is shown in Fig. 7.2. Samples cured in a nitrogen-purged cavity and in air resulted in essentially identical extent of reaction, showing that rapid, VFM-curing of PNB at low temperatures in air has no effect on the epoxy ring-opening reaction. This is reasonable because air or nitrogen are not consumed in the epoxy ring opening reaction. Other properties, such as modulus and degree of oxidation may be affected by curing in air. These properties will be investigated later in this section.

To investigate the minimum VFM processing time, PNB films were cured at 160°C for 1, 5, 15, and 30 min. The progress of the cure reaction was studied by FTIR and the results are shown in Figure 7.3. The extent of reaction for the sample cured for 1 min was 92.5%, showing that 1 min at 160°C is not sufficient for full reaction of the polymer. However, the extent of cure increased with the cure time and the full epoxy ring-opening was achieved at times as short as 5 min which is considerably faster than the 60 min cure at 160°C in a traditional, thermal oven [54].
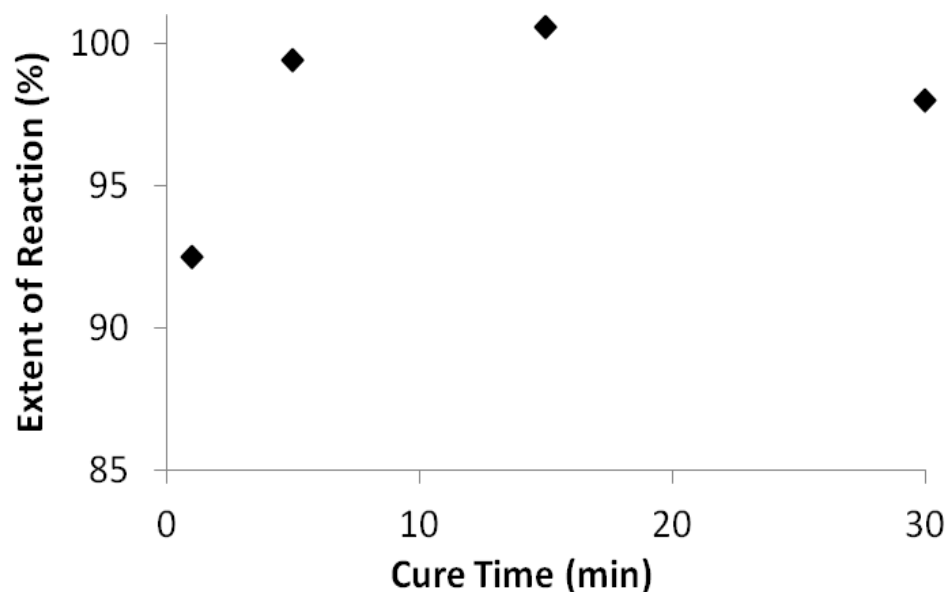
Figure 7.3 The extent of cure of Avatrel 8000P films, VFM cured at 160°C, as function of cure time.

While the FTIR results show epoxy ring opening, the FTIR technique has a degree of uncertainty, as indicated by the 4% standard deviation obtained here. Although FTIR indicates full ring opening, mechanical properties are a better indicator of cross-linking. Nano-indentation was used to determine the mechanical properties indicative of full cross-linking. Samples cured for 15 min at 140 to 180°C were examined. Figure 7.4 shows the reduced modulus of the PNB films as a function of cure temperature using a 15 min VFM cure in air. The reduced modulus increased nearly 12% for cure temperatures from 140°C to 150°C. The modulus reached a maximum value of 3.3 GPa, indicative of a higher cross-link density as the cure temperature was increased. When the cure temperature was further increased to 180°C, the reduced modulus decreased from 3.3 GPa to 2.7 GPa. The decrease in modulus at higher than the optimum cure temperature was previous shown to be due to a slight degradation of the cross-links, such as the polyether linkages between the multifunctional epoxy additives. The maximum reduced modulus value, 3.3 GPa, was obtained after curing at 150°C for 15 min. As shown in

Table 7.1, the same trend with temperature was observed for the film hardness. The maximum hardness was obtained for the sample cured at 150˚C for 15 min in VFM. The hardness increased from 0.13 GPa to 0.18 GPa with increasing temperature from 140°C to 150˚C followed by a drop to 0.13 GPa when the cure temperature was further increased to 180˚C. The average standard deviation for the hardness values reported in Table 7.1 was 0.005 GPa. These results show that the optimum hardness and modulus can be achieved at a relatively low temperature of 150°C for a 15 min VFM cure.
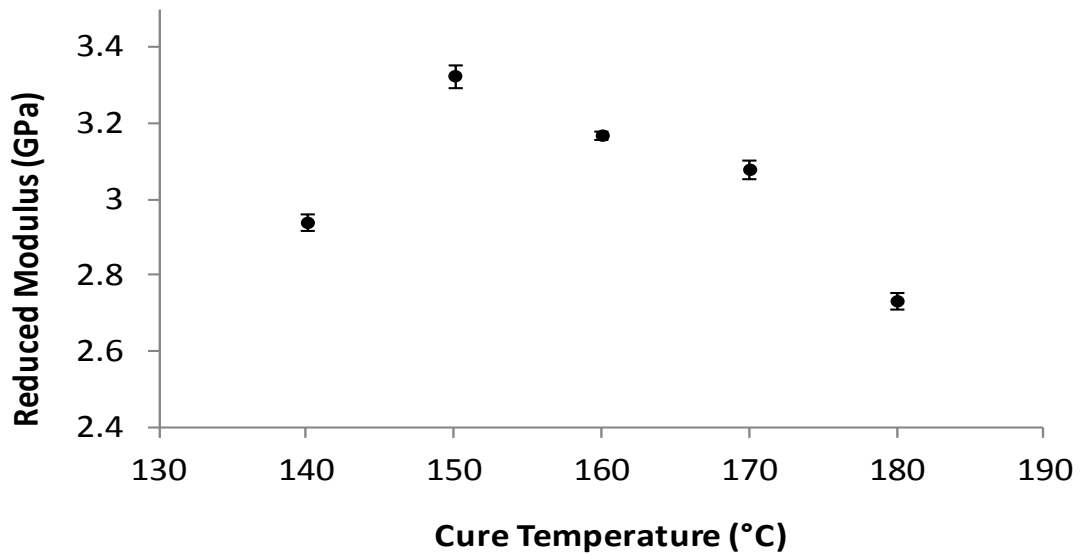
Figure 7.4 The reduced modulus of VFM-cured Avatrel 8000P in air ambient as a function of cure temperature (SB: 100°C for 5 min; exposure dose: 170 mJ/cm^2; PEB: 100°C for 5 min; VFM cure for 15 min in air).

Table 7.1 Summary of hardness measurements for cured Avatrel 8000P films in a VFM system and a thermal oven at different cure conditions

Cure Condition →	15 min VFM-cure in air	15 min VFM-cure in N$_2$	15 min Thermal-Cure in Air
Cure Temp. (°C) ↓	Hardness (GPa)	Hardness (GPa)	Hardness (GPa)
140	0.13	0.13	0.12
150	0.18	0.18	0.13
160	0.17	0.17	0.13
170	0.15	0.14	0.14
180	0.13	0.13	0.13

An identical set of samples were cured in nitrogen in order to evaluate the difference between air and nitrogen environments during curing. The reduced modulus and hardness for the VFM-cured samples in nitrogen for 15 min at 140˚C to 180°C are shown in Figure 7.5 and Table 7.1, repectively. The nano-indentation results for the nitrogen cured samples are nearly identical to the air cured ones at each cure temperature. The maximum reduced modulus and hardness values were once again 3.3 GPa and 0.18 GPa, respectively, when cured at 150˚C for 15 min. The results indicate that 15 min curing ambient did not affect the properties.
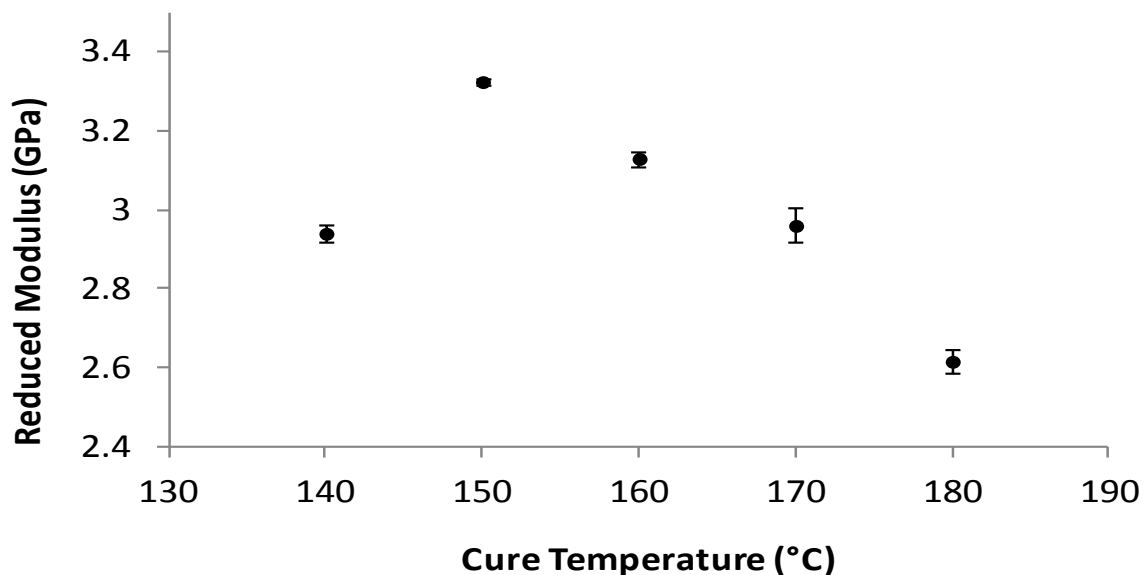
Figure 7.5 The reduced modulus of VFM-cured Avatrel 8000P in nitrogen ambient as a function of cure temperature (SB: 100°C for 5 min; exposure dose: 170 mJ/cm^2; PEB: 100°C for 5 min; VFM cure for 15 min in nitrogen).

Nano-indentation was also performed on samples cured in a thermal furnace for 15 min in air to show that the lower degree of epoxy ring opening results in a lower degree of cross-linking. As shown in Figure 7.6 and Table 7.1, both the modulus and hardness of thermally-cured samples for 15 min were lower than the VFM samples at the same conditions. The modulus and hardness for the thermally-cured samples were approximately 2.7 and 0.13 GPa, respectively. These values are much lower than the values obtained for the VFM-cured film at 150°C for 15 min confirming that a lower degree of epoxy ring opening results in a lower degree of cross-linking.
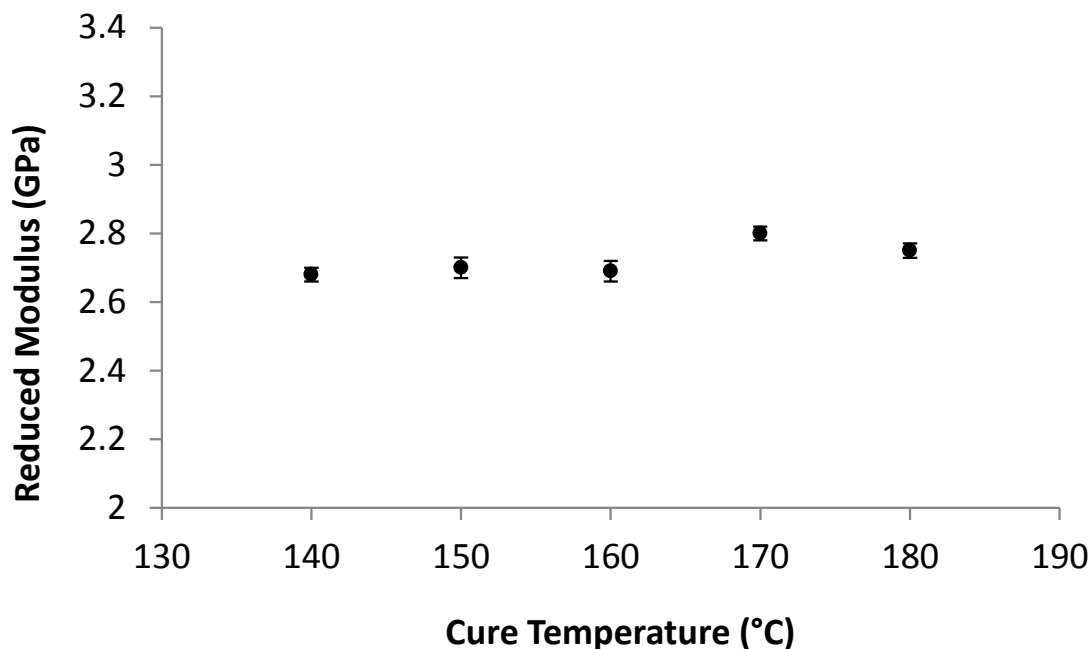
Figure 7.6 The reduced modulus of thermally-cured Avatrel 8000P as a function of cure time (SB: 100°C for 5 min; exposure dose: 170 mJ/cm^2; PEB: 100°C for 5 min; thermal cure for 15 min in air).

The nano-indentation results for the VFM-cured samples also shows that the 5 min exposure at 160°C was the shortest cure time tested where maximum values were obtained. Figure 7.7 shows the values for the 160˚C cures for 1, 5, 15, and 30 min. The reduced modulus of the film cured at 160˚C for 1 min was 2.3 GPa which increased to 3.1 GPa for the samples cured for 5 min and longer. The same trend was observed for hardness where the value increased from 0.13 GPa for the 1 min cure to its maximum value of 0.17 for the 5 min cure, Table 7.2. The lower values confirm that the 1 min VFM cure is not adequate to fully react within the film. However, full curing appears to be achieved after 5 min.
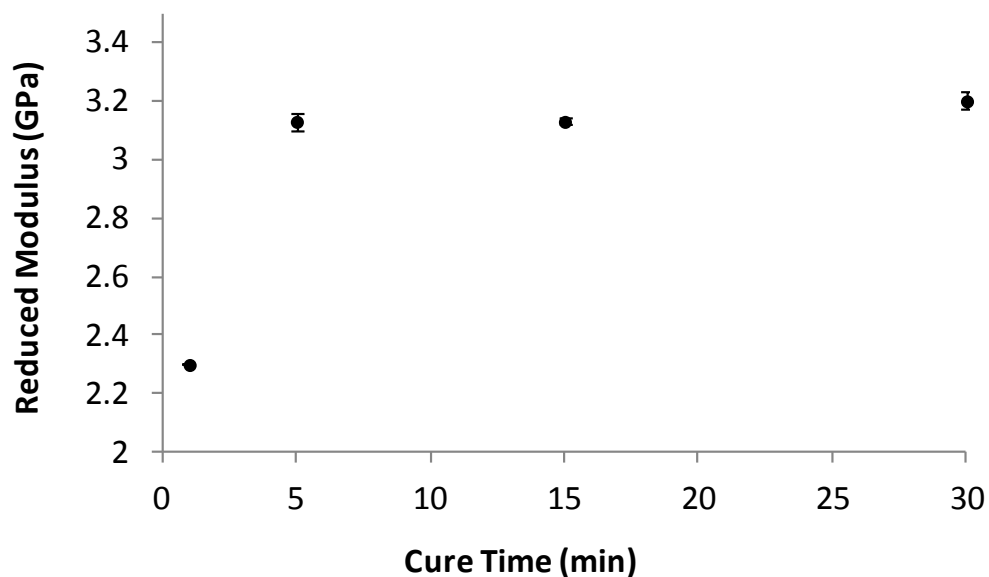
Figure 7.7 The reduced modulus of VFM-cure Avatrel 8000P at 160˚C as a function of cure time (SB: 100°C for 5 min; exposure dose: 170 mJ/cm^2; PEB: 100°C for 5 min; VFM cure at 160 °C in air).

Table 7.2 Summary of measured hardness for VFM-cured Avatrel 8000P films at 160°C in air.

Cure Time (min)	Hardness (GPa)
1	0.13
5	0.17
15	0.17
30	0.17

The solvent swelling in a polymer film is inversely related to the degree of cross-linking between polymer chains, other factors remaining constant [50, 94, 122, 123]. The swelling results for the VFM cured samples for 15 min in air are shown in Figure 7.8. Lower swelling values were found for samples cured at 150°C compared to those cured at 140°C confirming that a higher degree of cross-linking occurred for the 150°C sample.

The swelling ratio then increased about 18% by raising the cure temperature from 150°C to 180°C. This increase in swelling is consistent with the degradation of cross-link density at elevated temperatures.
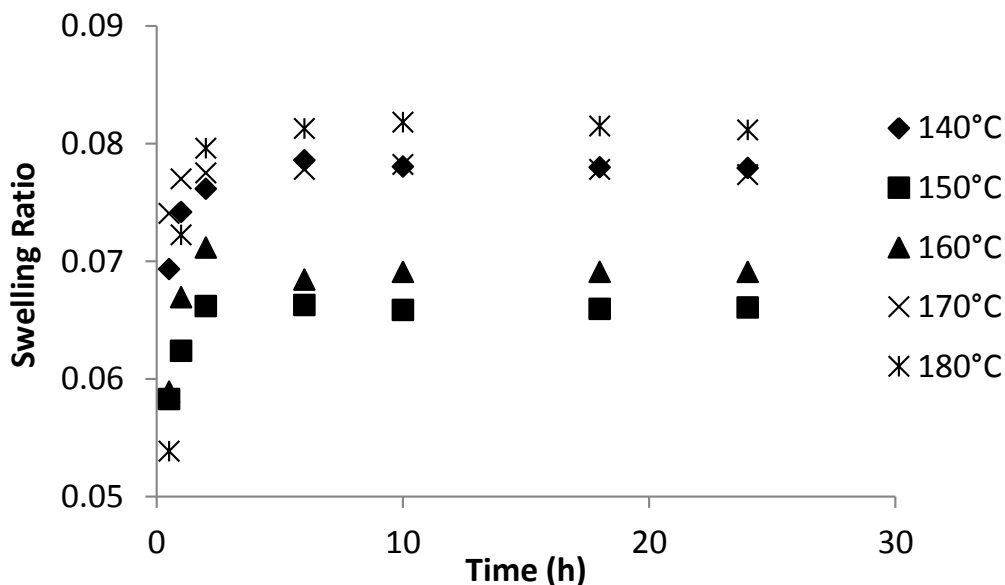
Figure 7.8 Effect of cure temperature on swelling ratio of VFM-cured Avatrel 8000P in air ambient.

The swelling experiments were repeated on the VFM samples cured in nitrogen for 15 min. The same trend in swelling was observed for the nitrogen cured samples as those cured in air. As shown in Figure 7.9, the swelling ratio decreased when the temperature increased from 140˚C to 150˚C followed by a 15% increase in swelling when the cure temperature was raised to 180˚C. The swelling ratio for the samples cured in nitrogen were nearly the same as the air cured samples at each cure temperature, showing there was no significant effect of air curing, in terms of cross-linking, as measured by solvent swelling or nano-indentation. The VFM swelling results were then compared to the swelling results for thermally cured samples. Figure 7.10 shows that the samples cured in a thermal oven for 15 min showed greater swelling (i.e. lower degree of cross-linking) than the VFM-cured samples. This is congruent with the FTIR and nano-

140

indentation results. Figure 7.11 shows the swelling results for the VFM-cured films at 160˚C for different cure times. The sample cured for 1 min resulted in a higher swelling ratio than samples cured for 5 and 15 min due to lower degree of cross-linking. Samples cured for 5 min and 15 min resulted in similar swelling ratios indicating that 5 min cure at 160˚C is sufficient for fully cross-linking the PNB polymer in VFM, which agrees with the FTIR and nano-indentation results.
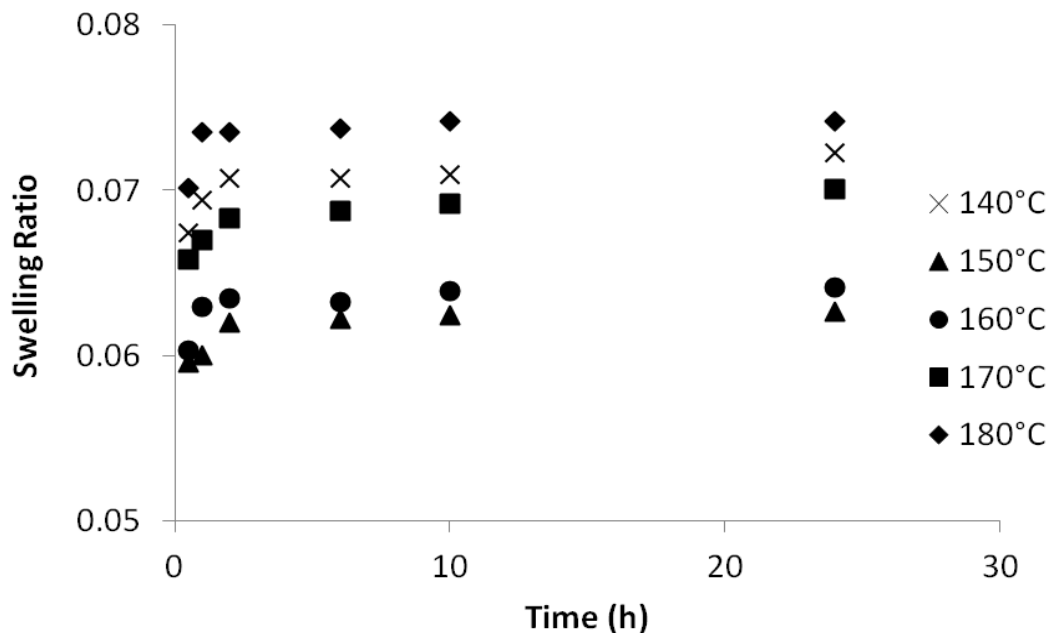
Figure 7.9 Effect of cure temperature on swelling ratio of VFM-curd Avatrel 8000P in nitrogen ambient.
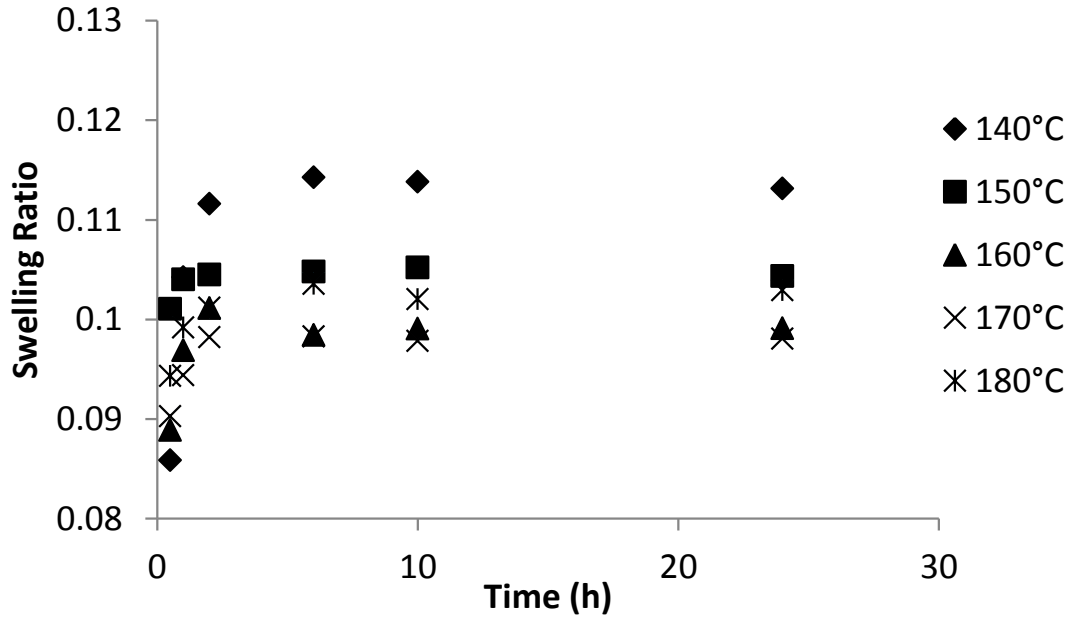
Figure 7.10 Effect of cure temperature on swelling ratio of thermally-cured Avatrel 8000P in air ambient.
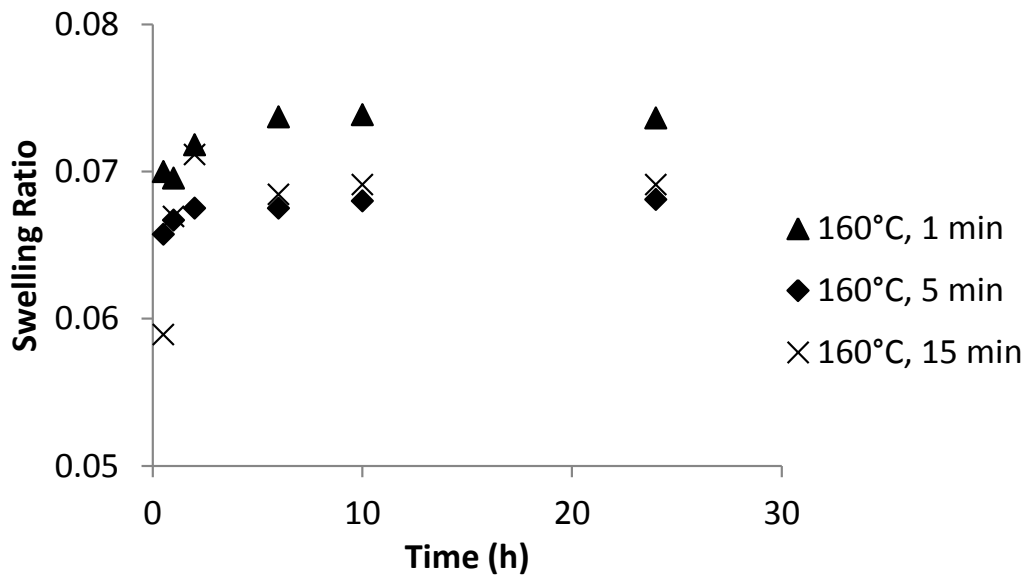
Figure 7.11 Swelling ratio of VFM-cured Avatrel 8000P at 160°C in air as a function of VFM cure time.

The residual stress of the polymer films was evaluated for the different cure conditions. The residual stress can be caused by CTE mismatch between the substrate and

the polymer film, or shrinkage during the cross-linking of the polymer film or solvent evaporation. The magnitude of the film stress is affected by Poisson's ratio, the biaxial modulus of the polymer film, CTE of the polymer, and the magnitude of the departure from the stress neutral temperature of the polymer film. These properties can be affected by the cure temperature through the type of three-dimensional cross-link network produced in the film [54]. The residual stress of the PNB films was characterized after each process step in the lithographic sequence and for samples VFM cured at temperatures from 140°C to 180°C. The measurements were repeated on six different samples (10 measurements each) for each processing step. The standard deviation of each set of samples was 1.1MPa.

The residual stress of a PNB film at different points in the lithographic process ranged from 13 MPa after SB to 24MPa after VFM curing at 150°C for 15 min in air, as shown in Figure 7.12. The creation of residual stress in the soft-baked film was primarily due to film shrinkage due to solvent evaporation. The modulus of the polymer film increased during PEB due to the acid-catalyzed cross-linking of the film at high temperature creating a zero stress state at high temperature. The residual stress resulted from cooling the sample back to room temperature due to the CTE mismatch between the polymer film and the substrate. The decrease in the polymer film stress after developing was the result of film softening and swelling from incorporation of the developer. The highest stress state, 24MPa, occurred after cure, again due to film shrinkage and deviation from the stress-neutral temperature during sample cool down.
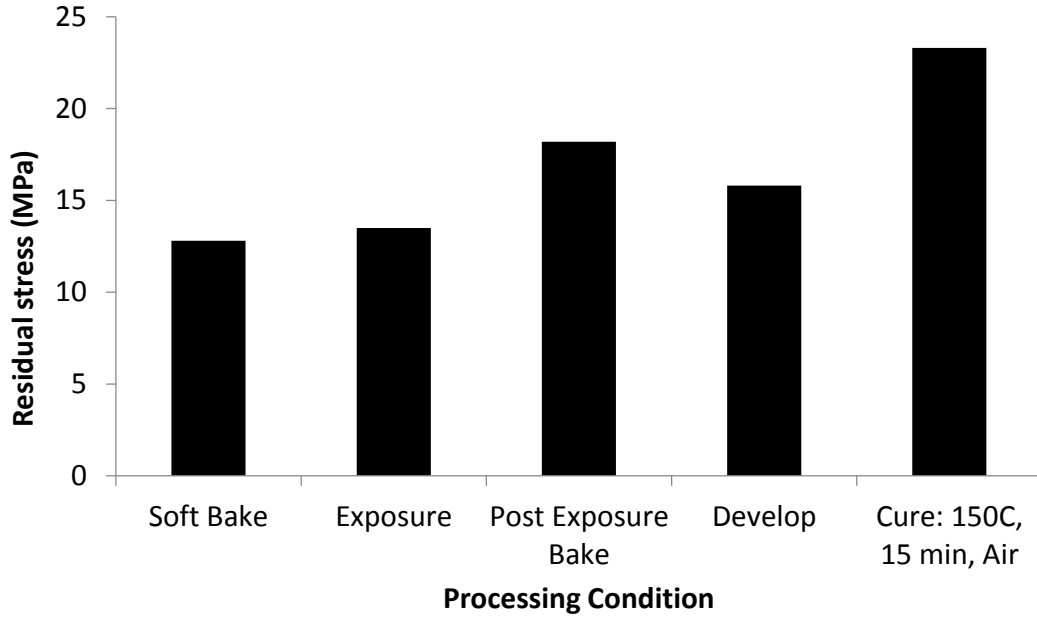
Figure 7.12 Changes in internal film stress of Avatrel 8000P as a function of processing conditions (SB: 100°C for 5 min; PEB: 100°C for 5 min; develop for 3 min; VFM cure at 150°C for 15 min in air).

The residual stress of the PNB films was also measured for VFM-cured samples for 15 min at temperatures from 140°C to 180°C. The measurements were performed on two different samples at each cure temperature with each data point being the average of 10 measurements on each sample. The standard deviation was 0.4 MPa. The residual stress increased with increasing cure temperature from 140°C to 150°C, as shown in Figure 7.13. This increase of residual stress is likely due to higher cross-link density and resulting increase in film rigidity along with a higher stress neutral temperature. The decrease in the film stress with temperature for films cured at temperatures from 150°C to 180°C can be attributed to the slight degradation of cross-linkages in the polymer at higher cure temperatures. The film stress decreased about 14% from the lowest to highest value for cures from 150°C to 180°C. The change in the individual factors contributing to the stress (i.e. degradation of cross-links, change in stress neutral point, CTE mismatch, and changing modulus of the film) contributed to total stress change. In addition, the stress values obtained for the VFM-cured samples are higher than the corresponding ones

for the thermally-cured samples reported by Raeis-Zadehet. al. [54]. It is known that different processing methods can impact the evolution of intrinsic stress in the film [135, 136]. For example, the rate of solvent and photoproduct evolution relative to the rate of epoxy ring-opening reaction could be different in VFM-cured films as compared to thermally-cured films.
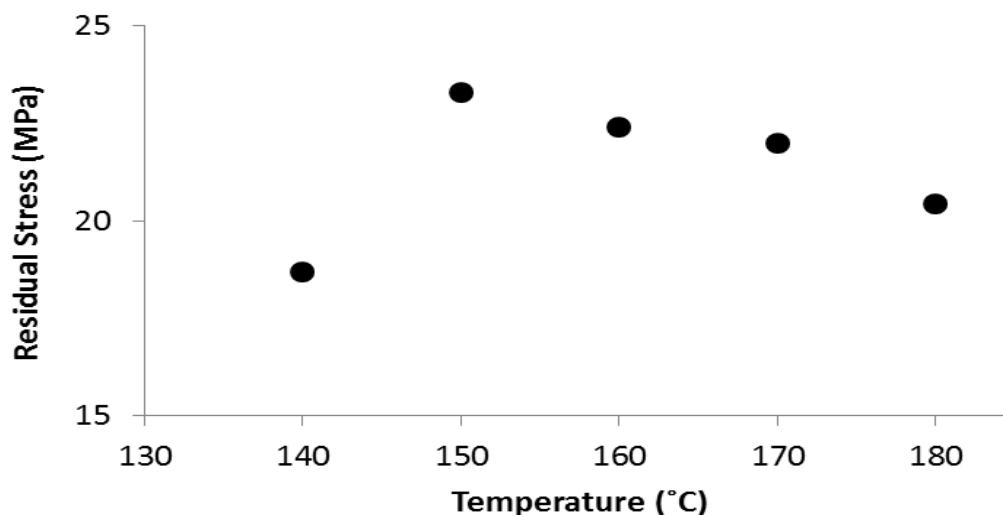
Figure 7.13 Residual stress of Avatrel 8000P as a function of cure temperature from 140°C to 180°C, 15 min VFM cure in air.

The extent of cross-linking can also change the dielectric properties of the PNB polymer due to the polarizability of the structures and products. The impact of cure temperature on the dielectric constant of VFM-cured films at temperatures from 140°C to 180°C was evaluated. Samples were cured for 15 min in air and parallel plate capacitors were fabricated, as described in the Experimental Section. Measurements were repeated four times for each cure temperature. The standard deviation was 0.04. The dielectric constant values for the samples cured from 140°C to 180°C are shown in Figure 7.14. The dielectric constant for the VFM-cured samples decreased from 5.2 to 4.3 with increasing cure temperature from 140°C to 150°C due to a decrease in film polarizability (electron and dipole polarization) when the epoxy is cross-linked. Since the C-O bond in

the epoxy ring has a dipole moment of 0.7 is higher than the dipole moment of the C-C (0.0) and C-H (0.4) bonds, the reaction of the epoxy rings lowers the dipole polarization. The dielectric constant increased from 4.3 to 4.7 with increasing the cure temperature from 150°C to 180°C as the cross-link density decreased due to thermal degradation.
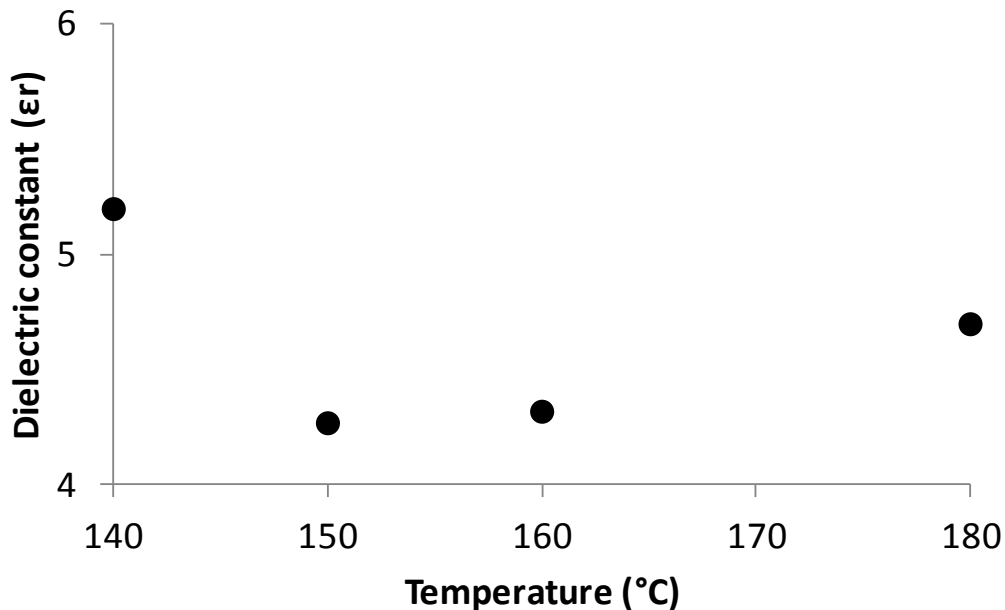
Figure 7.14 Dielectric constant of Avatrel 8000P at cure temperatures of 140°C, 150°C, 160°C, and 180°C.

The formation of species such as C=O (dipole moment of 2.3) with higher dipole moments than C-O (0.7) bonds [125] results in higher electron and induced dipole polarization. Curing the PNB polymer at 150°C for 15 min resulted in the lowest relative dielectric constant, $\varepsilon_r = 3.9$. This cure temperature is congruent with the cross-linking and modulus results shown above. The dielectric constant measured at each cure temperature was higher than that of samples thermally cured at the same temperature in a one hour cure[54]. At shorter cure times, trapped residual solvent and photoproducts may be responsible for the higher dielectric constant values [23]. This observation is consistent

with previous studies reporting somewhat higher values of dielectric constant for rapid cured photosensitive dielectric films [19].

TGA of VFM cured Avatrel 8000P which is shown in Figure 7.15 was compared to the TGA of the thermally cured films, shown in Figure 7.16. Both samples were cured at 150°C for 15 min in a nitrogen atmosphere. The results indicate that degradation in the VFM cured films began around 319°C which was similar to the decomposition temperature obtained for the thermally cured films, 329°C. However, the thermally cured sample showed additional weight loss especially above 200°C. The thermally cured sample and the VFM cured sample lost 26% and 22% up to 300°C, respectively. This additional weight loss in the thermally cured film (4%) may be due to the removal of the solvent which was not entirely removed during the low-temperature thermal cure.
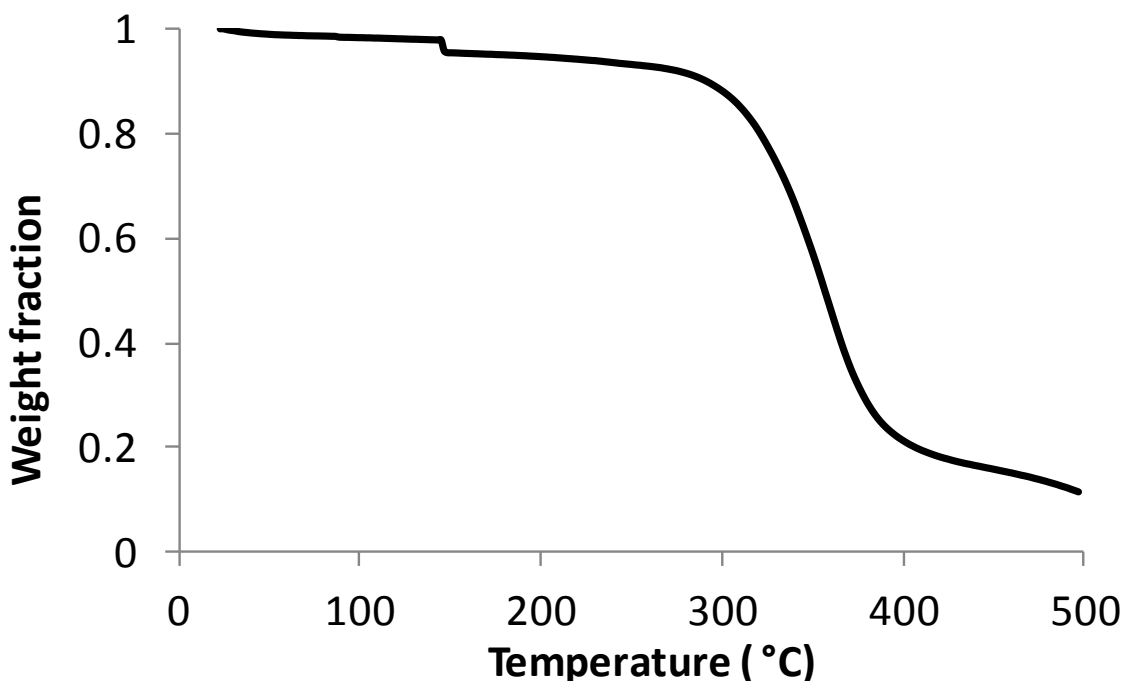
Figure 7.15 TGA scans for VFM cured Avatrel 8000P.
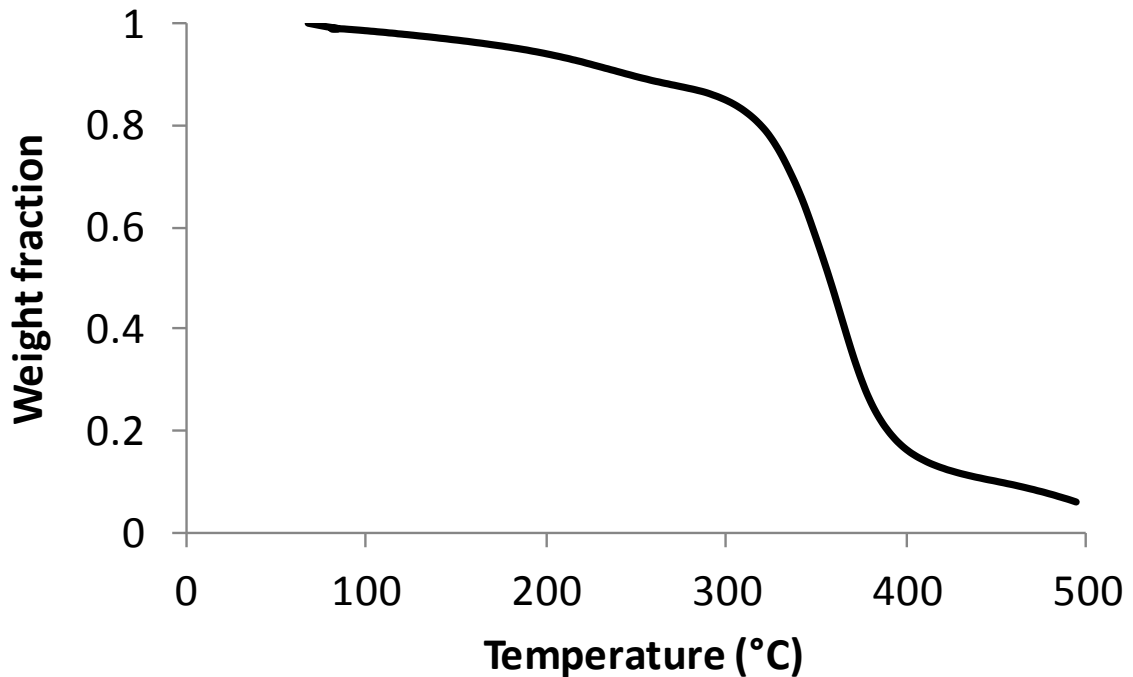
Figure 7.16 TGA scans for thermally cured Avatrel 8000P.

Polymer films are often cured in nitrogen to decrease the extent of oxidation, which can degrade the film properties and cause yellowing of an otherwise colorless material. Although the physical properties measured above do not show negative effects from curing in air vs. nitrogen, the yellowing effect in films can be a sensitive measure of oxidation. The absorbance of the polymer film in the visible range of the spectrum was measured under different cure conditions to monitor any change in color and the results are shown in Table 7.3. To quantify the yellowing effect, the absorbance at 400 nm and 650 nm wavelength was compared for each cure condition. Yellowing of a film would exhibit an increase in absorbance at 400 nm with respect to the value at 650 nm, $(\frac{Absorbace\ at\ 400\ nm}{Absorbance\ 1t\ 650\ nm})$.

Table 7.3 Yellowing effect on the base polymer (PNB polymer only) at different cure conditions (bake: 100°C for 10 min; no UV exposure; VFM cure in air and nitrogen).

VFM-Cure Condition	$\dfrac{Absorbance\ at\ 400\ nm}{Absorbance\ at\ 650\ nm}$
180°C, 15 min in N$_2$	1.06
180°C, 15 min in air	1.07
180°C, 60 min in air	1.06
220°C, 60 min in air	7.75

The PAG was not added to the polymer mixture so as not to distort the absorbance at 400 nm. The PNB film was first VFM cured for 15 min in nitrogen at 180°C as a control. This sample resulted in the normalized absorbance, ($\frac{Absorbace\ at\ 400\ nm}{Absorbance\ 1t\ 650\ nm}$), of 1.06. The sample was taken through a second VFM cure at 180°C for 15 min in air, and a third cure cycle at the same temperature for 1 h, which did not affect the normalized absorbance at 400 nm. To show the effect of oxidation, the sample was then VFM-cured in air at 220°C for 60 min, which resulted in significant increase in the absorbance at 400 nm, showing high degree of oxidation and yellowing. The results show that oxidation of the polymer occurs at temperature above 180°C and there is little or no detectable effect of oxidation during the cure cycle at temperatures below 180°C, especially for the short times used in VFM processing.

7.3 Discussion

PNB-based dielectric resins are known for their attractive physical properties and low moisture uptake. VFM processing has been shown to provide a significant reduction in cure time and temperature for several thin films polymers [137]. Previously, the thermal processing of Avatrel 8000P was optimized and full cross-linking of the polymer

was observed at 160°C for 1 h cure. The objective of this study was to investigate whether VFM processing of PNB could (i) produce equivalent or better PNB properties at a lower temperature, (ii) be carried out in air rather than nitrogen, and (iii) the overall processing time be shortened. To address these issues, the chemical, electrical, and mechanical properties of the VFM cured films were compared to thermally cured films.

The PNB-coated wafers had higher heating rates, compared to uncoated wafers showing that the polymer absorbed microwave energy even through the mass of the polymer was less than 2% of the mass of the silicon. That is, energy is directly absorbed by the polymer and is not simply convectively heated by the wafer. Furthermore, an increase in the polarizability of the film results in higher absorbance of microwave energy.

The local heating effect in VFM processing results in more rapid reactions even though the apparent temperature is the same as in a convection oven [19]. As seen in Fig. 7.2, the FTIR results clearly show a higher conversion rate at lower temperature by microwave processing. This result was confirmed by characterizing the mechanical properties for VFM cured temperatures. The maximum value of hardness and modulus, and lowest degree of solvent swelling was achieved at 150°C indicating that this is the cure temperature for the highest degree of crosslinking. The hardness, modulus and swelling properties also show that the VFM-cured samples were more highly cross linked than the thermally-cured ones. This also resulted in the highest residual stress, as shown in Fig. 7.13. The stress values obtained for VFM-cured samples were higher than those of thermally-cured at each cure temperature, which could be due to a number of factors including a different stress-neutral temperature, or mechanical properties. Additionally, the minimum dielectric constant was obtained at 150°C, shown in Fig. 7.14. However, the dielectric values obtained for VFM-cured samples at each cure temperature were higher than those of thermally-cured films, which could be due to retention of solvent or photoproducts since the time at high temperature was minimized. These observations are

consistent with other studies in literature that report increased dielectric constant for rapid cured photosensitive dielectric films [19, 23]. These results show that the physical properties for VFM cured films were generally similar to thermally cured ones, with most properties being better, even though the processing time was shorter.

The VFM curing in air was also studied, which would allow simpler and lower cost processing. Samples cured in nitrogen were compared with the samples cured in air. The FTIR results showed the same degree of reaction as those cured in nitrogen. Additionally, the mechanical properties and moisture uptake of the samples air-cured were almost identical in reduced modulus, hardness, and swelling ratio to the nitrogen cured samples and showed no oxidation effect. There was no indication of film yellowing which is important for optical applications.

Samples cured at 160°C in VFM were examined to investigate the minimum cure time. As shown in Fig. 7.3, full conversion was achieved at times as short as 5 min. This observation was supported by monitoring the nano-indentation and swelling results. A highest degree of crosslinking, which resulted in the maximum hardness and reduced modulus, was achieved for the sample cured for 5 min at 160°C, Fig. 7.7 and Table 7.2. This corresponded to the lowest degree of swelling which supports the claim of the highest degree of cross-linking. The values were also more favorable than the corresponding ones for thermally-cured films.

Thus, it can be concluded that the PNB can be cured by VFM in shorter times and lower temperature, compared to traditional oven curing, resulting in similar or improved properties.

7.4 Conclusions

VFM processing of Avatrel 8000P was investigated. The results showed that the microwave reaction rates were higher at each isothermal cure temperature compared to convective heating, indicating that the rapid VFM curing of the PNB at low temperatures

151

is feasible. The PNB film was fully cross-linked after 15 min VFM cure at low temperature of 150˚C. The shortest cured time to fully cure the polymer was found to be 5 min at 160°C. Also, the feasibility of rapid VFM curing of PNB in air was studied. All air cured VFM samples (140˚C-180˚C) showed no effect of oxidation. The degree of cross-linking in PNB films were studied by FTIR spectroscopy. The FTIR studies showed no significant difference in chemical structure between VFM and thermally cured samples. A higher degree of epoxy ring-opening and cross-linking was observed in VFM-cured samples than thermally-cured samples. The chemical, electrical, and mechanical, properties of VFM-cured films were characterized and compared with thermally cured films to determine the effectiveness of VFM processing. VFM-cured films showed equivalent or improved properties compared to thermally-cured films.

CHAPTER 8

APPLICATION OF POLYNORBORNENE DIELECTRICS IN
MICROFLUIDIC DEVICES

The research undertaken in this chapter was a collaboration with the Photonics Group at the Georgia Institute of Technology, where Ehsan Shah Hosseini carried out the photonic device fabrication and characterization aspects and Mehrsa Raeisazdeh carried out the fluidic-channels fabrication aspects. Epoxy-functionalized polymers, such as PNB, are valuable for forming micrometer-size structures, such as in permanent dielectrics. However, high spatial resolution features are not feasible through optical lithography due to wavelength and chemical reactivity restrictions. Nanometer size features made from inherently patternable, epoxy-based polymers are of interest and beyond the capabilities of conventional, photosensitive epoxy systems.

Micro/Nanochannels have applications in various new technologies such as micro/nanofluidic devices. Some key application areas for micro/nanofluidics are molecular biology, cellular biophysics, fuel cells, and photonics. Specially, applications in micro/nanofluidics in biosensing are of interest.   Micro/nanofluidics technology allows for novel developments such as integration and multimode sensing. Microfluidic circuitry can be mass-produced, making it inexpensive and accessible. Moreover, the reduction of size greatly reduces the analysis time. Another benefit of micro/nanosystems is the reduction in sample size needed.

Incorporating advanced micro/nano fluidics with high-sensitivity photonic sensors will provide compact, effective sensors for lab-on-a-chip tools [138]. Thus, optofluidic sensors are gaining widespread use in biosensing and chemical analysis applications [139]. Some potential applications of optofluidic sensors are clinical screening, medical

diagnostics, screening of chemical compounds in drug discovery and development, and toxic detection [140].

The microfluidic integration of optical chips with the usually aqueous solutions can be done by three major methods. One common method is SU-8 photolithography with glass/polymer/polydimethylsiloxane (PDMS) capping [141]. SU-8 (Micro-Chem Corp. MCC, Newton MA) is a negative-tone, solvent-developable epoxy-based formulation, first developed at IBM, which has been used extensively for making high aspect-ratio MEMS device structures and packaging components with high thermal stability [87, 90, 142-145]. PDMS replica-molding process is also used for such integrations [146]. Decomposable polymers can also be used for channel fabrication in microfluidic devices [147, 148]. The first method uses SU-8 as the channel material. After the channels are designed using photolithography (with a dark-field mask), the liquid can be dropped on top of the reaction area or flown into the channels. If pressure driven flow (PDF) is required, channels can be covered either by a PDMS layer or a glass cover. In the latter case, access holes need to be etched through the glass cover. In the second method, a clear field mask is used to define the channel molds in SU-8. SU-8 mold is made hydrophobic with a layer of Au evaporated and PDMS is poured over the mold. The cured PDMS can then be peeled off the mold. The PDMS piece should be made hydrophilic if a permanent and watertight structure is needed. To achieve this, the sample is exposed to oxygen plasma in a reactive ion plasma machine [149]. After the oxygen treatment, the PDMS surface retains its hydrophilic property for 15 minutes, which is enough for a proper alignment and integration with the optical devices.

The two aforementioned approaches, despite being commonly used in glass-based fluidic devices, lack several essential capabilities necessary for successful post-CMOS integration. The PDMS molding technique most often relies on rough alignment of the large channels with sensing devices, requires manual tubing, and relies on the degradable hydrophilic bonding of the bulky PDMS mold to the substrate. The SU-8-based devices,

154

despite having micrometer-scale alignment accuracies, require a capping layer making them unsuitable for compact CMOS integrated optofluidic lab-on-a-chip solutions. Moreover, both of these polymers are subject to chemical degradation and swelling when exposed to different chemical solvents.

In this work, an alternative approach was demonstrated based on channels formed by thermally decomposable polymers at relatively low and CMOS-compatible temperatures. A negative-tone PNB-based sacrificial material, Unity 4698P, was used to make micro/nanochannels. Avatrel 8000P and silicon dioxide were used as the overcoat materials. In this processing, no etchant is necessary to remove the polymer, thus the underlying sensing devices are not affected. The channels are then integrated with integrated photonic devices fabricated in silicon nitride and operating in the visible wavelength range.

The design of the proposed optofluidic sensor is shown in Figure 8.1. The device consists of a silicon nitride (SiN) microdisk resonator covered by a microfluidic channel. The device is designed in a way that the evanescent light traveling in the ring resonator interacts with the upper fluidic cladding. At resonance, light circulates many times within the ring, which leads to a large enhancement in the interaction length between the evanescent field and the cladding liquid (with micro/nanochannels, the interaction with the cladding fluid will be maximized [150].)
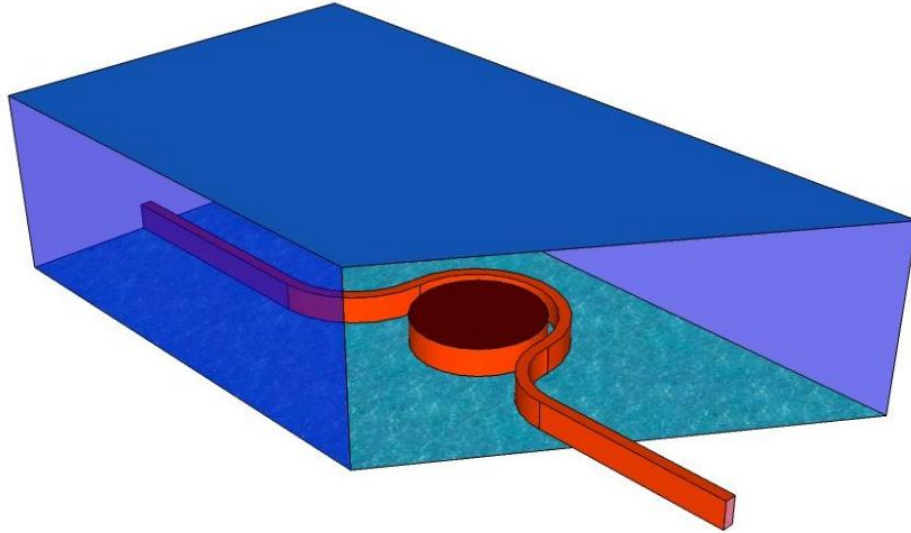
Figure 8.1 Optofluidic sensor design with a waveguide coupled to a microdisk resonator and a microfluidic channel on top. The waveguide and resonator in this work are fabricated in silicon nitride. The channel is created by thermal decomposition of the polymer through the Avatrel 8000P or oxide cladding.

There are several possible schemes for the sensing operation. For example, in the refractive index sensing scheme, by injection of each refractive index fluid, the resonance spectrum of the microring resonator will vary [151]. Figure 8.2 shows the variation of the resonance wavelength of the microring resonator when the refractive index of the fluid on top of the resonator is changed. High quality optical resonators can demonstrate very sharp resonances, which can be the core of very sensitive and accurate integrated sensing devices [115]. Epoxy-functionalized polymers, such as PNB, are valuable for forming micrometer-size structures due to their ease of reaction. Epoxy-based polymers can also be used as sacrificial polymers. PNB-based epoxy-containing decomposable polymers can be exposed with UV or e-beam radiation and subsequently solvent-developed to form free-standing structures. In this work, a negative-tone, PNB-based sacrificial material, identified as Unity 4698P, has been used to make microchannels. Unity 4698P has a simple process flow which can be accomplished in five process steps to form arbitrary microfluidic shapes and channel structures. The developed sacrificial-

polymer patterns can be encapsulated with a thick layer of Avatrel 8000P or silicon

dioxide, which will not affect the optical performance of the photonic device (e.g.,

resonators) underneath [151]. The thermal decomposition products of Unity 4698P are

able to diffuse through the encapsulating silicon dioxide/ Avatrel 8000P to leave clean

channels with exact shapes. In this chapter, the methods utilized in photonic and fluidic

microfabrication of this device are explained. The sample flow schemes and optofluidic

integration strategies are also reviewed.
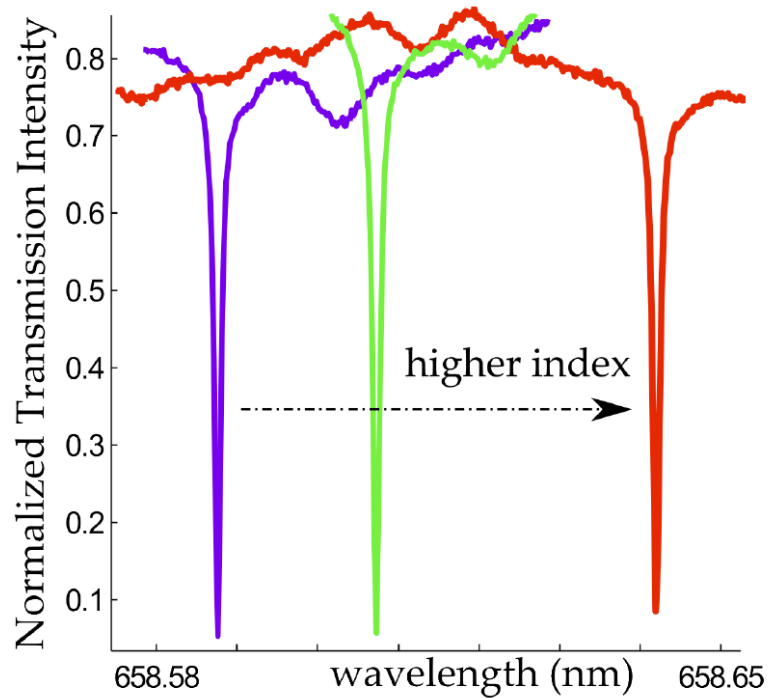
Figure 8.2 Change of the resonant frequency of the optical cavity due to the change in the
refractive index of the ambient or selective attachment of the biomolecules to the
resonator surface.

8.1 Experimental

8.1.1 Fabrication of the Photonic Device

The Fabrication process starts with a silicon substrate. The first step of fabrication is to grow a thick isolating oxide layer on prime silicon wafers. As the dry oxidation rate is very low, the majority of the oxidation process is done in a hydrogen-rich environment (wet oxidation). The temperature during the oxidation is limited to 1100°C. The required time for the production of 3 μm oxide is 32 h. During this process, 1.76 μm of the silicon is consumed.

The light guiding SiN layer can be deposited by either plasma enhanced chemical vapor deposition (PECVD) or low-pressure chemical vapor deposition (LPCVD). The films deposited by LPCVD are of higher quality than the PECVD films [152]. PECVD SiN is etched approximately twice as fast as the LPCVD material by dry etching (e.g., by inductively coupled plasma (ICP) or reactive ion etching (RIE)), somewhat reducing the difficulty of the fabrication. However the much higher impurity density (primarily hydrogen) and higher optical absorption of the PECVD material makes it inappropriate for high quality devices [152]. Nevertheless, the initial devices fabricated using PECVD films demonstrated a moderate quality factor ($Q{\sim}10^5$ for a microdisk with 20 μm radius and 200 nm SiN film thickness). To achieve high Q's and low loss waveguides, LPCVD to deposit the SiN device layer for all structures reported here.

The photonic patterns are e-beam written with MaN 2403 resist provided by Micro Resist Technology GmbH. MaN requires significantly lower dosage than HSQ, a more common negative resist, which results in a writing time almost a quarter of that of the HSQ. A major issue with the MaN resist is its weak adhesion to the substrate. The delamination failure, often happening in aqueous developers (e.g., 0.26N TMAH used in the MaN case), can be partially alleviated by hexamethyldisilazane (HMDS) priming.

Nevertheless, the results with this method are not repeatable. Instead, a SurPass 3000 (provided by DisChem Inc.) is used as a primer [153]. The wafers are submerged in SurPass 3000 for 30 seconds, rinsed with deionized (DI) water and covered with MaN immediately. After the development of the exposed patterns, an optional reflow of the resist at 145°C for 3 minutes can significantly lower the sidewall roughness of the final device. This step, although very beneficial for ultra-high quality photonics, can lead to feature size changes or sticking of patterns if the MaN resist does not perfectly adhere to the substrate.

After developing the patterns in the 0.26N TMAH developer, the samples are etched in a CF_4 ICP etcher with better than 1:1 selectivity [115]. The resist is stripped away, and the samples are then cleaned in a piranha solution for 5 min. After dehydration, samples are ready for fluidic integration described in subsection 8.1.2.

8.1.2 Fabrication of the Fluidic Channels

Unity 4698P sacrificial material contains a PNB backbone with functional groups dissolved in 2-heptanone. (Promerus LLC, Brecksville, OH). The chemical structure of Unity 4698P is shown in Figure 8.3. When Unity 4698P is irradiated with UV radiation or an e-beam, an acid catalyst is produced. Once reacted, the acid catalyst initiates epoxy ring opening and polymer cross-linking. An unstable carbocation from the epoxy, which forms a covalent bond with other PNB chains, results in cross-linking between chains. After the polymer has been cross-linked, Unity 4698P can be thermally decomposed at temperatures above 350°C. The fabrication sequence of the microchannels is shown in Figure 8.4. For microchannel fabrication, Unity 4698P films were spin coated on the processed wafer described in subsection 8.1.1 using a Brewer Science CEE 100 spinner. An 8-9 mm thick film was obtained at a spin speed of 500 rpm for 10 sec followed by 900 rpm for 60 s. The films were soft baked at 110°C for 5 min on a hotplate (air ambient) to remove most of the residual solvent. In this work, EBL has been used to

achieve very high spatial resolution. EBL was performed with a JEOL JBX-9300FS tool at 100 kV accelerating voltage and 50 pA beam current. After exposure, the samples were baked at 90°C for 4 min on a hotplate followed by a four-minute delay.
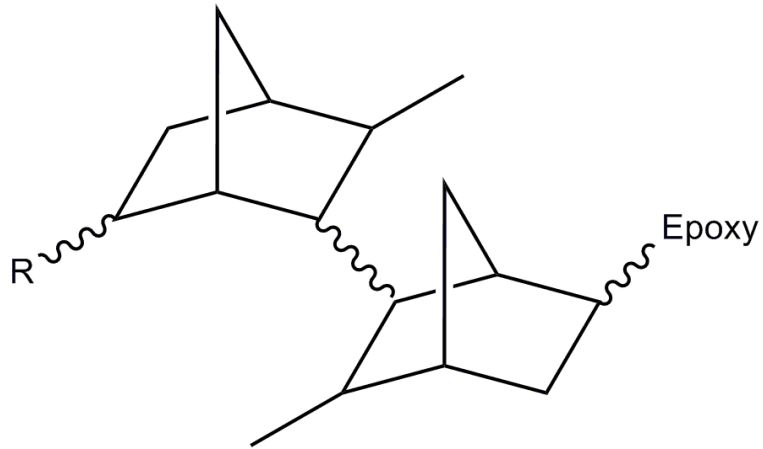
Figure 8.3 The chemical structure of Unity 4698P.
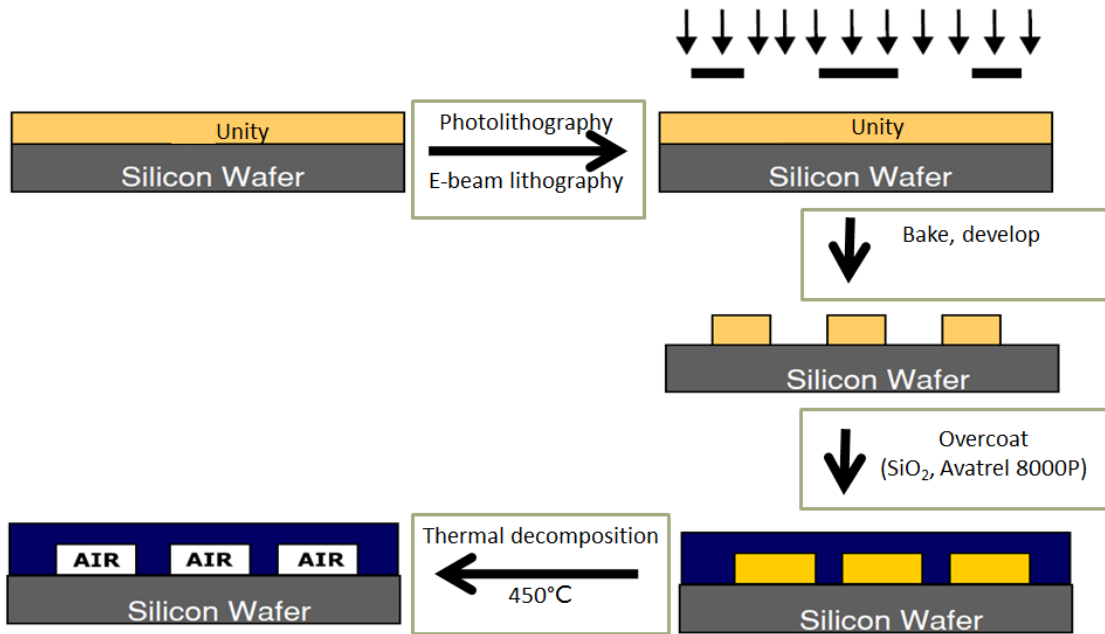
Figure 8.4 Fabrication sequence of air channels.

The samples were then developed with cyclopentanone for 5 min and spray rinsed with isopropanol (IPA) for 1 minute. Removal of any polymer residue from the developed patterns was accomplished with a PlasmaTherm RIE system using the following conditions: 45 sccm O_2, 250 mTorr, and 300 W at 25°C. The etch rate of the polymer under these conditions was approximately 700 nm/min. Deposition of the SiO_2 overcoat was performed with a PlasmaTherm PECVD tool using the following conditions: 380 kHz RF, 50Wpower, 300°C, 550 mTorr, and a gas mixture of N_2O 1400 sccm and 2% SiH4 diluted in N2 400 sccm. The SiO_2 deposition rate was approximately 35 nm/min. The encapsulated sacrificial polymer structures were thermally decomposed in a Lindberg tube furnace purged with nitrogen. It was found that a fast ramp rate, 20°C/min, resulted in cavities with lower residue. The heating cycle used for Unity 4698P decomposition is shown in Figure 8.5. The heating cycle was designed based on the decomposition profile of the polymer. Figure 8.6 shows the TGA scans for Unity 4698P which resulted in the decomposition temperature of 317°C. The final unity nanochannel structures are shown in Figure 8.7.
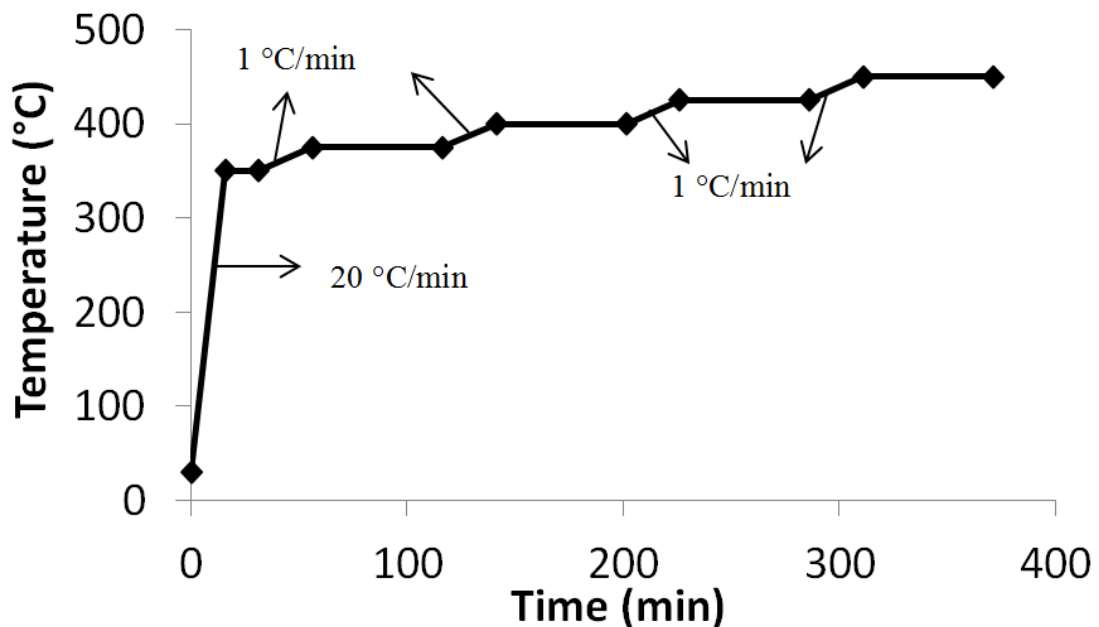
Figure 8.5 The heating program for the decomposition of Unity 4698P.
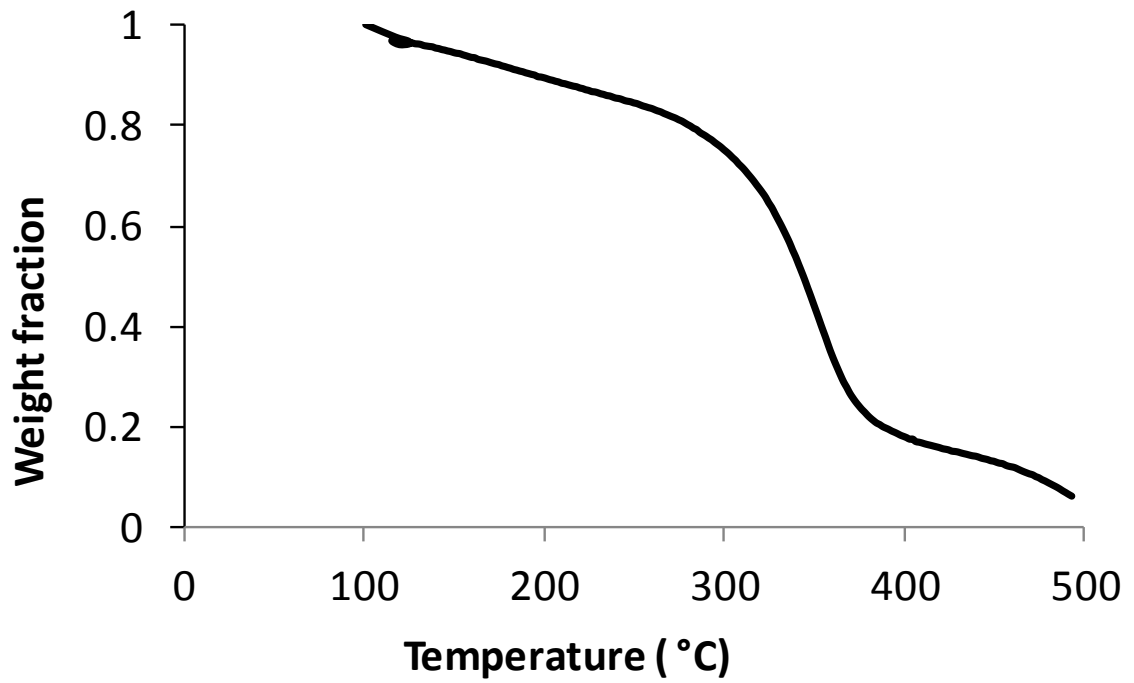
Figure 8.6 TGA scans for Unity 4698 (620 nm film; SB: 100°C for 5 min; exposure dose: 300 mJ/cm^2; PEB: 90°C for 30 s; develop for 45 s in toluene; 1 min isoproponal rinse).
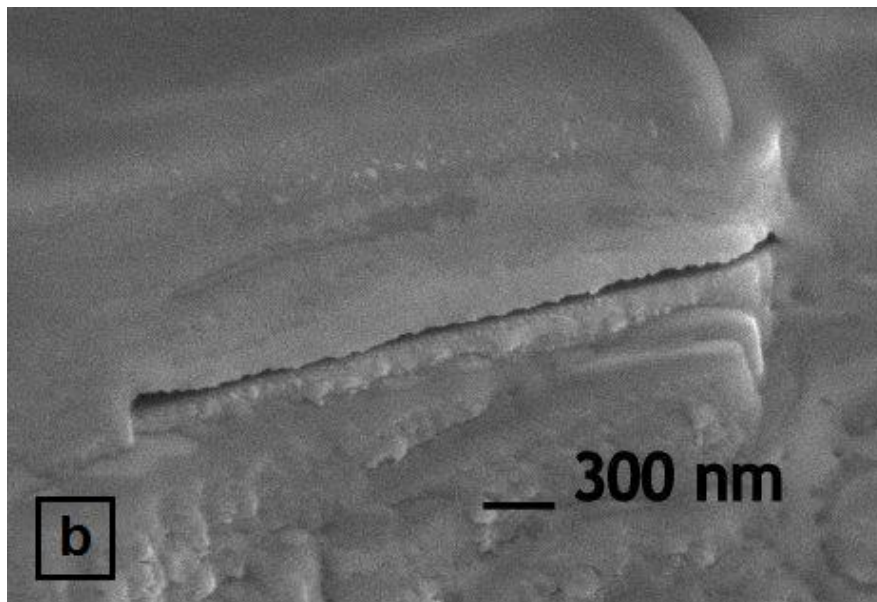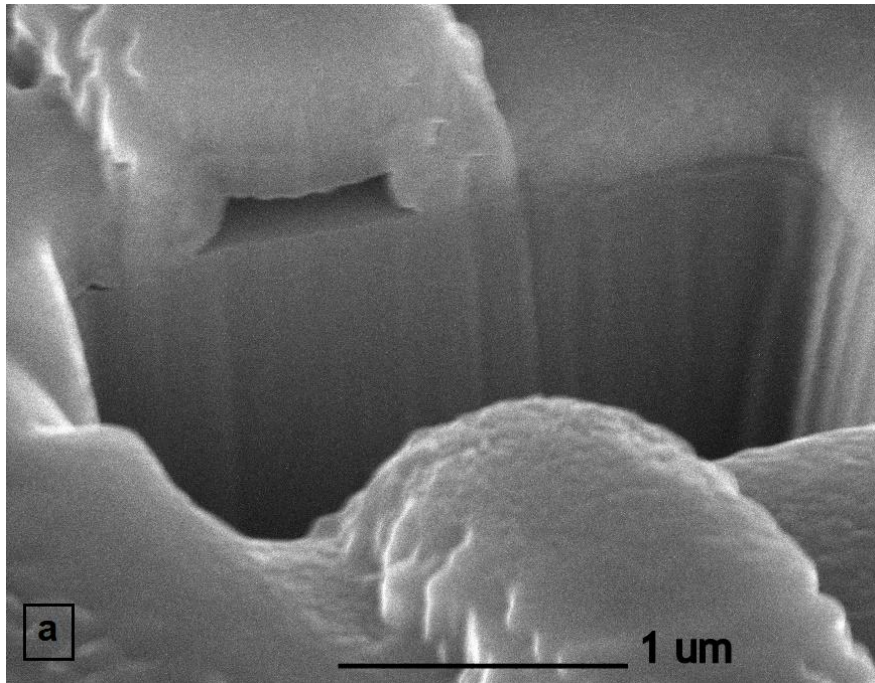
Figure 8.7 Nanochannels fabricated with Unity 4698P: (a) a nanochannel with vertical sidewalls; (b) a sub-100 nm thin channel.

One of the pertinent processing issues with SiO_2-covered air-channels was found to be the temperature for the deposition of the encapsulating layers. The oxide PECVD deposition temperature was limited to 300°C. Above these temperatures, the overcoat material severely cracked. The most important factor limiting the deposition temperature of the films is the mismatch between the CTE of PNB (CTE =127 ppm/°C) and SiO_2 (CTE = 0.6 to 0.9 ppm/°C). Due to this mismatch, the overcoat films crack from stress developed between the substrate and the film during cooling from the deposition temperature as shown in Figure 8.8. To address this issue, Avatrel 8000P was used as an alternative overcoat material which has a similar CTE to that of Unity 4698P due to the similar polymer structure of the PNB polymers. For the SiO_2-coated samples, the oxide cap was optimized and the decomposition model shown in Fig. 8.5 was developed which prevented the films from cracking. The resulting structures can be seen in Figure 8.9, which shows the microchannels with a width of 1, 5, 10, 15, and 20 µm and a 7.5 µm

pitch after decomposition. The AutoCAD patterns used for fabrication of the 1-20 μm width patterns are shown in Figure 8.10. Figure 8.11a and 8.11b show the cross-section image of the thermally treated samples with a width of 5 μm and 10 μm, respectively. As it can be seen in Fig. 8.11, there is no residue inside the channels, which is promising for optofluidic integration, as otherwise the performance of the optical devices would be highly degraded.
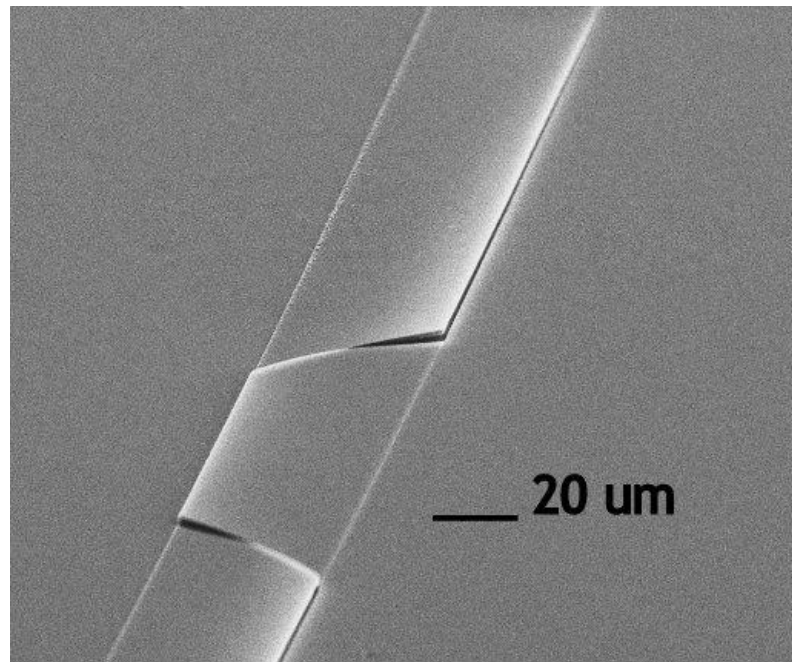
Figure 8.8 Cracking in channel fabricated with Unity 4698P and oxide capping due to the thermal stress built up in the film.
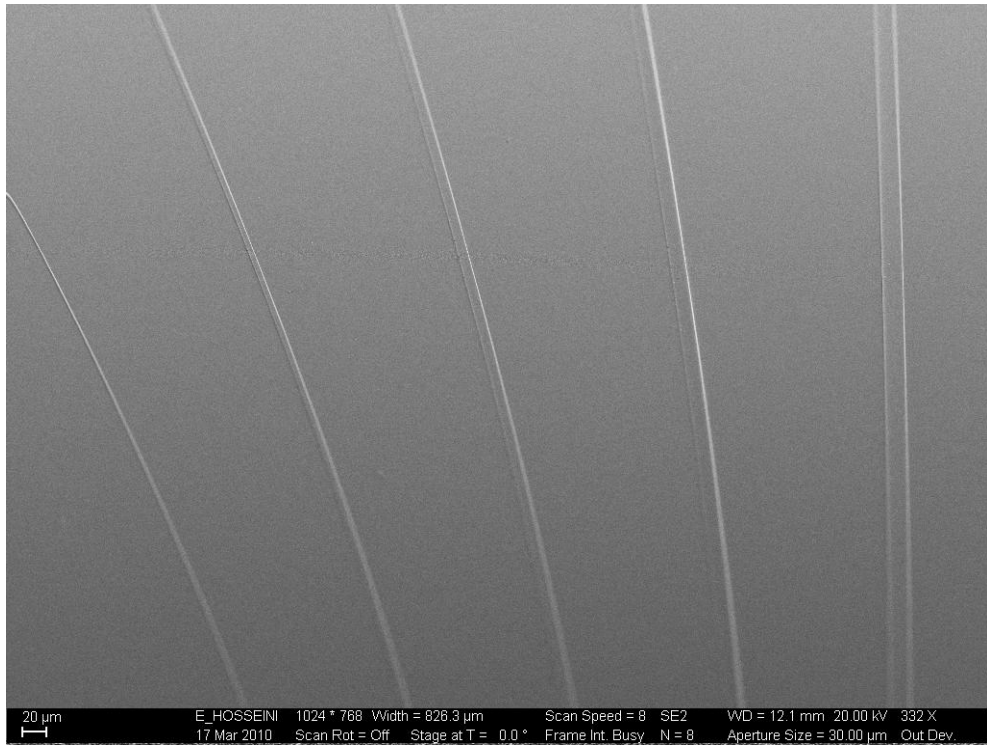
Figure 8.9 Microchannels with 1, 5 µm,10 µm, 15 µm, 20 µm width fabricated with Unity 4698P after decomposition.
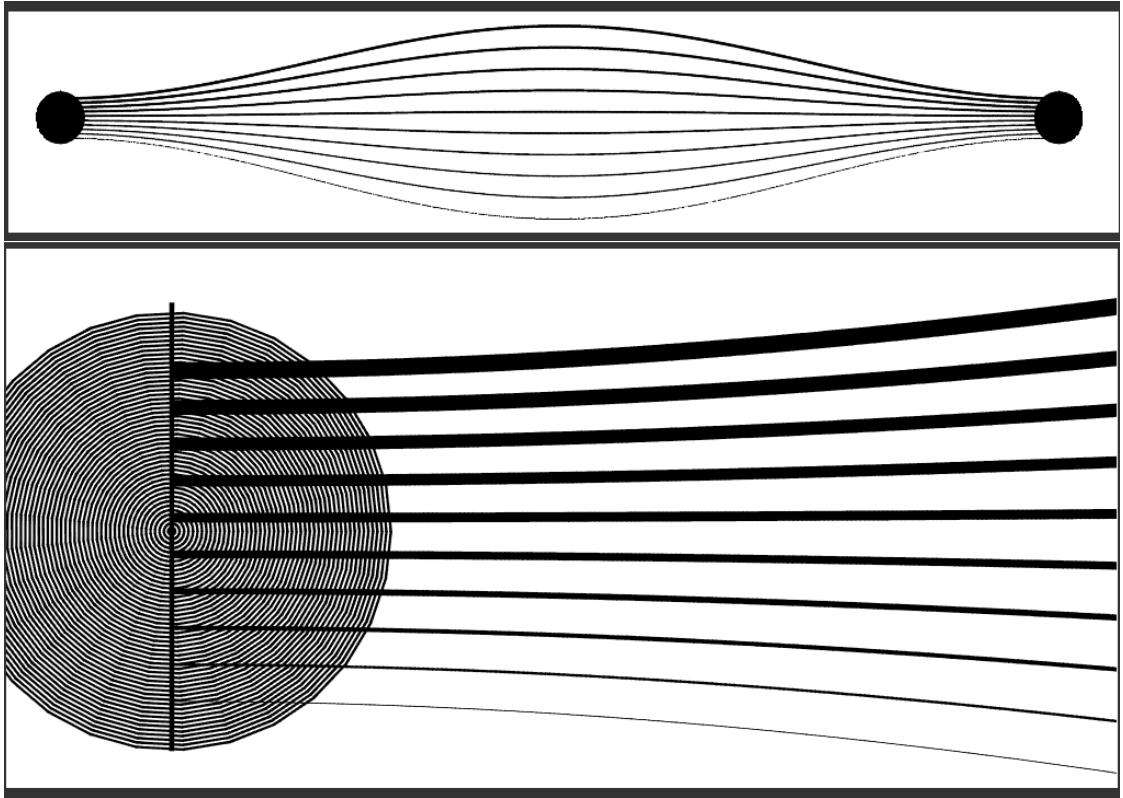
Figure 8.10 AutoCAD Patterns used for EBL of Unity 4698P.
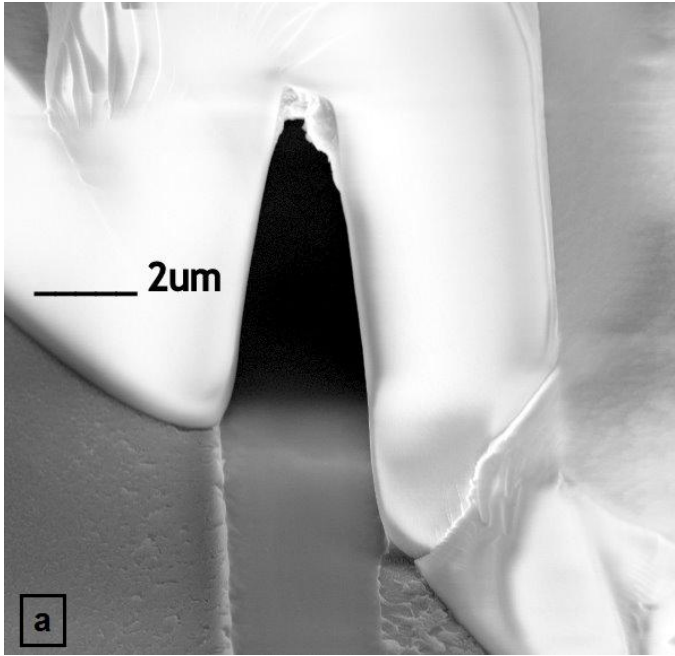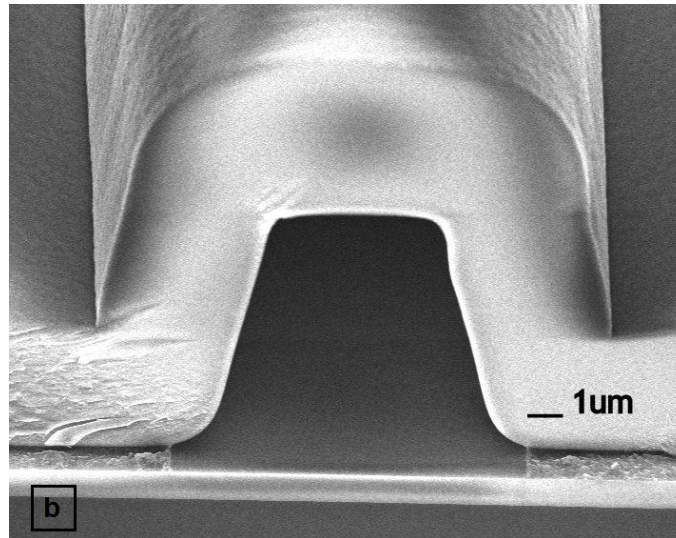
Figure 8.11 Channels fabricated with Unity 4698P using oxide cladding and EBL: (a) a high aspect ratio and (b) a wide channel.

8.2 Results

After the channel fabrication is optimized, integration with optical devices and the specimen flow is investigated. Several issues of this process needed to be addressed. The first challenge was that the very first devices would not pass the fluid. Further investigation showed that the decomposition process leaves the inside surfaces of the channels hydrophobic. It is virtually impossible to flow a liquid through a narrow hydrophobic channel. A high temperature oxygen plasma in an asher makes the channels hydrophilic, and the fluid flows inside the channels (as can be seen from Figure 8.12).
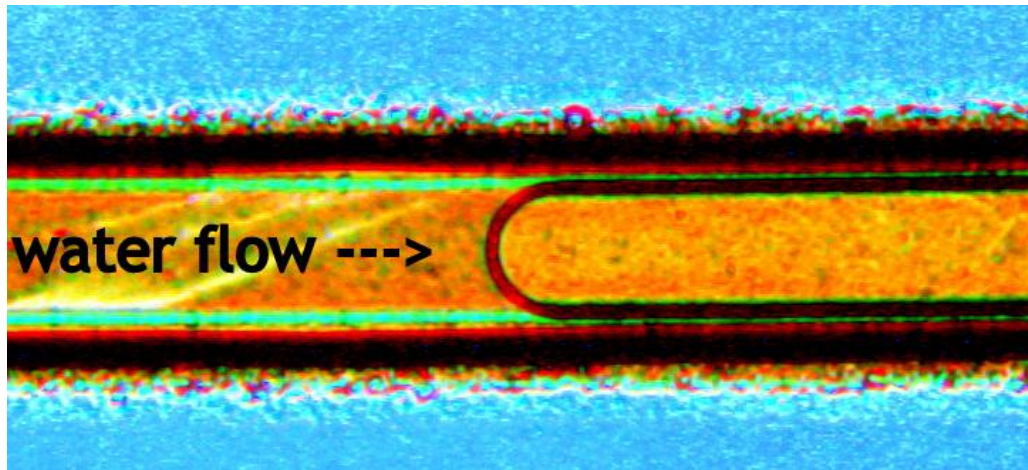
Figure 8.12 Flow of water inside the channel. The picture is taken using an optical microscope while water was flowing inside the channel due to the capillary effect. The channel opening was 5 μm wide.

The next challenge was to make sure no residue is left inside the channels (otherwise, the performance of the optical devices would be degraded). Usually, for conventional photonic devices a piranha clean (a mixture of sulfuric acid and hydrogen peroxide) removes the residues effectively. Because the mixture is a strong oxidizer, it will remove most organic materials, and it will also hydroxylate (add OH groups) most surfaces making them extremely hydrophilic. Unfortunately, due to the bubbles generated during the piranha etch, this process is not compatible with these channels. Instead, we used a solution of chromic acid made by adding concentrated sulfuric acid to a dichromate (which may contain a variety of compounds, including solid chromium trioxide). After establishing a reliable and scalable mico/nanochannels fabrication and a post processing method, a specimen flow (appropriate for the target channel size) is required.

To flow the liquids into the channels there are two common methods. The first method, i.e. PDF, utilizes a pressure build-up between two reservoirs. The other major method is the electro-osmotic flow (EOF). As a measure for the type of flow inside the channel, the dimensionless Reynolds number, Equation 8.1, is used [154].

$$Re = \frac{wb}{v} \qquad (8.1)$$

Where w[m/s] is the characteristic flow velocity, b[m] is the characteristic dimension and n[m2/s] is kinematic viscosity of the fluid. The n parameter for water is 1.01; b is typically the smallest dimension along the channel. The typical properties of pressure-driven microfluidic systems, namely small channel size, small velocity, and large viscosity combine in devices to result in generally small values of the Reynolds number. Re is usually much less than 100, often less than 1. In this Reynolds number regime, flow is completely laminar and no turbulence occurs. The transition to turbulent flow generally occurs when Re is around 2000 [154]. Laminar flow provides a means by which molecules can be transported in a relatively predictable manner through micro-channels. One of the basic laws of fluid mechanics for pressure driven laminar flow, the so called no-slip boundary condition, states that the fluid velocity at the walls must be zero. This produces a parabolic velocity profile within the channel.

Despite the simplicity of the pressure driven approach, which only needs a syringe pump or a vacuum line, the drawback is non-scalability of the devices. As for a typical rectangular channel with a characteristic dimension of d or a circular shaped tube with a radius r, the pressure needed for a certain velocity (ΔP) scales with $\alpha \ 1/wd^3$ for the rectangular shape, and $\Delta P \ \alpha \ 1/r^4$ for the tube. This imposes a limit on the size of the channels and makes nanofluidic with manageable pressures impossible. Therefore, if the channel sizes are smaller than roughly 10 mm, the electro-osmotic flow is the preferred method. EOF is the motion of liquid induced by an applied potential across a porous material, capillary tube, membrane, micro-channel, or any other fluid conduit. Because electro-osmotic velocities are independent of conduit size, as long as the double layer is much smaller than the characteristic length scale of the channel, EOF is most significant for channels. Therefore, in the smaller channels described in this work the flow is

achievable by applying a high voltage (200 V) through a pair of platinum electrodes across the LB conductive medium obtained from Faster Better Media LLC.

Another issue to be considered is the scattering of light from the waveguide-channel interface. As the index mismatch between the oxide-covered sections and the channel is large (especially if no fluid is flowing inside the channel), a large portion of the optical guided wave is scattered at the boundary (Figure 8.13). To alleviate this problem, large multi-mode waveguides were used at the intersection and the waveguide was tapered down to a single mode profile inside the channels (as schematically shown in Fig. 8.13). Considering this issue, it is undesirable to cover a ring resonator with the channels only partially, as this would lead to very low quality factors due to the scattering.

As we need to cover the resonators with the channel, the width of the channel should be larger than the diameter of the resonators used (20-40 μm). This leads to fragile overcoats (Fig. 8.8) unless a thick oxide layer is used, which in turn leads to longer and higher temperature decomposition conditions. Here, at least 5 μm of oxide coating and 6 hours of decomposition were used to achieve mechanically robust overcoats while maintaining
residue-free channels.

To characterize the fabricated structures, the output light of a tunable laser diode source (New Focus™TLB-6305) is coupled to the cleaved facet of the waveguide using a Mitutoyo 20x long distance objective lens. A quarter-wave plate and a polarizer ensure the light energy is in the TE mode. The wavelength of the laser is swept across the 652-660 nm wavelength range in 0.25 pm steps, and the transmission is measured as a function of wavelength by a Si detector at the waveguide output. The data is then transferred to the computer through a data acquisition (DAQ) card. One long distance working lens and one regular objective lens are used to collect the light from the top and the output of the waveguide respectively.

A custom-built microscope in the z direction is used for most of the analysis. Using 50/50 polarizing beam splitters to deliver the collected light to the measurement devices, a spectrometer, a detector, and a camera are integrated in the microscope. For all the set-up structures a Thorlabs 30 mm cage system was used. The cage system is very versatile and stable and allows fast and easy reconfiguration in the set-up without requiring an extensive alignment readjustment. As a test of the capabilities of our system to measure fluorescence, the output of a waveguide covered with 60 mg/lit Oxazine dye (Abs/Em at 646/670 nm) is measured with a spectrometer (Ocean Optics USB-2000). A sharp edge filter with an OD of over 70 is used to filter out the pump. The unfiltered and filtered spectra are shown in Figure 8.14a and 8.14b, respectively. Fig. 8.14 clearly suggests that the waveguide-channel structure is a reliable platform for a variety of sensing applications.
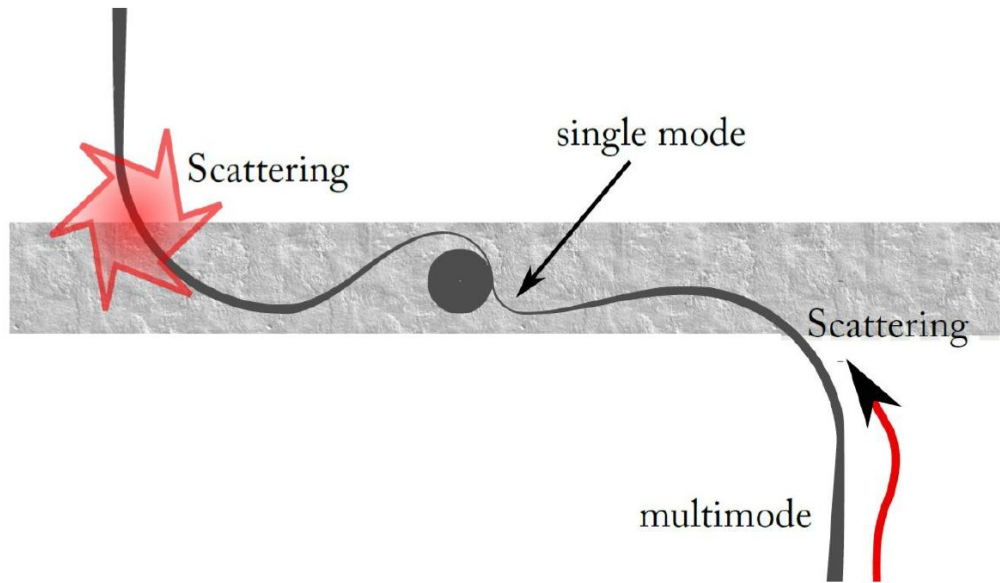
Figure 8.13 Scattering of the guided optical wave by the interface between the oxide cladding and the fluidic channel. The size of the disk puts an upper limit on the width of the channel. Using a multimode waveguide at the interface can reduce the scattering from the waveguide-channel interface.
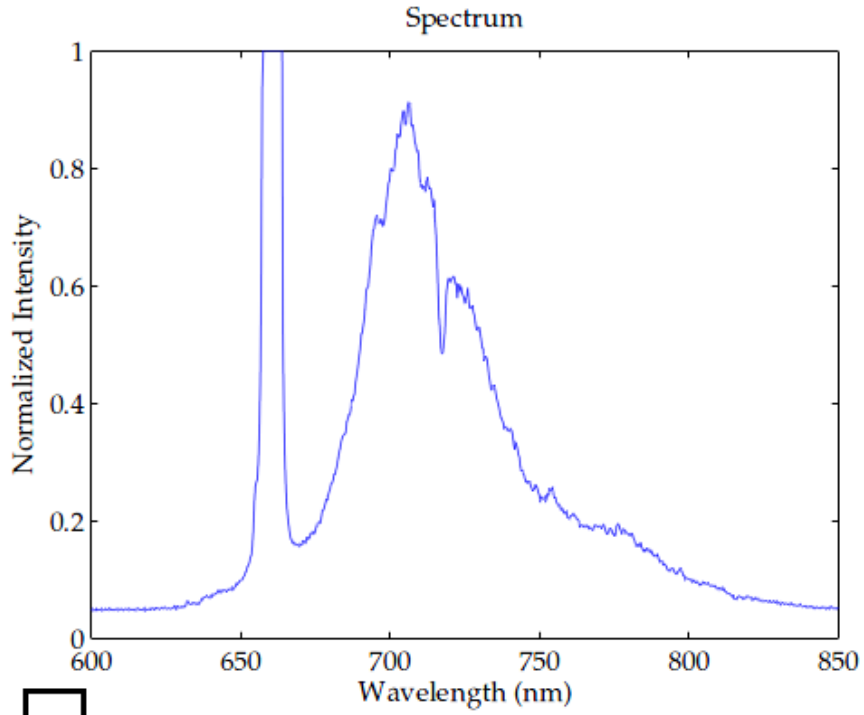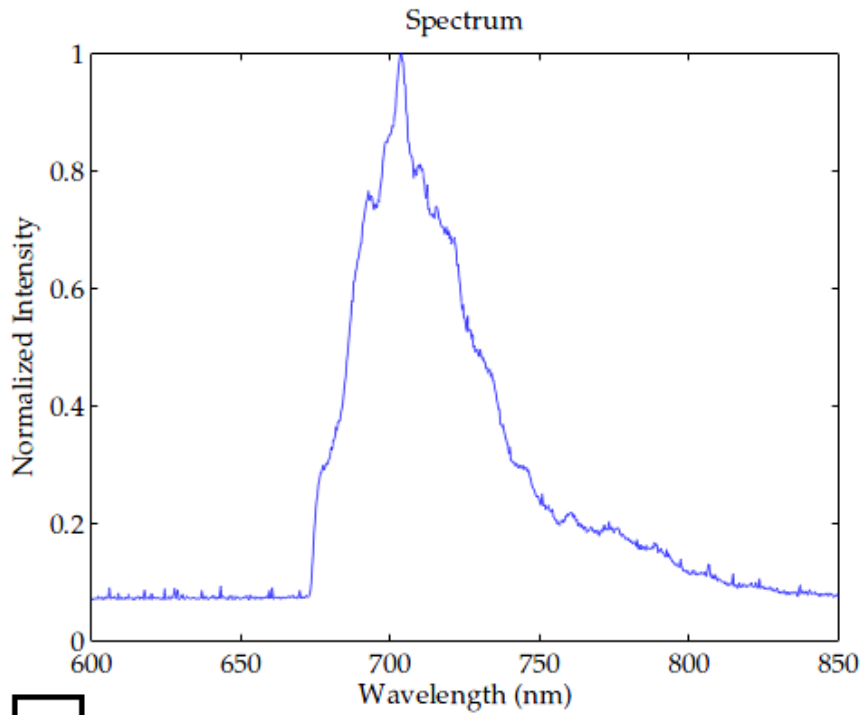
Figure 8.14 (a) Fluorescence from Oxazine pumped and collected with SiN waveguides.
(b) The pump signal is filtered out.

8.3 Conclusions

In this study, it was shown that it is possible to integrate micro/nanochannels, fabricated using Avatrel 8000P and thermally decomposable PNB polymers, with integrated photonics in a lab- on-a-chip platform. Low loss silicon nitride photonic structures, functioning in a broad optical range (visible through infra-red), were created with conventional micro-fabrication techniques by Dr. E. Shah Hosseini. The photonic structures were then covered with a decomposable PNB polymer, which can be patterned with UV or e-beam exposure. The channels then were formed by decomposition of the decomposable PNB polymer through the cladding layer of Aquatrel 8000P or SiO_2. The channels made with low-temperature decomposability are the most promising for future applications, especially considering the possibility of integration with CMOS processes without potential chemical or thermal damage to the CMOS circuitry. The robust and residue-free channels, demonstrated here, can be varied in size in accordance with the photonic design and the specimen flow procedure. If very compact photonics are utilized, the channels can be fabricated with sub-micrometer EBL, and EOF can be used for the sample delivery. On the other hand, microring/microdisk resonators fabricated in SiN require large channels and are suitable for pressure driven flows. The high resolution and compact channels will enable multi-mode sensing functionalities through refractive index, florescence and Raman sensors. The potential small size of the channels and sensors can pave the way for single molecule sensing schemes using ultra-small sample sizes.

CHAPTER 9

PERSPECTIVES AND SUGGESTIONS FOR FUTURE WORK

A challenging application space exists for high-sensitivity, high-fidelity dielectrics in MEMS, microelectronic, and photonics. Polymers are widely used in these fields because of their superior properties. The scope of this work was to study the cross-linking of a PNB-based polymer as a dielectric for these applications. The PNB dielectric must meet the needs in terms of patternability, mechanical stability, and dielectric properties as well as easy processing. Both the UV and e-beam induced cross-linking of the PNB dielectric were studied and the effect of epoxy additives, a PAG, a UV sensitizer on the polymer cross-linking, patternability, sensitivity, and resolution was investigated. In addition, the processing of the PNB dielectric was optimized to achieve the optimum mechanical and electrical properties at low thermal cure temperatures. The final goal of this wok was to develop a rapid, low-temperature cure process for the PNB dielectric using VFM to avoid the degradation of the polymer properties and the increase in the processing cost.

The addition of the tetra-functional epoxy cross-linker, TPEGE, showed significant improvement in the sensitivity and photo-patternability of the PNB dielectric. While this improvement was expected, the magnitude of the effect was unforeseen. Coupling the epoxy cross-linker with the UV absorber resulted in effective energy transfer between the epoxy cross-linker and PAG and improved the polymer cross-linking. The origin of the effect of TPEGE on the polymer sensitivity and patternability is unclear and could be the subject of future work. Additionally, the tetra-functional epoxy cross-linker significantly improved the polymer to substrate adhesion as shown in the contrast curves and by the longer DT. The exact nature of the improved adhesion for

this compound, beyond its higher epoxy functionality and absorbance, was not investigated and could also be the subject of future studies.

In addition, PNB formulations with additional PAG and epoxy cross-linkers showed extremely high e-beam sensitivity and high contrast. In order to understand these effects, the cross-linking and bond breaking reactions occurring due to the e-beam radiation must be studied which opens avenues for future investigations. Also, the reactions in other polymer systems with lower sensitivity need to be studied to understand why they require higher e-beam energy for cross-linking and/or bond breaking reactions involved in pattering the polymers. Additionally, Avatrel 8000P showed satisfying resolution and LER for the structures patterned with EBL. The PNB used in this study has a relatively high molecular weight. Improvements in minimum feature size and LER may be expected with lowering the molecular weight of the PNB formulations.

Developing also showed an interesting effect on the polymer cross-linking reactions. A higher degree of cross-linking and epoxy ring opening was observed for the samples developed in the TMAH developer prior to the cure process compared to the undeveloped samples. This effect was unexpected since TMAH is an aqueous base developer which could cause some degree of neutralization and dissolution of the photogenerated acids created during exposure, decreasing the amount of acid catalyst. However, this may provide more free volume and thus higher mobility for the activated epoxy moieties within the film to move, improving the polymer cross-linking. Alternatively, incorporation of the TMAH base in the PNB can plasticize the film. However, the exact nature of the effect of the TMAH developer on the polymer cross-linking is unclear and could be the subject of further studies.

It was also observed that the PNB dielectric was fully cross-linked at a low temperature of 150°C for the very short time of 15 min by VFM. This shows the high energy absorptivity of the PNB polymer at the microwave frequencies used in the study

176

and the effective cross-linking within the polymer when cured by VFM. To further investigate the effective cross-linking of PNB by VFM, the kinetics of the cross-linking reactions of the VFM-cured PNB films can be studied and compared to those of the thermally-cured PNB films.

Lastly, to further improve the polymer dielectric properties, the concentration of the epoxy cross-linkers in the polymer can be lowered. Epoxies suffer from high dielectric constants ($\varepsilon_r = 3.5$ to 5) and the addition of epoxy-based compounds can degrade the dielectric properties of the polymer. As mentioned previously, Avatrel 8000P is a mixture of a di-functional and a tri-functional epoxy cross-linker, which make about 17% of the polymer solution. On the other hand, the addition of a small amount (1 wt% or 3 wt%) of the tetra-functional epoxy cross-linker, TPEGE, showed significant improvement in the polymer cross-linking and patternability. Replacing the already existing epoxy cross-linkers in Avatrel 8000P with small amount of TPEGE can lower the overall dielectric constant of the dielectric.

REFERENCES

1.   Tummala, R.R. and M. Swaminathan, *Introduction to System-on-package (SOP): Miniaturization of the Entire System*2008: McGraw-Hill Professional.

2.   Tummala, R., E. Rytmaszewski, and A. Klopfenstein, *Microelectronics Packaging Handbook: Technology drivers*1997: Kluwer Academic Publishers.

3.   Rajarathinam, V., *Imprint lithography and characterization of photosensitive polymers for advanced microelectronics packaging.* 2010.

4.   Chiniwalla, P., *Crosslinking of polynorbornen based dielectrics for application in microelectronics*, in *Chemical Engineering*2001, Georgia Institue of Technology.

5.   Meindl, J.D., *Low power microelectronics: Retrospect and prospect.* Proceedings of the IEEE, 1995. **83**(4): p. 619-635.

6.   Golden, J., C. Hawker, and P. Ho, *Designing porous low-k dielectrics.* Semiconductor International, May, 2001: p. 79-88.

7.   Theis, T., *The future of interconnection technology.* IBM Journal of Research and Development, 2000. **44**(3): p. 379-390.

8.   Chu, J.K., et al., *Surface planarization method for VLSI technology*, 1988, Google Patents.

9.   Smythe, J.A., *Spin-on-dielectrics: Planarity modeling*2009: ProQuest.

10.   Rutter Jr, E., et al. *A Photodefinable Benzocyclobutene Resin For Thin Film Microelectronic Applications*. 1992.

11.   Moyer, E., et al., *Photodefinable Benzocyclobutene formulations for Thin film microelectronic Applications.* IEPS Proceedings, Austin, September, 1992.

12.   Bai, Y., *Photodefinition and structure-property relations for polynorbornene based dielectric.* 2001.

13.   May, G. and C. Spanos, *Fundamentals of semiconductor manufacturing and process control*2006: Wiley-IEEE Press.

14.   Rai-Choudhury, P., *Handbook of microlithography, micromachining, and microfabrication*1997: SPIE Optical Engineering Press.

15.   Campbell, S.A., *The science and engineering of microelectronic fabrication*. Vol. 476. 1996: Oxford University Press Oxford, UK.

16.   Jaeger, R.C., *Introduction to microelectronic fabrication*. Modular series on solid state devices ;1988, Reading, Mass. :: Addison-Wesley Pub. Co.

17.   Thompson, L.F., et al., *Introduction to microlithography: Theory, materials, and processing*1983: American Chemical Society.

18.   Crivello, J., J. Lam, and C. Volante, *Photoinitiated cationic polymerization using Diaryliodonium Salts.* Journal of Radiation Curing, 1977. **4**: p. 2.

19.   Famsworth, K., et al., *Variable frequency microwave curing of photosensitive polyimides.* Components and Packaging Technologies, IEEE Transactions on, 2001. **24**(3): p. 474-481.

20.   Sung, T., *Variable frequency microwave curing of polymer dielectrics on metallized organic substrates.* 2003.

21.   Tanikella, R.V., S.A. Bidstrup Allen, and P.A. Kohl, *Variable-frequency microwave curing of benzocyclobutene.* Journal of Applied Polymer Science, 2002. **83**(14): p. 3055-3067.

22.   FARNSWORTH, K.D., et al., *Variable frequency microwave curing of 3, 3', 4, 4'-biphenyltetracarboxylic acid dianhydride/P-phenylenediamine (BPDA/PPD).* The International journal of microcircuits and electronic packaging, 2000. **23**(2): p. 162-171.

23.   Tanikella, R.V., et al., *Rapid curing of positive tone photosensitive polybenzoxazole based dielectric resin by variable frequency microwave processing.* Components and Packaging Technologies, IEEE Transactions on, 2006. **29**(2): p. 411-419.

24.   Tanaka, K., S.A.B. Allen, and P.A. Kohl, *Variable Frequency Microwave curing of Amide-Epoxy Based Polymers.* Components and Packaging Technologies, IEEE Transactions on, 2007. **30**(3): p. 472-477.

25.   Kuekes, P., R. Williams, and J. Heath, *Molecular wire crossbar memory*, 2000, Google Patents.

26.   Lieberman, M., et al., *Quantum-dot cellular automata at a molecular scale.* Annals of the New York Academy of Sciences, 2002. **960**(MOLECULAR ELECTRONICS II): p. 225-239.

27.   Kawano, H., et al., *Development of an electron-beam lithography system for high accuracy masks.* Journal of Vacuum Science & Technology B: Microelectronics and Nanometer Structures, 2009. **21**(2): p. 823-827.

28.   Chou, S., et al., *Sub-10 nm imprint lithography and applications.* Journal of Vacuum Science & Technology B: Microelectronics and Nanometer Structures, 2009. **15**(6): p. 2897-2904.

29.   Hu, W., et al., *Sub-10 nm electron beam lithography using cold development of poly (methylmethacrylate).* Journal of Vacuum Science & Technology B: Microelectronics and Nanometer Structures, 2004. **22**: p. 1711.

30.   Sun, S. and G. Leggett, *Matching the resolution of electron beam lithography by scanning near-field photolithography.* Nano Letters, 2004. **4**(8): p. 1381-1384.

31.   Hosaka, S., et al., *Nanosilicon dot arrays with a bit pitch and a track pitch of 25 nm formed by electron-beam drawing and reactive ion etching for 1 Tbit/ in. storage.* Applied Physics Letters, 2006. **89**: p. 223131.

32.   Henschel, W., Y. Georgiev, and H. Kurz, *Study of a high contrast process for hydrogen silsesquioxane as a negative tone electron beam resist.* Journal of Vacuum Science & Technology B: Microelectronics and Nanometer Structures, 2003. **21**: p. 2018.

33.   Baek, I., et al., *Electron beam lithography patterning of sub-10 nm line using hydrogen silsesquioxane for nanoscale device applications.* Journal of Vacuum Science & Technology B: Microelectronics and Nanometer Structures, 2005. **23**: p. 3120.

34. Chen, W. and H. Ahmed, *Fabrication of sub 10 nm structures by lift off and by etching after electron beam exposure of poly (methylmethacrylate) resist on solid substrates.* Journal of Vacuum Science & Technology B: Microelectronics and Nanometer Structures, 2009. **11**(6): p. 2519-2523.

35. Voigt, A., et al. *Nanometer patterning using ma-N 2400 series DUV negative photoresist and electron beam lithography.* 1999.

36. Anderson, E.H., et al., *Influence of sub-100 nm scattering on high-energy electron beam lithography.* Journal of Vacuum Science & Technology B: Microelectronics and Nanometer Structures, 2001. **19**(6): p. 2504-2507.

37. Namatsu, H., et al., *Three-dimensional siloxane resist for the formation of nanopatterns with minimum linewidth fluctuations.* Journal of Vacuum Science & Technology B: Microelectronics and Nanometer Structures, 1998. **16**: p. 69.

38. Jedrasik, P. and M. Hanson, *Application of floatable oxide (FOx-12) for nanometer magnetic particle fabrication.* Microelectronic Engineering, 2002. **61**: p. 811-817.

39. Mollard, L., et al., *HSQ hybrid lithography for 20 nm CMOS devices development.* Microelectronic Engineering, 2002. **61**: p. 755-761.

40. van Delft, F.C., et al., *Hydrogen silsesquioxane/novolak bilayer resist for high aspect ratio nanoscale electron-beam lithography.* Journal of Vacuum Science & Technology B: Microelectronics and Nanometer Structures, 2000. **18**: p. 3419.

41. Maile, B.E., et al. *Sub-10 nm linewidth and overlay performance achieved with a fine-tuned EBPG-5000 TFE electron beam lithography system.* 2000. IEEE.

42. Zhao, J.H., et al., *Thermomechanical properties and moisture uptake characteristics of hydrogen silsesquioxane submicron films.* Applied Physics Letters, 1999. **74**: p. 944.

43. Hacker, N.P., *Organic and inorganic spin-on polymers for low-dielectric-constant applications.* MRS bulletin, 1997. **22**(10): p. 33-38.

44.   Loboda, M., C. Grove, and R. Schneider, *Properties of a-SiO: H Thin Films Deposited from Hydrogen Silsesquioxane Resins.* Journal of The Electrochemical Society, 1998. **145**: p. 2861.

45.   Bremmer, J., et al., *Material Research Society Symposium Proceedings.* San Francisco, CA, 1997: p. 1-4.

46.   Zeng, Y., et al., *Effectiveness of Ti, TiN, Ta, TaN, and WN as barriers for the integration of low-k dielectric hydrogen silsesquioxane.* Journal of Vacuum Science & Technology B: Microelectronics and Nanometer Structures, 2000. **18**: p. 221.

47.   Rooks, M., et al., *Low stress development of poly (methylmethacrylate) for high aspect ratio structures.* Journal of Vacuum Science & Technology B: Microelectronics and Nanometer Structures, 2002. **20**: p. 2937.

48.   Pantenburg, F., S. Achenbach, and J. Mohr, *Influence of developer temperature and resist material on the structure quality in deep X-ray lithography.* Journal of Vacuum Science & Technology B: Microelectronics and Nanometer Structures, 1998. **16**: p. 3547.

49.   *Positive Electron Beam Resists*, Nanothechnology Research Center Website, Georgia Institute of Technology.

50.   Rosen, S., *Fundamental principles of polymeric materials*1982: Wiley New York.

51.   Liu, C., *Recent developments in polymer MEMS.* Advanced Materials, 2007. **19**(22): p. 3783-3790.

52.   Wang, X., J. Engel, and C. Liu, *Liquid crystal polymer for MEMS: processes and applications.* Journal of Micromechanics and Microengineering, 2003. **13**: p. 628-633.

53.   Rajarathinam, V., et al., *Aqueous-Develop, Photosensitive Polynorbornene Dielectric: Properties and Characterization.* Journal of Electronic Materials, 2009. **38**(6): p. 778-786.

54.   Raeis-Zadeh, M., et al., *Aqueous-Develop, Photosensitive Polynorbornene Dielectric: Optimization of Mechanical and Electrical Properties.* Journal of Electronic Materials, 2011: p. 1-13.

55.   Bai, Y.Q., et al., *Photosensitive polynorbornene based dielectric. I. Structure-property relationships.* Journal of Applied Polymer Science, 2004. **91**(5): p. 3023-3030.

56.   Grove, N., et al., *Functionalized polynorbornene dielectric polymers: adhesion and mechanical properties.* Journal of Polymer Science Part B: Polymer Physics, 1999. **37**(21): p. 3003-3010.

57.   Grove, N., et al. *Polynorbornene for Low K Interconnection.* 1997. MATERIALS RESEARCH SOCIETY.

58.   Bai, Y.Q., et al., *Photosensitive polynorbornene based dielectric. II. Sensitivity and spatial resolution.* Journal of Applied Polymer Science, 2004. **91**(5): p. 3031-3039.

59.   Goodall, B. *US Patent 5,468, 819, 1995.(k) Goodall, BL; Benedikt, GM; McIntosh, LH, III: Barnes, DA; Rhodes, LF PCT Int.* 1995.

60.   Goodall, B., L. McIntosh III, and D. Barnes. *WO Pat., 9637529, 1997, BF Goodrich Company (USA).* 1997.

61.   Rosen, S.L., *Fundamental principles of polymeric materials*1982: Wiley New York.

62.   Decker, C., *Photoinitiated crosslinking polymerisation.* Progress in polymer science, 1996. **21**(4): p. 593-650.

63.   Plesch, P., *The chemistry of cationic polymerization*1963, New York: Pergamon.

64.   Fouassier, J. and J. Rabek, *Radiation Curing in Polymer Science and Technology: Fundamentals and Methods*1993: Springer.

65.   Cai, G. and W.P. Weber, *Synthesis of terminal Si-H irregular tetra-branched star polysiloxanes. Pt-catalyzed hydrosilylation with unsaturated epoxides.*

Polysiloxane films by photo-acid catalyzed crosslinking. Polymer, 2004. **45**(9): p. 2941-2948.

66.   Chiniwalla, P., et al., *Crosslinking and decomposition reactions of epoxide functionalized polynorbornene. Part I. FTIR and thermogravimetric analysis.* Journal of Applied Polymer Science, 2003. **89**(2): p. 568-577.

67.   Chiniwalla, P., et al., *Crosslinking and decomposition reactions of epoxide-functionalized polynorbornene. II. Impact of reactions on mechanical properties.* Journal of Applied Polymer Science, 2003. **91**(2): p. 1020-1029.

68.   Crivello, J., T. Lockhart, and J. Lee, *Diaryliodonium salts as thermal initiators of cationic polymerization.* Journal of Polymer Science Polymer Chemistry Edition, 1983. **21**(1): p. 97-109.

69.   Yu, H.S., T. Yamashita, and K. Horie, *Synthesis and Chemically Amplified Photo-Cross-Linking Reaction of a Polyimide Containing an Epoxy Group.* Macromolecules, 1996. **29**(4): p. 1144-1150.

70.   Cupta, M., P. Joseph, and P. Kohl, *Photoacid generators for catalytic decomposition of polycarbonate.* Journal of Applied Polymer Science, 2007. **105**(5): p. 2655-2662.

71.   Suss, *Technical Specifications for MA6 [cited; Available from: http://www.suss.com].*

72.   JEOL, *Technical Specifications for JBX-9300 [cited; Available from: http://www.jeol.com].*

73.   Yao, K., et al., *Swelling kinetics and release characteristic of crosslinked chitosan: Polyether polymer network(semi-IPN) hydrogels.* Journal of Polymer Science Part A Polymer Chemistry, 1994. **32**(7): p. 1213-1223.

74.   Bigi, A., et al., *Mechanical and thermal properties of gelatin films at different degrees of glutaraldehyde crosslinking.* Biomaterials, 2001. **22**(8): p. 763-768.

75.   Shaw, G., et al., *Thermomechanical high-density data storage in a metallic material via the shape-memory effect.* Advanced Materials, 2005. **17**(9): p. 1123-1127.

76.   Loubet, J., et al., *Vickers indentation curves of magnesium oxide (MgO).* Journal of Tribology, 1984. **106**: p. 43.

77.   Briscoe, B.J., L. Fiori, and E. Pelillo, *Nano-indentation of polymeric surfaces.* Journal of Physics D-Applied Physics, 1998. **31**(19): p. 2395-2405.

78.   VanLandingham, M., et al. *Nanoindentation of polymers: An overview*. 2001. John Wiley & Sons.

79.   Shen, L., et al., *Nanoindentation and morphological studies on nylon 66/organoclay nanocomposites. II. Effect of strain rate.* Polymer, 2004. **45**(24): p. 8221-8229.

80.   Oliver, W. and G. Pharr, *Improved technique for determining hardness and elastic modulus using load and displacement sensing indentation experiments.* Journal of Materials Research, 1992. **7**(6): p. 1564-1583.

81.   Wornyo, E., et al., *Nanoindentation of shape memory polymer networks.* Polymer, 2007. **48**(11): p. 3213-3225.

82.   *Thin films stress measurement system; Operational manual*, in *Model F2320*, Flexus Inc.: San Jose, CA.

83.   Klein, C.A., *How accurate are Stoney's equation and recent modifications.* Journal of Applied Physics, 2000. **88**(9): p. 5487-5489.

84.   Materials, A.S.f.T.a. *Standard Test Methods for AC Loss Characteristics and Permittivity (dielectric constant) of Solid Electrical Insulating Materials*. 1992.

85.   Lorenz, H., M. Laudon, and P. Renaud, *Mechanical characterization of a new high-aspect-ratio near UV-photoresist.* Microelectron. Eng, 1998. **41**(42): p. 371–4.

86.   Wei, X., et al., *Thick photoresists for electroforming metallic microcomponents.* Proceedings of the Institution of Mechanical Engineers, Part C: Journal of Mechanical Engineering Science, 2008. **222**(1): p. 37-42.

87.   Lee, C. and K. Jiang. *KMPR photoresist for fabrication of thick microstructures*. 2007.

88.   Chiniwalla, P., et al., *Crosslinking and decomposition reactions of epoxide functionalized polynorbornene. Part I. FTIR and thermogravimetric analysis.* Journal of Applied Polymer Science, 2003. **89**(2): p. 568-577.

89.   Chiniwalla, P., et al., *Crosslinking and decomposition reactions of epoxide-functionalized polynorbornene. II. Impact of reactions on mechanical properties.* Journal of Applied Polymer Science, 2004. **91**(2): p. 1020-1029.

90.   Feng, R. and R. Farris, *Influence of processing conditions on the thermal and mechanical properties of SU8 negative photoresist coatings.* Journal of Micromechanics and Microengineering, 2003. **13**: p. 80-88.

91.   Lee, C. and K. Jiang, *Fabrication of thick electroforming micro mould using a kmpr negative tone photoresist.* Journal of Micromechanics and Microengineering, 2008. **18**: p. 055032.

92.   Bogdanov, A. and S. Peredkov, *Use of SU-8 photoresist for very high aspect ratio x-ray lithography.* Microelectronic Engineering, 2000. **53**(1-4): p. 493-496.

93.   Mark, J., *Experimental determinations of crosslink densities.* Rubber Chemical Technology, 1982. **55**(3).

94.   Soh, M. and A. Yap, *Influence of curing modes on crosslink density in polymer structures.* Journal of dentistry, 2004. **32**(4): p. 321-326.

95.   Crawford, E. and A. Lesser, *The effect of network architecture on the thermal and mechanical behavior of epoxy resins.* Journal of Polymer Science-B-Polymer Physics Edition, 1998. **36**(8): p. 1371-1382.

96.   Thompson, Z., et al., *Block Copolymer Toughened Epoxy: Role of Cross-Link Density.* Macromolecules, 2009. **42**: p. 2333-2335.

97.   Raeis Zadeh, M., et al., *Cross linking of aqueous base developable, photosensitive polynorbornene.* Journal of Applied Polymer Science, 2010. **120**(4): p. 1916-1925.

98.   Horie, K. and T. Yamashita, *Photosensitive polyimides: fundamentals and applications*1995: CRC.

99.   Glendinning, W.B. and J.N. Helbert, *Handbook of VLSI Microlithography: Principles, Technology, and Applications*1991: William Andrew Publishing.

100.   Thompson, L., E. Feit, and R. Heidenreich, *Lithography and radiation chemistry of epoxy containing negative electron resists.* Polymer Engineering & Science, 1974. **14**(7): p. 529-533.

101.   Manepalli, R., et al., *Multilayer electron-beam curing of polymer dielectric for electrical interconnections.* Electrochemical and Solid State Letters, 2000. **3**(5): p. 228-231.

102.   Aktary, M., et al., *High-resolution pattern generation using the epoxy novolak SU-8 2000 resist by electron beam lithography.* Journal of Vacuum Science & Technology B: Microelectronics and Nanometer Structures, 2003. **21**: p. L5.

103.   Devlin, N.R., D.K. Brown, and P.A. Kohl, *Patterning decomposable polynorbornene with electron beam lithography to create nanochannels.* Journal of Vacuum Science & Technology B: Microelectronics and Nanometer Structures, 2009. **27**(6): p. 2508-2511.

104.   Argitis, P., et al., *An advanced epoxy novolac resist for fast high resolution electron beam lithography.* Journal of Vacuum Science & Technology B: Microelectronics and Nanometer Structures, 2009. **13**(6): p. 3030-3034.

105.   Lawson, R., et al., *Epoxide functionalized molecular resists for high resolution electron-beam lithography.* Microelectronic Engineering, 2008. **85**(5-6): p. 959-962.

106.   Hatzakis, M., et al., *New high resolution and high sensitivity deep UV, X-ray, and electron beam resists.* Microelectronic Engineering, 1990. **11**(1-4): p. 487-489.

107.   Yang, D., S.W. Chang, and C.K. Ober, *Molecular glass photoresists for advanced lithography.* Journal of Materials Chemistry, 2006. **16**(18): p. 1693-1696.

108. Young-Gil, K., et al., *A positive-working alkaline developable photoresist based on partially tert-Boc-protected calix [4] resorcinarene and a photoacid generator.* Journal of Materials Chemistry, 2002. **12**(1): p. 53-57.

109. Lawson, R.A., et al., *Influence of solubility switching mechanism on resist performance in molecular glass resists.* Journal of Vacuum Science & Technology B: Microelectronics and Nanometer Structures, 2007. **25**: p. 2140.

110. Raeis Zadeh, M., et al., *Cross linking of aqueous base developable, photosensitive polynorbornene.* Journal of Applied Polymer Science.

111. Chen, W. and H. Ahmed, *Fabrication of 5–7 nm wide etched lines in silicon using 100 keV electron beam lithography and polymethylmethacrylate resist.* Applied Physics Letters, 2009. **62**(13): p. 1499-1501.

112. Ocola, L. and A. Stein, *Effect of cold development on improvement in electron-beam nanopatterning resolution and line roughness.* Journal of Vacuum Science & Technology B: Microelectronics and Nanometer Structures, 2006. **24**: p. 3061.

113. Gnan, M., et al., *Fabrication of low-loss photonic wires in silicon-on-insulator using hydrogen silsesquioxane electron-beam resist.* Electronics Letters, 2008. **44**(2): p. 115-116.

114. Chen, Y., et al. *Fabrication of silicon microring resonator with smooth sidewalls*. 2009. SPIE.

115. Shah Hosseini, E., et al., *High quality planar silicon nitride microdisk resonators for integrated photonics in the visible wavelength range.* Optics Express, 2009. **17**(17): p. 14543-14551.

116. Leunissen, L., W. Lawrence, and M. Ercken, *Line edge roughness: experimental results related to a two-parameter model.* Microelectronic Engineering, 2004. **73**: p. 265-270.

117. Kozawa, T., et al., *Radiation-induced acid generation reactions in chemically amplified resists for electron beam and X-ray lithography.* Jpn. J. Appi. Phys. Vol, 1992. **31**: p. 4301-4306.

118. Kadota, T., et al., *Novel electron-beam molecular resists with high resolution and high sensitivity for nanometer lithography.* Chemistry Letters, 2004. **33**(6): p. 706-707.

119. Yang, J.K.W. and K.K. Berggren, *Using high-contrast salty development of hydrogen silsesquioxane for sub-10 nm half-pitch lithography.* Journal of Vacuum Science & Technology B: Microelectronics and Nanometer Structures, 2007. **25**: p. 2025.

120. Robinson, A., et al., *Chemically amplified molecular resists for electron beam lithography.* Microelectronic Engineering, 2006. **83**(4-9): p. 1115-1118.

121. Plage, B. and H. Schulten, *Pyrolysis-field ionization mass spectrometry of epoxy resins.* Macromolecules, 1988. **21**(7): p. 2018-2027.

122. Zang, Y., R. Muller, and D. Froelich, *Determination of crosslinking density of polymer networks by mechanical data in simple extension and by swelling degree at equilibrium.* Polymer, 1989. **30**(11): p. 2060-2062.

123. Flory, P. and Y. Tatara, *The elastic free energy and the elastic equation of state: Elongation and swelling of polydimethylsiloxane networks.* Journal of Polymer Science: Polymer Physics Edition, 1975. **13**(4): p. 683-702.

124. Crivello, J. and J. Lee, *Redox initiated cationic polymerization: The diaryliodonium salt/benzoin redox couple.* Journal of Polymer Science: Polymer Chemistry Edition, 1983. **21**(4): p. 1097-1110.

125. Brydson, J., *Plastic Materials*. 7 ed1989, Woburn: Reed International Books.

126. Materials, N.R.C.C.o.M.P.o., et al., *Microwave processing of materials*. Vol. 473. 1994: Natl Academy Pr.

127. Jacob, J., L. Chia, and F. Boey, *Thermal and non-thermal interaction of microwave radiation with materials.* Journal of materials science, 1995. **30**(21): p. 5321-5327.

128. Surrett, A.D., et al., *Polymer curing using variable frequency microwave processing.* Microwave processing of materials IV, 1994: p. 691-696.

129. Zhou, S. and M.C. Hawley, *A study of microwave reaction rate enhancement effect in adhesive bonding of polymers and composites.* Composite structures, 2003. **61**(4): p. 303-309.

130. Tanikella, R.V., S. Bidstrup Allen, and P.A. Kohl. *Novel low-temperature processing of polymer dielectrics on organic substrates by variable frequency microwave processing.* 2002. IEEE.

131. Demeuse, M.T. and A.C. Johnson, *Variable frequency microwave processing of thermosetting polymer matrix composites.* Proceedings of Materials Research Society Symposium 1994. **347**: p. 723-728.

132. Lauf, R., et al., *2 to 8 GHz broadband microwave heating systems.* Microwave Journal 1993: p. 24-34.

133. Fathi, Z., et al., *Industrial applications of variable frequency microwave energy in materials processing.* Proceedings of Materials Research Society Symposium, 1996. **430**: p. 21-28.

134. Panchapakesan, B., et al., *Variable Frequency Microwave, A New Approach to Curing.* Advanced Packaging, 1997: p. 60-63.

135. Chung, H., Y. Joe, and H. Han, *The effect of curing history on the residual stress behavior of polyimide thin films.* Journal of Applied Polymer Science, 1999. **74**(14): p. 3287-3298.

136. Coburn, J.C. and M.T. Pottiger. *The influence of processing conditions on structure, properties, and stress development in spin coated polyimide films.* 1993.

137. Lewis, D.A., *Microwave processing of polymers-an overview.* Procedding of Materials Research Society Symposium, 1992. **269**: p. 21-29.

138. Erickson, D., et al., *Nanobiosensors: optofluidic, electrical and mechanical approaches to biomolecular detection at the nanoscale.* Microfluidics and nanofluidics, 2008. **4**(1): p. 33-52.

139. Nitkowski, A., L. Chen, and M. Lipson, *Cavity-enhanced on-chip absorption spectroscopy using microring resonators.* Opt. Express, 2008. **16**: p. 11930-11936.

140. Chao, C. and L. Guo, *Design and optimization of microring resonators in biochemical sensing applications.* Journal of Lightwave Technology, 2006. **24**(3): p. 1395.

141. Blanco, F., et al., *Microfluidic-optical integrated CMOS compatible devices for label-free biochemical sensing.* Journal of Micromechanics and Microengineering, 2006. **16**: p. 1006.

142. LaBianca, N. and J. Gelorme. *High-aspect-ratio resist for thick-film applications*. 1995.

143. Gelorme, J., R. Cox, and S. Gutierrez, *Photoresist composition and printed circuit boards and packages made therewith*, 1989, Google Patents.

144. Ruhmann, R., et al., *SU-8-a high performance material for MEMS applications.* NEXUS-Network of Excellence in Multifunctional Microsystems EUROPRACTICE-Microsystems Service for Europe: p. 45.

145. Lee, K., et al., *Micromachining applications of a high resolution ultrathick photoresist.* Journal of Vacuum Science & Technology B: Microelectronics and Nanometer Structures, 1995. **13**: p. 3012.

146. Jo, B.H., et al., *Three-dimensional micro-channel fabrication in polydimethylsiloxane (PDMS) elastomer.* Microelectromechanical Systems, Journal of, 2000. **9**(1): p. 76-81.

147. Bhusari, D., et al., *Fabrication of air-channel structures for microfluidic, microelectromechanical, and microelectronic applications.* Microelectromechanical Systems, Journal of, 2001. **10**(3): p. 400-408.

148. Schmidt, H., et al., *Hollow-core waveguides and 2-D waveguide arrays for integrated optics of gases and liquids.* Selected Topics in Quantum Electronics, IEEE Journal of, 2005. **11**(2): p. 519-527.

149.   Bhattacharya, S., et al., *Studies on surface wettability of poly (dimethyl) siloxane (PDMS) and glass under oxygen-plasma treatment and correlation with bond strength.* Microelectromechanical Systems, Journal of, 2005. **14**(3): p. 590-597.

150.   Soltani, M., *Novel integrated silicon nanophotonic structures using ultra-high q resonators.* 2009.

151.   Passaro, V., F. Dell'Olio, and F. De Leonardis, *Ammonia optical sensing by microring resonators.* Sensors, 2007. **7**(11): p. 2741.

152.   Yota, J., J. Hander, and A. Saleh, *A comparative study on inductively-coupled plasma high-density plasma, plasma-enhanced, and low pressure chemical vapor deposition silicon nitride films.* Journal of Vacuum Science & Technology A: Vacuum, Surfaces, and Films, 2000. **18**: p. 372.

153.   Cardenas, J., et al., *Wide-bandwidth continuously tunable optical delay line using silicon microring resonators.* Optics Express, 2010. **18**(25): p. 26525-26534.

154.   Tesar, V., *Pressure Driven Microfluidics.* Artech House: Norwood, MA, 2007.